Titre: Title:	Controlled Wetting in Multiphase Polymer Blends with Polylactide: Morphology and Performance
Auteur: Author:	Mohammad Ali Zolali
Date:	2016
Type:	Mémoire ou thèse / Dissertation or Thesis
Référence: Citation:	Zolali, M. A. (2016). Controlled Wetting in Multiphase Polymer Blends with Polylactide: Morphology and Performance [Ph.D. thesis, École Polytechnique de Montréal]. PolyPublie. https://publications.polymtl.ca/2375/

Document en libre accès dans PolyPublie
Open Access document in PolyPublie

URL de PolyPublie: PolyPublie URL:	https://publications.polymtl.ca/2375/
Directeurs de recherche: Advisors:	Basil D. Favis
Programme: Program:	Génie chimique

UNIVERSITÉ DE MONTRÉAL

CONTROLLED WETTING IN MULTIPHASE POLYMER BLENDS WITH POLYLACTIDE: MORPHOLOGY AND PERFORMANCE

MOHAMMAD ALI ZOLALI

DÉPARTEMENT DE GÉNIE CHIMIQUE

ÉCOLE POLYTECHNIQUE DE MONTRÉAL

THÈSE PRÉSENTÉE EN VUE DE L'OBTENTION

DU DIPLÔME DE PHILOSOPHIAE DOCTOR

(GÉNIE CHIMIQUE)

DÉCEMBRE 2016

UNIVERSITÉ DE MONTRÉAL

ÉCOLE POLYTECHNIQUE DE MONTRÉAL

Cette thèse intitulée:

CONTROLLED WETTING IN MULTIPHASE POLYMER BLENDS WITH POLYLACTIDE:
MORPHOLOGY AND PERFORMANCE

présentée par : ZOLALI Mohammad Ali

en vue de l'obtention du diplôme de : Philosophiae Doctor

a été dûment acceptée par le jury d'examen constitué de:

M. TAVARES Jason-Robert, Ph. D., président

M. FAVIS Basil, Ph. D., membre et directeur de recherche

M. VIRGILIO Nick, Ph. D., membre

M. HU Guo-Hua, Ph. D., membre

DEDICATION

To Raziyeh

To my parents

ACKNOWLEDGEMENTS

I would like to express my sincere thanks to my advisor, Professor Basil Favis, for his guidance throughout this research and his constant support and encouragement. I am honored to have had the opportunity to work as a Ph.D. candidate under his supervision. His accurate, practical and realistic attitude toward scientific research will certainly hold positive influences on my career and personal life.

Thanks to Prof. Jason Tavares, Prof. Nick Virgilio, and Prof. Guo-Hua Hu for taking part in my thesis committee.

The experiences which I have had with members of my research group have not only provided me with a wealth of scientific resources, but memories which have allowed me to grow as a person. I wish to thank Vahid Heshmati, Ebrahim Jalali, Jun Wang, Ata Taghizadeh, and Mehdi Pakravan for fruitful discussions.

I would like to thank friends in the Department of Chemical Engineering. I greatly value their friendship and I deeply appreciate their help.

I also would like to thank the technical and administrative staff of the Department of Chemical Engineering at Polytechnique Montréal.

Most importantly I would like to thank my family. I never could have done it without their support and encouragement. To my parents and my parents-in-law who have always supported me to continue my studies. To my sons, Parsa and Borna, for being such wonderful little people, at least most of the time. To my wife, Raziyeh, thank you for your understanding and the sacrifices that you have made during the long drawn out process. You will never know how much I appreciate all that you have done for me. This never would have become a reality without your love and support.

RESUME

Le mélange de polylactide (PLA) avec d'autres polymères est une approche viable à l'expansion dans d'autres champs d'applications. La vaste majorité de la littérature concernant les mélanges à base de PLA ce concentrent sur les mélanges binaires. Malgré tout, récemment, les mélanges de polymères multi-phases ont reçu une attention particulière dû à leur potentiel en tant que matériaux multifonctionnel haute performance. La clé pour obtenir de tels matériaux est de contrôler la morphologie des phases et de comprendre sa relation avec les propriétés. Pour les mélanges multi-phases de polymères, particulièrement un système ternaire, deux grandes catégories d'états morphologiques sont définies : le mouillage complet, qui montre un comportement de contact entre deux phases, et le mouillage partiel, où trois sont en contact l'une avec l'autre et qui vient seulement de commencer à être étudié en détail récemment. Cette dissertation fait état de la morphologie de mélanges ternaires et quaternaires à base de PLA dans le contexte des deux états de mouillage et leur relation avec les propriétés mécaniques.

Dans la première partie de cet ouvrage, nous examinons la morphologie de mélanges ternaires et quaternaires du PLA avec le poly(butylene succinate) (PBS), le poly(butylene adipate-co-terephthalate) (PBAT) et le poly(3-hydroxybutyrate-co-hydroxyvalerate) (PHBV). Les échantillons mélangés à l'état fondu ont subi un traitement thermique subséquent afin de déterminer les états thermodynamiques les plus stables de mouillage complet ou partiel. Les tensions interfaciales entre les composantes ont été mesurées à l'aide de trois techniques différentes, à savoir : la rupture du fil (BT), la rétraction des fibres ancrées (IFR), et l'approche triangle-in situ de Neumann (NT). L'imagerie FTIR est présentée comme une nouvelle méthode d'identification de phase et d'analyse de la morphologie utile pour caractériser les systèmes multi-phases de structures chimiques similaires, tels que les bio-polyesters utilisées dans ce travail. Les mélanges ternaire 33PLA/33PBS/33PBAT montrent un comportement au mouillage complet tri-continu avant et après un traitement thermique, ce qui concorde étroitement avec l'analyse de la théorie d'étalement. Le système quaternaire PLA/PBS/PBAT/PHBV montre un comportement de mouillage dépendant de la concentration. Une morphologie complètement mouillée continue des quatre phases est trouvée pour 25PLA/25PBS/25PBAT/25PHBV après mélange. Durant le traitement thermique, il y a rupture des phases de PBAT qui forment des gouttelettes à l'interface PBS/PHBV. Cependant, à 10% volumique de PBAT, des gouttelettes partiellement mouillées de PBAT à l'interface de PBS et PHBV sont observés et ils restent stables après le recuit quiescent.

Les résultats morphologiques après recuit pour le mélange quaternaire sont fortement corrélés avec les prédictions thermodynamiques basées sur les mélanges ternaires constitutifs. Ces résultats montrent que le contrôle de la composition pour le mélange des systèmes multi-phases avec de faibles tensions interfaciales peut se traduire par un changement complet du comportement d'étalement.

Dans la deuxième partie de cette recherche, nous étudions le comportement de mouillage de trois phases intermédiaires différentes en fonction de la composition et du recuit de mélanges ternaires produit à l'état fondu PLA/PHBV/PBS, PLA/PBAT/PE et PLA/PE/PBAT. Ces systèmes ont tous montrés un comportement de mouillage partiel. Une transition d'un mouillage partiel à complet est observée pour les gouttelettes partiellement humides de PHBV et PBAT dans le PLA/PHBV/PBS et PLA/PBAT/PE, tandis que les gouttelettes de PE partiellement mouillées restent stables à l'interface du PLA/PBAT même à une concentration élevée en PE de 20% et après 30 min de recuit quiescent. La tension interfaciale des différentes composantes et les angles de contact des gouttelettes partiellement mouillées, confinées à l'interface de contact, ont été examinés en détail. L'analyse thermodynamique des coefficients d'étalement prédit une faible tendance au mouillage partiel pour les gouttelettes de PHBV et de PBAT dans le PLA/PHBV/PBS et le PLA/PBAT/PE, tandis qu'un mouillage partiel fort est prévu pour les gouttelettes de PE dans le PLA/PE/PBAT. Les trois systèmes de mélange présentent une coalescence considérablement améliorée en fonction de la composition et du temps de recuit, à cause du confinement des gouttelettes à l'interface. Un modèle de ségrégation est utilisé pour expliquer les divers phénomènes de mouillage et leur dépendance à la concentration et au temps de recuit. Les résultats indiquent le potentiel évident que le confinement interfacial, la composition, et le temps de recuit dans les systèmes multiphases ayant une morphologie avec mouillage partiel, puissent se traduire par un changement complet du comportement d'étalement. Ce travail montre l'excellent potentiel pour le mouillage contrôlé et la structuration des systèmes de polymères ternaires et présente une voie vers la préparation d'une panoplie de nouvelles structures morphologiques.

Dans la troisième partie de ce travail, nous examinons l'effet d'une structure de mouillage partiel sur la compatibilisation et la trempe d'un mélange co-continu de PLA/PA11. Quatre polymères différents : le PBS, le PBAT, l'EMA et l'EMA-GMA sont examinés pour leur capacité à mouiller partiellement l'interface PLA/PA11 dans un procédé de mélange en phase fondue, grâce à l'analyse de la morphologie et des propriétés physiques. Tous les mélanges présentent une morphologie de

mouillage partiel avec une gamme d'efficacités de compatibilisation et d'effets de durcissement. L'EMA-GMA montre le meilleur effet de compatibilisation en réduisant la taille de la phase co-continue à près de la moitié de celle du mélange binaire PLA/PA11 initial, en atteingnant 5-6 µm. Une augmentation significative de la ductilité des mélanges ternaires est obtenue, l'EMA montrant la plus forte amélioration avec un allongement à la rupture de 260% par rapport à 4% pour le mélange binaire. Une augmentation substantielle de la résistance au test de choc Izod est également obtenue avec l'EMA montrant quatre fois la résistance à l'impact du mélange binaire d'origine à 73 J/m. Nous croyons que les effets combinés de la morphologie compatibilisé, une bonne adhérence interfaciale et la cavitation interfaciale percolé de gouttelettes partiellement mouillées, suivis par la rupture en cisaillement de la matrice contribuent à l'effet de durcissement observé dans les mélanges ternaires partiellement mouillés. Ces résultats suggèrent une technique intéressante qui exploite les gouttelettes partiellement mouillées afin de compatibiliser et renforcer les structures co-continues.

Enfin, nous étudions la corrélation entre une morphologie de mouillage complet et l'augmentation de la ténacité dans un mélange ternaire à base de PLA/PA11. Nous montrons que lorsque du polyéther-b-amide (PEBA) est ajouté à au mélange PLA/PA11, il se propage entièrement à l'interface et s'assemble en une couche mince à l'interface du PLA et PA11 entièrement percolés. Ceci augmente considérablement la résistance à l'impact Izod, pour atteindre 142,4 J/m, par rapport à 17,3 J/m pour le mélange de PLA/PA11. L'addition supplémentaire d'oxyde de polyéthylène (PEO), dans la phase de PLA résulte en un matériau ultra-tenace manifeste par l'augmentation spectaculaire de la résistance à l'impact Izod qui atteint 728,6 J/m. Le PEBA est un élastomère thermoplastique capable de fortes interactions interfaciales avec le PLA et le composant amide dans le copolymère a une affinité naturelle pour le PA11. Le PEO ajoutée renforce également les interactions interfaciales et la mobilité de chaîne du PLA. La ténacité à la traction et la résistance à l'impact Izod sont fortement influencés par la région critique de la composition co-continue du système binaire PLA/PA11, les mélanges au-delà de cette région de composition démontrent une mauvaise ténacité. On constate que les effets combinés de la co-continuité, d'interactions interfaciales fortes, d'une interface déformable et d'une mobilité suffisante des chaînes de PLA sont tous essentiels à la réalisation du comportement ultra tenace dans le mélange PLA/PA11. Les surfaces de fracture des tests d'impact des mélanges ont été analysées et les résultats ont révélés une cavitation significative au sein de la phase PEBA déformable. Un mode de rupture ductile par

cisaillement est observé dans les mélanges ultras tenaces qui devrait être induite par le chevauchement des contraintes dans la phase PEBA déformable, conjointement à une adhérence interfaciale appropriée. Ces résultats établissent une stratégie pour l'augmentation de la ténacité des mélanges de polymères à phases multiples, en particulier à proximité de la région de co-continuité.

ABSTRACT

Blending of polylactide (PLA) with other polymers is a viable approach to promote its broader implementation. The vast majority of the PLA-based blend literature is based on binary blends, however, recently, multiphase polymer blends have received a marked interest due to their potential in generating high performance multi-functional materials. The key in achieving such materials is to control the phase morphology and understand its relationship with properties. For multiple phase polymer blends, particularly a ternary system, two broad categories of morphological states are defined: complete wetting, which demonstrates two phase contact wetting behavior, and partial wetting, in which three phases are in contact with each other and has only begun to be examined in detail recently. This dissertation reports on the morphology of ternary and quaternary PLA-based blends in the context of the two wetting regimes and its relationship with the mechanical properties.

In the first part of this work, we examine the morphology of ternary and quaternary blends of PLA with poly(butylene succinate) (PBS), poly(butylene adipate-co-terephthalate) (PBAT) and poly(3-hydroxybutyrate-co-hydroxyvalerate) (PHBV). Samples were melt blended and then annealed to determine the most stable complete or partial wetting thermodynamic states. The interfacial tensions between components were measured using three different techniques, i.e. breaking thread (BT), imbedded fiber retraction (IFR), and the in-situ Neumann triangle approach (NT). FTIR-imaging is presented as a new phase identification and morphology analysis method useful for characterizing multiphase systems of similar chemical structures such as the biopolyesters used in this work. The ternary 33PLA/33PBS/33PBAT blends demonstrate a tri-continuous complete wetting behavior before and after quiescent annealing which correlates closely with the spreading theory analysis. The quaternary PLA/PBS/PBAT/PHBV system shows a concentration dependent wetting behavior. A fully quadruple continuous completely wet morphology is found for 25PLA/25PBS/25PBAT/25PHBV after mixing where the PBAT phase breaks up and forms droplets at the PBS/PHBV interface upon quiescent annealing. However, at 10 vol.% PBAT, partially wet droplets of PBAT at the interface of PBS and PHBV are observed and they remain stable after quiescent annealing. The morphological results after annealing for the quaternary blend strongly correlate with the thermodynamic predictions based on the constituent ternary blends. These results show that composition control during the mixing of multiphase systems with low interfacial tensions can result in a complete change of spreading behavior.

In the second part of this research, we study the wetting behavior of three different intermediate phases as a function of composition and annealing in melt blended ternary PLA/PHBV/PBS, PLA/PBAT/PE and PLA/PE/PBAT systems all demonstrating partial wetting behavior. Although, partially wet PE droplets remain stable at the interface of PLA/PBAT even at a high PE concentration of 20% and after 30 min of quiescent annealing, a partial to complete wetting transition is found for both PHBV and PBAT partially wet droplets in the PLA/PHBV/PBS and PLA/PBAT/PE systems, respectively. The interfacial tension of the various components and the contact angles of the confined partially wet droplets at the interface were examined in detail. The thermodynamic analysis of the spreading coefficients predicts a weak partial wetting tendency for PHBV and PBAT droplets in PLA/PHBV/PBS and PLA/PBAT/PE, respectively, while a strong partial wetting is predicted for PE droplets in PLA/PE/PBAT. All three blend systems show significantly enhanced coalescence as a function of composition and annealing time due to the interfacial confinement of the droplets at the interface. A dewetting model is used to explain the various wetting behaviors and their dependence on concentration and annealing time. The results indicate the clear potential that interfacial confinement, composition, and annealing time in multiphase systems with partial wetting morphology can result in a complete change of spreading behavior. This work shows the excellent potential for controlled wetting and structuring in ternary polymer systems and presents a route towards the preparation of a range of new morphological structures.

In the third part of this work, we examine the effect of partial wetting structure on the compatibilization and toughening of a co-continuous PLA/PA11 blend. Four different polymers: PBS, PBAT, EMA and EMA-GMA are examined for their capacity to partially wet the PLA/PA11 interface in a melt-blending process. All the blends exhibit a partial wetting morphology with a range of compatibilization efficacies and toughening effects. EMA-GMA demonstrates the best compatibilization effect by reducing the co-continuous phase size to about half that of the original binary PLA/PA11 blend at 5-6 μm. A significant increase in the ductility of the ternary blends is achieved where EMA shows the highest enhancement with an elongation at break of 260% as compared to 4% for the binary blend. A substantial increase in the notched Izod impact strength is also obtained with EMA demonstrating four times the impact of the original binary blend at 73 J/m. The combined effects of compatibilized morphology, good interfacial adhesion and the interfacially percolated cavitation of partially wet droplets followed by shear yielding of the matrix

is believed to contribute to the toughening effect observed in the partially wet ternary blends. These results suggest an interesting technique exploiting partially wet droplets to compatibilize and toughen co-continuous structures.

Finally, we investigate the correlation between the morphology of a system demonstrating complete wetting behavior and toughening in a ternary blend based on PLA/PA11. We show that when polyether-*b*-amide (PEBA) is added to the PLA/PA11 blend, it completely spreads at the interface and assembles as a thin layer at the interface of a fully percolated PLA and PA11. This significantly increases the notched Izod impact strength from to 142.4 J/m as compared to 17.3 J/m for the PLA/PA11 blend. The further addition of polyethylene oxide (PEO) to the PLA phase results in an ultra-toughening effect and a dramatic increase in the Izod impact to 728.6 J/m is achieved. PEBA is a thermoplastic elastomer capable of strong interfacial interactions with PLA and the amide component in the copolymer has a natural affinity for the PA11. The added PEO is found to enhance the interfacial interactions and the chain mobility of PLA. The tensile toughness and notched Izod impact strength are significantly influenced by the critical co-continuous composition region of the PLA/PA11 binary system where the blends beyond this composition region demonstrate a poor toughness. It is found that the combined effects of co-continuity, strong interfacial interactions, a deformable interface and sufficient PLA chain mobility are all essential to achieving ultratough behavior in PLA/PA11. The impact fracture surface of the blends was analyzed and the results revealed significant cavitation within the deformable PEBA phase. A shear yielding failure mode is observed in the ultratough blends which is believed to be induced by the stress-field overlap within the deformable PEBA phase in conjunction with suitable interfacial adhesion. These results establish a strategy for the toughening of multiphase polymer blends, especially in the vicinity of the co-continuous region.

TABLE OF CONTENTS

LIST OF TABLES

LIST OF FIGURES

LIST OF SYMBOLS AND ABBREVIATIONS

Symbols:

α	amplitude of distortion
Ca	Capillary number
μ	chemical potential
G^*	complex modulus
θ_e	contact angle
h_{crit}	critical thickness of film between two drops in rupture
ρ	density of polymers
ν	dewetting speed
D	diameter
p	dispersed phase/matrix viscosity ratio
γ_i^d	dispersive component of surface tension
η_e	effective viscosity
N_1	first normal stress difference
χ_{AB}	Flory-Huggins interaction parameter
ω	frequency
G	Gibbs free energy
γ_{ij}/γ	interfacial tension
G''	loss modulus
M_w	molecular weight of the polymers
n	number of moles
γ_i^p	polar component of surface tension
ΔP	pressure difference

P_c probability of the droplet collision

R radius

$\dot{\gamma}$ shear rate

λ spreading coefficient

F Stokes drag force

G' storage modulus

γ surface/interfacial tension

Ω Tomotika function

η viscosity

φ volume fraction

η_0 zero shear viscosity

Abbreviations:

ABS   acrylonitrile-butadiene-styrene

AFM   atomic force microscopy

ATBC   acetyl tri-n-butyl citrate

BT   breaking thread

DSC   differential scanning calorimetry

EBA-GMA   ethylene/n-butyl acrylate/glycidyl methacrylate copolymer

EMA   ethylene methyl acrylate

EMA-GMA   ethylene-methyl acrylate-glycidyl methacrylate

EMAA-Zn   zinc ionomer of ethylene/methacryalic acid copolymer

EPDM   ethylene-propylene-diene terpolymer

EPR   ethylene-propylene-rubber

FTIR	Fourier transform infrared spectroscopy
HDPE	high density polyethylene
HDT	heat deflection temperature
HIPS	high impact polystyrene
IFR	imbedded fiber retraction
LbL	layer-by-layer
NT	Neumann triangle
PA11	polyamide-11
PA6	polyamide 6
PANI	polyaniline
PBAT	poly(butylene adipate-co-terephthalate)
PBS	poly(butylene succinate)
PBT	polybutylene terephthalate
PC	polycarbonate
PCL	polycaprolactone
PDLA	poly(D,L-lactic acid)
PE	polyethylene
PEBA	poly(ether-b-amide)
PEG	polyethylene glycol
PEO	poly(ethylene oxide)
PHBV	poly(3-hydroxybutyrate-co-hydroxyvalerate)
PLA	polylactide
PLLA	poly(L-lactic acid)
PMMA	polymethyl methacrylate

PO	polyolefin
POE	polyethylene-octene elastomer
PP	polypropylene
PPG	poly(propylene glycol)
PS	Polystyrene
PSS	poly(styrene sulfonate)
PVC	poly(vinyl chloride)
PVDF	polyvinylidene fluoride
SAN	styrene acrylonitrile resin
SBR	styrene-butadiene rubber
SEB	styrene-(ethylene-butylene) diblock
SEBS	styrene-ethylene/butylene-styrene copolymer
SEM	scanning electron microscopy
TCP	1,2,3-trichloropropane
THF	Tetrahydrofuran
TPS	thermoplastic starch
TPSA	thermoplastic starch acetate
TPU	thermoplastic polyurethane

LIST OF APPENDICES

CHAPTER 1   INTRODUCTION AND OBJECTIVES

1.1 Introduction

Plastics have become an important aspect of our everyday lives. Synthetic plastics such as polyethylene (PE), polypropylene (PP), polystyrene (PS), polyethylene terephthalate (PET), and polyvinyl chloride (PVC) share a major portion of commodity plastics. The environmental concerns and limited fossil fuel resources compel industrial sectors and scientists to find alternatives to current petroleum-based plastics. Biodegradable plastics are generating significant interest in various industries because of their true potential for reducing the dependence on fossil-based resources and their related environmental impacts (Avérous & Pollet, 2012). The bioplastics and biopolymers market is projected to grow at a compound annual growth rate of 12% between 2016 to 2021 (MarketsandMarkets, 2016). The growth of the market is attributed to the stringent environmental regulations across the globe, compelling the manufacturer to reduce the carbon content in their products, and fluctuations in the price of petroleum, which forces companies to search for a stable source of raw materials. The production and applications of bioplastics, nevertheless, are still limited due to their high production cost and poor performance characteristics as compared to the commodity plastics (MarketsandMarkets, 2015; L Shen, Haufe, & Patel, 2009).

Polylactides are the leading bioplastics, which have been looked upon as sustainable alternatives to petroleum based plastics over the last decade (Babu, O'Connor, & Seeram, 2013; Erickson & Winters, 2012; Li Shen, Worrell, & Patel, 2010; Williams & Hillmyer, 2008). These polymers are biodegradable aliphatic polyesters derived from renewable resources, such as corn and starch, and has generated much interest due to its mechanical properties and favorable economics (Auras, Lim, Selke, & Tsuji, 2010). However, PLA suffers from inferior impact toughness and thermal stability when compared to the conventional polymers and this limits its wider applications. Previously, PLA was only used for biomedical applications but there is a strong increase in the number of research papers and patent applications pertaining to the modification of PLA in order to develop it as a high performance plastic. PLA must meet and even surpass the mechanical properties expected from petroleum based polymers such as high impact polystyrene (HIPS), acrylonitrile butadiene styrene (ABS), and high impact polyamides in order to successfully replace these plastics in value added applications. Different strategies have been mentioned in the literature to improve

the poor toughness and impact strength of PLA such as copolymerization, plasticization and blending with other bioplastics (Anderson, Schreck, & Hillmyer, 2008; H. Liu & Zhang, 2011; Rasal, Janorkar, & Hirt, 2010).. Generally, polymer blending is considered as an important route to overcome the mechanical property deficiencies of PLA since it is the most versatile and cost-effective approach which is easily adapted to the classic compounding capabilities. PLA has been blended with different polymers to prepare materials with the desired set of properties (Anderson et al., 2008; Paul & Bucknall, 2000).

A remarkable research has been reported on binary polymer blends with a matrix/dispersed or co-continuous phase morphology, nevertheless, understanding the development of complex morphologies in multiphase polymers is still a major challenge in the field of polymer blending. To achieve the desired properties, we need to acquire a good knowledge of structure-property relationships in such systems. Generally, for a multiple phase system two distinct broad category of wetting regimes are possible: complete wetting and partial wetting (de Gennes, Brochard-Wyard, & Quere, 2004; Torza & Mason, 1970). Complete wetting is the most stable thermodynamic state where one phase segregates the two other phases from each other in a ternary system. In contrast, partial wetting is the thermodynamically favorable structure where all phases form a three phase contact and none of the phases completely spreads at the interface of the two others. The majority of studies of ternary immiscible polymer blends deal with complete wetting behavior in which interfacial dynamics can result in a broad range of phase separated structures. It has been shown that through control of composition, interfacial dynamic, and viscoelastic properties of components of a multiphase polymer blend, encapsulated structures can be converted to multiple percolated structures such as the transition of core-shell droplets to tri-continuous structure in a ternary blend (S Ravati & Favis, 2010a, 2010b; Reignier & Favis, 2000a; J. H. Zhang, Ravati, Virgilio, & Favis, 2007). Ravati and Favis (S Ravati & Favis, 2010a) conducted a detailed composition-morphology analysis of binary, ternary, quaternary, and quinary model systems and generated multiple percolated and onion-type structures. The formation of partially wet droplets has just begun to be reported in ternary and quaternary systems (Horiuchi, Matchariyakul, Yase, & Kitano, 1997; Virgilio, Marc-Aurele, & Favis, 2009). Virgilio et al. (Virgilio, Marc-Aurele, et al., 2009) were first to detail the generation of an entirely novel close-packed droplet array of polystyrene (PS) at the interface of high density polyethylene (HDPE) and polypropylene (PP).

However, it is still not clear how the incorporation of partially wet droplets can influence the mechanical properties in a ternary system.

Binary blends of PLA with other polymers are among the most widely studied bioplastic systems (H. Bai et al., 2012; Imre et al., 2013; Z. Liu, Luo, Bai, Zhang, & Fu, 2016a; Ojijo, Ray, & Sadiku, 2013; Stoclet, Seguela, & Lefebvre, 2011; Thurber, Xu, Myers, Lodge, & Macosko, 2015; M. Wu, Wu, Wang, Zhang, & Fu, 2014), however, researchers have shown an increased interest in multicomponent blends with PLA (H. Liu, Chen, Liu, Estep, & Zhang, 2010; K. Zhang, Mohanty, & Misra, 2012). High performance polymeric materials with high levels of toughness, mechanical strength, and thermal resistance can be obtained by combining plastics with complementary properties (Yongjin Li & Shimizu, 2009; H. Liu, Song, Chen, Guo, & Zhang, 2011; Luzinov, Pagnoulle, & Jerome, 2000a). They usually exhibit a more balanced performance compared with binary systems where improvement in one property can lead to a substantial decrease in other properties. However, a wide variety of complex morphologies in the study of ternary and quaternary polymer blends have been reported which must be determined and quantified in the case of bioplastic based multicomponent systems. The formation of a variety of partial and complete wet structures has been reported in ternary blends of bioplastics with some novel tunable morphologies (Sepehr Ravati & Favis, 2013b). To the best of our knowledge, little attention has been paid to the detailed characterization and control of the morphology in multiphase bioplastic blends, despite the clear role of phase morphology in controlling the physical properties (Dou et al., 2015; Luzinov, Xi, Pagnoulle, Huynh-Ba, & Jerome, 1999; Sepehr Ravati, Beaulieu, Zolali, & Favis, 2014). What is still unknown are how the development of morphologies such as multiple encapsulated, multiple percolated as well as partially wet structures contribute to the mechanical properties and particularly the toughness of multiple phase bioplastic blends. In addition, the effect of the level of continuity and interfacial interactions of phases are required to be thoroughly investigated in such heterophase systems.

1.2 Objectives

The main objective of this project is to *control the morphology in ternary and quaternary PLA-based blends to generate ultratough materials*. Thus, the following sub-objectives are envisaged as the main milestones to achieving the main objective of this research:

a) Establish the principal parameters which control partially and completely wet morphological structuring in ternary and quaternary PLA-based blends.

b) Determine the effect of partially wet droplets on the mechanical performance of co-continuous PLA-based systems.

c) Establish the correlation between the tri-continuous structure and mechanical properties of co-continuous PLA-based blends.

d) Develop ultratough materials based on partial and complete wetting in PLA-based blends.

In this work, the structuring of morphology in blends composed of the most relevant bioplastics with PLA are investigated. The effect of composition and interfacial dynamics on the morphology development of the ternary and quaternary systems are studied in detail. A simple melt mixing method, either using internal melt mixing or twin screw extrusion, is used to generate new structures based on two wetting behaviors of partial and complete wetting. The effect of these wetting behaviors on mechanical properties, and in particular notched Izod impact toughness, is examined. Attempts are made to understand the relationship between these structures and the mechanical properties.

CHAPTER 2   LITERATURE REVIEW

2.1   Biobased and Biodegradable plastics

Bioplastics have been used for food, furniture, and clothing for many years. In the 1860s, the first bioplastic namely "Celluloid" was invented and since then many other biobased polymers from renewable resources were developed. However, their development remained at the laboratory stage due to the discovery of crude oil and production of synthetic petroleum-based polymers in the 1930s and 1940s. Nowadays, the environmental concerns and limited fossil fuel resources motivated scientists and industrial sectors to find alternatives to petroleum-based polymers. Bioplastics are newly emerging materials which are expected to completely replace petroleum-based plastics. The term bioplastics or biopolymers refers to a whole family of polymeric materials which are either biodegradable or biobased, or both. Biodegradable means that the product degrades under certain conditions. Two specific standards, EN 13432 and ASTM D-6400, classify the biodegradable or compostable plastics fate. Based on the EN 13432 standard, a plastic must undergo 90% degradation in a lab within 180 days to be called biodegradable while this condition is 60% degradation threshold within 180 days for ASTM D-6400. On the other hand, when a significant portion of carbon in a polymeric product comes from renewable resources, it will be considered as a bioplastic per the ASTM D6866 standard. The most relevant biobased and biodegradable plastics are presented in Figure 2.1.

Bioplastics still present relatively small volume of the global plastic production; however, according to the recently published report by the Utrecht University (L Shen et al., 2009), the worldwide capacity of bioplastics will increase from 360 Kt in 2007 to 2.33 Mt in 2013 and to 3.45 Mt in 2020. Also, based on this report, the most important bioplastics in terms of production volume are starch plastics and PLA with 150 Kt for each product which are expected to increase to 1.3 Mt and 800 Kt by 2020, respectively. Biobased polyethylene with production volume of 600 Kt will be amongst the most influential bioplastics by 2020. However, bioplastics must provide the cost-performance requirements of the commodity polymers to be accepted as an alternative for the petroleum-based polymers. The available materials on the market suffer from some performance weaknesses such as low heat deflection, brittleness, processing window sensitivity, barrier

properties, and final product cost which limits their wider applications. The following section summarizes the most relevant bioplastics.
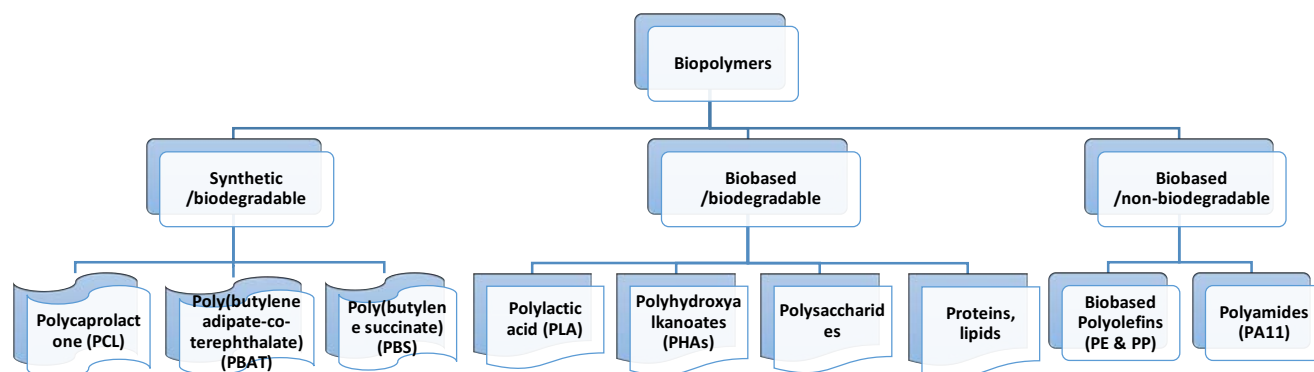
Figure 2.1. Classifications of bioplastics based on the source and biodegradability.

2.1.1 Poly(lactide)

Poly(lactic acid) or polylactide (see Figure 2.2) is one of the most promising biodegradable and compostable aliphatic polyesters derived from renewable sources, such as corn and sugar, which has received marked industrial and scientific attentions in research over the last decades (Auras et al., 2010; Jamshidian, Tehrany, Imran, Jacquot, & Desobry, 2010; Lim, Auras, & Rubino, 2008; Martin & Avérous, 2001). The polycondensation of lactic acid and the ring opening polymerization of lactide, the cyclic diester of lactic acid, are two methods which PLA can be produced by, while the ring opening polymerization is the more commonly used method. Commercial PLA grades are copolymers of poly(L-lactic acid) (PLLA) and poly(D,L-lactic acid) (PDLLA), in which the ratio of L- to D,L-enantiomers affects the properties of PLA, however, the mechanical properties are not significantly influenced by the synthesis method (Ajioka, Enomoto, Suzuki, & Yamaguchi, 1995; Sodergard & Stolt, 2002). Generally, PLA is a rigid, semi-crystalline polymer with tensile strength in the range of 50-70 MPa and elastic modulus of 3000-4000 MPa, and elongation at break of 2-5% (Perego & Cella, 2010). Mechanical properties of PLA including tensile strength, tensile modulus, and crystallinity are affected by the molecular weight, structure, and crystallinity of PLA (Engelberg & Kohn, 1991). Applications of PLA due to its good appearance, high mechanical strength, and relatively good barrier properties are broadened especially in the packaging industry (Jamshidian et al., 2010; Lim et al., 2008). Several companies such as Natureworks LLC, Mitsui

Chemicals produce PLA which Ingeo the brand of PLA produced from corn and other feedstock by Natureworks LLC is commercially available in the market.
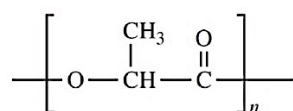
Figure 2.2. The molecular structure of PLA.

Although PLA has many advantages such as excellent biocompatibility, eco-friendly properties, better thermal processing as well as less energy dependence compared to petroleum-based plastics that distinguish this bioplastic from the other available biopolymers, it has some drawbacks which limit its broader applications. The main weaknesses of PLA are poor toughness and low heat deflection temperature (Auras et al., 2010; Rasal et al., 2010).

2.1.2 Poly(butylene adipate-co-terephthalate)

Poly(butylene adipate-co-terephthalate) (PBAT) is an aliphatic-aromatic copolyester which has been commercialized by BASF and Eastman under the trademarks of Ecoflex and Easter Bio, respectively. The molecular structure of PBAT consists of butylene terephthalate (BT) and butylene adipate (BA) segments as shown in Figure 2.3. PBAT is a flexible and ductile biodegradable polymer which degrades within a few weeks with the aid of naturally occurring enzymes (Gu, Zhang, Ren, & Zhan, 2008). Witt et al. (Witt et al., 2001) assessed the risk of introduction of PBAT into composting process and found that there is no indication for an environmental risk as well as no significant toxicological effect after degradation. Considering its high toughness and biodegradability, PBAT is a good candidate for toughening of biobased plastics such as PLA, PHAs, etc. while retaining the biodegradability of the final materials. Ecovio® is the commercial trademark of the blend of PLA/PBAT which is currently produced by BASF and shows the importance of PBAT in commercial applications.
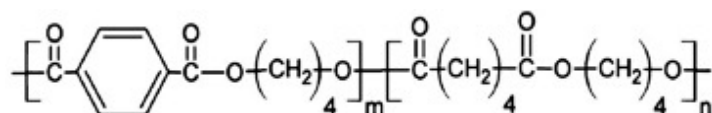
Figure 2.3. The molecular structure of PBAT.

2.1.3 Poly(butylene succinate)

Poly(butylene succinate) (PBS) (Figure 2.4), is a biodegradable polymer with possibility to be produced both from renewable and non-renewable resources. Its building monomers, i.e. 1, 4-butanediol and succinic acid, can be derived from renewable feedstocks (Florence & Mechael, 2015; Ichikawa & Mizukoshi, 2012; Momoko Ishii, Masaki Okazaki, Yuji Shibasaki, Ueda*, & Teranishi, 2001; Shirahama, Kawaguchi, Aludin, & Yasuda, 2001). PBS is a semi-crystalline thermoplastic polyester which exhibits balanced performance in thermal and mechanical properties, i.e. high heat deflection temperature and toughness, and has been extensively studied for potential applications as a feasible green polymer.
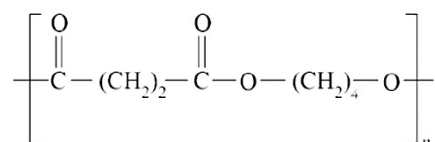
Figure 2.4. The molecular structure of PBS.

2.1.4 Poly(3-hydroxybutyrate-co-hydroxyvalerate)

Poly(3-hydroxybutyrate-co-hydroxyvalerate) (PHBV) is among one of the biggest group of biopolyesters, i.e. polyhydroxyalkanoates (PHA), which are directly produced by bacterial fermentation of sugars or lipids. It is also completely biosynthetic and biodegradable with zero toxic waste and recyclable into organic waste (Braunegg, Lefebvre, & Genser, 1998; Corre, Bruzaud, Audic, & Grohens, 2012). PHBV shows excellent thermal resistance and biodegradability that provide many potential applications in packaging and biomedical. Its chemical structure is shown in Figure 2.5.
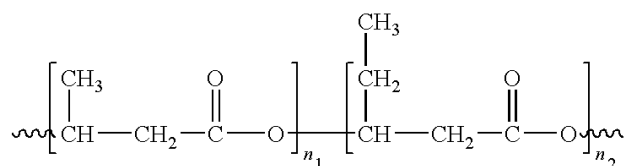
Figure 2.5. The molecular structure of PHBV.

2.1.5 Polyamide 11

Polyamide (PA) polymers, which can be derived from biobased resources such as castor oil(Rulkens & Koning, 2012), are engineering plastics with high thermal stability impact and chemical resistance as well as excellent dimensional stability. The main application of PA11 is in automotive and flexible pipe applications for offshore oilfield exploration. The typical water absorption characteristics of PA11 is significantly reduced because of the high hydrocarbon proportion of the repeat unit in comparison with those of PA6 and polyamide 66. The molecular structure of PA11 is presented in Figure 2.6.
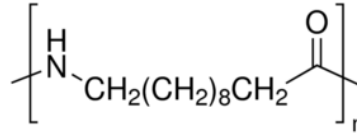
Figure 2.6. The molecular structure of PA11.

2.2   Polymer Blends

2.2.1 Miscibility

The miscibility of binary polymer mixtures can be assessed by the Gibbs free energy of mixing:

$$\Delta G_m = RT\chi_{AB}\varphi_A\varphi_B + RT\left[\frac{\rho_A\varphi_A\ln\varphi_A}{M_{w_A}} + \frac{\rho_B\varphi_B\ln\varphi_B}{M_{w_B}}\right] \qquad (2.1)$$

where ΔG_m is Gibbs free energy of mixing, χ_{AB} is the Flory-Huggins interaction parameter, φ_i is the volume fraction of the polymer components, ρ_i is the density of polymers, M_{w_i} is the molecular weight of the polymers, and R and T are gas constant and absolute temperature, respectively. This equation shows that Gibbs free energy includes the enthalpy and the entropy of mixing, the first and the second terms on the right side of the equation. Three classes of polymer blends are defined: a) miscible polymer blends which show $\Delta G_m < 0$ and $\partial^2\Delta G/\partial\varphi^2 > 0$ over the entire composition range; b) partial miscible polymer blends which only demonstrate miscibility in some compositions; and c) immiscible polymer blends which always possess $\Delta G_m > 0$ and $\partial^2\Delta G/\partial\varphi^2 < 0$. Most polymer mixtures are categorized as immiscible systems since the entropy

of mixing is negligible due to high molecular weights and a low degree of freedom of polymers. In addition, the mixing of polymers is usually endothermic which results in a positive Gibbs energy of mixing. The morphology of immiscible phases in an immiscible polymer blend significantly influence the final properties and can be manipulated towards achieving desired set of properties. Figure 2.7 shows the main possible phase morphologies in binary polymer blends and their potential applications. It will be shown later that interfacial tension between components is dominant factor controlling the final morphology in immiscible polymer blends.
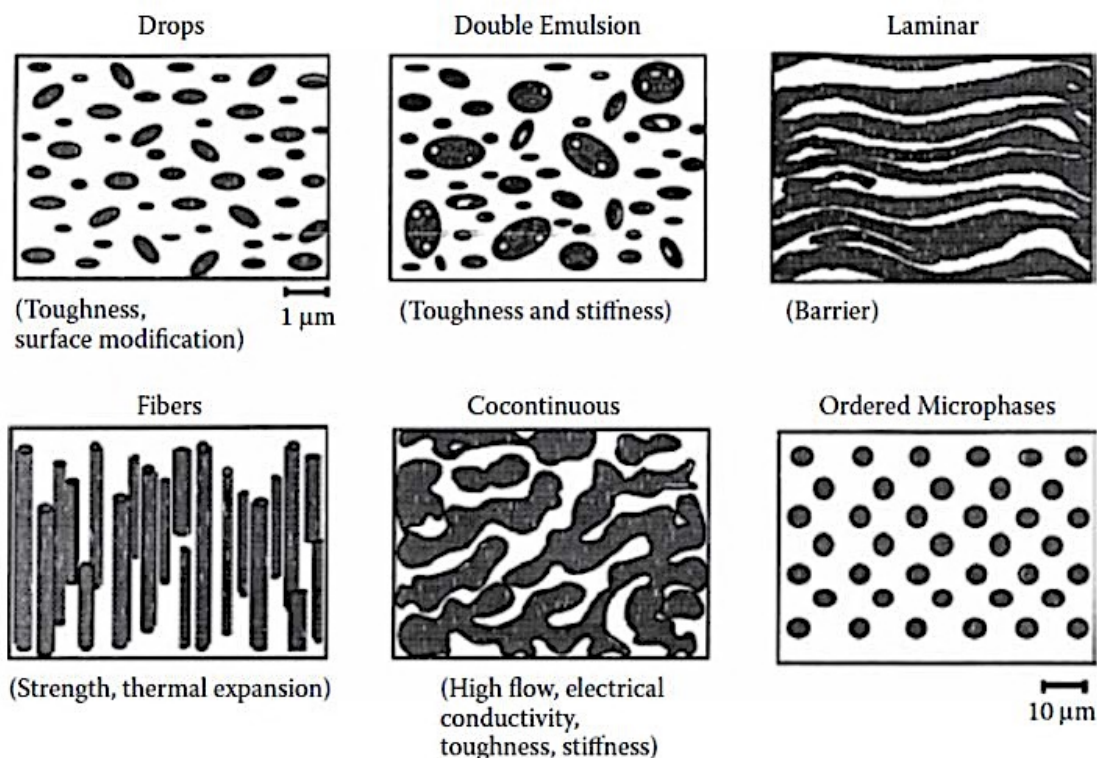
Figure 2.7. Morphologies of immiscible polymer blends with their potential applications (Macosko, 2000).

2.2.2 Interfacial Tension

The interfacial tension between the components of a blend is one of the most important parameters significantly influences the morphology and performance of the polymer blend. The interfacial tension is defined as the reversible work required to create an interfacial area by the unit of area between two immiscible phases (S Wu, 1982). Interfacial tension originates from the imbalanced molecular forces at the interface as compared to the bulk and has the same unit as the surface

tension (N/m or J/m^2). Experimental techniques used to determine interfacial tension can be divided into two categories: static (pendant drop, sessile drop and spinning drop) and dynamic (breaking thread, imbedded fiber retraction and deformed drop retraction) methods as well as estimation from surface tension and rheological techniques (Demarquette, 2003; Xing, Bousmina, Rodrigue, & Kamal, 2000). Some of the main techniques that are used to determine the interfacial tension between two polymers are briefly reviewed below.

2.2.2.1 Estimation from surface tension

One of the widely used methods to determine interfacial tension between polymers is to estimate it from the surface energy data of pure components. Harmonic and geometric mean equations have been proposed by Wu (Souheng Wu, 1971, 1974) for systems with low and high surface energies, respectively:

$$\gamma_{12} = \gamma_1 + \gamma_2 - 4\left(\frac{\gamma_1^d \gamma_2^d}{\gamma_1^d + \gamma_2^d} + \frac{\gamma_1^p \gamma_2^p}{\gamma_1^p + \gamma_2^p}\right) \quad \textit{Harmonic mean equation}$$

(2.2)

$$\gamma_{12} = \gamma_1 + \gamma_2 - 2\left(\sqrt{\gamma_1^d \gamma_2^d} + \sqrt{\gamma_1^p \gamma_2^p}\right) \quad \textit{Geometric mean equation}$$

(2.3)

where γ_{ij} is the interfacial tension, γ_i^d and γ_i^p are the dispersive (or nonpolar) and polar components of the surface tension, respectively.

2.2.2.2 Breaking Thread Method

In this technique, a thread of a given polymer sandwiched between two films of another polymer is heated at a desired temperature until it breaks up into several small droplets. When heated above the melting temperature of both polymers, distortions forms at the surface of the thread due to pressure differences between the inside and outside of the thread. Interfacial tension and a tendency to minimize the interfacial area intensify these distortions when the wavelength of distortions becomes greater than the initial thread circumference. Elemans et al. (Elemans, Janssen, & Meijer, 1990) showed that the amplitude of the sinusoidal distortions can be described by Tomotika's theory (Tomotika, 1935):

$$\alpha = \alpha_0 e^{qt} \tag{2.4}$$

where α_0 is the initial amplitude of distortions and q is the growth rate and is defined as:

$$q = \frac{\gamma_{12} \Omega(x, p)}{\eta_0 D_0} \tag{2.5}$$

in which γ_{12} is the interfacial tension between two liquids, η_0 is the zero shear viscosity of the matrix, D_0 is the initial thread diameter, and $\Omega(x, p)$ is a function tabulated by Tomotika and is a function of the viscosity ratio p between the thread and matrix. Figure 2.8 shows a typical breakup process of a PA6 thread in a matrix of PS at 230 °C.
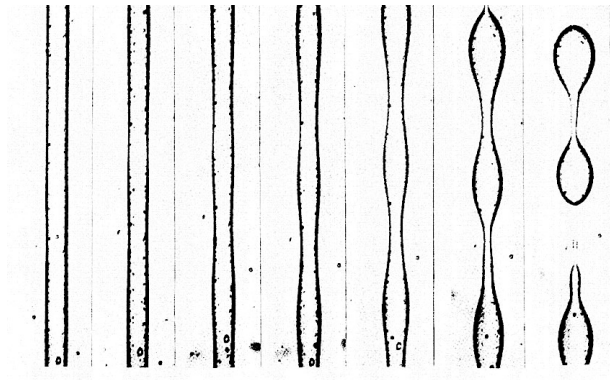
Figure 2.8. Distortions of PA6 thread in PS matrix at 230 °C as a function of time from left to right (Xing et al., 2000).

2.2.2.3 Imbedded Fiber Retraction Method

This technique is similar to the breaking thread method but with a shorter thread to prevent the thread breakup process. Thus, the initial length/diameter ratio of the fiber should be less than 12 (Demarquette, 2003; Xing et al., 2000). Figure 2.9 shows the evolution of a short thread during a retraction experiment. The short fiber relaxes back to a sphere which this process is function of the interfacial tension and viscosity ratio between fiber and matrix. The theory for this technique was first proposed by Carriere and Cohen (Carriere, Cohen, & Arends, 1989; Cohen & Carriere, 1989).

They showed that the evolution of the radius of the imbedded fiber can be described by the following equation:

$$f\left(\frac{R(t)}{R_d}\right) - f\left(\frac{R(0)}{R_d}\right) = t\frac{\gamma}{R_d\eta_e} \tag{2.6}$$

where $R(t)$ is the radius at time t, $R(0)$ is the initial radius, R_d is the radius of the final spherical droplet, t is time, γ is the interfacial tension, and η_e is the effective viscosity which is given by:

$$\eta_e = \frac{\eta_m + 1.7\eta_d}{2.7} \tag{2.7}$$

in which η_m and η_d are the zero shear viscosities of the matrix and fiber, respectively. The function used in Equation 2.7 is defined as:

$$f(x) = \frac{3}{2}\ln\left(\frac{\sqrt{1 + x + x^2}}{1 - x}\right) + \frac{3^{1.5}}{2}\arctan\left(\sqrt{3}\frac{x}{2 + x}\right) - \frac{x}{2} - \frac{4}{x^2} \tag{2.8}$$

where x is $R(t)/R_d$. It has been shown that the plot of $f(R(t)/R_d) - f(R(0)/R_d)$ vs time is linear (Demarquette, 2003; Xing et al., 2000). Thus, one can calculate the interfacial tension from the slop of a linear fit to the data with the knowledge of the effective viscosity and final droplet radius.
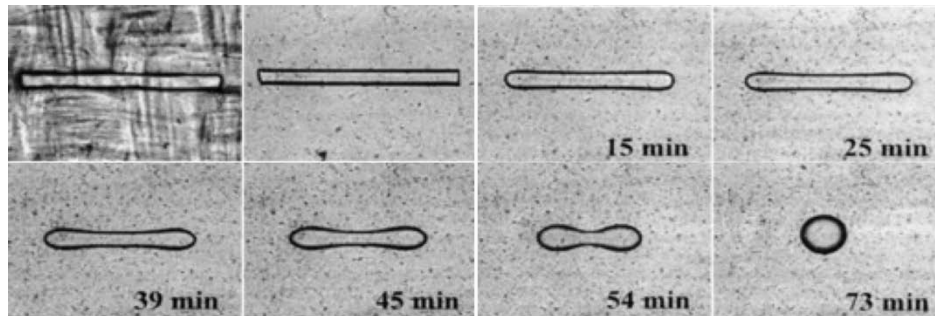
Figure 2.9. Typical evolution of short fiber (ethylene vinyl alcohol copolymer in low density polyethylene at 200 °C) (Demarquette, 2003).

2.2.2.4 Rheological Method

Palierne (Graebling, Muller, & Palierne, 1993) developed a model that relates the rheological properties of a binary emulsion to the rheological properties of its constituent components. Several studies have successfully utilized this model and shown that the interfacial tension between two polymers can be determined using the rheological properties of the binary polymer blend with the knowledge of its phase morphology (Bousmina, 1999; Lacroix, Bousmina, Carreau, Favis, & Michel, 1996; Shi, Hu, Ke, Li, & Yin, 2006). The model describes the modulus of a binary immiscible mixture in terms of the moduli of the individual phases and the ratio of interfacial tension to the size of the dispersed phase (γ/R) as described in the following equations:

$$G_b^*(\omega) = G_m^*(\omega) \frac{1 + 3\sum_i \phi_i H_i(\omega)}{1 - 2\sum_i \phi_i H_i(\omega)} \tag{2.9}$$

where $G_b^*(\omega)$ and $G_m^*(\omega)$ are complex moduli of the blend and the matrix, respectively, ϕ_i is the volume fraction of the dispersed phase and $H_i(\omega)$ is defined as:

$$
\begin{aligned}
&H_i(\omega) \\
&= \frac{4(\gamma/R)[2G_m^*(\omega) + 5G_d^*(\omega)] + [G_d^*(\omega) - G_m^*(\omega)][16G_m^*(\omega) + 19G_d^*(\omega)]}{40(\gamma/R)[G_m^*(\omega) + G_d^*(\omega)] + [2G_d^*(\omega) + 3G_m^*(\omega)][16G_m^*(\omega) + 19G_d^*(\omega)]}
\end{aligned}
\tag{2.10}
$$

in which $G_d^*(\omega)$ is the modulus of the dispersed phase. The value of (γ/R) can be determined from fitting Palierne model on the experimental data and, thus, one can calculate the interfacial tension by knowing the average radius of the dispersed phase.

2.3 Binary Polymer Blends

Two possible major categories of morphologies for a binary blend of polymers A and B are: dispersed phase/matrix or co-continuous morphologies. At low concentration of one phase, say phase B, the dispersed droplets of phase B are distributed in the matrix of phase A. The influence of composition, viscosity ratio, and processing condition on the droplet/matrix morphology have been extensively studied (Favis, 1990, 1991; Favis & Chalifoux, 1988; Favis & Willis, 1990). The co-continuous morphology has also received considerable interests over the last two decades

(Hedegaard, Gu, & Macosko, 2015; Huang, Bai, Trifkovic, Cheng, & Macosko, 2016; J. Li & Favis, 2001; Mekhilef, Favis, & Carreau, 1997). By increasing the dispersed phase content (phase B) in the blend, coalescence of the phase B droplets results in reaching a percolation threshold point. Further increasing the minor phase concentration above the percolation threshold point, various levels of continuity form until a fully-interconnected co-continuous morphology is achieved. In other words, co-continuity is a state that each polymer phase is fully interconnected through a continuous pathway. It was believed that the point of phase inversion and co-continuity occur at the same point, however, it was recently shown that co-continuity can be obtained in a domain of composition rather than at a single point (J. Li & Favis, 2001; Omonov, Harrats, Groeninckx, & Moldenaers, 2007; Willemse, Ramaker, Van Dam, & De Boer, 1999; Willemse, Speijer, Langeraar, & de Boer, 1999).

Morphology development of immiscible polymers under various melt-mixing conditions involves different processes such as droplet breakup, stretching of liquid droplets into threads, breakup of threads into smaller droplets, and coalescence of the droplets into larger droplets (Favis, 2000). The final morphology is a balance between these competing processes, thus a detail knowledge of blending condition and deformation-disintegration phenomena and coalescence is essential in order to obtain polymer blends with desired morphology. In the following sections, processes involved in the development of different morphologies in binary polymer blends are reviewed.

2.3.1 Droplet Deformation and Breakup

Most of the theories in the literature describe the deformation of a Newtonian droplet in another Newtonian liquid subjected to shear or elongational flow fields, in which it deforms and then breaks into smaller droplets. Taylor (Taylor, 1932, 1934) carried out the pioneering work on deformation and breakup of a single Newtonian liquid droplet suspended in another Newtonian liquid in a well-defined deformation field. He estimated the possible maximum droplet diameter by balancing the maximum difference in pressure between the inside and outside of droplet and proposed two dimensionless parameters: capillary number Ca and the blend viscosity ratio p. Capillary number is the ratio of the deforming stress τ (viscous force) exerted on the droplet by the flow field to the restoring interfacial stress σ/R, where σ is the interfacial tension and R is the radius of the droplet. In steady uniform shearing flow, shear stress is $\tau = \eta_m \dot{\gamma}$ where η_m is the viscosity of the matrix and $\dot{\gamma}$ is the shear rate. The capillary number and the blend viscosity ratio are defined as:

$$Ca = {\eta_m \dot{\gamma} R}/{\gamma} \tag{2.11}$$

and

$$p = \eta_d / \eta_m \tag{2.12}$$

where η_d and η_m are the viscosity of dispersed and matrix phases, respectively. A critical capillary value, Ca_{crit}, is defined in which below that the interfacial forces dominate and a steady drop shape develops. For capillary numbers larger than the critical capillary number, the drop becomes unstable and breaks into smaller droplets.
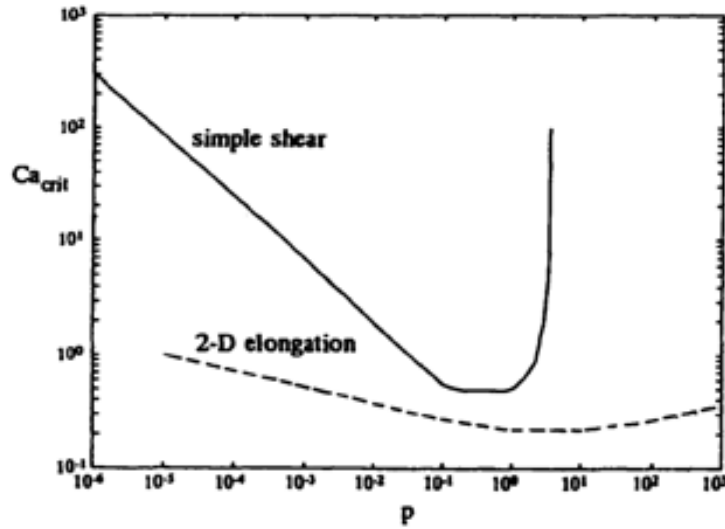
Figure 2.10. Critical capillary number vs. the viscosity ratio in simple shear and elongational flow fields (Grace, 1982).

A U-type dependence of droplet breakup on the viscosity ratio was reported for Newtonian mixtures under shear flow which indicates that there are upper and lower limits of the viscosity ratio beyond which no droplet breakup can occur (Favis, 2000). Karam and Bellinger (Karam & Bellinger, 1968) observed droplet breakup when $0.005 \leq p < 3.0$. Several studies have examined the breakup of Newtonian systems under shear flow field and reported comparable results (Grace, 1982; Rumscheidt & Mason, 1961; Serpe, Jarrin, & Dawans, 1990). Different modes of deformational and burst were observed for a Newtonian droplet in elongational flow. Rumscheidt (Rumscheidt & Mason, 1961) reported two basic mechanisms for dispersing one liquid in another:

steady drop breakup and disintegration of a deformed thread. They found that for a certain range of viscosity ratio, the drop extended into a fine thread, which then disintegrated into small droplets due to the instabilities, known as capillary instabilities (Rayleigh, 1878; Tomotika, 1935), in the thread. Grace (Grace, 1982) compared the breakup of Newtonian drops in both simple shear and extensional flow fields and showed that breakup is possible in pure extensional flow for all viscosity ratios, but is limited to a range where above $p = 4.0$ the breakup becomes impossible (Figure 2.10).

However, these models were developed for Newtonian fluids and cannot be applied to polymer blend systems which are composed of non-Newtonian fluids. Few studies have investigated the deformation and breakup of immiscible polymer blends in common polymer processing operations which is a mixed shear and elongational flow field. Bentley and Leal (Bentley & Leal, 1986) and Han and Funatsu (Dae Han & Funatsu, 1978) conducted studies on the droplet deformation in these transient flows, but little quantitative information was generated to describe the effect of viscoelasticity and viscosity ratio on the droplet deformation. The influence of viscosity ratio on the phase morphology of polymeric systems (non-Newtonian liquids) has been investigated by several researchers. Wu (Souheng Wu, 1987) proposed the following empirical relation between the final droplet diameter d and the interfacial tension σ, shear rate $\dot{\gamma}$ and the viscosity ratio p in a twin-screw extrusion process of polymer blends:

$$d = {4\gamma p^{\pm 0.84}}\Big/{\dot{\gamma}\eta_m} \tag{2.13}$$

where the positive sign in the exponent applies to $p > 1$ and the negative sign applies to $p < 1$. However, this relation does not explain the breakup of a single drop nor the limits estimated from Taylor's theory. In addition, the shear rate used in the equation is approximated as an effective shear rate, which is difficult to be evaluated as it is the result of a complex deformation fields including shear, elongational flows. Mighri et al. (Mighri, Carreau, & Ajji, 1998) showed that the elasticity of blend components plays a very important role in determining the critical capillary number.

2.3.2 Coalescence

The process of collision and possible coalescence for two droplets in a flow field in much more difficult to study. Several studies have examined the flow induced coalescence in binary Newtonian

liquid mixtures (Bai Chin & Han, 1979; Coulaloglou & Tavlarides, 1977; Jeelani & Hartland, 1991). When two droplets collide and come to a close contact, a thin film is formed between them which upon its rupture the droplets coalesce. Therefore, a three-step process was proposed for the flow induced coalescence of two droplets as shown in Figure 2.11: collision of two droplets, drainage of the trapped film between two droplets and rupture of the film (Roland & Böuhm, 1984). Many recent studies have proposed theories to describe the flow induced collisions of droplets with neglected interdroplet interactions followed by fusion of the droplets (Elmendorp & Van Der Vegt, 1986; Meijer, Janssen, & Anderson, 2009). The coalescence rate is determined by the product of the collision frequency and the coalescence efficiency. Two measureable quantities, the drainage and collision times, are evaluated in studying the flow induced coalescence. The collision process has been modeled for spheres with the same size in simple shear flow and the collision frequency of a drop is given by (Chesters, 1991):

$$C = \frac{8}{\pi} \dot{\gamma} \varphi \tag{2.14}$$

where φ is the concentration of dispersed phase and $\dot{\gamma}$ is shear rate. It has been shown that the required collision time is much shorter than the available mixing time in a conventional mixing process. As two droplets approach each other, hydrodynamic interactions between the droplets become important. Chesters (Chesters, 1991) described the process of coalescence and summarized results of theories describing drainage of the matrix film between spherical and highly flattened droplets. The process of film drainage has been theoretically shown to be governed by three different interfacial mobility between the droplet and the matrix: immobile, partially mobile and fully mobile interfaces (Chesters, 1991). Assuming that the drainage of the thin film between two droplets is a viscous flow and a constant contact force F acts along the interface, the drainage time for the coalescence to occur was determined for different conditions:

a) immobile interface,

$$t_d \sim \frac{3\eta_m R^2 F}{16\pi\gamma^2} \left(\frac{1}{h_{crit}^2} - \frac{1}{h_0^2} \right) \tag{2.15}$$

b) partially mobile interface,

$$t_d \sim \frac{\pi \eta_d F^{1/2}}{2(2\pi \gamma/R)^{3/2}} \left(\frac{1}{h_{crit}} - \frac{1}{h_0} \right) \tag{2.16}$$

c) and fully mobile interface

$$t_d \sim \frac{3\eta_m}{2\gamma} \left(\frac{h_0}{h_{crit}} \right) \tag{2.17}$$

where, h_0 and h_{crit} are respectively, the distance between two droplets and the critical distance that rupture occurs, and F is the Stokes drag force acting on the droplets. h_0 and h_{crit} can be estimated using models developed for each condition. For example, h_{crit} is estimated to be about 5 nm for droplets with radius 1 µm (Chesters, 1991). All three models predict longer drainage time for larger droplets, which is mainly due to the smaller pressure peak at the center of the trapped film at larger drop radii. This means that small droplets coalesce until a certain drop size beyond which no coalescence occurs under given conditions. Lower interfacial tension seems to result in longer drainage times and stabilize droplets. Although longer drainage times is expected for polymers due to a relatively immobile interface, it was found that polymers have a high coalescence probability during mixing suggesting a mobile interface (Elmendorp & Van Der Vegt, 1986). It has been shown that at concentrations as low as 0.5 to 1 wt% of the dispersed phase, flow induced coalescence can occur in polymeric systems (Elmendorp & Van Der Vegt, 1986; Sundararaj & Macosko, 1995).
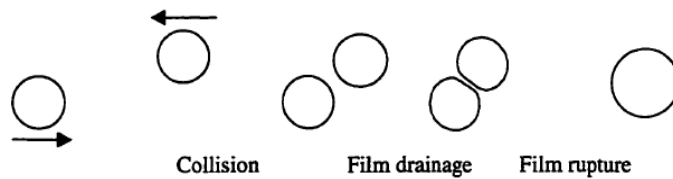
Figure 2.11. Coalescence model.

Generally, dynamic equilibrium between the breakup and coalescence of monodispersed droplets can be described by the equation 2.18 (Fortelný, 2001, 2006):

$$F(R) = \frac{4}{\pi} \dot{\gamma} \varphi P_c(R)$$

<div align="right">(2.18)</div>

where $F(R)$ is breakup frequency, and $P_c(R)$ is probability of the droplet collision. It has been shown that P_c is independent of R for droplets smaller than a critical droplets size (Fortelný & Jůza, 2012; Fortelný & Jůza, 2013; Rother & Davis, 2001). Al-Mulla and Gupta (Al-Mulla & Gupta, 2000) studied dependence of P_c on droplet radius and found an order of magnitude of R to agree with theory where experimentally determined and theoretical dependences of R on shear rate differed strongly. Recent studies have examined the matrix drainage theory and have shown reasonable agreement between the theory and experimental results in polymeric systems (Filippone, Netti, & Acierno, 2007; Gabriele, Pasquino, & Grizzuti, 2011; Hsu, Roy, & Leal, 2008).

2.3.3 Continuity and Co-Continuity Development

Coalescence plays an important role in the morphology development of polymer blends. In a binary polymer blend, increasing the concentration of a minor dispersed phase results in a large number of coalescence between the droplets of the minor component. By further increasing the concentration of the dispersed phase, a continuous phase morphology forms (Figure 2.12a). The transition from a dispersed morphology to a continuous morphology can be explained by percolation theory. Percolation theory defines the value of percolation threshold at which an infinite connectivity of randomly distributed sites first occurs in a system. It is basically a mathematical term defined to explain the formation of long-range connectivity in random systems in which the probability of formation of an infinite network is either zero below that value or 1 above that value (Stauffer & Amnon, 1994). Percolation threshold has been calculated to be at a volume fraction of 0.156 for a random distribution of mono-dispersed spheres (Scher & Zallen, 1970). Dynamic equilibrium between breakup and coalescence changes in favor of coalescence as concentration increases. Above the percolation threshold, different levels of continuity are possible until a fully-interconnected morphology is obtained upon a further increase of minor phase concentration (Figure 2.12c). Continuity development is described using two mechanisms: droplet-droplet coalescence and thread-thread coalescence (J. M. Li, Ma, & Favis, 2002; Pötschke & Paul, 2003).
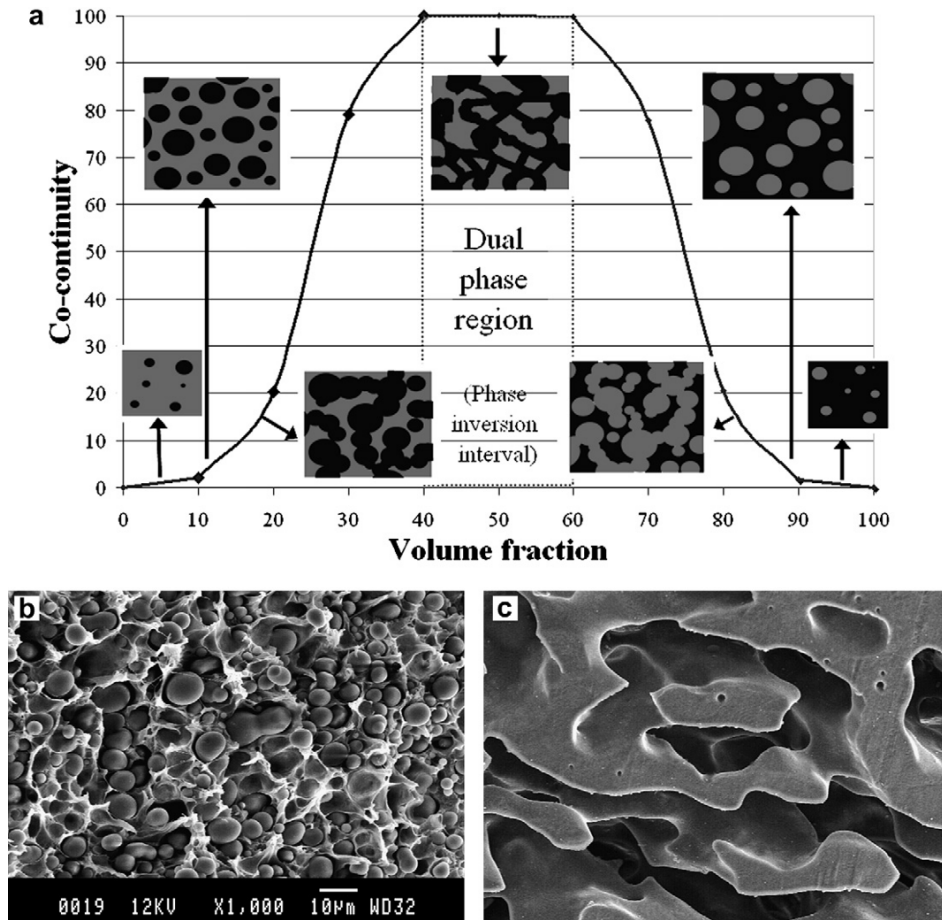
Figure 2.12. (a) A schematic representing a typical evolution of morphology in a binary blend, (b) and (c) typical matrix/dispersed and co-continuous morphologies, respectively (S Ravati & Favis, 2010b).

Several predictive models have been proposed to understand all parameters involved in the development of co-continuous structures. Several studies have investigated the effect of viscosity and composition on the formation of dual phase continuity. Paul and Barlow (Paul & Barlow, 1980) suggested a model based on the viscosity ratio of the components at low shear rates for phase inversion. Per their model, phase inversion occurs at a composition obtained from the following equation:

$$\frac{\varphi_1}{\varphi_2} = \frac{\eta_1}{\eta_2} \tag{2.19}$$

where φ_i and η_i are volume fraction and zero-shear viscosity of each component, respectively. This equation has been examined by several researchers (Miles & Zurek, 1988), while some

discrepancies have been reported for systems that exhibit viscoelastic asymmetry between the melt components (Favis & Chalifoux, 1988). Miles and Zurek (Miles & Zurek, 1988) corrected the equation by substituting the viscosity with effective viscosity ratio instead of zero-shear viscosity. A number of theoretical models have been proposed which each of them demonstrated some limitations in describing the experimental results (Luciani & Jarrin, 1996; Lyngaae-Jørgensen & Utracki, 1991).

A semi-empirical model was developed by Willemse et al. (Willemse, de Boer, van Dam, & Gotsis, 1998) which is based on geometrical requirements for the formation of co-continuous structures:

$$\frac{1}{\varphi_d} = 1.38 + 0.0213 \left(\frac{\eta_m \dot{\gamma}}{\sigma} R_0 \right)^{4.2} \tag{2.20}$$

where φ_d is the volume fraction of the dispersed phase, η_m is the viscosity of the matrix, $\dot{\gamma}$ is the shear rate, σ is the interfacial tension, and R_0 is the radius of the thread. This equation determines the composition rage of co-continuity by providing the lower and upper limits of continuity for the components. It should be noted that this model is not a predictive one because the thread radius must be determined experimentally first. Another predictive semi-empirical model assuming the phase inversion occurs at maximum shape relaxation times of domains of components developed by Steinmann et al. (Steinmann, Gronski, & Friedrich, 2002) as follows:

$$\varphi_1 = \frac{1}{\left(\dfrac{\eta_1}{\eta_2} \right)^{1/z} + 1} \tag{2.21}$$

where z is a dependent parameter on the blend system and should be first evaluated for each system.

Bourry and Favis (Bourry & Favis, 1998) introduced elasticity as an important parameter in the understanding of phase inversion. They proposed two criteria, first based on the elasticity ratio of blend components and the other based on the ratio of the loss moduli with:

$$\frac{\varphi_1}{\varphi_2} = \frac{G_2'(\omega)}{G_1'(\omega)} \qquad (2.22)$$

$$\frac{\varphi_1}{\varphi_2} = \frac{\tan \delta_1(\omega)}{\tan \delta_2(\omega)} \qquad (2.23)$$

where $\tan \delta = G_i''/G_i'$ and G_i' and G_i'' are storage and loss moduli of component i (i=1,2), respectively. They compare the predicted value from their equation with the values obtained from the viscosity ratio models and found that their model is in accordance with observed experimental results for the PS/HDPE blend system.

2.3.4 Effect of Interfacial Tension

It is known that interfacial tension has a remarkable effect on the morphology of polymer blends. Domain size is strongly dependent on interfacial tension, i.e., generally, reduction of interfacial tension results in decrease in the dispersed phase size. Wu (Souheng Wu, 1987) studied the effect of interfacial tension on the formation of dispersed phase in the blend of incompatible polyamide/rubber. He found that the particle size was directly proportional to the interfacial tension. Favis and Willis (Favis & Willis, 1990) indicated that the presence of good adhesion at the interface can reduce the coalescence effect with increasing the composition of minor phase which was confirmed by other studies (Elmendorp & Van Der Vegt, 1986; Willis, Favis, & Lunt, 1990). Willemse et al. (Willemse, de Boer, van Dam, & Gotsis, 1999) investigated the effect of interfacial tension on the morphology of binary blends of polyethylene (PE)/PS, PP/PE, and PE/polyamide 6 (PA6). They found that the co-continuity limits are dependent on the interfacial tension where increasing the interfacial tension narrows the dual-phase continuity interval.

Li et al. (J. M. Li et al., 2002) examined the role of the blend interface type on the morphology development in a co-continuous blend. They summarized three types of morphology developments based on droplet and thread lifetimes during a melt mixing process. For a system comprised of immiscible but compatible components demonstrating a low interfacial tension (Type I), continuity development is dominated by a thread-thread coalescence mechanism; whereas, the dominant mechanism in immiscible incompatible blend with a high interfacial tension (Type II), is droplet-droplet coalescence. An immiscible and incompatible system that is compatibilized with a third

component (Type III), develops co-continuity through reduced droplet-droplet coalescence. Thread lifetime for Type I is proposed to be longer than droplet lifetime, while the droplet lifetime is longer than thread lifetime for Type II and III. Figure 2.13 shows the morphology of the three different types of a blend interface and is a direct evidence of thread/droplet lifetime mechanism.
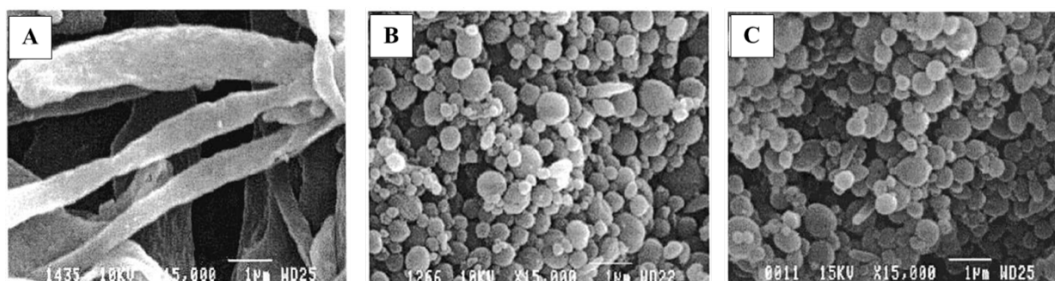
Figure 2.13. SEM photomicrographs of the dispersed HDPE phase after the matrix dissolution technique: (A) 5HDPE/95SEBS (Type I); (B) 5HDPE/95PS (Type II); (C) 5 HDPE/90 PS/20 SEBS (Type III) (J. M. Li et al., 2002).

2.3.5 Coarsening of Co-Continuous Morphology

It has been observed that the phase size of blends with co-continuous morphology significantly coarsens under quiescent annealing conditions (Favis, 1990; Lee & Han, 1999; Mekhilef et al., 1997; Veenstra, Van Dam, & de Boer, 2000; Veenstra, van Lent, van Dam, & de Boer, 1999; Willemse, Ramaker, et al., 1999). The energy stored at the interface due to a highly curved interface in co-continuous systems, which leads to a thermodynamically unstable system, is the driving force for the growth of the phase size. McMaster (McMASTER LEE P, 1975) provided a model for interpreting the early stages of coarsening. He observed a linear growth with time for spinodally decomposed blends of styrene-acrylonitrile copolymer and polymethyl methacrylate. He considered a collection of interconnected threads for the fluid structure surrounded by a second fluid. He assumed that the rate of coarsening is determined by growing capillary instabilities along the interface and used Tomotika's model (Tomotika, 1935) for the breakup of cylindrical threads under the action of the interfacial tension and viscous forces to explain the breakup of the interconnected domains. Assuming an exponential growth with time for the sinusoidal disturbances occurring on the thread interface, the dominant instability as a function of time is:

$$\alpha = \alpha_0 e^{qt} \tag{2.24}$$

where α_0 is the initial amplitude and the growth rate of the dominant disturbance is given by:

$$q = \frac{\gamma\Omega}{2R\eta_m} \tag{2.25}$$

where γ is the interfacial tension, Ω is Tomotika's function, R is the thread radius, and η_m is the matrix viscosity. Thus, the initial growth rate of the disturbances is:

$$\frac{d\alpha}{dt}\bigg|_{t=0} = \frac{\alpha_0 \Omega}{2R} \frac{\gamma}{\eta_m} \tag{2.26}$$

Assuming the rate of coarsening is controlled by the breakup of the elongated domains, McMaster equated the rate of coarsening with the growth rate of these small amplitude interfacial instabilities which leads to a dimensionless coarsening rate k for the early stages of coarsening:

$$k = \alpha_0 \Omega / 2R \tag{2.27}$$

It should be noted that several concerns have been raised with this model (Hedegaard et al., 2015; López-Barrón & Macosko, 2010). The dominant wavelength of a capillary disturbance should be at least more than 5 times an equivalent filament diameter which significantly exceeds the size of a domain in interconnected structures. In addition, local curvature of the fluid structure is predominantly hyperbolic, particularly in low interfacial tension systems, as opposed to the parabolic curvature of a filament-like structure. The model also requires a protocol to decide which of the two co-continuous phases to treat as the internal and external phases. The model is also unable to describe the impact of final film drainage and domain retraction which has been observed by Saito et al. (Saito, Yoshinaga, Mihara, Nishi, & Jinnai, 2009) for a phase separated system. Veenstra et al. (Veenstra, Van Dam, et al., 2000) also reported a linear growth with time for different immiscible blends with co-continuous structures. They suggested a coarsening process based on an interfacial driven breakup and retraction of polymer fibers opposed by viscous forces in a polymer matrix. Therefore, the coarsening rates follow McMaster's model and are proportional

to the ratio between interfacial tension and matrix viscosity. Yuan and Favis (Yuan & Favis, 2005) experimentally measured coarsening rates over broad viscosity and viscosity ratio ranges for two melt mixed polymer systems having a co-continuous structures and found a good agreement between the experimental results and Equation 2.27.

Most recently, Lopez-Barron and Macosko (López-Barrón & Macosko, 2010) proposed an alternative model to describe the coarsening in immiscible polymer blends with a dual continuous structure. They extended the scaling approach of Siggia (Siggia, 1979) who assumed that the capillary flow within the interconnected channels with a pressure gradient created by the interfacial tension of a two phase fluid system is responsible for the global coarsening. Using the Young-LaPlace equation ($\Delta P = 2\gamma H$, where H is the mean curvature) and the average velocity for Poiseuille flow inside a channel with a radius a which is given by:

$$v = \frac{a^2}{8\eta} \frac{\Delta P}{d}$$

(2.28)

where d is the characteristic size of the microstructure, $\Delta P/d$ is the pressure gradient which drives the flow, and η is the fluid viscosity, Siggia arrived at a constant dimensionless coarsening rate. One limitation of this approach is that it does not consider the impact of viscosity ratio on coarsening rate. Also, the assumption of uniform curvature along the channels and the characteristic length equal to the inverse of the average value of the mean curvature is not valid (López-Barrón & Macosko, 2010). However, Lopez-Barron and Macosko (López-Barrón & Macosko, 2010) utilized a measure of the interfacial curvature of the fluid structure as the driving force for coarsening. The use of their model requires detailed knowledge of system variables such as interfacial tension, viscosity ratio and phase volume ratios on local curvature since the five tuning parameters needed in the model are system dependent.

2.4 Multicomponent Blends

2.4.1 Wetting in Immiscible Polymer Blends

Generally, wetting refers to the study of how a liquid spreads out when it is deposited on a solid (or liquid) substrate. The wetting behavior is categorized into two main regimes: complete wetting and partial wetting which are depicted in Figure 2.14. Harkins, in his pioneering work in the early

1920s, proposed a model, the so called spreading coefficient λ, to distinguish these wetting behaviors (Harkins, 1941; Harkins & Feldman, 1922). The parameter measures the difference between the surface energy (per unit area) of the substrate when dry and wet:

$$\lambda = [E_{substrate}]_{dry} - [E_{substrate}]_{wet} \tag{2.29}$$

or

$$\lambda = \gamma_S - (\gamma_{SL} + \gamma_L) \tag{2.30}$$

where γ_S and γ_L are the solid and liquid surface tensions, respectively, and γ_{SL} is the solid/liquid interfacial tension between. This parameter demonstrates the tendency of a liquid to spontaneously spread across a liquid or solid surface. Two wetting regimes are defined based on the spreading coefficient: complete wetting and partial wetting. For positive spreading coefficients, the liquid drop completely spreads and forms a thin film on the substrate to minimize the surface energy. However, the liquid drop does not spread and rather forms a spherical cap with an equilibrium contact angle on the substrate when the spreading coefficient is negative (see Figure 2.14).
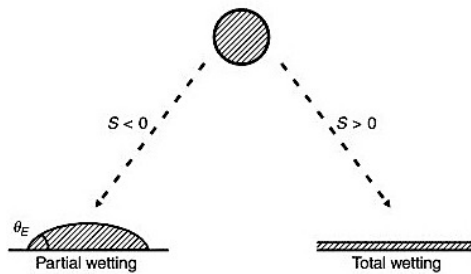
Figure 2.14. The two wetting regimes for a drop on a substrate.

Torza and Mason (Torza & Mason, 1970) showed that Harkins' equation can be generalized for a three phase liquid system by substituting the appropriate interfacial tensions for the surface tensions:

$$\lambda_{31} = \gamma_{12} - (\gamma_{32} + \gamma_{13}) \tag{2.31}$$

where the γ's are the interfacial tensions between components. In this case, λ_{31} demonstrates the tendency of component 3 to encapsulate/spread on component 1. Hobbs et al. (Hobbs, Dekkers, & Watkins, 1988), later, applied the spreading coefficient model in different ternary polymer mixtures and showed that the predictions of the model are in good agreement with experimental results. Four

morphological states in a ternary immiscible polymer system with components A, B, and C are presented in Figure 2.15. Two categories of morphological states are displayed for ternary polymer blends: 1) complete wetting (Figure 2.15a-c) or 2) partial wetting at the interface (Figure 2.15d).
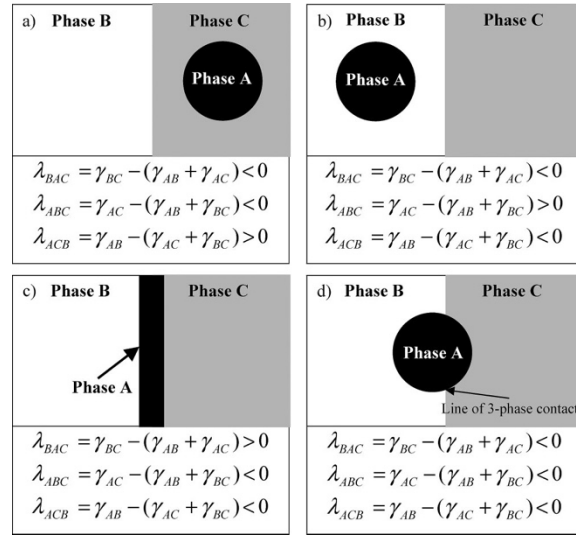
Figure 2.15. Possible equilibrium morphologies in a ternary polymer system composed of two major phases B and C and one minor phase A. The cases (a) to (c) describe complete wetting morphologies, and the case (d) displays partial wetting morphology (Virgilio, Marc-Aurele, et al., 2009).

2.4.2 Thermodynamic Models

As discussed, Hobbs et al. (Hobbs et al., 1988) used the concept of Harkins spreading coefficient and proposed an equation to interpret their observation on morphology of ternary polymer blends. They did several experiments on ternary model systems comprised of polymethyl methacrylate (PMMA), PS, polycarbonate (PC), polybutylene terephthalate (PBT), and styrene acrylonitrile resin (SAN) and showed that the spreading theory is capable to predict the wetting state of ternary polymer blends. However, three spreading coefficients are needed to predict possible morphologies that each of them defines the tendency of one phase to spread on the other phase in the matrix of the third phase. These coefficients for an A/B/C system are defined as follows:

$$\lambda_{BAC}=\gamma_{BC}-(\gamma_{AB}+\gamma_{AC}) \tag{2.32}$$

$$\lambda_{ABC}=\gamma_{AC}-(\gamma_{AB}+\gamma_{BC}) \tag{2.33}$$

$$\lambda_{\text{ACB}} = \gamma_{\text{AB}} - (\gamma_{\text{AC}} + \gamma_{\text{BC}}) \tag{2.34}$$

if one spreading coefficient is positive and the other two are negative, it indicates the complete wetting case; while the partial wetting case will be observed when all three spreading coefficients are negative (see Figure 2.15). Several researchers have examined the spreading theory and have validated the predictions with experimental results (de Freitas, Valera, Catelli de Souza, & Demarquette, 2007; Hemmati, Nazokdast, & Panahi, 2001b; Reignier & Favis, 2003a; Valera, Morita, & Demarquette, 2006; Virgilio, Marc-Aurele, et al., 2009), while some discrepancies have been reported in the literature (Nemirovski, Siegmann, & Narkis, 1995; Reignier, Favis, & Heuzey, 2003).

Guo et al. (Guo, Gvozdic, & Meier, 1997; Guo, Packirisamy, Gvozdic, & Meier, 1997) developed a model incorporating interfacial area based on a concept that a system tends to minimize its free energy of mixing. They considered the interfacial area of each component and introduced the interfacial free energy of mixing:

$$G = \sum_i n_i \mu_i + \sum_{i=j} A_i \gamma_{ij} \tag{2.35}$$

where G is the Gibbs free energy; n, the number of moles; μ, the chemical potential; A, the interfacial area and γ is the interfacial tension. They neglected the first term in right hand side of the equation (2.35) and proposed the following relations for the relative interfacial energy as follows:

$$\left(\sum A_i \gamma_{ij} \right)_{\text{B+C}} = \left(4\pi \right)^{1/3} \left[n_{\text{B}}^{1/3} x^{2/3} \gamma_{\text{AB}} + n_{\text{C}}^{1/3} \gamma_{\text{AC}} \right] \left(3V_{\text{C}} \right)^{2/3} \tag{2.36}$$

$$\left(\sum A_i \gamma_{ij} \right)_{\text{B/C}} = \left(4\pi \right)^{1/3} \left[n_{\text{B}}^{1/3} \left(1+x \right)^{2/3} \gamma_{\text{AB}} + n_{\text{C}}^{1/3} \gamma_{\text{BC}} \right] \left(3V_{\text{C}} \right)^{2/3} \tag{2.37}$$

$$\left(\sum A_i \gamma_{ij} \right)_{\text{C/B}} = \left(4\pi \right)^{1/3} \left[n_{\text{B}}^{1/3} x^{2/3} \gamma_{\text{BC}} + n_{\text{C}}^{1/3} \left(1+x \right)^{2/3} \gamma_{\text{AC}} \right] \left(3V_{\text{C}} \right)^{2/3} \tag{2.38}$$

where A_i is the interfacial area of each phase, V_i is the volume of each phase, $x = V_{\text{B}}/V_{\text{C}}$, and n_{B} and n_{C} are the number of particles in the B and C phases, respectively. In this model, the lowest value of the relative interfacial energy corresponds to the most stable morphology. Based on this model, the interfacial tensions play the major role in establishing the morphology, whereas the

surface areas have less important effect on morphology development. They used the model to predict the morphology of the HDPE/PP/PS ternary systems and found that the predictions are in good agreement with experimental results, but they did not discuss the partial wetting case.

Reignier et al. (Reignier et al., 2003) examined the HDPE/PS/PMMA ternary polymer blend and reported discrepancy between the predictions of the previous models and the experimental results. In one case, unexpectedly, PMMA encapsulated PS phase while the encapsulation of PS phase by PMMA was predicted. Following Van Oene's concept (Van Oene, 1972), they introduced a dynamic interfacial term for polymer blends which accounts the effect of the melt elasticity for morphology development. They replaced the interfacial tension term in Guo's equation with the interfacial tension obtained from Van Oene's equation and proposed the dynamic interfacial energy model:

$$\left(\sum A_i \gamma_{ij}\right)_{B/C} = 4\pi R_e^2 \left[\gamma_{BA} + \frac{R_e}{6}\left(N_{1,B} - N_{1,A}\right)\right] + 4\pi R_i^2 \left[\gamma_{CB} + \frac{R_i}{6}\left(N_{1,C} - N_{1,B}\right)\right] \quad (2.39)$$

$$\left(\sum A_i \gamma_{ij}\right)_{C/B} = 4\pi R_e^2 \left[\gamma_{CA} + \frac{R_e}{6}\left(N_{1,C} - N_{1,A}\right)\right] + 4\pi R_i^2 \left[\gamma_{BC} + \frac{R_e}{6}\left(N_{1,B} - N_{1,C}\right)\right] \quad (2.40)$$

$$\left(\sum A_i \gamma_{ij}\right)_{B+C} = 4\pi R_i^2 \left[\gamma_{BA} + \frac{R_i}{6}\left(N_{1,B} - N_{1,A}\right)\right] + 4\pi R_i^2 \left[\gamma_{CA} + \frac{R_i}{6}\left(N_{1,C} - N_{1,A}\right)\right] \quad (2.41)$$

where N_1 is the first normal stress difference for A, B, and C components, R_i and R_e are the internal and external radii of core-shell droplets. They showed that this dynamic interfacial tension model was able to predict the results observed in their study.

Valera et al. (Valera et al., 2006) studied the ternary PMMA/PP/PS blends and examined the three thermodynamic theory of the spreading coefficient, free interfacial energy, and dynamic interfacial energy. They observed that for most samples both spreading coefficient and dynamic interfacial energy models predicted the experimental results very well while the free interfacial energy model only predicted the case where PS was the matrix. However, none of the models could predict the presence of PS droplets in the matrix of PMMA.

2.4.3 Ternary Polymer Blends

Ternary blends comprise a major part of the studies on multicomponent polymer blends. The morphology of these systems is mainly influenced by either thermodynamic effect, which tends to

minimize the surface free energy of a system (Guo, Packirisamy, et al., 1997; Hobbs et al., 1988), or rheological effect, which is due to the entrapment of sub-inclusions in a more viscose phase near the phase inversion region (Favis & Chalifoux, 1988). Based on the wetting behavior, different structures are reported in the literature. Ravati and Favis (S Ravati & Favis, 2010b) did a comprehensive study on possible morphological states for a model HDPE/PS/PMMA ternary system demonstrating complete wetting behavior. They proposed four sub-categories of morphologies that can be achieved by varying the composition including: a) matrix/core-shell dispersed phase; b) tri-continuous; c) matrix/two separated dispersed phases; and d) bi-continuous/dispersed phase morphologies (Figure 2.16). They showed that all morphologies were in good agreement with Harkins spreading theory predictions. In this section, however, we review some of the most relevant morphologies reported for ternary polymer blends and structures reported for systems demonstrating partial wetting behavior.
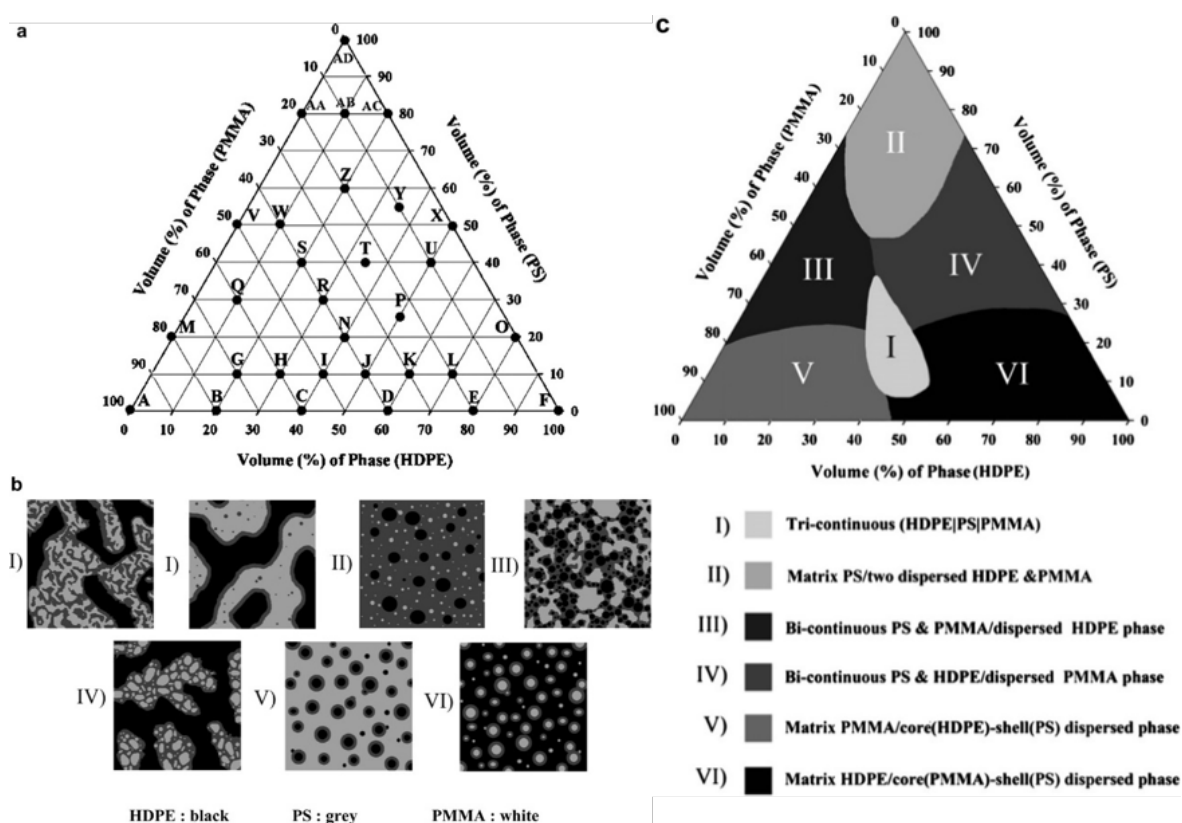
Figure 2.16. a) Triangular concentration diagram showing the composition of the various ternary HDPE/PS/PMMA blends examined in this study, b) various morphological states for ternary HDPE/PS/PMMA, and c) triangular concentration diagram showing the various regions (S Ravati & Favis, 2010b).

2.4.3.1 Composite Droplet Morphology

The composite droplet morphology is an interesting microstructure formed in ternary systems in which a minor phase is encapsulated by a second minor phase in the matrix of a third phase. Luzinov et al. (Luzinov et al., 1999) reported on the formation of a core-shell structure in ternary PS/PE/styrene-butadiene rubber (SBR) blends which changed to a multicore structure upon increasing the relative content of PE with respect to SBR in the PS matrix. Tchomakov et al. (Tchomakov, Favis, Huneault, Champagne, & Tofan, 2004) prepared ternary blends of HDPE/PS/PMMA by twin-screw extrusion and investigated the core-shell encapsulation phenomenon in composite droplets. Their results agreed with the theory of spreading and revealed a stable morphology for blends with a 1:1 composite droplet volume fraction over a wide range of processing conditions.
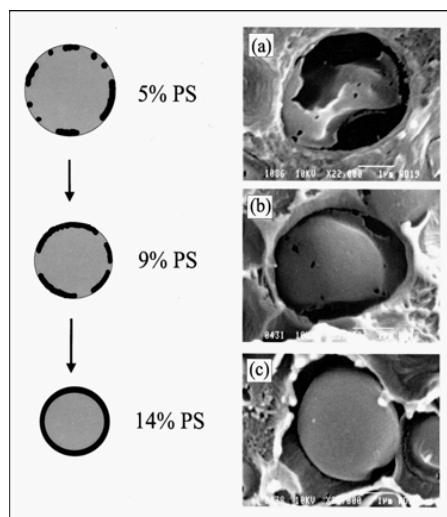
Figure 2.17. Evolution of the shell formation process with increasing PS content (vol. % based on the dispersed phase) for the 80(HDPE)/20(PS/L-PMMA) (cryo-fractured samples after being etched for 10 s with acetic acid) (Reignier & Favis, 2003a).

Reignier and Favis (Reignier & Favis, 2000b, 2003a) observed composite droplet morphology of PMMA encapsulated by PS in the matrix of HDPE. They found that at the early stages of melt mixing, almost all the PMMA phase was encapsulated by the PS dispersed phase and a stable morphology formed. They proposed a schematic for the evolution of the sell formation process with increasing PS content in the dispersed composite. The shell thickness was shown to be controlled from 40 to 300 nm by changing the relative amount of the PS to PMMA phases (see

Figure 2.17). They concluded that the interfacial dynamics is the main driving force controlling the encapsulation effects rather than the viscosity ratio.

Ha et al. (Ha, Kim, & Kim, 2004) reported that in PP/HDPE/mPE ternary blends, the HDPE droplets are encapsulated by mPE in the matrix of PP. They showed that the particle size of dispersed phase (HPDE/mPE) decreased with decreasing the viscosity ratio of the dispersed phase to the PP matrix.

Kim et al. (Kim, Kim, & Kim, 1993) found that in a ternary polyolefin system with two minor phases with equal compositions, the phase with a lower viscosity tends to form a shell layer and encapsulate the other phase. Hemmati et al. (Hemmati, Nazokdast, & Panahi, 2001a) prepared two different ternary polymer blends comprised of PP as the matrix and different combinations of minor phases including ethylene-propylene-diene terpolymer (EPDM) or ethylene-propylene-rubber (EPR) as shell phase, and HDPE or PS as the core phase. They claimed that the droplet size is determined by the average viscosity ratio of minor phases, which they calculated by the mixture law, to the matrix. Based on these results, viscosity ratio only affects the size of dispersed phases and have no influence on the type of morphology. Several other studies have reported that the composition of minor phases in ternary polymer blends with the core/shell morphology does not influence the encapsulation phenomenon and just changes the size of the dispersed composite droplets (Hemmati et al., 2001b; Yan Li, Wang, Zhang, & Xie, 2010; C. Shen et al., 2015).
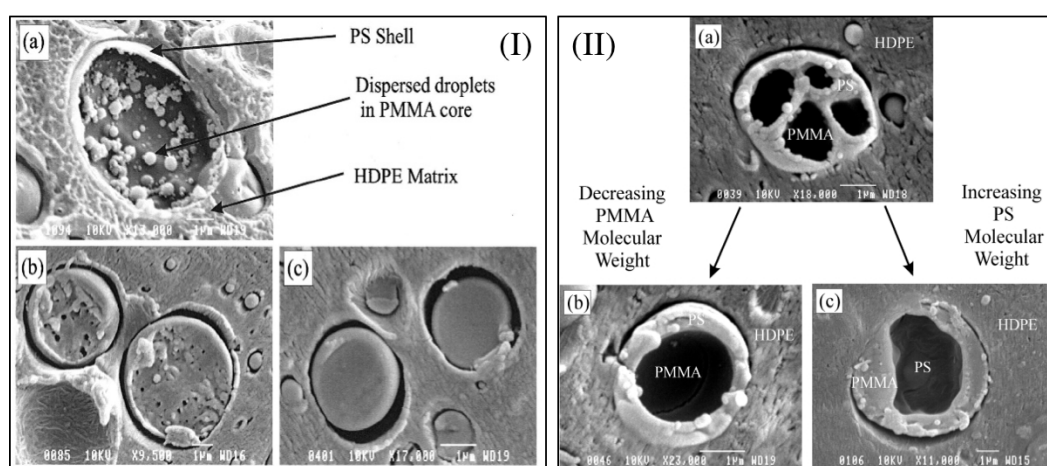
Figure 2.18. SEM micrographs of the 80 HDPE/20 (PS/PMMA), (I): (a) fractured surface etched with acetic acid for 2 min (14%PS/86%PMMA); (b) microtomed surface etched 24 h with cyclohexane (9%PS/91%PMMA); and (c) microtomed surface etched 24 h with cyclohexane

(9%PS/91%PMMA), (a and b with high viscosity and c with low viscosity PMMA) (Reignier & Favis, 2003b); (II) (a) low viscosity PS/high viscosity PMMA, PMMA is extracted by acetic acid; PS encapsulates PMMA; (b) low viscosity PS/low viscosity PMMA, PMMA is extracted by acetic acid; PS encapsulates PMMA; (c) high viscosity PS/high viscosity PMMA, PS is extracted by cyclohexane; PMMA encapsulates PS (Reignier et al., 2003).

Reignier and Favis (Reignier & Favis, 2003a) used PMMA with two different viscosities as a core phase encapsulated by the PS phase dispersed in the HDPE matrix. They showed that the PS/PMMA dispersed composite droplets with low viscosity PMMA form a complete PS shell structure at a significantly lower concentration than the high viscosity PMMA, while a large number of PS sub-inclusions were trapped within the high viscosity PMMA encapsulated by PS phase (Figure 2.18 I). Similar results have been reported by Shen et al. (C. Shen et al., 2015) in the ternary PA6/EPDM-g-MA/HDPE blend. When they used a low viscosity HDPE, a single HDPE core in EPDM-g-MA shell was formed whereas a multicore core/shell was formed in case of a high viscosity HDPE. In another work (Reignier et al., 2003), when they replaced the PS component with a high viscosity PS while keeping the high viscosity PMMA, an inversion in encapsulation occurred and PMMA completely segregated the PS phase in the HDPE matrix. They related this discrepancy to the high viscosity of PS that does not allow the PS phase to spread and encapsulate the PMMA phase (Figure 2.18 II).

2.4.3.2 Tri-continuous Morphology

Luzinov et al. (Luzinov, Pagnoulle, & Jerome, 2000b) investigated the transition from core-shell morphology to tri-continuous structure in PE/PS/SBR ternary blends through changing the relative composition of the PE phase to the PS phase while kept the SBR composition at 25 wt%. They observed that when PE or PS is the matrix, the dispersed phase has a core/shell morphology with SBR forming the shell phase. However, at some compositions a tri-continuous morphology is obtained. The observed morphologies agreed with the spreading coefficient predictions. Omonov et al. (Omonov, Harrats, & Groeninckx, 2005) examined the PA6/PP/PS (40/30/30) ternary blends demonstrating a double percolated structure where the PA6 phase formed the intermediate layer and separated the co-continuous PP/PS phase. They evaluated continuity of all phases by gravimetric measurements and found that the continuity of each phase was above 97%. They used

compatibilizing agents to improve the interface adhesion; however, it only reduced phase sizes and it did not change the morphology and the order of phases.

Preparation of double-percolated structure in HDPE/PS/PMMA ternary polymer blends has been reported by Zhang et al. (J. H. Zhang et al., 2007) in which PS forms a continuous sheath structure layer at the interface of the co-continuous HDPE/PMMA system. They showed that by controlling the composition of the components, it is possible to diminish the percolation threshold of the PS phase to below 3 vol%. Recently, Ravati and Favis (S Ravati & Favis, 2010b) studied the effect of viscosity ratio of PS to PMMA phases within the matrix of HDPE in the HDPE/PS/PMMA ternary blend demonstrating complete wetting structure. They observed that at a fixed 35/40/25 HDPE/PS/PMMA composition, although, the PMMA phase size decreases in the blend containing the high viscosity PMMA, the type of the morphology was not affected by the viscosity ratio (Figure 2.19).
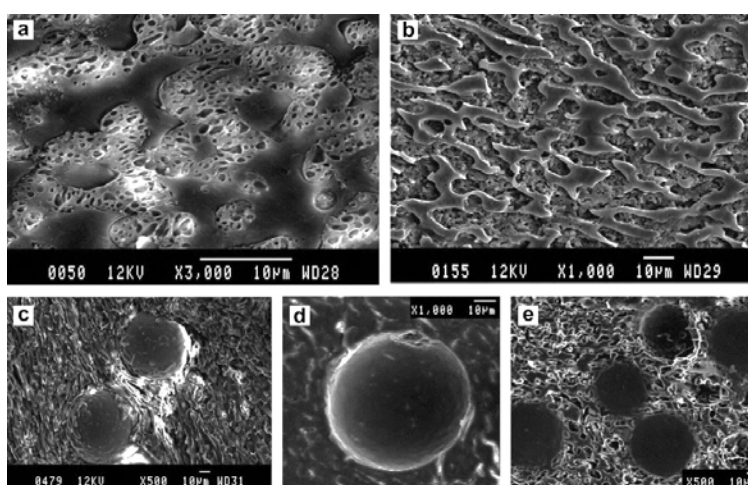
Figure 2.19. SEM micrograph of morphology of (a) and (b) 35/40/25 HDPE/PS/PMMA with low molecular weight PMMA after extraction of PMMA by acetic acid and extraction of PS by cyclohexane, respectively; (c) 35/40/25 HDPE/PS/PMMA with low molecular weight PMMA (cryofracture), (d) and (e) 35/40/25 HDPE/PS/PMMA with low molecular weight PMMA after extraction of PMMA by acetic acid and extraction of PS by cyclohexane (S Ravati & Favis, 2010b).

Dou et al. (Dou, Li, Shao, Yin, & Yang, 2016; Dou, Shao, Li, Yin, & Yang, 2016) examined the ternary polyvinylidene fluoride (PVDF)/PS/HDPE blend and reported a tri-continuous structure where the PS phase forms a percolated sheath structure at the PVDF/HDPE interface. The morphology was found to be supported by the thermodynamic spreading coefficients. They showed

that its morphology evolves at the interface by increasing the concentration of the PS phase until forms a continuous structure. However, it was observed that the composition of PS has little influence on the formation of sub-inclusions in the HDPE phase and it is the viscosity ratio of HDPE/PS that controls the morphology evolution of PS at the interface (Shao, Dou, Li, Yin, & Yang, 2016). The thickness of the intermediate PS layer has shown a linear growth with the content of PS in the tri-continuous structure.
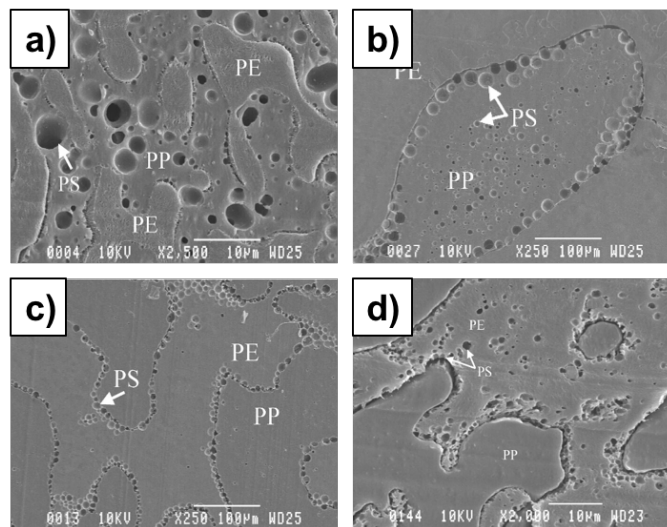
Figure 2.20. SEM micrographs of morphology of HDPE/PP/PS 45/45/10 vol% blends (a) immediately after melt processing without SEB modifier; (b) without SEB modifier after 120 min of annealing time at 200 °C; (c) with 1% SEB based on the PS content after 120 min of annealing time at 200 °C; (d) with 15% SEB based on the PS content after 60 min of quiescent annealing time. Note that the PS phase has been extracted by cyclohexane (Virgilio, Marc-Aurele, et al., 2009)

2.4.3.3 Partially Wet Structure

The case of partial wetting morphology, for the first time, was examined in detail by Virgilio et al. (Virgilio, Marc-Aurele, et al., 2009) in the HPDE/PS/PP blend with a close-packed array of PS droplets at the interface of HDPE and PP (Figure 2.20). They showed that self-assembling of PS droplets at the interface was accentuated by quiescent annealing due to a sweep and grab effect induced by the coarsening of the HDPE/PP co-continuous microstructure. They found 1% of 1,4-hydrogenated styrene-(ethylene-butylene) (SEB) diblock copolymer very effective in the localization of the all PS droplets at the HDPE/PP interface after 15 min of annealing. By increasing

the copolymer content, the PS droplets migrated from the PP phase at the interface to the HDPE side of the interface. It was shown that the self-assembling of the PS droplets at the interface and the effect of block copolymer on the migration of the PS droplets at the interface can be thermodynamically predicted using the spreading coefficient theory.

Taking advantage of the partial wetting behavior, Virgilio et al. (Virgilio, Desjardins, L'Esperance, & Favis, 2009) developed a method based on the Neumann triangle method combined with a focused ion beam sample preparation technique combined with atomic force microscopy to measure interfacial tension ratios in PS/PP/HDPE, PMMA/PS/PP, PS/polycaprolactone (PCL)/PP, and PLLA/PCL/PS ternary polymer blends demonstrating partial wetting behavior. They showed that with the knowledge of one of the interfacial tensions values between the components of a ternary blend, one can calculate the two other interfacial tensions. The results were confirmed and were in good agreement with results obtained from the breaking thread method. They also evaluated the effect of an interfacial modifier (an SEB diblock copolymer) on the interfacial tension of PS/PP/HDPE ternary blend and found that by addition of 1 wt% modifier the measured interfacial tension by this new method decreased from 4.2±0.6 to 3.3±0.4 mN/m. In another attempt, they measured the interfacial tension of HDPE/PS in ternary HDPE/PP/PS blends demonstrating partial wetting behavior modified with different modifiers including SEB, SB, and SEBS copolymers (Virgilio, Desjardins, L'Esperance, & Favis, 2010). They showed that a symmetric copolymer was very effective in decreasing the interfacial tension and relocating the position of the PS droplets at the interface, while the SEBS triblock copolymer had no effect. The measured interfacial tension from the in-situ Neumann triangle-focused ion beam-atomic force microscopy technique were higher than the results of the breaking thread method, which they attributed this difference to the interfacial elasticity of the compatibilized interface.

For systems with partial wetting phenomenon, Le Corroller and Favis (Le Corroller & Favis, 2011) examined the effect of the viscosity of the PE phase in 40/40/10 PE/PP/PS ternary polymer blends. The size of the PS droplets and the thickness of the co-continuous PE/PP phase were found to be similar in both systems with low and high viscosity PE right after melt mixing process. However, the coverage and size of PS droplets were dominated by viscous effects after quiescent annealing. The system containing the low viscosity PE showed increase in the PS droplet size within the PP continuous phase with disengagement of larger droplets from the PE/PP interface. In contrast, the

system with the high viscosity PE demonstrated a close-packed array of PS droplet at the interface with no significant change in the PS droplet size. They attributed the results to the more induced mobility of the PE/PP interface in the low viscosity PE system compared to the high viscosity PE system. These indicate that viscous effects can play a significant role in the morphology development of a system with weak driving for partial wetting behavior.

Ravati and Favis (Sepehr Ravati & Favis, 2013a, 2013b) reported a partially wet structure in the ternary PCL/PLA/PBS blend. They showed that each component can assemble as partially wet droplets at the interface of the co-continuous structure of the other components in an interchangeable manner which was supported by thermodynamic predictions. They observed a substantial growth of the PLA interfacial droplets due to the coalescence at the PBS/PCL interface upon quiescent annealing. They showed that the drainage of the trapped film between droplets and intermolecular forces are the main mechanisms controlling interfacial coarsening. In a recent work, Wang et al. (Wang, Reyna-Valencia, & Favis, 2016) showed that ionically conductive polyether-b-amide (PEBA) assembles at the co-continuous interface of PLA/PET. They observed that at low concentration (3%), PEBA forms partially wet droplets which then transits to a complete wet layer by increasing its concentration to about 10%. They explained this phenomenon by a mechanism based on the competition between dewetting and coalescence of the PEBA phase at the interface which is attributed to the dominant effect of coalescence over dewetting with increasing PEBA composition.

2.4.4 Quaternary Polymer Blends

The number of works reported on the morphology analysis of quaternary polymer blends is very limited (Guo, Gvozdic, et al., 1997; Virgilio & Favis, 2011a; Virgilio, Marc-Aurele, et al., 2009; Virgilio, Sarazin, & Favis, 2010). Guo et al. (Guo, Gvozdic, et al., 1997) extended their total interfacial energy theory to quaternary polymer blends and successfully predicted the phase morphologies of quaternary blends comprised of HDPE, PP, PS and PMMA. They proposed four out of 16 possible morphological states for quaternary (A/B/C/D) system where three minor phases (B, C, and D) are dispersed in the phase A as the matrix: (1) B, C and D form separate phases (B+C+D); (2) the phase D is encapsulated by the C phase while the B phase stays separate (B+C/D); (3) the C and D phases disperse separately in the B phase (B/(C+D)); (4) the B phase encapsulates the C phase while the C phase encapsulates the D phase (B/C/D). They observed the

case 2 when PP was the matrix phase and the PMMA phase was encapsulated by the PS phase while the PE particles were dispersed separately in the matrix (Figure 2.21a). The case 2, again, was observed when PS was the matrix and the HDPE phase was encapsulated by the PP phase while the PMMA phase was remained separately dispersed in the matrix (Figure 2.21b). For PMMA and HDPE matrices, the multi-encapsulated structures, the case 4, where structures of PS/PP/HDPE (Figure 2.21c) and PP/PS/PMMA (Figure 2.21d) were observed, respectively. Their experimental results were in agreement with the predicted phase structures and confirmed that the phase morphology is primarily determined by interfacial tensions. They also showed that the morphology of a quaternary blend can be converted from multi-encapsulated (PP/PS/PMAA) structure to (PP+PS/PMMA) structure by using a small amount of an interfacial modifier.
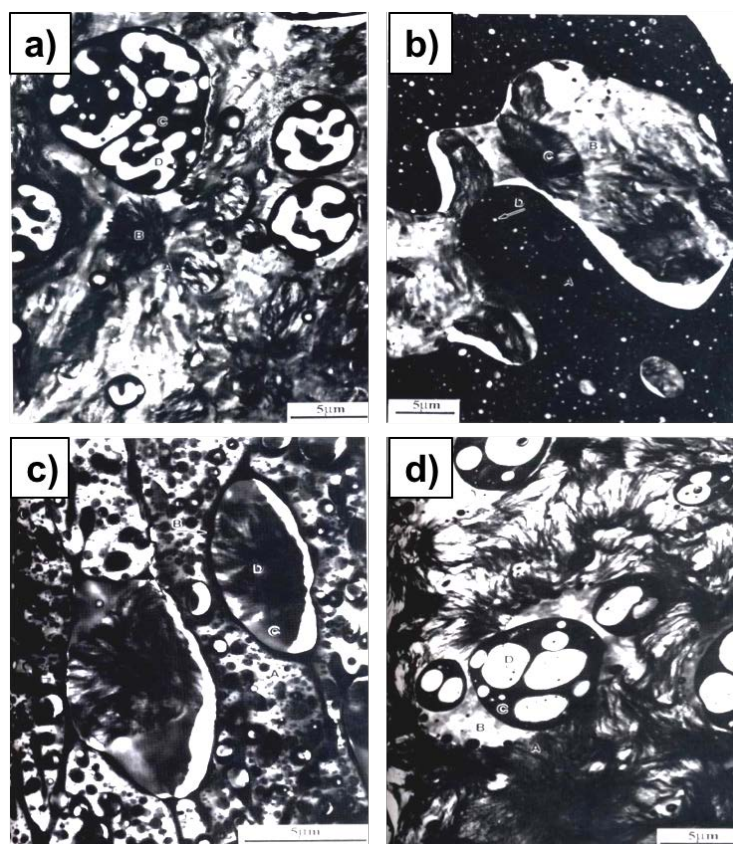
Figure 2.21. SEM photomicrograph of a) 10/10/60/20 PMMA/PS/PP/HDPE, b) 10/60/20/20/10 PMMA/PS/PP/HDPE, c) 60/20/10/10 PMMA/PS/PP/HDPE, and d) 10/10/20/60 PMMA/PS/PP/HDPE (Guo, Gvozdic, et al., 1997).
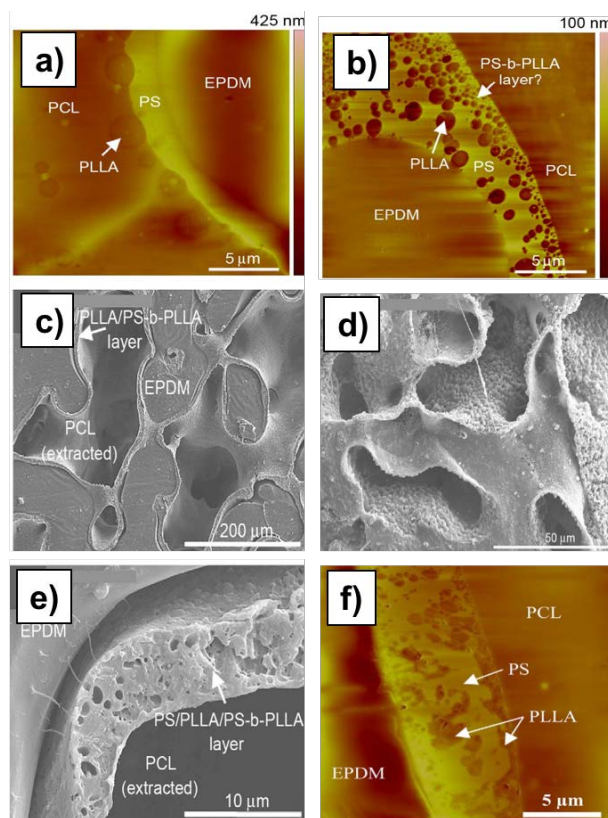
Figure 2.22. (a) FIB-AFM images of (a) unmodified EPDM/PCL/PS/PLLA 45/45/5/5 blend after 30 min of quiescent annealing time, (b) the PS/PLLA/PS-b-PLLA sheath structure at the EPDM/PCL interface in the EPDM/PCL/PS/PLLA/PS-b-PLLA blend after 60 min of quiescent annealing; (c) morphology of the EPDM/PCL/PS/PLLA/PS-b-PLLA 45/45/5/5/(30 g/100 ml PLLA) blend annealed at 200 °C for 60 min; (d) SEM micrographs showing the asymmetric layer structure of the remaining PLLA + PS-b-PLLA material after 15 min of quiescent annealing time. The first micrograph clearly shows that one side of the layer is relatively smooth, while the other is rough and covered with submicron droplets; (e) the layer structure in the EPDM/PCL/PS/PLLA/PS-b-PLLA blend after the selective extraction of the PCL phase after 60 min of annealing (Virgilio, Sarazin, et al., 2010); (f) FIB-AFM images of the blends modified with the PS-b-PMMA copolymers after melt processing and 60 min of quiescent annealing time (Virgilio, Sarazin, & Favis, 2011).

Virgilio et al. (Virgilio, Sarazin, et al., 2010) prepared ultraporous PLLA scaffolds (with a 95% void volume) by melt-blending quaternary (45/45/5/5 vol%) ethylene propylene diene rubber (EPDM)/PCL/PS/PLLA polymer blend. This quaternary blend showed very interesting structure with both complete and partial wetting behaviors. The PS layer completely segregated the EDPM

phase from the PCL phase while the droplets of the PLLA phase were located at the interface of the PS and PCL phases demonstrating partial wetting behavior (Figure 2.22a). They showed that through elaborate control of interfacial properties in multicomponent blends, it is possible to develop complex microstructures with a desired morphology. By addition of 30 wt% PS-*b*-PLLA copolymer based on the PLLA volume fraction to the EPDM/PCL/PS/PLLA quaternary blend and subsequent quiescent annealing, the PLLA droplets migrated to the PS phase due to the increased affinity of the PLLA droplet to the PS phase by addition of the copolymer (Figure 2.22b). Then, by selective extraction of the PS, EPDM, and PCL phases, an ultraporous PLLA+PS-*b*-PLLA scaffold was generated (Figure 2.22d, e). They also examined the activity of PS-*b*-PMMA block copolymer in comparison with PS-*b*-PLLA in the same quaternary blend system (Virgilio et al., 2011). By addition of PS-*b*-PMMA block copolymer, the modified quaternary system presented a co-continuous blend of EPDM/PCL with PS/PLLA/PS-*b*-PMMA sub-blend layers at the EPDM/PCL interface, while the morphology of the sub-blend layer was completely different with the system modified using the PS-*b*-PLLA copolymer. They attributed this observation to the activity and swelling power of the copolymer brushes where the PLLA homopolymer phase penetrates and swell the PMMA blocks due to the mutual affinity.

The formation of Janus composite droplets comprised of PS and PMMA hemispheres was reported by Virgilio and Favis (Virgilio & Favis, 2011b) in unmodified and interfacially modified quaternary HDPE/PP/PS/PMMA 45/45/5/5/ blends as a result of the combined effect of partial and complete wetting behavior. These axisymmetric composite droplets were located at the interface of the co-continuous HDPE/PP interfaces where for unmodified blends the PS side was in contact with both the HDPE and PP phases while the PMMA side was only in contact with the PP phase. The addition of a small amount of a PE-*b*-PMMA block copolymer (2 wt% based on the PMMA content) altered the structure and position of the Janus droplets. The modified blends showed Janus droplets with amphiphilic behavior where the PS hemisphere was only in contact with the PP phase, and the PMMA hemisphere was only in contact with the HDPE phase. They also, for the first time, reported the formation of a four-phase line of contact as point for each droplet in modified quaternary blends.

Ravati and Favis (S Ravati & Favis, 2010a) reported on the formation of a low percolation threshold conductive material device through the control of multiple encapsulation and multiple percolation effects in a five component HDPE/PS/PMMA/PVDF/polyaniline (PANI) system. To

investigate the multiple encapsulation and multiple percolation structures, they presented a detailed morphology and continuity concentration dependence diagrams of binary, ternary, quaternary and quinary systems. They showed that through the control of the composition of the components, an onion-type multiple encapsulated dispersed phase structure with multiple complete wetting behavior between components, can be converted to a hierarchical-self-assembled, multiple-percolated structure (Figure 2.23). Using this strategy, they successfully reduced the percolation threshold of the core component, PANI, to below 5 vol%. In another work, they prepared ternary and quaternary multi-percolated systems comprised of HDPE, PS, PMMA, and PVDF which were predicted by the Harkins spreading theory (S Ravati & Favis, 2011). The double and tri-percolated structures of the blend systems allowed them to extract the PS, PMMA, and PVDF phases through obtaining a fully interconnected porous HDPE substrate. Using a layer-by-layer (LbL) approach, poly(styrene sulfonate) (PSS)/PANI layers were deposited on the internal surface of the substrate and a low percolation threshold concentration of PANI was reported to be prepared with the percolation threshold no more than 0.19%.
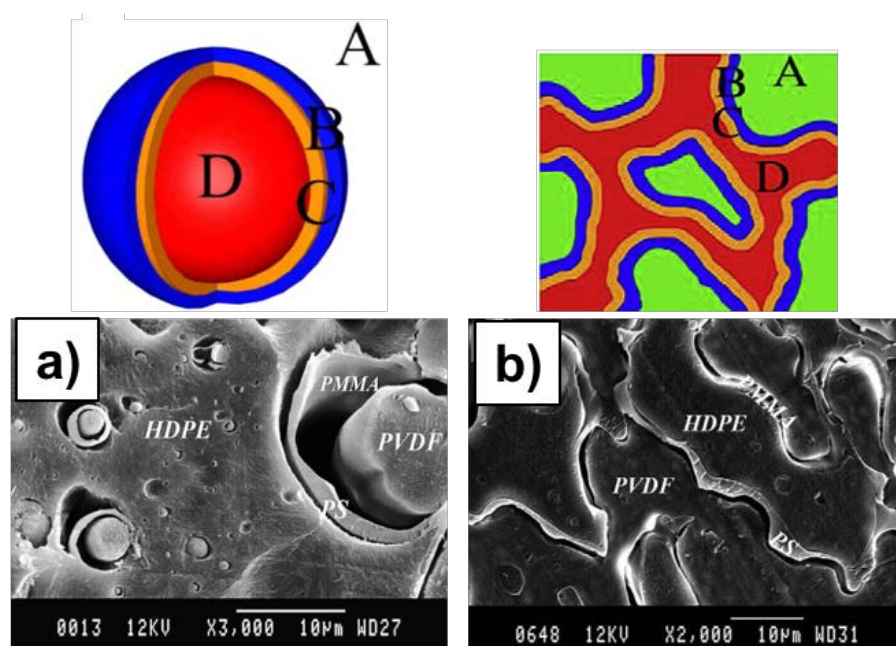
Figure 2.23. SEM micrograph of a) onion morphology in an HDPE matrix for 60/13/13/13 HDPE/PS/PMMA/PVDF; b) triple-percolated morphology of 30/15/15/40 (microtomed surface) (PMMA extracted) (S Ravati & Favis, 2010a).

2.5 Toughening Mechanisms

In a materials science context, the term toughness denotes the ability to resist fracture by absorbing energy and is usually expressed in terms of the work done in a unite area of fractured surface. Polymeric materials should sustain loads in various loading modes or deform in a non-catastrophic way under sudden impact as required by several applications (Paul & Bucknall, 2000). Generally polymers are brittle showing low resistance to fracture at low temperatures and high strain rates (Argon & Cohen, 2003). The brittle-ductile transition temperature (T_{BD}) is a unique temperature at which the brittle behavior changes to a ductile behavior at a fixed strain rate (Young, 1991). Since polymers show ductile behavior above T_{BD}, lowering this temperature, which is usually obtained by decreasing the plastic resistance of a polymer, can result in an enhanced toughness (Argon & Cohen, 2003).

Toughening of glassy polymers can be achieved by incorporation of a dispersed rubbery phase as it alters the plastic resistance of the polymer. The energy absorbing process can be initiated by the rubbery discrete particles leading to a multiple-deformation mechanism, which enhances the toughness in these multiphase systems. High impact polystyrene (HIPS) and acrylonitrile-butadiene-styrene (ABS) are two well-known examples of rubber toughened polymers. The incorporation of butadiene rubber greatly improved toughness compared to the unmodified PS and SAN, respectively (Kinloch & Young, 1995). A number of different theories have been proposed for the toughening mechanism of rubbery particles within a glassy brittle matrix. In general, crazing, shear yielding, and cavitation/debonding are commonly known theories to explain the increase in toughness of modified materials. However, the toughness mechanism depends on the intrinsic ductility of the matrix material and morphology of the blends (Souheng Wu, 1992). For instance, multiple crazing is the main toughening mechanism in rubber modified brittle polymers such as PS and SAN, whereas pseudoductile PC and poly(vinyl chloride) (PVC) undergo the shear yielding mechanism.

2.5.1 Crazing

Crazing is an important deformation mechanism in polymers which can be distinguished by stress whitening and increase in specimen volume since crazes are microvoids bridged by fibrils (Paul & Bucknall, 2000). Crazes are usually initiated under a dilational stress field at zones of imperfections

such as weakly bonded and loosely packed chain segments containing structural defects in pure polymers or at zones of stress concentration at the rubber particles, i.e. in the equatorial zones of the matrix perpendicular to the loading direction in rubber modified plastics (Michler & Bucknall, 2001). The energy can be dissipated by yielding during fibril formation and stored as surface energy in the fibrillated matter during the crazing process of polymers. A negligible volume of sample is involved in the energy dissipation process due to the severe strain localization within the craze. However, increased toughness can be achieved by multiple crazing created in larger volumes of the sample by high number of dispersed rubber particles. On the other hand, fibrils tend to break down and form crack due to the high stress caused by the localized crazes. This leads to the premature fracture of the polymer upon propagation of the cracks, however, the rapid propagation of cracks can be retarded and prevented by the rubber particles. A certain level of interfacial adhesion between the matrix and rubbery phase is required to prevent premature craze failure. Therefore, the dispersed rubber particles can act both as craze initiators and crack terminator to promote toughness of a brittle polymers. Several parameters have been reported to contribute to the enhanced toughness of rubber modified polymers: intrinsic properties of the matrix, size and size distribution of the rubber particles, modulus of the rubber particles, and adequate interfacial adhesion (Paul & Bucknall, 2000). Generally, the crazing mechanism even when is developed into multiple crazing is not a desirable toughening mechanism because of it can easily evolve into a crack due to the negligible volume involved in energy dissipation process.

2.5.2 Shear Yielding

Shear yielding, in the form of microshear bands, is a major plastic deformation mechanism which takes place essentially at constant specimen volume without the creation of an internal surface and leads to a permanent change in the shape of specimen. Shear yielding is a complex mechanism and is much more difficult to interpret in multiphase systems. Nevertheless, shear yielding is considered much more effective toughening mechanism than crazing particularly in rubber modified systems. Considerable energy is absorbed through shear yielding since a large volume of the material is involved in plastic deformation in the form of relatively homogeneous yielding within deformation zones. In unmodified polymers, shear bands mainly form in the matrix but in the case of rubber modified systems, diffuse regions of plastic deformation also develop in addition to the shear bands. Three-dimensional stress concentration is developed by dispersed particles in multiphase

systems which induces the dilation processes such as cavitation and interfacial debonding. The overlap of these stress fields can expand the shear yielding regions throughout the sample caused at a certain interparticle distance (SJOERDSMA, n.d.). A basic difference of shear yielding compared to crazing mechanism is the need for the local dilational processes in or at the rubber particles to enable yielding of the adjacent matrix. It enables the blend to yield at moderate stresses and thus facilitates the plastic deformation of the matrix around the particles. In addition, the plastic deformation that occurs around the particles can effectively blunt the formed crack tips and contribute to the overall toughness. It is worth mentioning that brittle fracture mode may be observed due to highly localized shear yielding about the crack tip followed by little plastic energy dissipation (Bucknall & Paul, 2009).

2.5.3 Cavitation or Debonding

For a long time, it was believed that the cavitation/debonding phenomenon in rubber modified plastics is a secondary deformation process following yielding of the matrix and is not an important toughening mechanism (Paul & Bucknall, 2000). However, opinions gradually changed as numerous studies reported that the cavitation in rubber particles reduce the detrimental dilational stress in the matrix polymer without forming cracks in the matrix or at the interface of rubber with matrix. Extensive studies have shown that the cavitation process promotes both crazing and shear yielding mechanisms (Kinloch & Young, 1995).) It induces formation of multiple crazes in systems with crazing as the dominant toughening mechanism and favors the plane stress situation in systems with shear yielding toughening mechanism which multiplies shear yielding. Stress concentrates at the equatorial plane of dispersed particles which results is the interfacial debonding between the dispersed particle and matrix, leading to the formation of microvoids. In case of strong interfacial adhesion between the dispersed rubbery phase and matrix, cavitation forms in the dispersed rubbery phase due to its lower Young's modulus and different Poisson's ratio compared to the matrix (Guild & Young, 1989). The mechanism of rubber cavitation in polymers has been studied both theoretically and experimentally in the literature (Merz, Claver, & Baer, 1956; Sue, Huang, & Yee, 1992).

2.6 Mechanical Properties of Polymer Blends

2.6.1 Matrix/Dispersed Morphology

The majority of studies on the mechanical properties of multicomponent polymer blends is on systems with a matrix/dispersed morphology. In a pioneering work, Cheng et al. (Cheng, Keskkula, & Paul, 1992) showed that the toughness of ternary blends of PC strongly depends on the morphology, interfacial adhesion and inherent properties of components. Significant improvements in the impact strength and tensile properties have been obtained through the formation of core-shell structures in ternary blends. The ultra high impact of PA6 have been achieved through the incorporation of well-controlled in-situ formed core-shell droplets in a matrix of PA (Ke, Shi, Yin, Li, & Mai, 2008; Z.-Z. Yu, Ou, Qi, & Hu, 1998; Z. Yu, Lei, Ou, & Hu, 1999). Yu et al. (Z.-Z. Yu et al., 1998) used maleic anhydride grafted polyethylene-octene rubber/semicrystalline polyolefin blend as an impact modifier to toughen PA6. They showed that the maleic anhydride grafted polyethylene-octene rubber forms a shell around the polyolefin core and significantly enhances the impact strength due to a good interfacial adhesion with both the PA6 matrix and the polyolefin core.

In a series of studies, Luzinov et al. (Luzinov et al., 2000a, 2000b, 1999) investigated the morphology and mechanical properties of PS/SBR/polyolefin (PO) ternary blends. They observed a PE core/SBR shell morphology in the matrix of PS with a constant content of 75 wt% in agreement with the thermodynamic prediction of the spreading coefficients (Luzinov et al., 1999). They successfully controlled the shell thickness and the core diameter by changing the weight ratio of the two minor components. The mechanical properties of the blends were found to strongly depend on composition. They evaluated the mechanical properties of the blends with different predictive models which revealed the existence of a perfect stress transfer from the PS matrix to the SBR shell and through the shell to the PE core due to a strong interfacial adhesion. Some synergism in the tensile strengths at yield was observed while the mechanical properties of the blends showed no negative deviation from the mixing rules. They also studied the effect of melt viscosity and stiffness of POs on the mechanical properties (Luzinov et al., 2000b). The mechanical properties of the blends were found to be dependent on the stiffness of the PO core. It was found that the impact strength decreases with the increase in the modulus of the core PO phase while the elongation at break is independent of the core-forming polymer.

The morphology, mechanical properties and toughening mechanism have been investigated in ternary PP/PA6/polyethylene-octene elastomer (POE) blends where the POE phase separates PA6 dispersed droplets from PP by forming a middle layer between them (S. L. Bai, G'Sell, Hiver, & Mathieu, 2005; S. L. Bai, Wang, Hiver, & G'Sell, 2004; G'Sell, Bai, & Hiver, 2004). The dilatometry results reveal that the volume strain decreases with increasing (PA6+POE) content from 0 to 60 wt% where the PA6/POE weight ratio was maintained at 2. In other words, the amount of POE interphase cavitation at the interface of PP and PA6 was reduced, implying the profuse expansion of plastic shear yielding in the PP matrix through the development of the intermediate completely wet phase of POE at the interface of the PP/PA6 system.

2.6.2 Co-continuous Structure

It has been shown that changing from a matrix/dispersed structure to a co-continuous morphology can significantly improve the impact and tensile properties in different binary blends. Willemse et al. (Willemse, Speijer, et al., 1999) showed that co-continuous blends of PE with PP or PS exhibit high tensile moduli as compared with a matrix/dispersed phase morphology. Two separate studies have supported that generating co-continuous morphologies leads to the important improvement of impact and tensile properties of binary blends (Inberg & Gaymans, 2002; Mamat, VuKhanh, Cigana, & Favis, 1997; Veenstra, Verkooijen, et al., 2000). Mamat et al. (Mamat et al., 1997) studied the tensile and impact properties of uncompatibilized PA6 with ABS over the entire range of compositions and observed a peak in the elongation at break and the impact performance around 70% ABS which is attributed to the co-continuous morphology of the blend. Inberg and Gaymans (Inberg & Gaymans, 2002) reported a reduced brittle to ductile transition temperature in a co-continuous PC/ABS blend prepared in an extrusion process. The intrinsic properties of ABS, i.e. the rubbery polybutadiene content, appeared to effectively influence the impact resistance. In another study, styrene-acrylonitrile-glycidyl methacrylate copolymer (SAN-GMA) was added to the PLA/ABS blends to modify the mechanical properties (Yongjin Li & Shimizu, 2009). The impact and elongation at break is significantly improved when SAN-GMA was incorporated to the PLA/ABS system with a co-continuous morphology. Recently, Liu et al. (Z. Liu, Luo, Bai, Zhang, & Fu, 2016b) prepared a ternary poly(L-lactide) (PLLA)/thermoplastic polyurethane (TPU)/poly(D-lactide) (PDLA) blend with remarkably improved impact toughness as compared to the binary PLLA/TPU blend. They showed that the interaction of PDLA chains with PLLA matrix

chains results in a rapid co-crystallization into stereocomplex crystallites, which modifies the melt viscoelasticity of the PLLA matrix. This induces a morphological change from a dispersed TPU phase to a co-continuous PLLA/TPU morphology and renders the significantly improved impact strength of about 65 kJ/m^2 compared to 4.9 kJ/m^2 of the neat PLLA.

2.7   Toughening of PLA

Toughening of PLA has been the subject of several research studies and a number review papers have extensively discussed different aspects of this topic (Anderson et al., 2008; H. Liu & Zhang, 2011; Rasal et al., 2010). There are several methods reported in the literature to modify the toughness of PLA, such as copolymerization, plasticization, and blending. In this section, the plasticization and blending are reviewed with an emphasis on the multicomponent blending of PLA.

2.7.1   Plasticization

Since plasticization has been a common technique to improve the processability and toughness of glassy polymers (Mascia & Xanthos, 1992), PLA has been blended with different plasticizers in order to modify its brittleness. Lactide as the first choice of plasticization of PLA has been used in several studies which shows a positive effect on elongation at break (Jacobsen & Fritz, 1999; Sinclair, 1996). Martin and Averous (Martin & Avérous, 2001) utilized several plasticizers to modify PLA brittleness. They observed that low molecular weight polyethylene glycol (PEG) and oligomeric lactic acid result in the best plasticization effects. Aging phenomenon is one of the main problems that occur in using small molecule or low molecular weight plasticizers. A number of other studies have dealt with the brittleness of PLA using various plasticizers such as triacetine, tributyl citrate, tributyl citrate oligomers, and diethylene glycol (Ljungberg, Colombini, & Wesslen, 2005; Ljungberg & Wesslen, 2002, 2003) and concluded that phase separation and migration of plasticizers toward surface are critical for mechanical properties improvement.

Baiardo et al. (Baiardo et al., 2003) examined different molecular weights of acetyl tri-*n*-butyl citrate (ATBC) and PEGs as PLA plasticizers and found that by increasing the molecular weight miscibility decreases. Their results showed a significant increase in elongation at break at the cost of strength and tensile modulus. The effect of ATCB was confirmed by Labrecque et al. (Labrecque, Kumar, Dave, Gross, & McCarthy, 1997) as an effective plasticizer at a concentration

of 20 wt%. Kulinski and Piorkowska (Kulinski & Piorkowska, 2005) studied the effect of PEG containing hydroxyl end groups on plasticization of PLA. Lai et al. (Lai, Liau, & Lin, 2004) showed that these end groups influence the crystallinity and miscibility behavior of PLA. High molecular weight poly(ethylene oxide) (PEO) found to be very effective in improving mechanical properties of PLA at 20 wt% (Nijenhuis, Colstee, Grijpma, & Pennings, 1996). Recently, poly(propylene glycol) (PPG) was used and significantly improved the elastic properties due to its good miscibility with PLA with no influence on the crystallinity of PLA (Kulinski, Piorkowska, Gadzinowska, & Stasiak, 2006; Piorkowska, Kulinski, Galeski, & Masirek, 2006).

2.7.2 Multicomponent Blends

Generally, polymer blending is considered as an important route to overcome the mechanical property deficiencies of polylactide (PLA). Binary blends of PLA with other polymers are among the most widely studied bioplastic systems and comprise a high proportion of the studies on the toughening of PLA (H. Bai et al., 2012; Imre et al., 2013; Z. Liu et al., 2016a; Ojijo et al., 2013; Stoclet et al., 2011; Thurber et al., 2015; M. Wu et al., 2014). However, recently, researchers have shown an increased interest in multicomponent polymer blends (H. Liu et al., 2010, 2011; K. Zhang et al., 2012). High performance polymeric materials with high levels of toughness, mechanical strength, and thermal resistance are reported by combining plastics with complementary properties (Yongjin Li & Shimizu, 2009; H. Liu et al., 2011; Luzinov et al., 2000a). They usually exhibit a more balanced performance compared with binary systems where improvement in one property can lead to a substantial decrease in other properties. In this section, we intend to review the studies on the toughening of PLA through the multicomponent blending approach.

A melt blended fully biodegradable and biorenewable ternary blend comprised of PLA, PBS, and PHBV was reported by Zhang et al. (K. Zhang et al., 2012) which has demonstrated a good balanced set of stiffness-toughness properties. In both PLA and PHBV based blends, a brittle to ductile transition has been observed which was not present in the pure PLA and PHBV and the binary constituent blends. They showed that the addition of PHBV and PBS improves the thermal resistance of PLA by slightly increasing its heat deflection temperature (HDT). A balanced mechanical and HDT results with an elongation at break of about 70% and an HDT of 87.5 °C as compared with 55.5°C of PLA were obtained in the PHBV/PLA/PBS 60/30/10 blend which was reported to demonstrate a core-shell morphology.

Zhang and coworkers (H. Liu et al., 2010; H. Liu, Guo, Guo, & Zhang, 2012; H. Liu et al., 2011; Song, Liu, Chen, & Zhang, 2012) investigated the mechanical properties of a ternary blend system consisting of PLA, ethylene/n-butyl acrylate/glycidyl methacrylate copolymer (EBA-GMA), and a zinc ionomer of ethylene/methacryalic acid copolymer (EMAA-Zn). They observed that the dispersed EBA-GMA and EMAA-Zn phases form a composite droplet morphology where the EBA-GMA phase encapsulates the EMAA-Zn droplets in the matrix of PLA. Blending at high temperature of 240 °C rendered a supertough PLA blend demonstrating notched Izod impact strength up to 777.2 J/m with moderate levels of tensile strength and modulus. It was found that the carboxyl groups in the EMAA-Zn ionomer reacts with the epoxy groups in the EBA-GMA phase and the Zn ions in the ionomer catalyzes the reactions which further enhances the interfacial adhesion. None of the binary blends and non-reactive ternary blends were able to yield such enhanced impact properties. The results are attributed to the composite droplet morphology and the effective interfacial compatibilization achieved due to the interfacial reaction. They also found that the EBA-GMA/EMAA-Zn ratio plays a critical role in determining phase morphology and the ultimate impact performance. Increasing the EMAA-Zn content resulted in a phase inversion where the EMAA-Zn phase encapsulates the EBA-GMA droplets in the PLA matrix. As a result of this morphology change the impact strength significantly deteriorates to a low value of 45.8 J/m. An optimum range of particle sizes of the dispersed composite domains for high impact toughness was identified to be about 1 μm. Through the analysis of fractured surfaces, it was suggested that the low cavitation resistance of dispersed particles in conjunction with suitable interfacial adhesion was responsible for the optimum impact toughness observed.

A supertoughened PLA-based material demonstrating impact strength of about 500 J/m was reported in a ternary blend comprised of PLA, ethylene-methyl acrylate-glycidyl methacrylate (EMA-GMA) terpolymer, and poly(ether-b-amide) elastomeric copolymer (PEBA) by Mohanty and coworkers (Nagarajan, Zhang, Misra, & Mohanty, 2015; K. Zhang, Nagarajan, Misra, & Mohanty, 2014). The phase morphology analysis revealed that a partial wetting behavior exists between the dispersed EMA-GMA and PEBA phases in the PLA matrix which results in a unique multiple stacked structure. The highest impact strength was achieved at a blending composition of 70%PLA/20%EMA-GMA/10%PEBA. They suggested that the combined effect of good interfacial adhesion and interfacial cavitation followed by shear yielding of the matrix contributes to the high toughness observed in the ternary blends. They later examined the effect of addition of various

nucleating agents on the crystallinity of PLA in order to enhance the thermal and impact strengths. A dramatic increase in the crystallinity content of 42% was obtained by the addition of 1 wt% aromatic sulfonate as a nucleating agent which increased the HDT of PLA to 85 °C compared to 55 °C of the neat PLA.

Zhou et al. (Zhou, Zhao, Feng, Yin, & Jiang, 2015) prepared high impact resistant fully biodegradable PLA/polyether-block- amide-graft-glycidyl methacrylate (PEBA-g-GMA)/thermoplastic starch acetate (TPSA) blends. A composite droplet morphology was observed for the dispersed PEBA-g-GMA and TPSA where the TPSA phase was encapsulated by the PEBA-g-GMA rubbery phase within the PLA matrix. It was found that the mechanical properties strongly depend on the esterification degree of starch acetate, which significantly influences the phase morphology. At an esterification degree 0.04, a high impact strength ~47 kJ/m^2 and an elongation at break of ~85% were achieved which are attributed to a more uniform and smaller composite PEBA-g-GMA/TPSA droplets.

Sarazin et al.(Sarazin, Li, Orts, & Favis, 2008) reported a brittle-ductile transition in ternary blends of PLA/PCL/thermoplastic starch (TPS). When TPS with higher glycerol content as a plasticizer was blended with PLA, an increase in the ductility of the samples is achieved and this effect increases with increasing volume fraction of TPS. It is observed that the PCL phase forms an intermediate layer between the PLA and TPS phases generating a tri-continuous structure at PLA/PCL/TPS 40/10/50 wt%. Significant improvements in elongation at break and impact strength are achieved through the addition of PCL and TPS to PLA giving promise to the ternary blend approach as a useful technique to expand the property range of PLA materials.

A high impact strength PLA blend with significantly enhanced heat resistance was reported for quaternary blends of PLA, PC, styrene-ethylene/butylene-styrene copolymer (SEBS), and EGMA (Hashima, Nishitsuji, & Inoue, 2010). In that case, as the result of the compatibilization effect of EGMA at the interface of PLA and PC, the negative pressure effect of dispersed SEBS droplets effectively dilated the highly continuous PLA and PC matrices. This results in a high performance PLA blend with an HDT as high as 95 °C, elongation at break of about 90%, and Izod impact strength of about 65 kJ/m^2.

CHAPTER 3   ORGANIZATION OF THE ARTICLES

Based on the specific objectives, the following CHAPTER 4-7 present the results obtained during this research work.

CHAPTER 4 is dedicated to the study of morphology development in ternary and quaternary biodegradable blends comprised of PLA, PBS, PBAT, and PHBV. The first article is entitled: "Partial and Complete Wetting in Ultralow Interfacial Tension Multiphase Blends with Polylactide". The melt blended samples were subjected to quiescent annealing to assess the morphological stability. The interfacial tension between components were measured using different methods including the breaking thread, imbedded fiber retraction, and in situ Newmann triangle methods. Different microscopy techniques including SEM, atomic force microscopy along with solvent extraction/gravimetry methods were employed to investigate the phase structure of the blends. Furthermore, FTIR-imaging is developed for the purpose of unambiguous phase identification which is quite useful for complex systems comprised of polymers with similar molecular structure. A concentration dependent wetting behavior for ternary and quaternary multiphase polymer blends was observed. Increasing the concentration of the intermediate phase results in a transition from self-assembled droplets at the interface (partial wetting) to a fully formed layer structure at the interface (complete wetting). This behavior is placed in context through a rigorous examination of interfacial tension-based thermodynamic models.

The second article is entitled "Partial to Complete Wetting Transitions in Immiscible Ternary Blends with PLA: The Influence of Interfacial Confinement" which is presented in CHAPTER 5. Through a study of three ternary systems comprised of PLA/PHBV/PBS, PLA/PBAT, and PLA/PE/PBAT, this work reports on the influence of interfacial confinement and thermodynamic tendency of the intermediate towards partial wetting on wetting transitions for multiphase polymer blends. Increasing the concentration of the confined intermediate phase results in a transition from self-assembled droplets at the interface (partial wetting) to a fully formed layer structure at the interface (complete wetting). A conceptual dewetting/coalescence model is used to examine the results and the confinement effect imposed on the intermediate phase.

CHAPTER 6 presents the third article entitled: "Compatibilization and Toughening of Co-Continuous Ternary Blends via Partially Wet Droplets at the Interface". From the knowledge acquired on partial wetting in ternary polymer blends from the first and second papers, in this work,

the effect of the interfacial assembly of partially wet polymeric droplets at a co-continuous PLA/PA11 interface is examined and indicated its significant implications for the compatibilization and toughening of co-continuous multiphase systems in general. Four different polymers: ethylene methyl acrylate (EMA), ethylene methyl acrylate–glycidyl methacrylate (EMA-GMA), poly(butylene succinate (PBS) and poly(butylene adipate-co-terephthalate) (PBAT) were employed which all form partially wet droplets at the PLA/PA11 interface. The partially wet droplets at the interface result in a compatibilization effect and a brittle to ductile transition is observed for the various blends. The PLA/EMA/PA11 blend, in particular, shows a 4-fold increase in the impact strength (73 J/m) and a substantial increase in the elongation at break to 260% as compared to the brittle PLA/PA11 50/50 binary blend. An analysis of the fracture surfaces shows that the very significant increase in impact strength is due to the interfacial cavitation of the self-assembled rubbery EMA droplets which percolate across the co-continuous PLA/PA11 interface and result in the shear yielding of the major phases.

CHAPTER 7 reports on the profound impact of a tri-continuous structure and strong interfacial interactions on the ultra-toughening of ternary and quaternary multiphase polylactide (PLA)-based blends. The results are presented as the fourth article entitles: "Ultratough Co-Continuous PLA/PA11 by Interfacially Percolated Polyether-b-amide". It is found that when PEBA elastomer is assembled as a thin layer at the interface of fully percolated PLA and PA11, the notched Izod impact strength increases to 142.4 J/m as compared to 17.3 J/m for the PLA/PA11 blend. The further addition of polyethylene oxide (PEO) in the PLA phase results in an ultra-toughening effect and a dramatic increase in the Izod impact to 728.6 J/m is achieved. The article discusses the critical roles of triple continuity, strong interfacial interactions, the importance of plasticizing the PLA phase and interfacial cavitation as the main components controlling this ultratough behavior.

CHAPTER 4   ARTICLE 1: PARTIAL AND COMPLETE WETTING IN ULTRA-LOW INTERFACIAL TENSION MULTIPHASE BLENDS WITH POLYLACTIDE[1]

Ali M. Zolali, Basil D. Favis

CREPEC, Department of Chemical Engineering, École Polytechnique de Montréal, Montréal, QC, Canada H3C3A7

4.1   Abstract

The control of phase structuring in multiphase blends of polylactide (PLA) with other polymers is a viable approach to promote its broader implementation. In this paper ternary and quaternary blends of PLA with poly(butylene succinate (PBS), poly(butylene adipate-co-terephthalate) (PBAT) and poly(3-hydroxybutyrate-co-hydroxyvalerate) (PHBV) are prepared by melt blending followed by static annealing in order to determine their most stable complete or partial wetting thermodynamic states. The interfacial tensions between components are measured using three different techniques, i.e. breaking thread (BT), imbedded fiber retraction (IFR), and the in-situ Neumann triangle approach (NT). Also, an FTIR-imaging technique is developed for the purpose of unambiguous phase identification in these complex blends comprised of similar polyesters. A tri-continuous complete wetting behavior is observed in the ternary 33PLA/33PBS/33PBAT blends before and after quiescent annealing which correlates closely with spreading theory analysis. In the quaternary PLA/PBS/PBAT/PHBV blend a concentration dependent behavior is found. At 10 vol.% PBAT, partially wet droplets of PBAT at the interface of PBS and PHBV are observed and they remain stable after quiescent annealing. In contrast, at higher PBAT content (25 vol.%), a quadruple continuous system is observed after mixing. Upon quiescent annealing, the PBAT phase breaks up and forms droplets at the PBS/PHBV interface. The morphological results after annealing for the quaternary blend strongly correlate with the thermodynamic predictions based on the

---

constituent ternary blends. These results are important since they indicate the clear potential that composition control during the mixing of multiphase systems can result in a complete change of spreading behavior.

4.2 Introduction

Recently, researchers have shown a marked interest in studying ternary and quaternary polymer blends [1–4]. High performance polymeric materials with high levels of toughness, mechanical strength, and thermal resistance can be obtained by combining polymers with very different complementary properties and controlled structures [5–10]. Despite this potential and the clear relationship of phase morphology in controlling the physical properties [11,12], to date, little attention has been paid to the detailed characterization and morphological structuring in multiphase blends. In particular, polylactide (PLA), an important bioplastic, has significant inherent weaknesses as a neat polymer and its morphological structuring in ternary and quaternary polymer blend form is only beginning to be explored.

Generally, for a three-phase liquid system two distinct broad categories of wetting regimes are possible: complete wetting and partial wetting. Complete wetting is the most stable thermodynamic state where one phase segregates the two other phases from each other in a ternary system. In contrast, partial wetting is the thermodynamically favorable structure where all phases form a three phase contact and none of the phases completely spreads at the interface of the two others [13,14]. The spreading coefficient proposed by Harkins in the spreading theory [15,16] was first generalized for emulsions of three immiscible liquids [13] and then successfully employed in predicting the wetting behavior of polymeric systems [17]. For a ternary system, three spreading coefficients can be derived from the following equation:

$$\lambda_{ijk} = \gamma_{ik} - \left(\gamma_{ij} + \gamma_{jk}\right) \tag{4.1}$$

where λ_{ijk} is the spreading coefficient and the γ's are the three interfacial tensions between the dissimilar pairs of components. A positive spreading coefficient technically delineates the tendency of a component to encapsulate the second minor component in the matrix of the third component or to spread at the interface of the two other components. Therefore, for a particular ternary blend

of A/B/C with three possible spreading coefficients of λ_{BAC}, λ_{ABC}, and λ_{ACB}, the phase morphology is complete wetting if one out of the three coefficients is positive and is partial wetting if all the coefficients are negative.

The majority of studies of ternary immiscible polymer blends deal with complete wetting behavior in which interfacial dynamics can result in a broad range of phase separated structures including percolated and encapsulated structures. Reignier et al. [18] examined the formation of the core-shell composite droplets of the minor polystyrene (PS) and poly(methyl methacrylate) (PMMA) phases in the matrix of high density polyethylene (HDPE). They showed that the morphology is controlled by composition, thermodynamics, and the viscoelastic properties of the components. Omonov et al. [19] reported on the formation of a tri-continuous phase morphology from a PP/PS core-shell dispersed in PA6 matrix in ternary PA6/PS/PP blends upon controlling the composition.

The critical role of the interfacial tension in controlling morphology in completely wet ternary polymeric systems has also been reported in several studies [4,10,20]. The addition of a small amount of interfacial modifier to an HDPE/PS/polypropylene (PP) system modified the morphology from composite droplets of PS encapsulated by PP to separately dispersed PS and PP droplets in the matrix of HDPE [4]. Wilkinson et al. [21] observed a morphology transition from separate dispersed phases of polyamide-6 (PA6) and poly[styrene-b-(ethylene-co-butylene)-b-styrene] (SEBS) triblock copolymer to partially and then finally completely engulfed PA6 droplets upon the progressive replacement of SEBS with a reactive maleic anhydride-grafted SEBS-g-MA in a matrix of PP. They attributed the results to the reduced interfacial tension as the result of the reaction between the reactive SEBS and PA6 phases. A reaction induced morphology change has also been reported in ternary PA6/PS/PP blends [19]. The continuous PA6 phase in the tri-continuous morphology converted to finely dispersed droplets in the PS phase upon incorporation of maleic anhydride grafted polypropylene and styrene maleic anhydride copolymer to PP and PS, respectively. Several studies have successfully employed the use of spreading coefficients to predict the morphology in ternary polymer blends [19,22,23].

It has also been shown in the literature that solid particles can partially wet, and stabilize, a fluid-fluid interface in systems known as Pickering emulsions [24–29] and bijels [30–33]. Multiple studies of fluid/fluid/solid particle systems show that an interplay between viscous forces,

capillarity, and wettability control the final microstructure [34,35]. Although the effect of the particle concentration and phase ratio are also important, the influence of the wettability of the particles, and the dominant role of minimizing surface free energy, has also been shown to be a first order parameter in the adsorption behavior of solid particles to the interface.

The formation of partially wet droplets in multiple phase polymeric systems, where three-phase contact is generated, has only just begun to be reported in ternary and quaternary systems [36,37]. Virgilio et al. [37] were first to detail the generation of a closed-pack array of partially wet droplets of PS at the interface of HDPE/PP. Through the addition of an SEBS copolymer, they controlled the localization of PS droplets at the interface, and were also able to migrate the PS from the interface to the HDPE phase. Their results were supported by the thermodynamic analysis of the spreading coefficients. The formation of a variety of partial and complete wet structures was also reported in ternary blends of bioplastics with some novel tunable morphologies [38]. Very low interfacial tensions between components were perceived to be responsible for three different, but stable morphological states of complete, partial, and combined complete-partial wetting. In addition to interfacial dynamics, kinetics can also play an important role in the morphology development of multiphase blends particularly, with respect to phase size and shape [11,39–41].

Although the use of biodegradable or compostable polymers in the plastics industry has seen dramatic growth in the last decade, there is an important need to develop next generation high value-added applications for these materials. The goal of this study is to generate ternary and quaternary blends comprised of biodegradable/compostable components with novel phase structures through controlled wetting behavior. These new structures will potentially pave the way for entirely new property sets. In terms of the scientific context, the vast majority of the polymer blend literature is based on systems which demonstrate two phase contact wetting behavior for binary systems. The study of the controlled wetting of ternary, quaternary and quinary polymer systems is still in its infancy.

The objective of this paper is to study the effect of interfacial dynamics and composition on wetting behavior in ternary and quaternary blends with ultra-low interfacial tensions between components. For this purpose, multiphase blends of polylactide (PLA) with three other polyesters, poly(butylene succinate (PBS), poly(butylene adipate-co-terephthalate) (PBAT) and poly(3-hydroxybutyrate-co-

hydroxyvalerate) (PHBV) were prepared by melt blending. The addition of PBS, PBAT, and PHBV to PLA is also interesting since it results in compostable polymer blends which can offer a range of complementary property sets [42,43]. Since phase characterization is a major hurdle in multiphase system morphology analysis, this paper will examine FTIR imaging as route to clear phase identification. Static annealing will be used to clearly determine the most stable thermodynamic states and the tendency of phases to form complete or partially wet structures will be supported by spreading theory analysis.

4.3 Experimental

4.3.1 Materials

We used four different commercially available homopolymers in this work. PLA (98.7 mol% L-isomer) was supplied by NatureWorks LLC (Ingeo™ Biopolymer 3001D). PBAT was obtained from BASF (Ecoflex™) and PBS was obtained from Showa Denko America Inc. (Bionelle™ 1001MD). PHBV (8 mol% hydroxyvalerate) was provided by Tianan Biopolymer (Enmat™ Y1000P). A grade of poly(ε-caprolactone) (PCL) from Solvay (PCL6800) was also used. The main characteristics of the materials are listed in Table 4.1. All the materials were dried at 70 °C under vacuum for at least 8 hours before being used in the experiments.

Table 4.1. Main characteristics of materials used in the study.

Material	Melt density (g/cm^3) at 190°C	M_n/M_w (kg/mol)	T_m (°C)	η^* (Pa.s) at 190°C and 25 s^{-1}	$\eta_0 \times 10^3$ (Pa.s) at 190°C
PLA	1.13	107/152[a]	170	630	680
PBS	1.1	47/140[b]	113	470	660
PBAT	1.15	72/126[c]	120	540	670
PHBV	1.1	92/240[d]	172	150	-
PCL	1.0	-/120[e]	60	-	-

a[59]; b[60]; c[61]; d[62]; e: GPC data reported by the supplier.

M_n: number average molecular weight.

M_w: weight average molecular weight.

T_m: melting temperature determined from DSC experiments.

η* complex viscosity

4.3.2 Blend preparation and annealing

All samples were prepared in a 30 mL Brabender internal mixer at 190 °C and 50 rpm for 8 min under a nitrogen blanket. All compositions are in volume percent. After blending, the samples were cut and quenched in ice-water to freeze-in the morphology. Quiescent annealing was performed using a hot press at 190 °C for 10 min under a nitrogen flow. The annealed samples were also plunged into ice-water to freeze-in the morphology.

4.3.3 Rheological measurements

The rheological analyses were carried out on a controlled-stress rheometer (Physica MCR 301, Anton Paar) equipped with a 25 mm parallel plate disk geometry with a gap of 1 mm. The samples were first prepared by compression molding at 190 °C on a Carver hot plate hydraulic press to obtain 1.2 mm thick and 25mm diameter discs. All rheological measurements were performed at 190 °C under nitrogen atmosphere. Dynamic strain sweep tests were made to determine the linear viscoelastic region and then, dynamic frequency sweep tests were carried out and the results are presented in Figure 4.1. The zero shear viscosities (η_0) of the neat polymers were calculated using the Carreau-Yassuda model and are shown in Figure 4.1. All polymers were found to be stable at the set temperature in the time sweep experiment at 10% strain and 1 rad/s after 40 min except PHBV which shows degradation as reported elsewhere [44] and which limits the estimation of its zero shear viscosity.
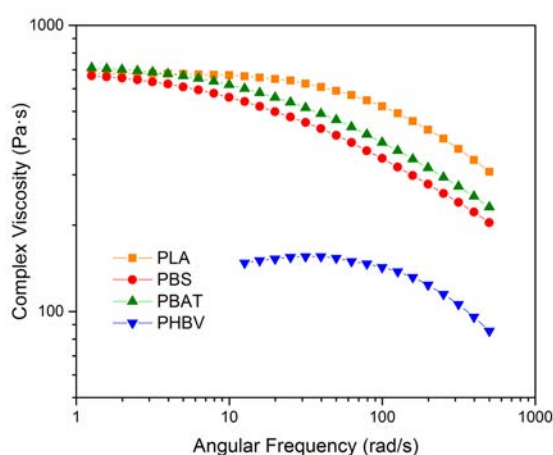
Figure 4.1. Complex viscosity vs. frequency of the neat polymers at 190°C.

4.3.4 Interfacial tension measurement

Three different methods were used to measure the interfacial tension between polymer pairs used in this study.

Breaking Thread Method (BT)

The well-known breaking thread method is based on the growth of distortions related to the break-up of a liquid cylinder in a liquid matrix [45]. For each pair, a thread of component with the higher melting temperature was spun out of melt with diameters ranging from 40-70 μm and then annealed at 60 °C for 24 h under vacuum to remove the residual stress. The threads were afterwards sandwiched between films of the other pair. Measurements were then performed at 190 °C using a hot-stage (Mettler FP-82HT) under an optical microscope from Nikon (Optiphot-2). SigmaScan v.5 software was used to analyze digital images captured during the experiments using Streampix v.III software. This method, however, requires long times to develop distortions due to the very low interfacial tensions of components employed in this work. Also, PHBV demonstrates a very low and heat sensitive complex viscosity, it is thus impossible to measure the interfacial tension through the BT method for that component. A minimum of ten measurements were performed for each reported interfacial tension value in order to get the most reliable data. The error associated with the interfacial tension measurements was less than 10%.

Imbedded Fiber Retraction Method (IFR)

In order to validate these results and measure the interfacial tension between PHBV and the other components, a retraction method called the IFR technique was explored as it requires much shorter times [46–49]. The technique is similar to the BT method, except that in this method the fiber is short, in the range of 0.9-1.2 mm, in order to prevent the fiber distortion phenomenon. The kinetics of the retraction of a cylindrical fiber to a spherical shape, which is determined by the interfacial tension and the viscous resistance to retraction, has been modeled previously [46,47]. The interfacial tension is obtained by fitting the theoretical model to the experimental shape evolution results. In the experiment, the short fiber of the component with higher melting temperature was placed between films of the other polymer and annealed at 190 °C under a flow of dry nitrogen. The retraction of the fiber was recorded and analyzed using Streampix v.III software. The average

result of at least ten repetitions in which the theoretical model is perfectly fitted to experimental results is reported.

Neumann Triangle Method (NT)

Finally, a third method based on the Neumann triangle method combined with a microscopy technique is also used to measure the interfacial tensions of PHBV with PBS and PLA with PBS. This technique is based on the geometrical analysis of contact angles between an in-situ assembled partially wet droplet at the interface of the two other major components in a ternary immiscible polymer blend. The balance between three interfacial tensions at the line of 3-phase contact is described by a Neumann triangle. This method gives relative values of the interfacial tensions between components, therefore, one can calculate the interfacial tensions when one of the interfacial tensions is known. Micrographs of the phase morphology of partially wet systems were analyzed and contact angles of a minimum of 20 partially wet droplets at the interface were measured for each system. The absolute values of interfacial tensions were calculated through the Neumann triangle method. Further details of the technique can be found elsewhere [36,50].

4.3.5 Field emission scanning electron microscopy

The specimens were cut and microtomed under liquid nitrogen using a microtome (Leica RM 2065) equipped with a glass knife and a cryo-chamber (LN21). In order to create a contrast between phases, selective solvent extraction method was performed. Tetrahydrofuran (THF) was used to extract PLA and PBAT at 35 °C, and dichloromethane (DCE) for PLA, PBAT, and PBS. The microtomed surface of the specimens were coated with gold/palladium by plasma deposition and the morphology was observed with a FE-SEM machine (JSM 7600F, JEOL) operated at a voltage of 2-5 keV.

4.3.6 Atomic force microscopy

Atomic force microscopy (AFM) nano-mechanical mapping was carried out using a Dimension Icon atomic force microscope (Bruker, USA) in PeakForce tapping mode with quantitative nanomechanical analysis (QNM). In order to obtain a smooth surface, samples were ultra-microtomed using a Leica EM UC7 ultra-microtome equipped with Leica EM FC7 cryo-chamber

and a cryo 45° DiAtome diamond knife. All scans were performed on the ultra-microtomed surface using ScanAsyst-Air probes (Bruker, CA) with 5 nm nominal tip radius and a 0.4 N/m nominal spring constant. Nanoscope (v8) and Nanoscope Analysis (v1.40) software were used for AFM operation and image analysis.

4.3.7 Solvent extraction and gravimetry

The solvent extraction technique, which is an absolute measurement of continuity, was used to extract and measure the % continuity of various components. The volume of components before and after extraction was measured by weighing samples and converting weight to volume. The continuity of each phase was determined using the following equation:

$$\%continuity\ of\ A = \left(\frac{V_{initial} - V_{final}}{V_{A,initial}}\right) \times 100 \tag{4.2}$$

where, 'A' represents the extracted component, $V_{initial}$ and V_{final} are the volume of sample before and after extraction while $V_{A,initial}$ is the volume of component 'A' before extraction, respectively. THF was used to extract PLA and PBAT and DCE was utilized to extract PLA, PBAT, and PBS. The values reported are the average of at least four measurements done in this way. A homogenous blend is assumed when carrying out the selective solvent extraction. The extraction measurements were carried out for ten days using a soxhlet extractor setup at a temperature of about 40 °C.

4.3.8 FTIR-Imaging

A Perkin Elmer Spotlight 400 imaging system (Perkin Elmer, Waltham, MA) was used to collect IR spectroscopic imaging data of the microtomed samples. FTIR images were acquired in ATR imaging mode using a Germanium crystal (Approx. 600 μm × 600 μm). Data over the nominal free-scanning spectral range, 4000–600 cm−1, were recorded with an interferometer speed of 1.0 cm/s and collected using a linear MCT detector array. In ATR mode, spectral images were acquired with a pixel size of 1.56 μm by 1.56 μm, with 16 scans per pixel at a spectral resolution of 4 cm−1. ATR images were collected across a 150 μm × 150 μm region of the ATR crystal. The ATR crystal was placed in contact with the microtomed sample using minimal pressure to ensure good contact. An ATR crystal fitted to a microscope enables one to map the surface of microtomed samples. The

machine collects spectra at regularly-spaced points along a line and then assembles all lines to form a 2D spectrum of the surface. SpectrumIMAGE software was used to analyze the surface data of samples. The program extracts the most significant features in the surface spectra using a basic Principal Component Analysis (PCA). It basically considers the difference between each point-spectrum and the average spectrum and then defines common factors which are called principal components. These factors show how absorbances at different wavelengths change together and can be plotted in the form of a spectra. For example, in a sample containing two different polymers with different proportions of OH and CO chemical groups, these two factors may account for the majority of variance occurring in the set of spectra. The first factor has a prominent feature at 3450 cm^{-1}, corresponding to the differing absorption of OH groups. The second factor has a prominent feature at 1735 cm^{-1}, showing that it is largely associated with the CO group. Based on the difference between each spectrum and the average spectrum, PCA calculates the amount of each kind of variation in each spectrum. The most significant results are then rendered in the form of a 2D surface map based on a statistical analysis of the data set.

4.4 Results and Discussion

4.4.1 Interfacial Tensions

The polymers used in this study possess very low interfacial tensions, which make the thermodynamic analysis very delicate to perform [38]. For this reason, the interfacial tension was studied in a very detailed fashion using three different techniques: breaking thread, imbedded fiber retraction and the Newman triangle technique. The results of the BT, IFR, and in-situ NT methods are listed in Table 4.2. Typical optical microscopy images showing the fiber breakup and retraction of the BT and IFR techniques respectively with time are shown in Figure 4.2.

It has been previously reported that the breakup of a PLA thread does not occur in a matrix of PBAT even after 56 min due to the very low interfacial tension between PLA and PBAT [38]. Although it is true that a very low interfacial tension will prolong the breakup time, it is not the only parameter involved in the capillary breakup phenomenon of a cylindrical melt thread embedded within another melt. The breakup time, t_b is also dependent on the initial radius of the thread and the viscosity ratio of thread to matrix [45]. Figure 4.2a displays the distortion and then

breakup of the thread of PLA with a low diameter of ca. 60 μm within the matrix of PBAT after about 30 min.
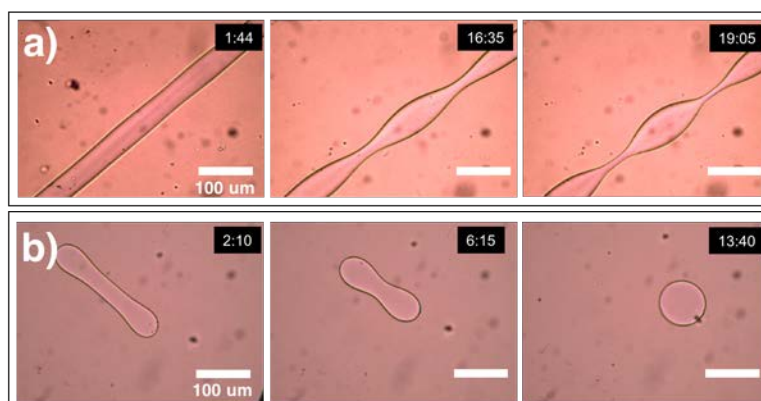
Figure 4.2. a) The breakup of the PLA thread in the matrix of PBAT; and b) The retraction of the imbedded fiber of PLA in the matrix of PBS at 190°C.

Table 4.2. Interfacial tension values (mN/m) at 190 °C.

Method	PLA/PBAT	PLA/PBS	PBS/PBAT	PBS/PHBV	PBAT/PHBV
BT	0.40 ± 0.04	0.20 ± 0.05	0.07 ± 0.02	-	-
IFR	0.48 ± 0.05	0.24 ± 0.06	0.17 ± 0.05	0.22 ± 0.03	0.23 ± 0.07
in-situ	-	0.27 ± 0.06	-	0.24 ± 0.05	-

The IFR method was also performed and the results compare well with those obtained from the BT method (Table 4.2). The advantage of this method is the shorter time of the experiment (about 10-15 min) in comparison with the BT method which reduces the possible thermal degradation effects on final interfacial tension values. In the case of PHBV, its low viscosity makes it impossible to perform the BT experiment accurately. For this reason, in addition to the IFR method, an in-situ Neumann triangle approach [50] was used to confirm the interfacial tension of blends with PHBV (see Table 4.2).

In order to determine the interfacial tension between PLA and PBS, a ternary blend of 50PLA/5PBS/45PCL was prepared. Since the interfacial tension of PBS/PCL is known from the literature, one can calculate the interfacial tension of PLA/PBS using the in-situ NT approach. The

microstructure of the 50/5/45 PLA/PBS/PCL system is shown in Figure 4.3. The angles $\phi_{PBS/PCL}$ and $\phi_{PBS/PCL}$ are measured to be 98 and 45 degrees. Knowing the interfacial tension between PBS/PCL to be 0.32±0.1 mN/m [38], the interfacial tension of PLA/PBS was calculated. The in-situ measured interfacial tensions between PLA/PHBV and PBS/PHBV are also taken from the ternary blend of PLA/PHBV/PBS. The interfacial tension of PLA/PBS and PBS/PHBV from this method are listed in Table 4.2.
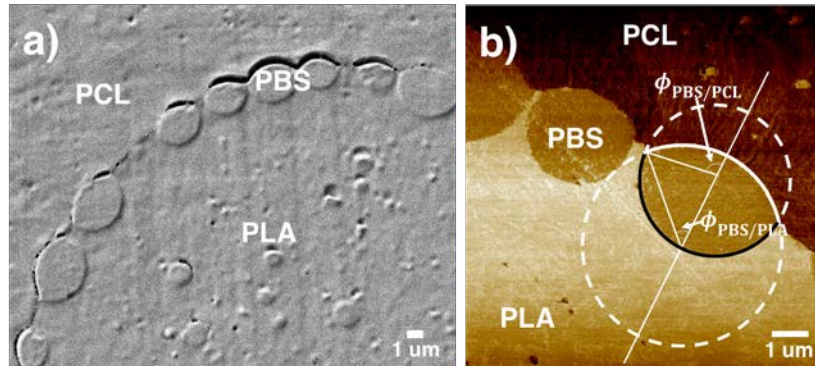
Figure 4.3. a) SEM and b) AFM micrographs of the partially wet system of 50/5/45 PLA/PBS/PCL. Note that the geometrical construction in (b) is used to measure the interfacial tension ratios between components.

4.4.2 Phase Identification

Morphology characterization and phase identification can be a complicated task in ternary, quaternary and quinary mixtures as compared to the straightforward morphology of binary mixtures. Complex structures such as multiple percolated, composite droplet, and partially wet droplet morphologies make the phase characterization a challenging task. Optical microscopy, Scanning Electron Microscopy (SEM), Transmission Electron Microscopy (TEM), and Atomic Force Microscopy (AFM) are commonly used in the morphological analyses of polymer blends [51], however, these techniques are limited in their ability to precisely characterize phases with chemically similar components [52]. Phase identification can also be problematic when multicomponent systems are designed for multiple percolation and where the concentrations of the individual components are quite similar.

In this part FTIR-imaging is developed as a phase identification technique for multicomponent polymer blends. The technique is non-destructive, chemically specific and can provide high lateral spatial resolution [53]. FTIR imaging spectroscopes are equipped with infrared array detectors in a grid pattern which provide spatial distribution of molecular components in a heterogeneous sample in a single measurement. FTIR imaging has been employed in the biomedical and pharmaceutical fields [54], and also recently in a phase separation study of polymer blends [55]. Vogel et al. [55] showed that the phase separation phenomenon could be detected in a polymer blend using FTIR-imaging. However, their results remain limited due to the large size of the single detector pixel, 61 μm by 61 μm, used in their study as compared to the typical micron and sub-micron phase dimensions of polymer blends.
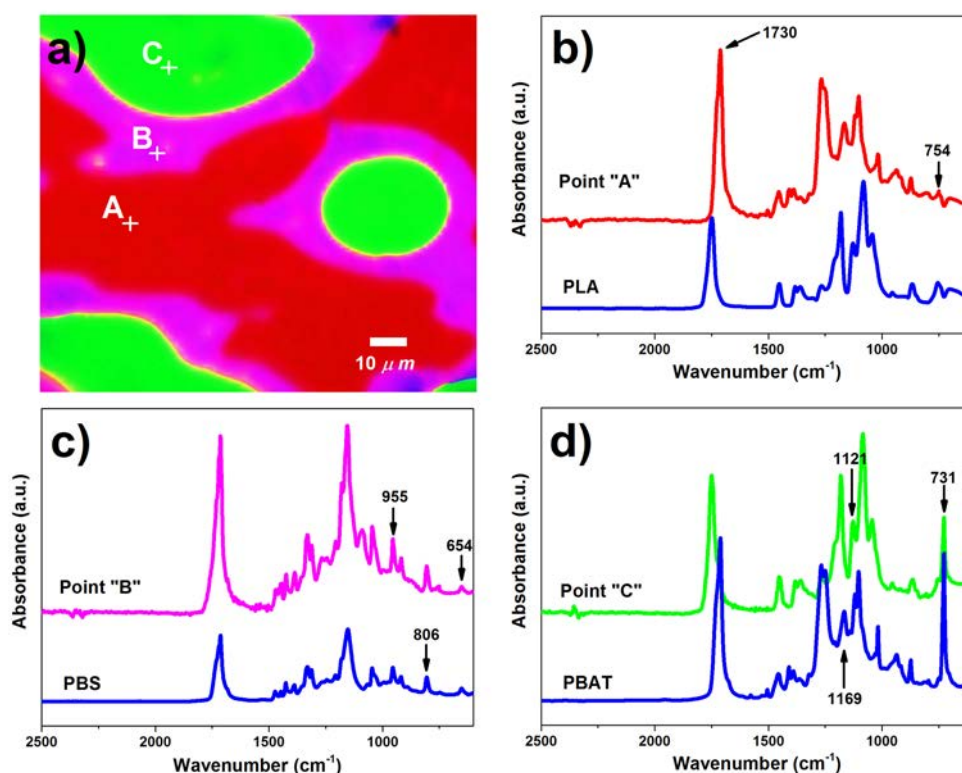
Figure 4.4. a) FTIR-imaging micrograph of 33/33/33 PLA/PBS/PBAT; b, c, d) FTIR spectra of points "A, B, and C" on FTIR-image versus pure components of PLA, PBS, and PBAT, respectively.

The FTIR-image micrograph of the 33/33/33 PLA/PBS/PBAT blend from this work is presented in Figure 4.4 along with the IR spectra associated with the different components in the FTIR-image (Figure 4.4a). Each color in this micrograph represents the phase structure of a component, which is unknown and needs to be identified. The IR spectrum of an arbitrary point on the 2D surface map can be extracted and compared with those obtained from the conventional IR spectrum of pure components. In this work the comparison has been done and the results have been matched with the spectra of the pure components in Figure 4.4b-c. The IR shift of the C = O stretching mode from 1730 to 1754 cm^{-1} and the wagging absorption of α-CH$_3$ at 757 are all reported to be characteristics in the identification of PLA [56]. Figure 4.4b compares the IR spectrum of point "A" on the FTIR-image micrograph with the spectrum of pure PLA. The two characteristic peaks of PLA are depicted by the arrows at 754 and 1730 cm^{-1} that are common among both spectra while the whole spectrum of point "A" perfectly matches that of PLA. This confirms that the red phase represents PLA. Figure 4.4c demonstrates the IR spectra of point "B" and pure PBS with the arrows indicating the three characteristic peaks of PBS. These peaks at 654 cm^{-1}, COO bending mode; 806 cm^{-1}, CH$_2$ in OC(CH$_2$)$_2$CO in-plane bending mode; and 955 cm^{-1}, C-O symmetric stretching mode; are noted as indicative IR shifts of PBS [56]. It can be seen that the IR spectrum of point "B" agrees well with the reference spectrum of PBS and thus the pink phase is PBS. A similar procedure is followed in the case of the "green" area on the FTIR-imaging micrograph in Figure 4.4 knowing the three characteristic IR peaks of PBAT to be 731 cm^{-1}, the out-plane bending of =C–H in benzene ring; 1121 and 1169 cm^{-1}, the stretching mode of the C–O in aliphatic acid [56]. Figure 4.4d shows that the IR spectrum of the "green" area obtained from the surface mapping corresponds closely to the reference spectrum of PBAT. Therefore, these results reveal that the "red" color corresponds to the PLA phase, and the "pink" and "green" colors depict the PBS and PBAT phases, respectively.

4.4.3 Ternary Systems with PLA

The thermodynamic spreading coefficients of the PLA/PBS/PBAT system are calculated based on the measured interfacial tensions and are tabulated in Table 4.3. The positive value of the λ_{ABC} spreading coefficient suggests a complete wetting behavior for the PLA/PBS/PBAT system in which the PBS phase completely segregates the PLA and PBAT phases from each other.

Table 4.3. Spreading coefficients (mN/m) of two possible ternary blends in the present work.

Spreading Coefficients	PLA/PBS/PBAT A/B/C	PBAT/PBS/PHBV A/B/C
λ_{BAC}	−0.53	−0.30
λ_{ABC}	+0.23	−0.18
λ_{ACB}	−0.27	−0.16
Prediction	Complete Wetting	Partial Wetting
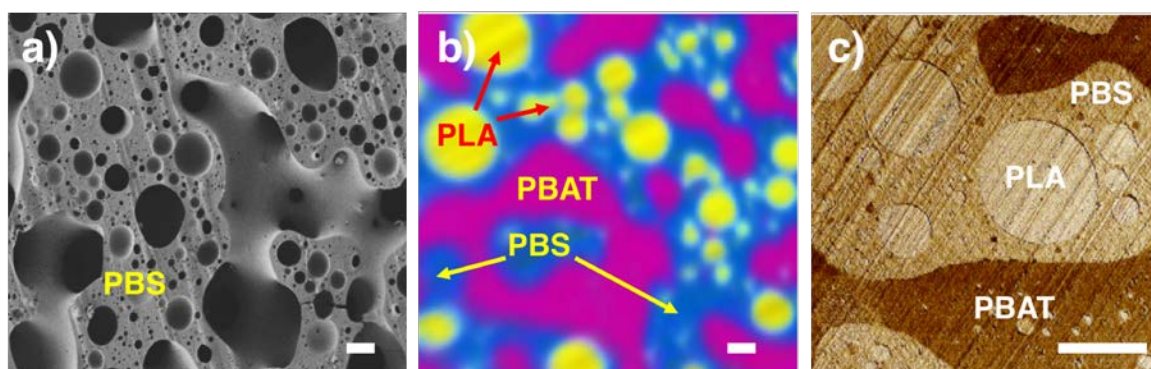
Figure 4.5. a) SEM, b) FTIR-image, c) AFM micrograph of PLA/PBS/PBAT 20/40/40 vol% blend after 10 min of annealing at 190 °C. Note that the PLA and PBAT phases have been extracted using tetrahydrofuran in the SEM micrograph and the white bars indicate 10 μm.

The morphology of the ternary PLA/PBS/PBAT system was then examined by SEM and AFM along with the FTIR-imaging technique and the results are presented in Figure 4.5. The SEM image of 20/40/40 PLA/PBS/PBAT after solvent extraction shows only the phase structure of PBS since there is no selective solvent to extract either PLA or PBAT without affecting the other one (Figure 4.5a). The FTIR-imaging micrograph in Figure 4.5b reveals a three-phase microstructure of dispersed PLA droplets (yellow phase), which are separated from the continuous PBAT phase (purple phase) by a continuous phase of PBS (blue phase). The AFM micrograph obtained from the microtomed surface of the 20/40/40 PLA/PBS/PBAT system is presented in Figure 4.5c. In the AFM method, a PeakForce QNM probe provides maps of sample moduli and adhesion simultaneously along with high-resolution topography which is quite useful in the case of materials with very similar chemical structures, but contrasting mechanical properties. It is clear that

20/40/40 PLA/PBS/PBAT forms a complete wetting (two phase contact) morphology with PBS separating the PLA and PBAT phases. This hierarchical form of complete wetting is in accordance with the thermodynamic prediction in Table 4.3.

Figure 4.6 shows AFM and SEM micrographs of the 33/33/33 PLA/PBS/PBAT blend. Figure 5b shows that the PBS phase forms a fully continuous structure with a continuity of 98% as measured by gravimetric analysis after extraction of both the PLA and PBAT phases (Table 4.4). The increase in concentration of PLA from 20-33% does not have any effect on the wetting behavior. The system is clearly completely wet with PBS separating PLA and PBAT. In order to examine the robustness of the obtained morphology, the PLA/PBS/PBAT system was subjected to annealing at 190 °C. Figure 4.7 demonstrates the morphologies of the 33/33/33 PLA/PBS/PBAT blend before and after annealing for 10 min. A coarsening of the phase morphology is evident following the annealing process. This behavior has been reported in the case of co-continuous blends in the literature [57] and can generally occur when the volume fraction of a component is above its percolation threshold. Although the phase size changes upon annealing, clearly the system maintains a complete wetting behavior. The results of gravimetry analyses after 10 min and even 30 min of annealing verify the inter-connectivity of the phases by showing a high level of combined continuity for PLA and PBAT, ca. 100%, for this system (Table 4.4).
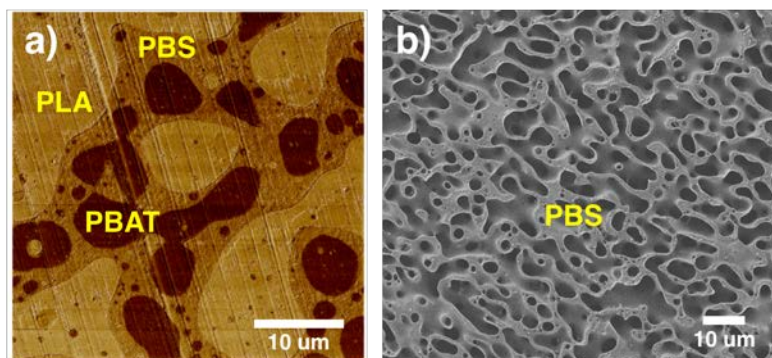
Figure 4.6. a) AFM micrograph of 33/33/33 PLA/PBS/PBAT blend; b) SEM micrographs of 33/33/33 PLA/PBS/PBAT blend after PLA and PBAT are extracted by tetrahydrofuran.

Thus, the interfacial tensions and subsequent calculated spreading coefficients for PLA/PBS/PBAT support a complete wetting behavior with PBS separating PLA from PBAT. This wetting behavior is observed both directly after mixing and is maintained even after static annealing. In a previous

work [38], where experimental surface tensions were used to estimate the interfacial tensions using the harmonic mean theory, a prediction of complete wetting with PBAT separating the PLA and the PBS was obtained. This clearly does not correlate with the experimental results shown in this work and underlines the importance of using a variety of precise interfacial tension methods as well as multiple phase identification techniques in order to characterize the phase structuring of multicomponent systems.

Table 4.4. Continuity (%) results obtained from gravimetry experiments.

Blend	Continuity of	Before annealing	10 min annealing	30 min annealing
PLA/PBS/PBAT 33/33/33 vol.%	PLA and PBAT	102 ± 2	100 ± 3	99 ± 2
PLA/PBS/PBAT/PHBV 25/25/25/25 vol.%	PLA and PBAT	101 ± 4	92 ± 2	76 ± 3
PLA/PBS/PBAT/PHBV 25/25/25/25 vol.%	PLA, PBAT and PBS	102 ± 5	103 ± 11	108 ± 5
PBS/PBAT/PHBV 33/33/33 vol.%	PBAT	92 ± 3	76 ± 2	45 ± 4
PBS/PBAT/PHBV 33/33/33 vol.%	PBAT and PBS	102 ± 4	101 ± 5	105 ± 4
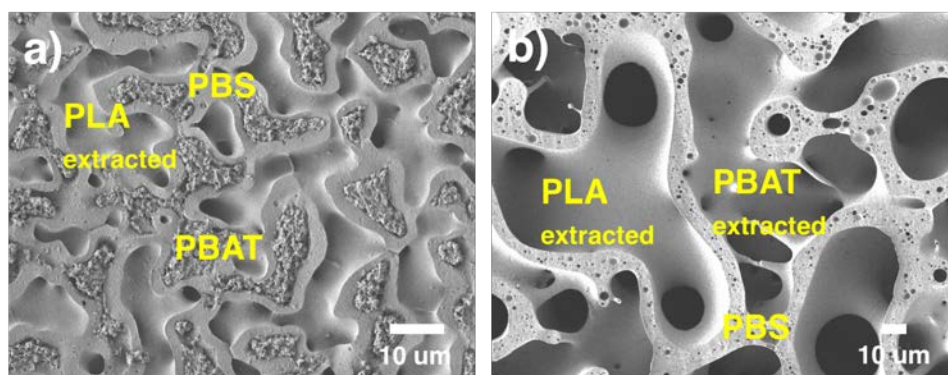
Figure 4.7. SEM micrographs of PLA/PBS/PBAT 33/33/33 (a) before and (b) after annealing for 10 min at 190 °C. Note that tetrahydrofuran has been used to completely extract PLA and partially influence PBAT.

4.4.4 Quaternary Systems with PLA

Figure 4.8 shows the morphology of the quaternary blend of 25PLA/25PBS/25PBAT/25PHBV. AFM micrographs (Figure 4.8a,b) illustrate a completely wet system with the following hierarchical ordering PLA/PHBV/PBS/PBAT. Thus, PHBV separates PLA and PBS; and PBS separates PHBV and PBAT. Although it is impossible to determine the continuity of each phase separately due to the lack of selective solvents, the continuity of each phase can be inferred from the results in Table 4. The simultaneous extraction of PLA and PBAT results in 101% continuity. Since PLA and PBAT are completely separated from each other, this unambiguously demonstrates that each of them are fully continuous. When PBS is then also extracted, a 102% continuity is achieved which clearly shows the continuous nature of the PBS phase. Finally, Figure 4.8d shows the micrograph of the remaining PHBV by itself and unambiguously presents a non-disintegrated, fully interconnected PHBV system. Thus, the above combined results clearly support a conclusion of quadruple complete continuity for the 25PLA/25PBS/25PBAT/25PHBV system.
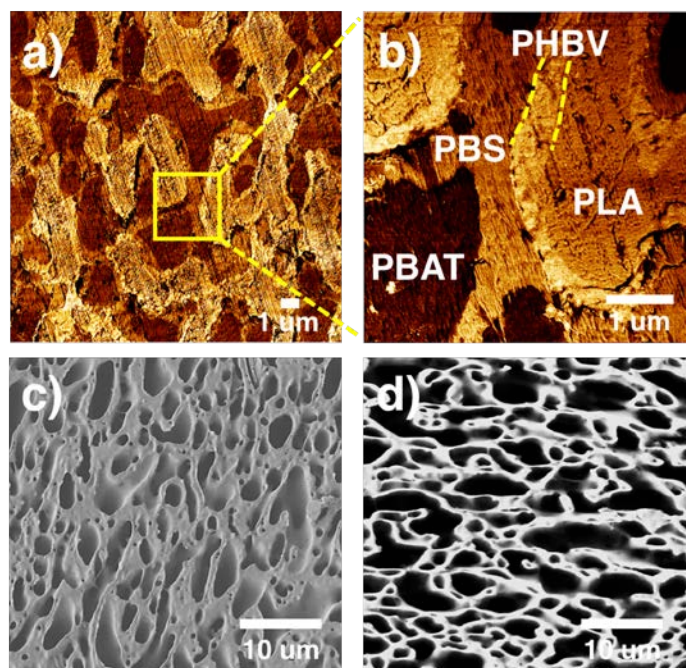
Figure 4.8. Micrographs of 25/25/25/25 PLA/PBS/PBAT/PHBV: a, b) AFM images; SEM images c) after extraction of PLA and PBAT using tetrahydrofuran and d) after extraction of all components except PHBV using dichloromethane.

The 25PLA/25PBS/25PBAT/25PHBV quaternary system was also annealed to examine the robustness of the obtained structures. Figure 4.9a displays FTIR-imaging micrographs of the blend after 10 min of annealing. It can be seen that annealing induces a morphology transition for the PBAT from a continuous phase to discrete droplets dispersed both at the PBS/PHBV interface and within the PBS phase. The AFM micrograph in Figure 4.9b confirms the FTIR-imaging observations. The loss of continuity of PBAT after 10 and 30 minutes of annealing is also reflected in the gravimetric extraction results shown in Table 4. The results of annealing the 25PLA/25PBS/25PBAT/25PHBV system point to a morphological transition where it appears that PBAT is partially wetting the PBS/PHBV interface.
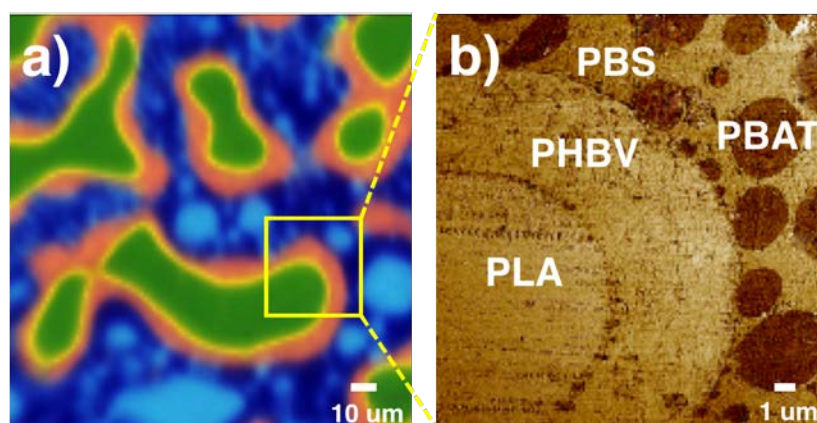
Figure 4.9. a) FTIR-imaging (PLA: green; PHBV: orange; PBS: dark blue; PBAT: light blue) and b) the close-up AFM micrographs of 25/25/25/25 PLA/PBS/PBAT/PHBV after 10 min of annealing at 190 °C.

In order to evaluate and model the thermodynamic tendency of a quaternary system, it can be broken down into its two ternary constituents. For the quaternary PLA/PBS/PBAT/PHBV system, these are PLA/PBS/PBAT and PBAT/PBS/PHBV. The spreading coefficients describing the thermodynamic behavior of these systems are calculated from the interfacial tensions and are presented in Table 4.3. Since all the spreading coefficients are negative for the PBAT/PBS/PHBV system, a partial wetting behavior is predicted, where all phases meet at a 3-phase line of contact. On the other hand, complete wetting behavior is predicted for the PLA/PBS/PBAT system, as was discussed earlier. Experimental confirmation for the morphology of the PBAT/PBS/PHBV blend is presented in Figure 4.10. The 33/33/33 PBAT/PBS/PHBV system shows a complete wetting

structure directly after mixing while a clear morphology transition towards partial wetting behavior occurs upon annealing after 10 min (Figure 4.10 a and a'). The PBAT droplets saturate the interface and the excess PBAT droplets remain within the PBS phase. The tendency for PBAT to partially wet the PBS/PHBV interface is even more clear when the PBAT content is lowered to 10 vol.%. The partially wet droplets of PBAT are clearly located at the interface of PBS and PHBV before annealing (Figure 4.10b). After annealing, partial wetting behavior is even more pronounced where almost all the PBAT droplets cover the interface of PBS/PHBV as shown in Figure 4.10b'.
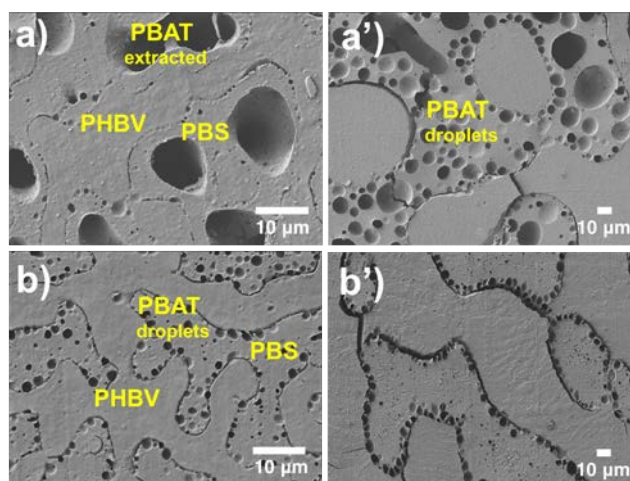
Figure 4.10. SEM micrographs of a and a') PBAT/PBS/PHBV 33/33/33 before and after annealing for 10 min at 190°C, respectively; b and b') PBAT/PBS/PHBV 10/45/45 before and after annealing for 10 min at 190°C, respectively.

Taking the data for the two ternary constituents of the quaternary blend together, the morphological observations for quaternary PLA/PBS/PBAT/PHBV in Figure 4.9 can now be confirmed. 25PLA/25PBS/25PBAT/25PHBV after mixing, and before annealing, is a fully quadruple continuous, completely wet system where PHBV separates PLA and PBS; and PBS separates PBAT and PHBV. After 10 and 30 min of annealing, the quaternary blend transits to a system where PBAT partially wets the PBS/PHBV interface and once the interface is saturated, the remaining PBAT droplets localize within the PBS phase (see Figure 4.11a and a'). When the concentration of PBAT is decreased to 10 vol.% as presented in Figure 4.11b,b', all the PBAT droplets were localized at the interface of PBS/PHBV even after 30 min of annealing. The results

after annealing for the quaternary system are completely in accordance with spreading theory predictions for each of the ternary constituent systems: PBAT/PBS/PHBV which predicts partial wetting; and PLA/PBS/PBAT which predicts complete wetting.

The morphology-composition dependence in a ternary immiscible blend with relatively high interfacial tensions between components demonstrating complete wetting behavior has been thoroughly examined [58]. It was shown that all the observed morphological states followed the complete wetting behavior over the entire composition range and the viscosity only influenced the phase size and interfacial area. Luzinov et al. [7] also reported similar results in which the wetting behavior in the ternary PS/SBR/PE blends was independent of the composition. The present study is one of the first to report on concentration dependent wetting behavior for ternary and quaternary multiphase polymer blends. This behavior has been placed in context through a rigorous examination of interfacial tension-based thermodynamic models. The results in the present study are important since they indicate the clear potential that composition control during the mixing of multiphase systems comprised of components with low interfacial tensions can result in a complete change of spreading behavior.
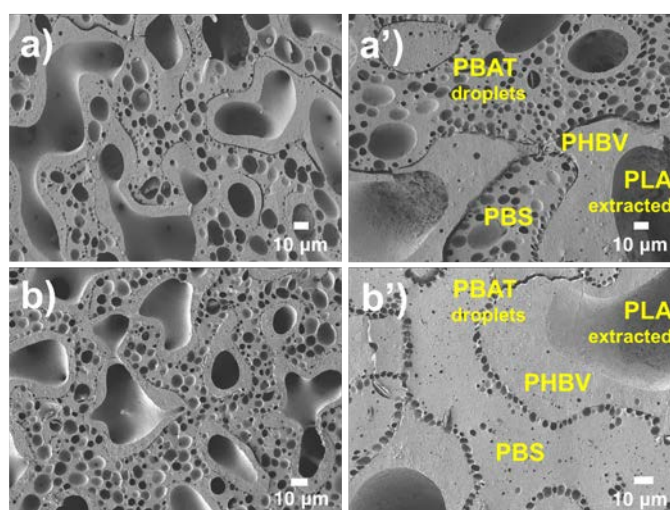
Figure 4.11. SEM micrographs of quaternary PLA/PBS/PBAT/PHBV blends: a) and a') 25/25/25/25 after 10 and 30 min of annealing respectively; b) and b') 30/30/10/30 after 10 and 30 min of annealing respectively.

4.5 Conclusion

This work underlines the importance of using a variety of precise interfacial tension methods as well as multiple phase identification techniques in order to characterize the phase structuring of immiscible ternary and quaternary polymer systems. FTIR-imaging is presented as a new phase identification and morphology analysis method useful for characterizing multiphase systems of similar chemical structures such as the biopolyesters used in this work.

A completely wet tri-continuous morphology with PBS separating PLA and PBAT is observed in the 33PLA/33PBS/33PBAT system. This morphology remains stable even after annealing and correlates well with the thermodynamic spreading coefficient predictions. Concentration dependent wetting behavior is found for the quaternary PLA/PBS/PBAT/PHBV system. For 25PLA/25PBS/25PBAT/25PHBV, a fully quadruple continuous completely wet morphology was obtained after mixing where PHBV separates PLA and PBS; and PBS separates PBAT and PHBV. However, after annealing, this quaternary blend transits to a system where PBAT partially wets the PBS/PHBV interface and once the interface is saturated, the remaining PBAT droplets localize within the PBS phase. When the concentration of PBAT is reduced to 10 vol.% in the quaternary blend, partial wetting is observed both after mixing and after annealing.

The morphological results after annealing for the quaternary blend strongly correlate with the thermodynamic predictions based on the constituent ternary blends where partial wetting and complete wetting were predicted for PBAT/PBS/PHBV and PLA/PBS/PHBV, respectively. These results are important since they indicate the clear potential that composition control during the mixing of multiphase systems with ultra-low interfacial tensions can result in a complete change of spreading behavior.

4.6 Acknowledgment

4.7 References

[1]   H. Liu, F. Chen, B. Liu, G. Estep, J. Zhang, Super toughened poly(lactic acid) ternary blends by simultaneous dynamic vulcanization and interfacial compatibilization, Macromolecules. 43 (2010) 6058–6066.

[2]   A. Rezaei Kolahchi, A. Ajji, P.J. Carreau, Surface Morphology and Properties of Ternary Polymer Blends: Effect of the Migration of Minor Components, J. Phys. Chem. B. 118 (2014) 6316–6323.

[3]   H.F. Guo, N. V Gvozdic, D.J. Meier, Prediction and manipulation of the phase morphologies of multiphase polymer blends: II. Quaternary systems, Polymer. 38 (1997) 4915–4923.

[4]   H.F. Guo, S. Packirisamy, N. V Gvozdic, D.J. Meier, Prediction and manipulation of the phase morphologies of multiphase polymer blends: 1. Ternary systems, Polymer. 38 (1997) 785–794.

[5]   H. Liu, W. Song, F. Chen, L. Guo, J. Zhang, Interaction of Microstructure and Interfacial Adhesion on Impact Performance of Polylactide (PLA) Ternary Blends, Macromolecules. 44 (2011) 1513–1522.

[6]   Y. Li, H. Shimizu, Improvement in toughness of poly(l-lactide) (PLLA) through reactive blending with acrylonitrile-butadiene-styrene copolymer (ABS): Morphology and properties, Eur. Polym. J. 45 (2009) 738–746.

[7]   I. Luzinov, C. Pagnoulle, R. Jerome, Dependence of phase morphology and mechanical properties of PS/SBR/PE ternary blends on composition: transition from core-shell to triple-phase continuity structures, Polymer. 41 (2000) 3381–3389.

[8]   S. Ravati, B.D. Favis, Low percolation threshold conductive device derived from a five-component polymer blend, Polymer. 51 (2010) 3669–3684.

[9]   N. Virgilio, P. Sarazin, B.D. Favis, Towards ultraporous poly(L-lactide) scaffolds from quaternary immiscible polymer blends, Biomaterials. 31 (2010) 5719–5728.

[10] P. Le Corroller, B.D. Favis, Droplet-in-Droplet Polymer Blend Microstructures: a Potential Route Toward the Recycling of Co-mingled Plastics, Macromol. Chem. Phys. 213 (2012) 2062–2074.

[11] I. Luzinov, K. Xi, C. Pagnoulle, G. Huynh-Ba, R. Jerome, Composition effect on the core-shell morphology and mechanical properties of ternary polystyrene/styrene butadiene rubber polyethylene blends, Polymer. 40 (1999) 2511–2520.

[12] R. Dou, Y. Zhou, C. Shen, L. Li, B. Yin, M. Yang, Toughening of PA6/EPDM-g-MAH/HDPE ternary blends via controlling EPDM-g-MAH grafting degree: the role of core–shell particle size and shell thickness, Polym. Bull. 72 (2015) 177–193.

[13] S. Torza, S.. G. Mason, Three-phase interactions in shear and electrical fields, J. Colloid Interface Sci. 33 (1970) 67–83.

[14] P.-G. de Gennes, F. Brochard-Wyard, D. Quere, Capillarity and Wetting Phenomena: Drops, Bubbles, Pearls, Waves, Springer, New York, 2004.

[15] W.D. Harkins, A. Feldman, Films. The spreading of liquids and the spreading coefficient, J. Am. Chem. Soc. 44 (1922) 2665–2685.

[16] W.D. Harkins, A General Thermodynamic Theory of the Spreading of Liquids to Form Duplex Films and of Liquids or Solids to Form Monolayers, J. Chem. Phys. 9 (1941) 552.

[17] S.Y. Hobbs, M.E.J. Dekkers, V.H. Watkins, Effect of interfacial forces on polymer blend morphologies, Polymer. 29 (1988) 1598–1602.

[18] J. Reignier, B.D. Favis, M.C. Heuzey, Factors influencing encapsulation behavior in composite droplet-type polymer blends, Polymer. 44 (2003) 49–59.

[19] T.S. Omonov, C. Harrats, G. Groeninckx, Co-continuous and encapsulated three phase morphologies in uncompatibilized and reactively compatibilized polyamide 6/polypropylene/polystyrene ternary blends using two reactive precursors, Polymer. 46 (2005) 12322–12336.

[20] D. Wang, Y. Li, X.-M. Xie, B.-H. Guo, Compatibilization and morphology development of immiscible ternary polymer blends, Polymer. 52 (2011) 191–200.

[21] A.N. Wilkinson, M.L. Clemens, V.M. Harding, The effects of SEBS-g-maleic anhydride reaction on the morphology and properties of polypropylene/PA6/SEBS ternary blends, Polymer. 45 (2004) 5239–5249.

[22] T.S. Valera, A.T. Morita, N.R. Demarquette, Study of morphologies of PMMA/PP/PS ternary blends, Macromolecules. 39 (2006) 2663–2675.

[23] H. Rastin, S.H. Jafari, M.R. Saeb, H.A. Khonakdar, U. Wagenknecht, G. Heinrich, On the reliability of existing theoretical models in anticipating type of morphology and domain size in HDPE/PA-6/EVOH ternary blends, Eur. Polym. J. 53 (2014) 1–12.

[24] B.P. Binks, S.O. Lumsdon, Influence of particle wettability on the type and stability of surfactant-free emulsions, Langmuir. 16 (2000) 8622–8631.

[25] E. Vignati, R. Piazza, T.P. Lockhart, Pickering emulsions: Interfacial tension, colloidal layer morphology, and trapped-particle motion, Langmuir. 19 (2003) 6650–6656.

[26] S. Sacanna, W.K. Kegel, A.P. Philipse, Thermodynamically stable pickering emulsions, Phys. Rev. Lett. 98 (2007) 158301.

[27] J. Guzowski, M. Tasinkevych, S. Dietrich, Capillary interactions in Pickering emulsions, Phys. Rev. E - Stat. Nonlinear, Soft Matter Phys. 84 (2011) 1–11.

[28] A. Kumar, B.J. Park, F. Tu, D. Lee, Amphiphilic Janus particles at fluid interfaces, Soft Matter. 9 (2013) 6604.

[29] M. Destribats, S. Gineste, E. Laurichesse, H. Tanner, F. Leal-Calderon, V. H??roguez, V. Schmitt, Pickering emulsions: What are the main parameters determining the emulsion type and interfacial properties?, Langmuir. 30 (2014) 9313–9326.

[30] K. Stratford, R. Adhikari, I. Pagonabarraga, J.-C. Desplat, M.E. Cates, Colloidal Jamming at Interfaces: A Route to Fluid-Bicontinuous Gels, Science (80-.). 309 (2005) 2198–2201.

[31] M.E. Cates, P.S. Clegg, Bijels: a new class of soft materials, Soft Matter. 4 (2008) 2132.

[32] L. Bai, J.W. Fruehwirth, X. Cheng, C.W. Macosko, Dynamics and rheology of nonpolar bijels., Soft Matter. 11 (2015) 5282–5293.

[33] M. Reeves, A.T. Brown, A.B. Schofield, M.E. Cates, J.H.J. Thijssen, Particle-size effects in the formation of bicontinuous Pickering emulsions, Phys. Rev. E - Stat. Nonlinear, Soft Matter Phys. 92 (2015) 32308.

[34] F. Fenouillot, P. Cassagnau, J.-C. Majesté, Uneven distribution of nanoparticles in immiscible fluids: Morphology development in polymer blends, Polymer. 50 (2009) 1333–1350.

[35] S.S. Velankar, A non-equilibrium state diagram for liquid/fluid/particle mixtures, Soft Matter. 11 (2015) 8393–8403.

[36] S. Horiuchi, N. Matchariyakul, K. Yase, T. Kitano, Morphology development through an interfacial reaction in ternary immiscible polymer blends, Macromolecules. 30 (1997) 3664–3670.

[37] N. Virgilio, C. Marc-Aurele, B.D. Favis, Novel Self-Assembling Close-Packed Droplet Array at the Interface in Ternary Polymer Blends, Macromolecules. 42 (2009) 3405–3416.

[38] S. Ravati, B.D. Favis, Tunable morphologies for ternary blends with poly(butylene succinate): Partial and complete wetting phenomena, Polymer. 54 (2013) 3271–3281.

[39] B.K. Kim, M.S. Kim, K.J. Kim, Viscosity effect in polyolefin ternary blends and composites, J. Appl. Polym. Sci. 48 (1993) 1271–1278.

[40] N. Nemirovski, A. Siegmann, M. Narkis, Morphology of ternary immiscible polymer blends, J. Macromol. Sci. Part B. 34 (1995) 459–475.

[41] I. Luzinov, C. Pagnoulle, R. Jerome, Ternary polymer blend with core-shell dispersed phases: effect of the core-forming polymer on phase morphology and mechanical properties, Polymer. 41 (2000) 7099–7109.

[42] K. Zhang, A.K. Mohanty, M. Misra, Fully Biodegradable and Biorenewable Ternary Blends from Polylactide, Poly(3-hydroxybutyrate-co-hydroxyvalerate) and Poly(butylene succinate) with Balanced Properties, ACS Appl. Mater. Interfaces. 4 (2012) 3091–3101.

[43] S. Ravati, C. Beaulieu, A.M. Zolali, B.D. Favis, High performance materials based on a self-assembled multiple-percolated ternary blend, AIChE J. 60 (2014) 3005–3012.

[44] T. Gerard, T. Budtova, Morphology and molten-state rheology of polylactide and polyhydroxyalkanoate blends, Eur. Polym. J. 48 (2012) 1110–1117.

[45] P.H.M. Elemans, J.M.H. Janssen, H.E.H. Meijer, The measurement of interfacial tension in polymer/polymer systems: The breaking thread method, J. Rheol. 34 (1990) 1311–1325.

[46] A. Cohen, C.J. Carriere, Analysis of a retraction mechanism for imbedded polymeric fibers, Rheol. Acta. 28 (1989) 223–232.

[47] C.J. Carriere, A. Cohen, C.B. Arends, Estimation of Interfacial Tension Using Shape Evolution of Short Fibers, J. Rheol. 33 (1989) 681–689.

[48] M. Tjahjadi, J.M. Ottino, H.A. Stone, Estimating Interfacial-Tension Via Relaxation of Drop Shapes and Filament Breakup, AIChE J. 40 (1994) 385–394.

[49] J. Martin, S. Velankar, Interfacial tension-errors from the Cohen and Carriere analysis of imbedded fiber retraction, Macromolecules. 38 (2005) 10614–10618.

[50] N. Virgilio, P. Desjardins, G. L'Esperance, B.D. Favis, In Situ Measure of Interfacial Tensions in Ternary and Quaternary Immiscible Polymer Blends Demonstrating Partial Wetting, Macromolecules. 42 (2009) 7518–7529.

[51] L.C. Sawyer, D.T. Grubb, G.F. Meyers, Polymer Microscopy, Springer New York, New York, NY, 2008.

[52] S. Ravati, S. Poulin, K. Piyakis, B.D. Favis, Phase identification and interfacial transitions in ternary polymer blends by ToF-SIMS, Polymer. 55 (2014) 6110–6123.

[53] M.J. Nasse, M.J. Walsh, E.C. Mattson, R. Reininger, A. Kajdacsy-Balla, V. Macias, R. Bhargava, C.J. Hirschmugl, High-resolution Fourier-transform infrared chemical imaging with multiple synchrotron beams, Nat. Methods. 8 (2011) 413–416.

[54] S.G. Kazarian, K.L.A. Chan, Applications of ATR-FTIR spectroscopic imaging to biomedical samples., Biochim. Biophys. Acta. 1758 (2006) 858–67.

[55] C. Vogel, E. Wessel, H.W. Siesler, FT-IR Imaging Spectroscopy of Phase Separation in Blends of Poly(3-hydroxybutyrate) with Poly(L-lactic acid) and Poly(ϵ-caprolactone), Biomacromolecules. 9 (2008) 523–527.

[56] Y. Cai, J. Lv, J. Feng, Spectral Characterization of Four Kinds of Biodegradable Plastics: Poly (Lactic Acid), Poly (Butylenes Adipate-Co-Terephthalate), Poly (Hydroxybutyrate-Co-Hydroxyvalerate) and Poly (Butylenes Succinate) with FTIR and Raman Spectroscopy, J. Polym. Environ. 21 (2012) 108–114.

[57] H. Veenstra, J. Van Dam, A.P. de Boer, On the coarsening of co-continuous morphologies in polymer blends: effect of interfacial tension, viscosity and physical cross-links, Polymer. 41 (2000) 3037–3045.

[58] S. Ravati, B.D. Favis, Morphological states for a ternary polymer blend demonstrating complete wetting, Polymer. 51 (2010) 4547–4561.

[59] C.-P. Wu, C.-C. Wang, C.-Y. Chen, Influence of asymmetric ratio of polystyrene-block-poly(methyl methacrylate) block copolymer on the crystallization rate of PLA, Eur. Polym. J. 66 (2015) 160–169.

[60] K. Yoshikawa, N. Ofuji, M. Imaizumi, Y. Moteki, T. Fujimaki, Molecular weight distribution and branched structure of biodegradable aliphatic polyesters determined by s.e.c.-MALLS, Polymer. 37 (1996) 1281–1284.

[61] E. Jalali Dil, P.J. Carreau, B.D. Favis, Morphology, Miscibility and Continuity Development in Poly(lactic acid)/Poly(butylene adipate-co-terephthalate) Blends, Polymer. 68 (2015) 202–212.

[62] V. Jost, Blending of Polyhydroxybutyrate-co-valerate with Polylactic Acid for Packaging Applications – Reflections on Miscibility and Effects on the Mechanical and Barrier Properties, Chem. Biochem. Eng. Q. 29 (2015) 221–246.

CHAPTER 5   ARTICLE 2: PARTIAL TO COMPLETE WETTING TRANSITIONS IN IMMISCIBLE TERNARY BLENDS WITH PLA: THE INFLUENCE OF INTERFACIAL CONFINEMENT[2]

Ali M. Zolali, Basil D. Favis

CREPEC, Department of Chemical Engineering, École Polytechnique de Montréal, Montréal, QC, Canada H3C3A7

5.1 Abstract

In this study, it is shown that the three different intermediate phases in melt blended ternary PLA/PHBV/PBS, PLA/PBAT/PE and PLA/PE/PBAT systems all demonstrate partial wetting, but have very different wetting behaviors as a function of composition and annealing. The interfacial tension of the various components, their spreading coefficients and the contact angles of the confined partially wet droplets at the interface are examined in detail. A wetting transition from partially wet droplets to a complete layer at the interface is observed for both PHBV and PBAT by increasing the concentration and also by annealing. In contrast, in PLA/PE/PBAT, the partially wet droplets of PE at the interface of PLA/PBAT coalesce and grow in size, but remain partially wet even at a high PE concentration of 20% and after 30 min of quiescent annealing. The dewetting speed of the intermediate phase is found to be the principal factor controlling these wetting transitions. This work shows the significant potential for controlled wetting and structuring in ternary polymer systems.

5.2 Introduction

Fluid interfaces are common in nature and play a crucial role in many industrial products and applications including pharmaceuticals, the food industry and biomaterials. Thermodynamically

---

unstable emulsions are typically stabilized by adsorption of molecular surfactants or amphiphilic polymers at the liquid-liquid interface. The use of soft particles to stabilize emulsions has recently gained attention as an alternative to Pickering emulsions which are stabilized by hard particles [1]. This class of emulsions is conceptually similar to Pickering emulsions, but the underlying mechanisms responsible for the stabilization of the emulsions are very different. Soft particles can stretch and adapt to the interface and this deformation can increase the adsorption energy, all energies associated with the adsorption of a particle on a surface, by orders of magnitude relative to solid particles even up to $10^6\ k_\mathrm{B}T$ [2].

Two distinct wetting regimes can be defined based on equilibrium interfacial forces in emulsions of 3-phase immiscible liquids: complete wetting and partial wetting. These equilibrium morphologies can be predicted by Harkin's spreading coefficients generalized by Torza and Mason [3,4]. For an A/B/C ternary emulsion system, they introduced a set of three spreading coefficients λ_{ijk} as follows:

$$\lambda_{BAC} = \gamma_{BC} - (\gamma_{AB} + \gamma_{AC}) \tag{5.1a}$$

$$\lambda_{ABC} = \gamma_{AC} - (\gamma_{AB} + \gamma_{BC}) \tag{5.1b}$$

$$\lambda_{ACB} = \gamma_{AB} - (\gamma_{AC} + \gamma_{BC}) \tag{5.11c}$$

where γ_{ij} are the interfacial tensions between components. λ_{ABC}, for example, indicates the tendency of component B to spontaneously spread at the interface of components A and C which is considered the complete wetting regime. However, when all the three coefficients are negative, partial wetting, where all phases meet at a three-phase line of contact, is predicted since the spreading does not occur. A negative but close to null spreading coefficient suggests a weak partial wetting driving force whereas the larger absolute value of a negative spreading coefficient implies a strong driving force towards partial wetting [5].

Thus, the partial wetting of a soft liquid, phase A, at the interface of B and C is completely determined by the interfacial tensions between components and the shape of these partially wet particles is defined by the Neumann triangle (NT) construction which relates the interfacial tensions and contact angles of a three phase liquid system in static equilibrium state (see Figure 5.1a) [6]. The shape of partially wet droplets at fluid-fluid interfaces has recently been the

subject of some experimental and theoretical studies [7–9]. Zhang and Kim [8] were among the first to employ the NT method to describe partially wet polymer particles of poly(buty1ene terephthalate) (PBT) layered between two sheets of polystyrene (PS) and poly(methy1 methacrylate) (PMMA). They also applied the in situ NT method in the interfacial tension measurement of interfacially reactive systems [10]. Virgilio et al.[9] employed the NT construction to self-assembled partially wet structures in ternary and quaternary polymer blends. They showed that the interfacial tension ratios achieved by the in situ NT construction compare well with the results obtained from the classical breaking thread (BT) method.

Immiscible polymer blends are a class of materials analogous to emulsions and the principals that govern them. A considerable literature has been published on the fundamental morphology development of binary polymer blends whereas much less work has been carried out on ternary immiscible polymer blends. Recently, Ravati and Favis [11] systematically studied the morphological states for a ternary polymer blend demonstrating complete wetting. Thermodynamically driven composite-droplet, double-percolated, and matrix/two separate dispersed morphologies have been reported by them which are in agreement with earlier observations [12–14]. Virgilio et al.[15] investigated novel highly organized microstructures which were induced by partial wetting in melt-processed ternary blends of HDPE, PS, and polypropylene (PP). Their work has revealed the self-assembling of a close-packed array of partially wet droplets of PS at the interface of HDPE and PP. In another work, they have exploited the concept of partial-complete wetting towards the design and generation of porous polylactic acid scaffolds in a quaternary polymer blend [16].

Ravati and Favis [17] have studied the phase evolution of partially wet droplets of PLA after a quiescent annealing process in a ternary blend of poly(butylene succinate) (PBS)/polylactide (PLA)/poly(ε-caprolactone) (PCL) and have concluded that the film drainage is the controlling stage in the interfacial coalescence of PLA droplets. An interfacial reaction induced morphology change has been reported in a ternary blend of polyamide-6/polycarbonate/polystyrene with partial wetting morphology [18]. Most recently, some preliminary studies examining the wetting transition of partially wet droplets to a completely wet layer at the interface have been examined [19–21]. The composition dependence of wetting was demonstrated in ternary PLA/PBS/poly(3-

hydroxybutyrate-co-hydroxyvalerate) (PHBV) blends and it was shown that partially wet PHBV droplets can be reorganized in the form of a complete wet layer at the interface [19]. Similar morphology transitions have recently been reported in the literature [20,21]. Wang et al.[21] observed a partial to complete wetting transition at a very low concentration of poly(ether-block-amide) (PEBA) in ternary low density PE/PEBA/polyethylene terephthalate demonstrating weak partial wetting. They attributed this anomalous wetting behavior to the competition between dewetting and coalescence at the interface.

The dynamics (breakup and coalescence) of fluid droplets dispersed in a fluid matrix have been addressed in numerous studies [22–25]. Coalescence is a complex process driven by the interfacial tension to reduce the total interfacial area of a system. Generally, the coalescence of dispersed phases in binary polymer blends has been shown to follow the $R^n \sim kt$ relation in which R is the droplet size at time t, n and k (the rate constant) are related to the coarsening mechanism [26–30] and does not change with time [26]. Fortelný et al.[28–31] have formulated theoretical models that describe the coalescence in polymer blends. They arrived at different mean particle size relations by the coalescence time for various interfacial mobility and driving forces. They showed that the contribution of gravitational force and Brownian motion are negligible in high viscosity systems and the only driving force inducing coalescence in the absence of an external driving force is intermolecular forces such as van der Waals forces. They concluded that the mean-radius-time relation of $R^3 \sim kt$ best describes such systems with immobile interfaces in which k is the coalescence rate.

So far, however, the underlying mechanisms related to the stability of partially wet ternary systems remain quite unclear. This paper aims to gain a fundamental understanding of the morphological transitions of partial wetting in ternary polymer blends demonstrating both weak and strong partial wetting tendencies. Dewetting and interfacial coalescence will be investigated by studying the influence of quiescent annealing time in model systems with low and high interfacial tensions. The influence of composition and interfacial tension will be studied and quantitative morphological analysis will be used to determine the principal underlying mechanisms related to the wetting transitions at the interface of co-continuous blends.

5.3 Experimental

5.3.1 Materials

Polylactide (PLA) Ingeo™ Biopolymer 3001D was supplied by NatureWorks. Poly(butylene adipate-co-terephthalate) (PBAT) (Ecoflex™) and poly(butylene succinate) (PBS) (Bionelle™ 1001MD) were respectively obtained from BASF and Showa Denko America Inc. Poly(3-hydroxybutyrate-co-hydroxyvalerate) (PHBV) was provided by Tianan Biopolymer (Enmat™ Y1000P). Sclair® 2710 a grade of high density polyethylene (PE) from Nova Chemicals was also used. Table 5.1 summarizes the main characteristics of the polymers used in this study. A vacuum oven at 70 °C was used to remove residual moistures from samples for at least 8 hours before being used in the experiments.

Table 5.1. Principal properties of the polymers used in the study.

Material	Melt density (g/cm^3) at 190°C	M_n/M_w (kg/mol)	T_m (°C)	η^* (Pa.s) at 190°C and 25 s^{-1}	$\eta_0 \times 10^3$ (Pa.s) at 190°C
PLA	1.13	107/152[a]	170	630	680
PBS	1.1	47/140[b]	113	470	660
PBAT	1.15	72/126[c]	120	540	670
PHBV	1.1	92/240[d]	172	150	-
PE	0.8	-/48[e]	128	380	565

a, b, c, and d were respectively obtained from Ref. [53], [54], [55], and [56]; e: obtained from the supplier.

M_n: number average molecular weight; M_w: weight average molecular weight.

T_m: melting temperature determined from DSC experiments.

η^*: complex viscosity; η_0: zero shear viscosity calculated by Carreau-Yassuda model.

5.3.2 Blend Preparation and Annealing

A 30 mL Plasti-Corder Digi-System internal mixer from Brabender Instruments Inc. was used to prepare three different ternary blends of PLA/PHBV/PBS, PLA/PBAT/PE and PLA/PE/PBAT with various volume compositions in a one-step mixing process at 190 °C and 50 rpm for 8 min under a constant nitrogen flow. A small amount (0.2 wt.%) of Irganox B-225 from CIBA was added

during the mixing process in order to prevent thermal degradation. In order to freeze-in the morphology, the samples were cut and quenched in ice-water. Quiescent annealing was performed using a hot press at 190 °C for 5, 10, 20, and 30 min under a nitrogen flow and the annealed samples were immediately immersed in ice-water to freeze-in the morphology. Annealing is an effective process to minimize kinetic effects due to the absence of mixing while maximizing thermodynamic effects to dictate the morphology development. In this way one can examine the stability of structures and understand the principal features of thermodynamically driven morphologies.

5.3.3 Rheological Measurements

A controlled-stress rheometer (Physica MCR 301, Anton Paar) equipped with a 25 mm parallel plate disk geometry with a gap of 1 mm was used to perform rheological measurements. All rheological measurements were performed on compression molded disks of 25mm diameter and 1.2mm thickness at 190 °C under nitrogen atmosphere. Strain and time sweep tests were performed to determine the linear viscoelastic region and thermal stability of samples. All polymers showed acceptable thermal stability (less than 10% viscosity reduction) at the set temperature in the time sweep experiment at 10% strain and 1 rad/s after 40 min except PHBV which shows some molecular weight loss as reported elsewhere [32].

5.3.4 Interfacial Tension Measurement

The breaking thread method which is based on the growth of capillary instabilities related to the break-up of a liquid cylinder in a liquid matrix was used to measure the interfacial tensions between polymer pairs [33]. A thread of diameter in the range of 40-70 micron of the component with the higher melting temperature was sandwiched between two films of the other polymer and was then placed in a Mettler FP-82HT hot-stage at 190 °C. The distortions of the threads were filmed by Streampix v.III software under an optical microscope from Nikon (Optiphot-2) and the captured images were then analyzed by SigmaScan v.5 software. Each value is the average of a minimum of ten BTM measurements.

A second in situ method based on the Neumann triangle combined with microscopy techniques is used to measure the interfacial tensions of PBS/PHBV and also PLA/PBAT. The geometrical characteristics of systems with a partially wet structure, i.e. contact angles between interfacial

tensions at a 3-phase line of contact, can be used to calculate the interfacial tension between components if one of the interfacial tensions is known. Therefore, the partially wet structure of the studied ternary blends was used to determine the interfacial tensions. Details of the technique can be found elsewhere [9]. This method is useful for the calculation of the interfacial tension of systems with ultra-low interfacial tensions which require long times to develop distortions in the BTM. It is also beneficial for systems with thermal-sensitive components such as PHBV, which demonstrates a very heat sensitive complex viscosity and which makes it impossible to measure the interfacial tension through the breaking thread method.

5.3.5 Microtoming/Field Emission Scanning Electron Microscopy

A Field Emission SEM machine (JSM 7600F, JEOL) operated at a voltage of 2 keV was employed for the morphology observation. The specimens were first cryo-microtomed using a microtome (Leica RM 2065) equipped with a glass knife and a cryo-chamber (LN21). Then, the PLA phase was extracted using tetrahydrofuran (THF) as a solvent in order to create a contrast between phases in the PLA/PHBV/PBS systems. For the PLA/PE/PBAT and PLA/PBAT/PE ternary systems no solvent was used. The specimens were then sputter coated with gold/palladium by plasma deposition and placed in the microscope.

5.3.6 Ultramicrotoming/Atomic Force Microscopy

A Bruker Dimension Icon atomic force microscope was used in PeakForce tapping mode with quantitative nanomechanical analysis (QNM) on ultra-microtomed samples to map the surface of the microtomed samples. The samples for AFM analysis were microtomed using a Leica EM UC7 ultra-microtome equipped with Leica EM FC7 cryo-chamber and a cryo 45° DiAtome diamond knife. ScanAsyst-Air probes (Bruker AFM Probes Camarillo, CA) consist of a SiN cantilever with Si probe, 5 nm nominal tip radius, and 0.4 N/m nominal spring constant were used for all experiments. Nanoscope (v8) and Nanoscope Analysis (v1.40) software were used for the AFM operation.

5.3.7 Image Analysis

Image analysis was performed on SEM and AFM micrographs using a digitizing table from Wacom and SigmaScan v.5 software. The interfacial presence (%) of partially wet droplets was calculated based on the area fraction of droplets located at the interface to the total area of the minor phase on the SEM or AFM micrographs. The number average diameter of PE droplets with a strong partial wetting tendency and the major axis of droplets (PHBV and PBAT) a with weak partial wetting tendency were measured using standard corrections [34] and by counting approximately 50-200 droplets. It is reported as a particle size. The thickness of the middle layer in the ternary blends and the phase size in the co-continuous binary blends were estimated by averaging the thicknesses at different points without taking into account the edges and the converging parts. The thickness values are the average of at least 5 images from two different samples.

5.4 Results and Discussion

5.4.1 Interfacial Tensions and Spreading Coefficients

It has been shown that the shape and contact angle of a soft partially wet droplet at the interface depends on the interfacial tension between components and its Young's modulus [7]. However, for a polymeric drop, both the shape and contact angle follow the Neumann triangle [7]. Blends of PLA/PHBV/PBS, PLA/PBAT/PE, and PLA/PE/PBAT were prepared and their morphologies clearly demonstrate partial wetting morphologies as shown in Figure 5.1. The goal here was to construct one system (PLA/PHBV/PBS) comprised of partially wet droplets with low interfacial tensions with the other components and another (PLA/PE/PBAT) with high interfacial tensions.

The interfacial tensions of these systems were calculated through the Neumann triangle method. Table 5.2 summarizes the average contact angles of N measurements at the three-phase line of contact between components of the different systems. The detailed geometrical constructions fitted to microscopy observations are provided in Supporting Information in ANNEX A. The interfacial tensions and the corresponding spreading coefficients for both the PLA/PHBV/PBS and PLA/PE/PBAT systems are summarized in Table 5.3 and Table 5.4, respectively. The PLA/PHBV/PBS blend is comprised of polymer pairs with very low interfacial tensions, while the ternary blend of PLA/PE/PBAT is comprised of components with one low and two high interfacial

tensions. Thermodynamic analysis predicts partial wetting for all the PLA/PHBV/PBS, PLA/PBAT/PE and PLA/PE/PBAT systems as all the spreading coefficients are negative. In other words, the most thermodynamically stable structure for these systems is when all phases are assembled in the form of a 3-phase line of contact.
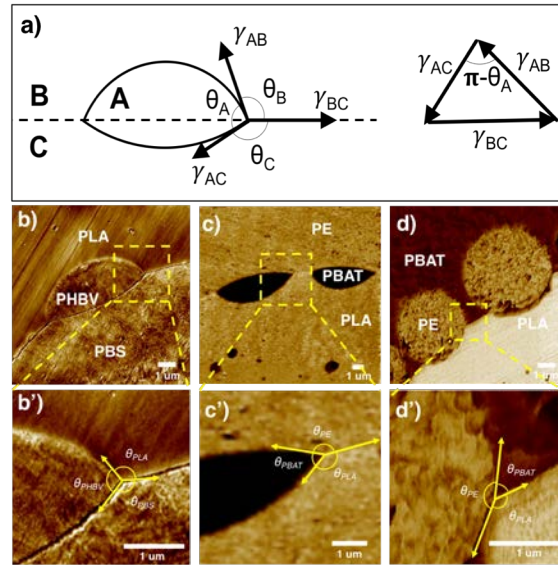
Figure 5.1. a) The equilibrium interfacial tensions at a 3-phase line of contact in a ternary A/B/C system with the corresponding Neumann triangle. AFM micrographs demonstrating contact angles in b, b') PLA/PHBV/PBS 50/5/50, c, c') PLA/PBAT/PE 50/5/50, and d, d') PLA/PE/PBAT 50/5/50.

Table 5.2. Average values of the geometrical constructions of the partially wet droplets in PLA/PHBV/PBS, PLA/PBAT/PE and PLA/PE/PBAT systems.

Blend	N	θ_A°	θ_B°	θ_C°	Γ_A	Γ_B	Γ_C
PLA/PHBV/PBS[a]	24	99 ± 10	114 ± 12	141 ± 8	1.4 ± 0.1	1.6 ± 0.2	1.1 ± 0.2
PLA/PE/PBAT[b]							
	33	65 ± 9	118 ± 6	174 ± 4	8.4 ± 0.6	8.7 ± 0.7	1.0 ± 0.1
PLA/PBAT/PE[c]							

[a] PHBV (A) droplet at the interface of PLA (B)/PBS (C).

[b] PBAT (A) droplet at the interface of PLA (B)/PE (C).

[c] PE (C) droplet at the interface of PBAT (A)/PLA (B).

Table 5.3. Interfacial tension values (mN/m) at 190 °C.

Method	PLA/PBS	PBS/PHBV	PLA/PHBV	PLA/PBAT	PLA/PE	PBAT/PE
BTM	0.20 ± 0.05	-	-	0.40 ± 0.04	5.0 ± 0.49[a]	4.7 ± 0.35
in-situ NT	0.27 ± 0.06	0.24 ± 0.07	0.17 ± 0.04	0.57 ± 0.07	-	-

[a] From Ref.[35]

The PLA/PHBV/PBS 50/5/50 blend, Figure 5.1b, represents a "weak partial wetting" tendency where a PHBV droplet with a low contact angle ($\lesssim 90°$) forms at the interface. Weak partial wetting is a term that has been proposed in this laboratory to describe the thermodynamic tendency of systems with a low driving force towards forming partially wet droplets at the interface [5,21]. Partial wetting behavior is also observed when PE is the partially wet droplet at the interface of PLA/PBAT in the PLA/PE/PBAT 50/5/50 system (Figure 5.1c). It forms a spherically shaped droplet with a wide contact angle of 174° which is characteristic of a droplet with a "strong partial wetting" tendency. Strong partial wetting is defined here as a high driving force towards generating segregated partially wet droplets at the interface.

Table 5.4. Spreading coefficients (mN/m) of the ternary blends.

Spreading Coefficients	PLA/PHBV/PBS[a]	PLA/PBAT/PE[b]	PLA/PE/PBAT[c]
λ_{BAC}	− 0.14	− 0.10	− 9.30
λ_{ABC}	− 0.20	− 0.70	− 0.70
λ_{ACB}	− 0.34	− 9.30	− 0.10
Prediction	Partial Wetting	Partial Wetting	Partial Wetting

[a] PLA/PHBV/PBS (A=PHBV, B=PLA, C=PBS)

[b] PLA/PBAT/PE (A=PBAT, B=PLA, C=PE)

[c] PLA/PE/PBAT (A=PE, B=PLA, C=PBAT)

The thermodynamic analysis of the spreading coefficients, λ, clarifies the weak and strong partial wetting terminology. For example, λ_{ABC} shows the tendency of phase B to completely segregate phases A and C by spreading at the interface whereas a negative λ indicates the partial wetting behavior and its value may indicate how one phase evades to spread at the interface. The absolute

value of the spreading coefficient of the partially wet PE is significantly larger than the two other spreading coefficients in the PLA/PE/PBAT system as calculated in Table 5.4. The opposite is the case for PLA/PHBV/PBS where the absolute values of the spreading coefficients are very small and close to nil which is observed when PHBV and PBAT are partially wet droplets at the interface of PLA/PBS and PLA/PE, respectively (Table 5.4). Therefore, a large value of the ratio between spreading coefficients (for example $\lambda_{BAC}/\lambda_{ACB} = 93$ in the PLA/PE/PBAT system) implies a strong tendency for PE to partially wet the PLA/PBAT interface while a small value (for example $\lambda_{BAC}/\lambda_{ABC} = 0.01$ in the PLA/PBAT/PE system) predicts a weak partial wetting behavior for PBAT at the PLA/PE interface. The comparison of these ternary polymer systems thus provides the opportunity to rigorously relate interfacial tension to the development and stability of weak and strong partial wettings at the interface as a function of composition.

5.5 Weak Partial Wetting
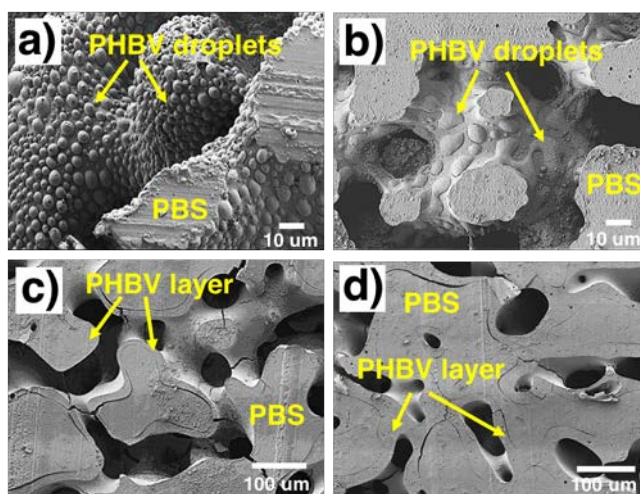
Figure 5.2. SEM micrographs of 50/x/50 PLA/PHBV/PBS with different concentrations of PHBV annealed for 10 min: a) 5%, b) 10%, c) 20%, d) 33%.

5.5.1 PLA/PHBV/PBS

Figure 5.2 shows the morphology of the PLA/PHBV/PBS blends after 10 min of annealing treatment. Partially wet droplets of PHBV, localized at the interface of PLA/PBS, are evident in Figure 5.2a after extraction of the PLA phase. These droplets start to coalesce at the interface upon

an increase in concentration of PHBV from 5 to 10% and finally form a continuous layer at the interface at 20% and 33% PHBV. From the thermodynamic point of view, a ternary liquid system should either demonstrate a complete wetting or a partial wetting structure unless kinetic parameters are influencing the morphology.

The morphology observation in Figure 5.2a is in agreement with the thermodynamic prediction but the results obtained for systems with a higher concentration of PHBV in Figure 5.2b-d diverge from the predictions in Table 5.4. One might speculate that the low composition of PHBV (<10%) could be considered insufficient to spread at the interface and construct a completely wet structure. However, it has been shown that polystyrene spreads and completely wets the interface of polyethylene and poly(methyl methacrylate) even at the very low concentration of 3% [13]. In order to examine validity of spreading theory in systems with ultralow interfacial tensions, the ternary blend of PLA/PBS/PBAT 50/5/50 was prepared, which is predicted to demonstrate complete wetting [36]. The submicron PBS layer segregates the PLA and PBAT phases and constructs a complete wet structure at 5% of PBS (see Supporting Information in ANNEX A). This proves that a minor component in a low interfacial tension system with a thermodynamic tendency for complete wetting can spread at the interface even at very low concentrations.
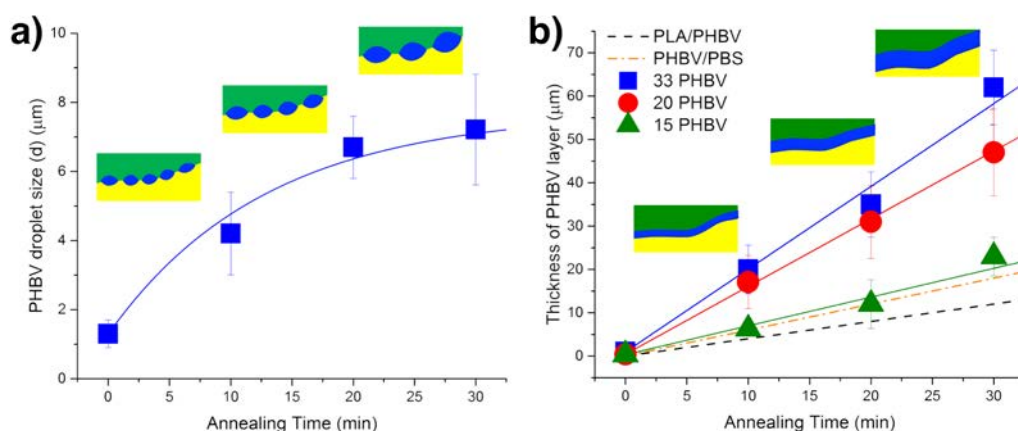
Figure 5.3. a) Diagram of diameter (d) of PHBV droplets in the PLA/PHBV/PBS 50/5/50 system as a function of annealing time and b) diagram of PHBV layer thickness in PLA/PHBV/PBS 50/x/50 with 15, 20, and 33% of PHBV compared with the predictions of PHBV coarsening in binary 50/50 PLA/PHBV (dashed line) and 50/50 PHBV/PBS (dashed-dotted line) as functions of annealing time.

In order to further examine the stability of the wetting behavior of PLA/PHBV/PBS, the system was subjected to quiescent annealing. Figure 5.3a shows the diagram of PHBV droplet size versus annealing time. The PHBV droplets grow in size with a slow growth rate as annealing time increases. However, upon increasing the PHBV content from 5 to 15%, the transition of morphology from partial wetting to complete wetting thoroughly changes the morphology evolution of the PHBV phase at the interface of PLA/PBS. 10% PHBV forms an extended, but incomplete layer structure at the interface which was not quantified here. The blends containing higher PHBV contents (15, 20 and 33%) demonstrate linear growth in the thickness of the PHBV layer with annealing time as illustrated in Figure 5.3b. The linear growth of the middle phase has been reported for different tri-continuous ternary polymer blends showing complete wetting behavior [17,20].

5.5.2 PLA/PBAT/PE

Figure 5.4 shows the morphology of the PLA/PBAT/PE system with PBAT as the minor phase. 5% PBAT clearly forms partially wet droplets at the interface of 50/50 PLA/PE even after being annealed for up to 30 min (only the results of 5 and 10 min of annealing are presented in Figure 5.4a', and a"). However, similar to what was observed in the PLA/PHBV/PBS system, the partially wet PBAT droplets coalesces and form a complete wet layer at the interface upon increasing the PBAT concentration to 10% and higher. The morphological results of PLA/PBAT/PE 50/10/50 before and after 5 and 10 min of annealing are demonstrated in Figure 5.4b, b', and b".

When PBAT is the minor component in the PLA/PBAT/PE system as can be seen in Figure 5.5a, the diameter of the partially wet droplets of 5% PBAT gradually grows with annealing time and levels off after 30 min. Apparently partially wet systems achieve a quasi-stable morphology at high annealing times and it may be an indication that the particle-particle distance between droplets at the interface increases to the point where further coalescence is difficult. On the other hand, increasing the PBAT content to 10% causes the PBAT droplets to evolve into a completely wet layer at the interface of PLA/PE. In this latter case a very different behavior with annealing is observed and the complete layer thickness grows linearly with annealing time with no apparent plateau evident even at 30 min of annealing. This behavior is similar to what was observed in the

PLA/PHBV/PBS system where a transition from partial to complete wetting occurred upon increasing the concentration of the minor phase.
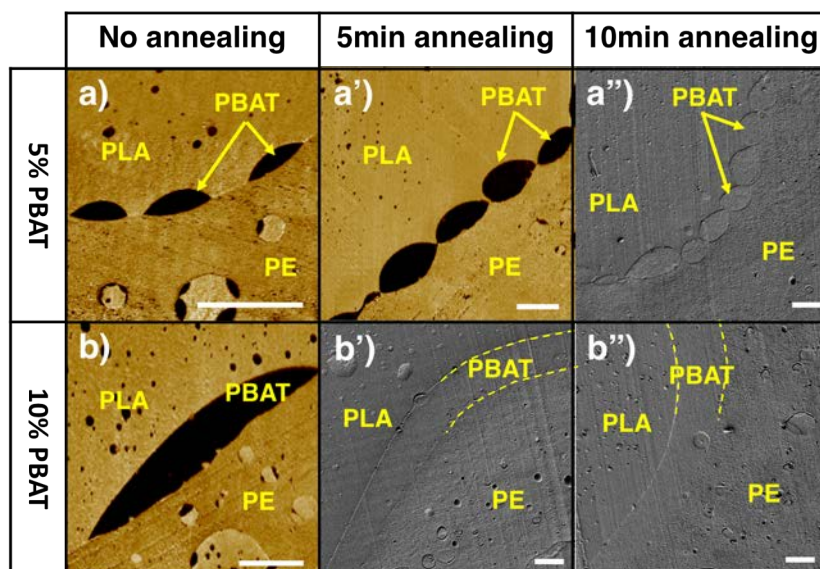
Figure 5.4. AFM and SEM micrographs of the PLA/PBAT/PE 50/x/50 system at 0, 5 and 10 minutes quiescent annealing. a, a', and a" are with 5% PBAT and b, b', and b") are with 10% PBAT. The white bars denote 10 µm.
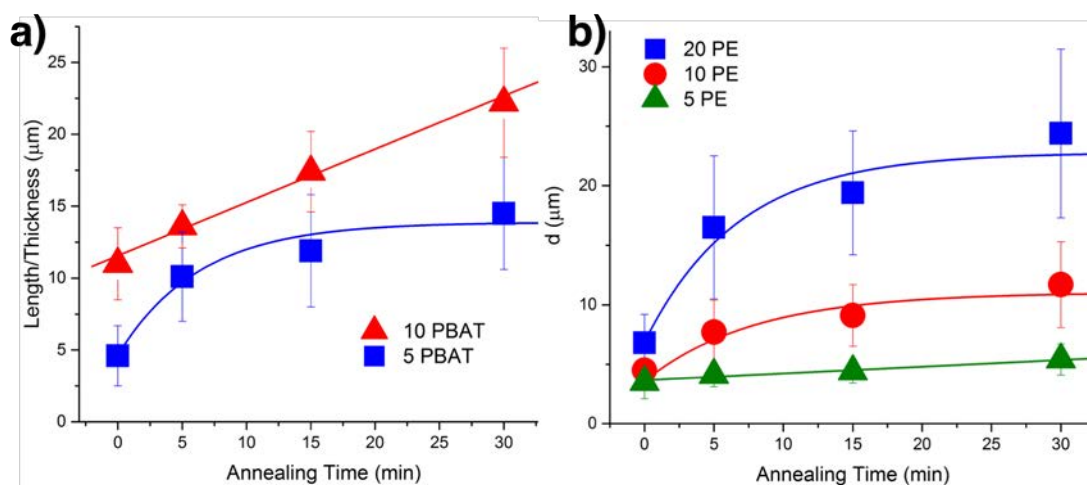
Figure 5.5. a) PBAT droplet length or layer thickness as a function of annealing time in PLA/PBAT/PE 50/x/50 system with 5 and 10% of PBAT. b) PE droplet diameter (d) as a function of annealing time in PLA/PE/PBAT 50/x/50 system with 5, 10, and 20% of PE.
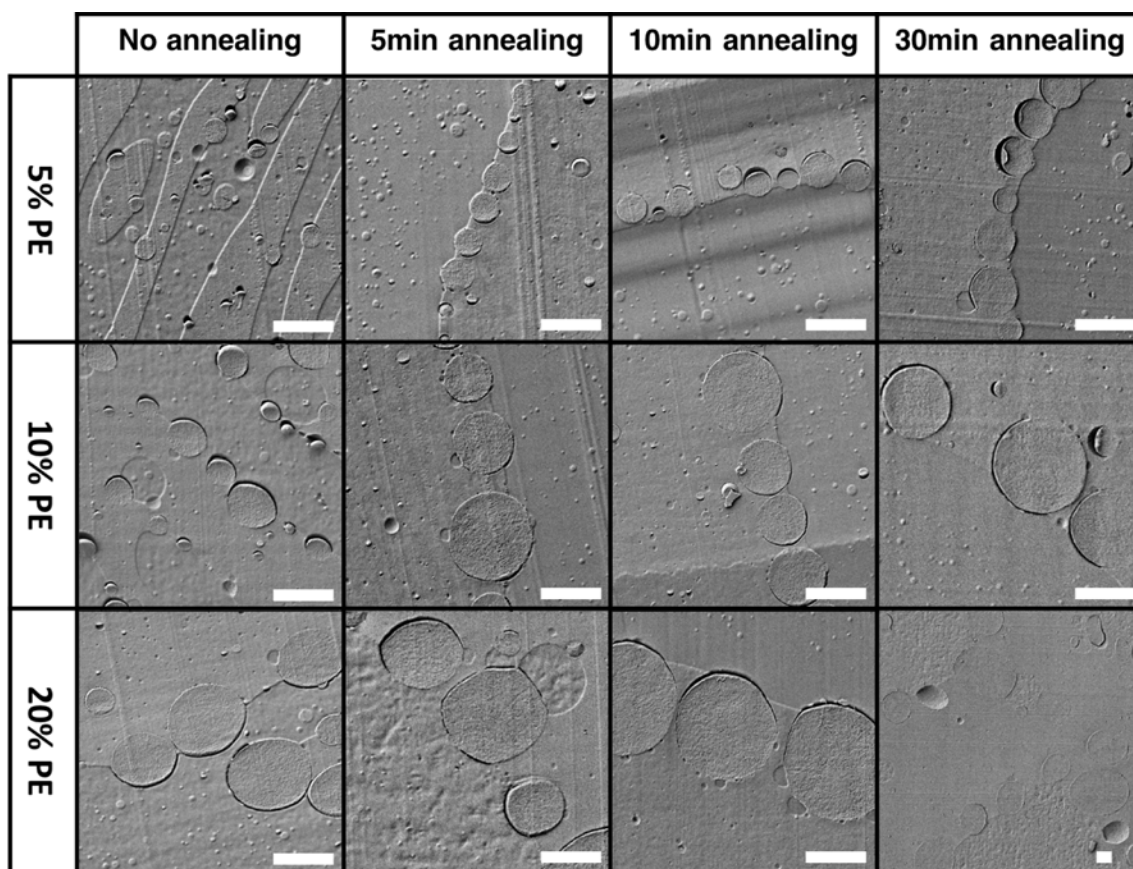
Figure 5.6. SEM micrographs of the PLA/PE/PBAT 50/x/50 system with 5, 10, and 20% of PE annealed for 5, 10, and 30 min. The white bars denote 10 μm.

5.5.3 Strong Partial Wetting

PLA/PE/PBAT. The minor PE phase in the PLA/PE/PBAT 50/x/50 ternary system generates a partial wetting structure as shown in Figure 5.6. The morphologies are stable and neither the composition nor the annealing change the partial wetting behavior. The size of the PE droplets increases with concentration of PE from 5 to 20% which suggests the development of interfacial coalescence while still preserving a partially wet structure at the interface of PLA/PBAT. The annealing of the blends also reveals a growth trend in the size of the partially wet PE particles with annealing time with a plateau behavior at higher annealing times (Figure 5.5b). This plateau behavior with annealing time was also observed for the weak partial wetting systems of PLA/PHBV/PBS at low concentrations of partially wet droplets. These results are in agreement with a recent report on the interfacial coarsening of partially wet droplets in ternary polymer blends

[17]. However, the wetting transitions observed in the PLA/PHBV/PBS system and the partially wet PBAT droplets in the PLA/PBAT/PE blend raise the important question of how morphology develops in the partially wet systems. In the following sections we will examine the causes of such wetting transitions at a liquid-liquid interface.

5.5.4 Interfacial Confinement and Coalescence

In all the systems examined in this study a third phase is situated between two others. Clearly this spatial limitation of the intermediate phase imposes a form of confinement. These systems thus present the very interesting possibility of studying the influence of interfacial confinement on coalescence for both the partially wet droplets and the completely wet layers observed in this work.
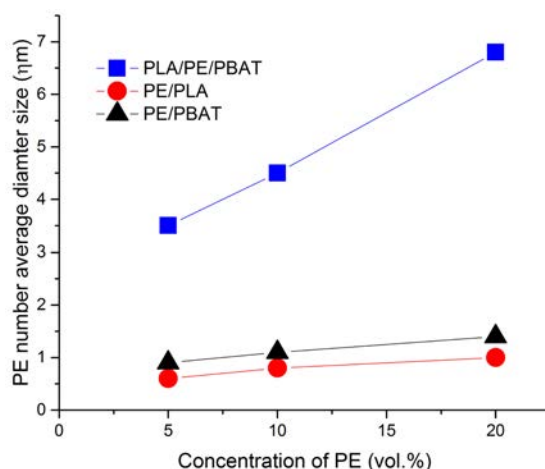
Figure 5.7. PE number-average droplet size as a function of composition comparing the confined partially wet droplets in the ternary blends with that for dispersed PE droplets in binary blends.

Partially wet confined droplets. Figure 5.7 compares the dependence of the PE number average droplet size on composition for the confined droplets showing strong partial wetting in PLA/PE/PBAT and that of the corresponding two binary systems PLA/PE and PBAT/PE. These data are obtained immediately after melt mixing and without any annealing whatsoever. At 5% PE, the ternary system already demonstrates a much higher phase size of 3.5 μm as compared to 0.6 and 0.8 μm for the two binary systems respectively. The slope of the ternary curve at 0.22 is also significantly greater than that of the binary systems, 0.02 (PLA/PE) and 0.03 (PBAT/PE). Thus, as

composition increases, the effects of coalescence for the confined PE droplets in the ternary system become even more marked. This is a clear and quantitative indication of the important effects of interfacial confinement on coalescence for a strong partially wet system.

The enhanced coalescence for partially wet confined droplets is even more evident when examining the systems after static annealing. The diagrams in Figure 5.8 demonstrate the third power of number average droplet size as a function of annealing time in which all of them follow the relationship of $R^3 \sim kt$ in which k is the coalescence rate i.e. particle growth rate. The results of the interfacial presence (%) and coalescence rate of the partially wet systems are presented in Table 5.5. It was found that more than 90% of the PE phase with the strong partial wetting tendency is located at the interface of PLA/PBAT while about 73% of PBAT and 75% of PHBV with the weak partial wetting tendency were present at the interfaces of PLA/PE and PLA/PBS, respectively, right after the melt mixing process.
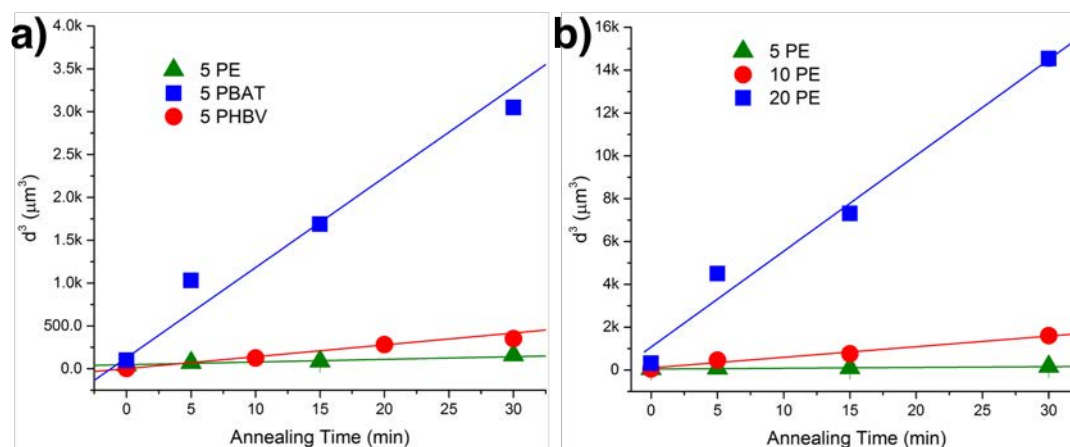
Figure 5.8. Diagrams of the third power of the number average diameter (d^3) as a function of annealing time: a) 5% PHBV in PLA/PHBV/PBS, 5% PBAT in PLA/PBAT/PE and 5% PE in PLA/PE/PBAT; b) 5, 10 and 20% PE in PLA/PE/PBAT.

The growth rates of these strong and weak partially wet droplets with annealing time were compared to the growth rates reported for binary matrix/dispersed systems reported in the literature (see Table 5.5). It can be seen that the interfacial growth rates of the partially wet systems, either with weak or strong partial wetting tendencies, are much higher than those of binary systems. It has been reported in the literature that geometrical confinement can significantly increase the

coalescence of droplets [43,44]. The growth rate of the strong partially wet PE droplets at the interface of PLA/PBAT during annealing dramatically increases with composition which further confirms the strong influence of interfacial confinement on the morphology development at the interface.

Table 5.5. Interfacial concentration and particle growth rates of partially wet droplets at the interface during annealing. Comparison of growth rates with binary systems.

Ternary systems with	PHBV 5% in PLA/PHBV/PBS (weak partial wetting)	PBAT 5% in PLA/PBAT/PE (weak partial wetting)	PE 5% in PLA/PE/PBAT (strong partial wetting)	PE 10% in PLA/PE/PBAT (strong partial wetting)	PE 20% in PLA/PE/PBAT (strong partial wetting)
PW phase (%) at the interface	75	73	95	93	92
Particle growth rate k (μm^3/min)	1.8 ± 0.1	13.2 ± 2.1	0.5 ± 0.06	6.2 ± 0.6	56.0 ± 5.8
Supporting phases (50/50) growth rate k' (μm/min)	PLA/PBS	PLA/PE	PLA/PBAT		
	1.5 ± 0.5	17.2 ± 1.4	2.1 ± 0.5		
Binary systems with 10-20 wt% typically show particle growth rates k (μm^3/min)	in the range of $10^{-4} - 1.0$*				

* Obtained from Ref.[30,31,37–42]

Comparing the 5% data in Table 5.5, it can be seen that significant differences in the coalescence rate, k, with annealing time can be observed. Firstly, the strong partially wet PE droplets show a much lower rate of coalescence (0.5 μm^3/min) than the weak partially wet systems PHBV (1.8 μm^3/min) and PBAT (13.2 μm^3/min). This significant difference is likely due to a high dewetting rate for the strong partially wet PE droplets and this will be discussed in more detail later in the paper. In the case of the two weak partially wet droplets, it should also be noted that the coalescence rate for 5% PBAT droplets is significantly higher than that of 5% PHBV.

The significant differences in the coarsening rate during annealing between 5% PBAT and 5% PHBV can be attributed, in part, to the differences in the coarsening rate of the supporting co-continuous phases. In the absence of any external forces, Brownian motion is usually held

responsible to cause contact between droplets in a binary dispersed/matrix system, but its effect is negligible due to high melt viscosity in polymer blends [28]. It is believed that the internal flow caused by the coarsening of the two co-continuous phases induces the force required for contact of the partially wet droplets confined at the interface [15,20]. The capillary flow inside continuous channels creates a mobile interface, and consequently the confined partially wet droplets move towards each other. It has been reported that the higher the interfacial tension in co-continuous systems, the faster the coarsening and consequently the higher the contact probability [45–47]. The growth rate k' of co-continuous PLA/PBS and PLA/PE systems were measured to be 1.5±0.5 µm/min and 17.2±1.4 µm/min, respectively. These results correlate well with the coalescence rates of the PHBV and PBAT droplets in Table 5.5 and imply that although they both have weak partial wetting behavior, the higher growth rate of the supporting PLA/PE phases contributes to the significantly higher coalescence rate of PBAT, i.e. 13.2±2.1 µm^3/min, while the lower growth rate of the supporting PLA/PBS phases only results in a PHBV particle coalescence rate of 1.8±0.1 µm^3/min.

Completely wet confined layer. In this part of the paper, the growth rate of the completely wet intermediate layer as a function of annealing time will be examined. In this case the coarsening rate, k', is estimated by following the growth of the thickness of the layer in the ternary systems using an approach to study the coarsening of co-continuous systems studied previously [46]. In addition, the coarsening rate k' of the middle phase in the ternary systems is compared to those of the constituent binary blends of the two ternary (PLA/PHBV/PBS and PLA/PBAT/PE) systems (see Table 5.6).

The growth rate of the completely wet intermediate layer comprised of 20% PHBV and 33% PHBV in PLA/PHBV/PBS is considerably higher than the coarsening rates estimated for the constituent co-continuous binary systems, PLA/PHBV (0.4 µm/min) and PHBV/PBS (0.6 µm/min) (see Figure 5.3b) which appears to indicate that a confined completely wet layer in ternary systems also demonstrates enhanced coalescence as was observed for the partially wet case. However, in contrast, the coarsening rate of the PBAT intermediate layer in PLA/PBAT/PE has a significantly lower coarsening rate than that for the constituent binary co-continuous systems of PLA/PBAT and PBAT/PE. Understanding this latter behavior will require further work.

Table 5.6. Coarsening rates of the middle phase in tri-continuous ternary blends of PLA/PHBV/PBS and PLA/PBAT/PE vs. their constituent co-continuous binary blends during annealing.

Ternary systems with	PHBV 20% in PLA/PHBV/PBS	PHBV 33% in PLA/PHBV/PBS	PBAT 10% in PLA/PBAT/PE	PBAT 20% in PLA/PBAT/PE
Coarsening rate k' (μm/min)	1.6±0.5	1.9±0.4	0.4±0.2	1.0±0.2
Binary systems (50/50)	**PLA/PHBV**	**PBS/PHBV**	**PLA/PBAT**	**PBAT/PE**
Coarsening rate k' (μm/min) [a]	0.4	0.6	1.5	23.4

a Estimated from the model in Ref.[46]

5.5.5 Dewetting/Coalescence

It is believed that dewetting and coalescence are two main parameters that influence the wetting behavior of a minor phase confined at the interface of two phases [17,19–21]. Wang et al. [21] proposed a conceptual model based on the dewetting of a polymer film to explain the formation of partially wet droplets at the interface of two other polymers. In the model, they generalized the dewetting of a film on solid/liquid substrates to a film at the interface of two different liquids since it has been shown that the concept of dewetting can be employed in polymer-polymer interfaces [48–50]. They showed that the dewetting speed (v) can be evaluated from Equation 5.2:

$$v = \frac{\gamma \theta_e^3}{k_d \eta} \tag{5.2}$$

where γ is the interfacial tension, θ_e is the equilibrium contact angle in radians, k_d is a dissipation factor, and η is the viscosity of the film phase. This relation implies that for high contact angle values, one would expect a faster dewetting process as it strongly depends on the third power of contact angle. This is the case of the PE droplets with a strong partial wetting tendency, a large contact angle ($\theta_e = 174° \approx 3.1$ radians) is observed at the interface (see Table 5.2). Also, note that PE has much lower viscosity than PBAT and PLA (see ANNEX A), which furthermore contributes to its dewetting at the interface. However, due to the very low interfacial tension of polymeric systems as compared to the surface tension of solids/liquids (about an order of magnitude), the dewetting velocity becomes much slower particularly in systems with lower contact angles, as in the cases of PHBV ($\theta_e = 99° \approx 1.7$ radians) and PBAT ($\theta_e = 65° \approx 1.1$

radians), at the interface of PLA/PBS and PLA/PE, respectively (Table 5.2). The higher viscosity of PBAT, compared to that of PE, also hinders the dewetting process by reducing the dewetting speed.

If one considers the contact angle, interfacial tension components and viscosity in equation 5.2, an estimate of the relative dewetting speeds of the various droplets at the interface can be made. In this case the contact angle used is taken from Table 5.2, the value of the interfacial tension used is the average value of the two constituent interfacial tensions (see Table 5.3) and the value of the viscosity at 25 rad/s is used from Table 5.1. This analysis results in about 61 times greater dewetting speed for the partially wet PE phase as compared to that for partially wet PBAT ($v_{PE}/v_{PBAT} \approx$ 61). The relative dewetting speed of the PE phase to the PHBV phase is estimated to be $v_{PE}/v_{PHBV} \approx 38$ and PHBV/PBAT is found to be 2 ($v_{PHBV}/v_{PBAT} \approx 2$). This very high dewetting speed for partially wet PE droplets explains why stable partially wet PE droplets are observed over a wide range of concentrations and even during annealing in the PLA/PE/PBAT ternary system. In the case of partially wet PBAT and PHBV droplets, the more than one order of magnitude lower dewetting speeds allow for coalescence to dominate at higher concentrations and/or at higher annealing times and hence partial wetting to complete wetting transitions are observed in the PLA/PBAT/PE and PLA/PHBV/PBS ternary systems, respectively. Although both PHBV and PBAT droplets can be considered to have low dewetting speeds, it should be noted that the dewetting speed of PBAT droplets is slower than that for PHBV droplets by a factor of ca. 2. This ordering of dewetting speeds is in line with virtually all of the morphological observations made in this work (see Figure 5.9). Thus, the dewetting behavior of droplets at the interface appears to be the dominant factor in determining strong or weak partial wetting behavior.

5.5.6 Principal Transitions in Wetting Behavior

When the concentration of PHBV and PBAT is increased above 5%, partially wet droplets, due to their low dewetting speed, transform into a completely wet layer at the interface of PLA/PBS and PLA/PE (see Figure 5.2 and Figure 5.4). At 5% of PHBV or PBAT at the interface, the coalescence/dewetting balance favors dewetting, however, increasing the minor phase content to 10%, shifts the coalescence/dewetting balance to favor coalescence. The coalescence of a high number of partially wet droplets at the interface leads to the development of the continuous layer

at the interface as coalescence overtakes dewetting. This case is schematically shown in Figure 5.9a,b.

Similar wetting behavior transitions for PHBV or PBAT at the interface can be observed as a function of annealing time. At 5% of PHBV or PBAT at the interface partially wet behavior is maintained over a wide range of annealing times. At 10% PHBV or PBAT, wetting behavior changes as a function of annealing time. Annealing time would be expected to principally influence coalescence over dewetting due to the well-known and very significant coarsening of the supporting co-continuous phases.[46,51,52] The high coarsening effects of the supporting co-continuous phases lead to a lower interfacial area and significantly increases coalescence for the confined droplets at the interface. Thus, in the case of annealing, the dewetting/coalescence equilibrium changes in the favor of coalescence and a complete wet layer forms from the coalescence of partially wet droplets at the interface. Some small differences in the transition behavior of the weak partially wet PHBV and PBAT droplets are also observed. The PBAT droplets transit to a complete layer at 10% with annealing (see Figure 5.4) while the partially wet PHBV droplets transform to a highly extended, but incomplete layer at that concentration (see Figure 5.2b). In the case of PHBV, the transition to the complete layer occurs at 15% PHBV. This enhanced morphological transition for partially PBAT droplets can be attributed to both the higher coarsening rate of the supporting co-continuous PLA/PE phase and the lower dewetting speed of PBAT at the interface as compared to PHBV. Both of these factors will enhance coalescence of PBAT in the PLA/PBAT/PE system as compared to PHBV in the PLA/PHBV/PBS system. These transitions are schematically shown in Figure 5.9a,b. The larger contact angle of PHBV at the PLA/PBS interface ($\theta_e = 1.7$ radians) implies a faster dewetting speed than that of PBAT at the PLA/PE interface with $\theta_e = 1.1$ radians. In addition, PHBV possesses a lower viscosity than PBAT which further facilitates its dewetting at the interface.

In contrast, the spherical-shape droplets of PE in PLA/PE/PBAT grow in size and maintain their partial wetting behavior with increasing PE content (see Figure 5.6 and schematic Figure 5.9c). Although increasing the concentration of PE favors coalescence, the high dewetting speed (more than an order of magnitude greater than that for PHBV or PBAT) prevents the transition of the partially wet droplets toward a complete wet layer. Even in the case of annealing, a partially wet

PE droplet structure at the interface of PLA and PBAT is maintained over the entire range of annealing times.

These results taken together strongly indicate that, although coalescence is a very important factor, it is principally the dewetting speed which determines the final wetting regime in any of the ternary systems studied here. Figure 5.9 schematically shows the range of morphological structures that can be achieved through a control of contact angle (dewetting speed), concentration and annealing time. This work shows the excellent potential for controlled wetting and structuring in ternary polymer systems and presents a route towards the preparation of a range of new morphological structures.
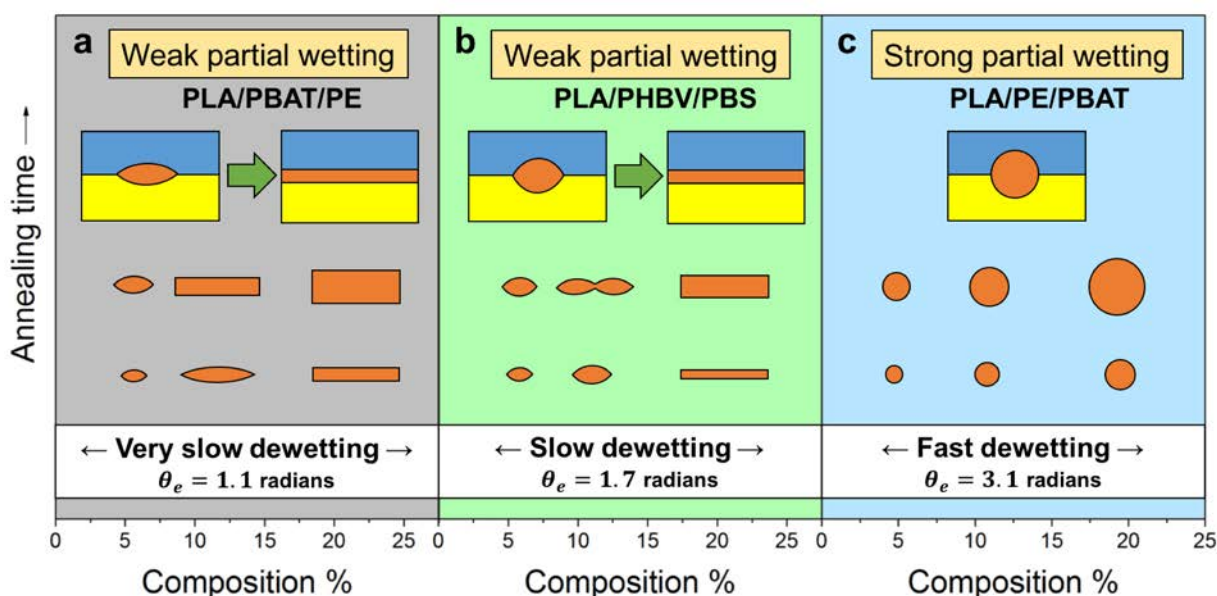
Figure 5.9. The range of morphological structures observed in this work based on dewetting behavior, composition and annealing time.

5.6 Conclusion

This work reports on the wetting transitions of confined intermediate phases at the interface of two other polymers. The three different melt blended ternary systems, PLA/PHBV/PBS, PLA/PBAT/PE and PLA/PE/PBAT, demonstrate diverse partial wetting behaviors. The detailed interfacial tension measurements through the breaking thread method and in-situ Neumann triangle approach allow for a rigorous thermodynamic analysis, which predicts weak partial wetting for

both PLA/PHBV/PBS and PLA/PBAT/PE ternary blends and strong partial wetting for the PLA/PE/PBAT system. In all systems, partially wet droplets of the 5% minor phase were developed at the interface right after mixing and retain the partially wet structure after annealing. However, at concentrations above 10%, a wetting transition from partial to complete wetting (complete layer forms) occurs in the systems with weak partially wet behavior. This is further accentuated through the application of quiescent annealing. It is found that due to the low dewetting speed and the interfacial confinement, the dewetting/coalescence equilibrium favors coalescence. During annealing, this effect is further intensified by the coarsening of the supporting co-continuous phase. Thus, partially wet droplets of PBAT or PHBV coalesce into a completely wet layer at the interface with increasing concentration and also by annealing. In contrast, the partially wet droplets of PE at the interface of PLA/PBAT coalesce and grow in size, but, due to a high dewetting speed, remain partially wet even at a high PE concentration of 20% and after 30 min of quiescent annealing. In all these systems, despite the enhanced coalescence imposed by the interfacial confinement, the wetting behavior is clearly dominated by the dewetting speed. It is shown that dewetting speed, concentration of the intermediate phase, annealing time and interfacial confinement significantly influence the morphology development in both partial and complete wetting morphologies and can be controlled to generate a wide range of new morphological structures.

5.7 Acknowledgment

5.8 References

[1]   B.P. Binks, T.S. Horozov, eds., Colloidal Particles at Liquid Interfaces, Cambridge University Press, Cambridge, U.K., 2006.

[2]   H. Monteillet, M. Workamp, J. Appel, J.M. Kleijn, F. a. M. Leermakers, J. Sprakel, Ultrastrong Anchoring Yet Barrier-Free Adsorption of Composite Microgels at Liquid Interfaces, Adv. Mater. Interfaces. 1 (2014) 1300121.

[3]   W.D. Harkins, A General Thermodynamic Theory of the Spreading of Liquids to Form

Duplex Films and of Liquids or Solids to Form Monolayers, J. Chem. Phys. 9 (1941) 552.

[4] S. Torza, S.. G. Mason, Three-phase interactions in shear and electrical fields, J. Colloid Interface Sci. 33 (1970) 67–83.

[5] P. Le Corroller, B.D. Favis, Effect of viscosity in ternary polymer blends displaying partial wetting phenomena, Polymer. 52 (2011) 3827–3834.

[6] P.-G. de Gennes, F. Brochard-Wyard, D. Quere, Capillarity and Wetting Phenomena: Drops, Bubbles, Pearls, Waves, Springer, New York, 2004.

[7] H. Mehrabian, J. Harting, J.H. Snoeijer, Soft particles at a fluid interface, Soft Matter. 12 (2015) 1–17.

[8] X. Zhang, J.K. Kim, Interfacial tension measurement with the Neumann triangle method, Macromol. Rapid Commun. 19 (1998) 499–504.

[9] N. Virgilio, P. Desjardins, G. L'Esperance, B.D. Favis, In Situ Measure of Interfacial Tensions in Ternary and Quaternary Immiscible Polymer Blends Demonstrating Partial Wetting, Macromolecules. 42 (2009) 7518–7529.

[10] J. Kim, W. Jeong, J. Son, H. Jeon, Interfacial tension measurement of a reactive polymer blend by the neumann triangle method, Macromolecules. 33 (2000) 9162–9165.

[11] S. Ravati, B.D. Favis, Morphological states for a ternary polymer blend demonstrating complete wetting, Polymer. 51 (2010) 4547–4561.

[12] J. Reignier, B.D. Favis, Control of the subinclusion microstructure in HDPE/PS/PMMA ternary blends, Macromolecules. 33 (2000) 6998–7008.

[13] J.H. Zhang, S. Ravati, N. Virgilio, B.D. Favis, Ultralow percolation thresholds in ternary cocontinuous polymer blends, Macromolecules. 40 (2007) 8817–8820.

[14] T.S. Valera, A.T. Morita, N.R. Demarquette, Study of morphologies of PMMA/PP/PS ternary blends, Macromolecules. 39 (2006) 2663–2675.

[15] N. Virgilio, C. Marc-Aurele, B.D. Favis, Novel Self-Assembling Close-Packed Droplet Array at the Interface in Ternary Polymer Blends, Macromolecules. 42 (2009) 3405–3416.

[16] N. Virgilio, P. Sarazin, B.D. Favis, Towards ultraporous poly(L-lactide) scaffolds from quaternary immiscible polymer blends, Biomaterials. 31 (2010) 5719–5728.

[17] S. Ravati, B.D. Favis, Interfacial coarsening of ternary polymer blends with partial and complete wetting structures, Polymer. 54 (2013) 6739–6751.

[18] S. Horiuchi, N. Matchariyakul, K. Yase, T. Kitano, Morphology development through an interfacial reaction in ternary immiscible polymer blends, Macromolecules. 30 (1997) 3664–3670.

[19] A.M. Zolali, B.D. Favis, Wetting behavior in ternary blends of PLA/PBS/PHBV, in: 65th Can. Chem. Eng. Conf., Calgary, AB, 2015.

[20] R. Dou, S. Li, Y. Shao, B. Yin, M. Yang, Insight into the formation of a continuous sheath structure for the PS phase in tri-continuous PVDF/PS/HDPE blends, RSC Adv. 6 (2016) 439–447.

[21] J. Wang, A. Reyna-Valencia, B.D. Favis, Assembling Conductive PEBA Copolymer at the Continuous Interface in Ternary Polymer Systems: Morphology and Resistivity, Macromolecules. 49 (2016) 5115–5125.

[22] Y. Liao, D. Lucas, A literature review on mechanisms and models for the coalescence process of fluid particles, Chem. Eng. Sci. 65 (2010) 2851–2864.

[23] A. Ramachandran, G. Leal, A scaling theory for the hydrodynamic interaction between a pair of vesicles or capsules, Phys. Fluids. 22 (2010) 17–21.

[24] D.Y.C. Chan, E. Klaseboer, R. Manica, Film drainage and coalescence between deformable drops and bubbles, Soft Matter. 7 (2011) 2235.

[25] I. Fortelný, Breakup and Coalescence of Dispersed Droplets in Compatibilized Polymer Blends, J. Macromol. Sci. Part B. 39 (2000) 67–78.

[26] W. Yu, C. Zhou, T. Inoue, Coalescence mechanism for the coarsening behavior of polymer blends during a quiescent annealing process. II. Polydispersed particle system, J. Polym. Sci. Part B Polym. Phys. 38 (2000) 2390–2399.

[27] R.C. Willemse, E.J.J. Ramaker, J. Van Dam, A.P. De Boer, Coarsening in molten quiescent

polymer blends: The role of the initial morphology, Polym. Eng. Sci. 39 (1999) 1717–1725.

[28] I. Fortelný, A. Živný, Coalescence in molten quiescent polymer blends, Polymer. 36 (1995) 4113–4118.

[29] I. Fortelný, A. Živný, Film drainage between droplets during their coalescence in quiescent polymer blends, Polymer. 39 (1998) 2669–2675.

[30] I. Fortelný, J. Jůza, B. Dimzoski, Coalescence in quiescent polymer blends with a high content of the dispersed phase, Eur. Polym. J. 48 (2012) 1230–1240.

[31] I. Fortelný, A. Živný, J. Jůza, Coarsening of the phase structure in immiscible polymer blends. Coalescence or ostwald ripening?, J. Polym. Sci. Part B Polym. Phys. 37 (1999) 181–187.

[32] T. Gerard, T. Budtova, Morphology and molten-state rheology of polylactide and polyhydroxyalkanoate blends, Eur. Polym. J. 48 (2012) 1110–1117.

[33] P.H.M. Elemans, J.M.H. Janssen, H.E.H. Meijer, The measurement of interfacial tension in polymer/polymer systems: The breaking thread method, J. Rheol. 34 (1990) 1311–1325.

[34] S.A. Saltikov, Proceedings of the Second International Congress for Stereology, in: H. Elias (Ed.), Proc. Second Int. Congr. Stereol., Springer-Verlag, Berlin, 1967: pp. 163–173.

[35] J. Wang, B.H. Lessard, M. Maric, B.D. Favis, Hierarchically porous polymeric materials from ternary polymer blends, Polymer. 55 (2014) 3461–3467.

[36] A.M. Zolali, B.D. Favis, Partial and Complete Wetting in Ultra-low Interfacial Tension Multiphase Blends with Polylactide, J. Phys. Chem. B. (2016) Submitted.

[37] J.G.M. van Gisbergen, Influence of electron beam irradiation on the microrheology of incompatible polymer blends: Thread break-up and coalescence, J. Rheol. 35 (1991) 63.

[38] F.M. Mirabella, J.S. Barley, Ostwald ripening in immiscible polyolefin blends, J. Polym. Sci. Part B Polym. Phys. 33 (1995) 2281–2287.

[39] F.M. Mirabella, Jr., Phase separation and the kinetics of phase coarsening in commercial impact polypropylene copolymers, J. Polym. Sci. Part B Polym. Phys. 32 (1994) 1205–1216.

[40] B. Crist, A.R. Nesarikar, Coarsening in Polyethylene-Copolymer Blends, Macromolecules. 28 (1995) 890–896.

[41] Z.H. Stachurski, G.H. Edward, M. Yin, Y. Long, Particle Coarsening in Polypropylene/Polyethylene Blends, Macromolecules. 29 (1996) 2131–2137.

[42] B. Dimzoski, I. Fortelný, M. Šlouf, M. Nevoralová, D. Michálková, J. Mikešová, Coalescence during annealing of quiescent immiscible polymer blends, E-Polymers. 11 (2011) 115–126.

[43] D. Chen, R. Cardinaels, P. Moldenaers, Effect of confinement on droplet coalescence in shear flow, Langmuir. 25 (2009) 12885–12893.

[44] P. De Bruyn, R. Cardinaels, P. Moldenaers, The effect of geometrical confinement on coalescence efficiency of droplet pairs in shear flow, J. Colloid Interface Sci. 409 (2013) 183–192.

[45] H. Veenstra, J. Van Dam, A.P. de Boer, On the coarsening of co-continuous morphologies in polymer blends: effect of interfacial tension, viscosity and physical cross-links, Polymer. 41 (2000) 3037–3045.

[46] Z. Yuan, B.D. Favis, Coarsening of immiscible co-continuous blends during quiescent annealing, AIChE J. 51 (2005) 271–280.

[47] J.R. Bell, K. Chang, C.R. Lopez-Barron, C.W. Macosko, D.C. Morse, Annealing of Cocontinuous Polymer Blends: Effect of Block Copolymer Molecular Weight and Architecture, Macromolecules. 43 (2010) 5024–5032.

[48] K. Shull, T. Karis, Dewetting dynamics for large equilibrium contact angels, Langmuir. (1994) 334–339.

[49] C. Wang, G. Krausch, M. Geoghegan, Dewetting at a Polymer−Polymer Interface: Film Thickness Dependence, Langmuir. 17 (2001) 6269–6274.

[50] F. Brochard Wyart, P. Martin, C. Redon, Liquid/liquid dewetting, Langmuir. 9 (1993) 3682–3690.

[51] E. Scholten, L.M.C. Sagis, E. van der Linden, Coarsening Rates of Bicontinuous Structures

in Polymer Mixtures, Macromolecules. 38 (2005) 3515–3518.

[52]   C.R. López-Barrón, C.W. Macosko, A new model for the coarsening of cocontinuous morphologies, Soft Matter. 6 (2010) 2637.

[53]   C.-P. Wu, C.-C. Wang, C.-Y. Chen, Influence of asymmetric ratio of polystyrene-block-poly(methyl methacrylate) block copolymer on the crystallization rate of PLA, Eur. Polym. J. 66 (2015) 160–169.

[54]   K. Yoshikawa, N. Ofuji, M. Imaizumi, Y. Moteki, T. Fujimaki, Molecular weight distribution and branched structure of biodegradable aliphatic polyesters determined by s.e.c.-MALLS, Polymer. 37 (1996) 1281–1284.

[55]   E.J. Dil, P.J. Carreau, B.D. Favis, Morphology, Miscibility and Continuity Development in Poly(lactic acid)/Poly(butylene adipate-co-terephthalate) Blends, Polymer. 68 (2015) 202–212.

[56]   V. Jost, Blending of Polyhydroxybutyrate-co-valerate with Polylactic Acid for Packaging Applications – Reflections on Miscibility and Effects on the Mechanical and Barrier Properties, Chem. Biochem. Eng. Q. 29 (2015) 221–246.

CHAPTER 6   ARTICLE 3: COMPATIBILIZATION AND TOUGHENING OF CO-CONTINUOUS TERNARY BLENDS VIA PARTIALLY WET DROPLETS AT THE INTERFACE[3]

Ali M. Zolali, Basil D. Favis

CREPEC, Department of Chemical Engineering, École Polytechnique de Montréal, Montréal, QC, Canada H3C3A7

6.1   Abstract

This work reports that a partially wet (PW) phase can compatibilize and toughen a co-continuous PLA/PA11 blend. Four different polymers: PBS, PBAT, EMA and EMA-GMA are examined for their capacity to partially wet the PLA/PA11 interface in a melt-blending process. All the blends exhibit a partial wetting morphology, but offer very different compatibilization efficacies and toughening effects. EMA-GMA demonstrates the best compatibilization effect as it reduces the co-continuous thickness to 5-6 μm, which is about half that of the original binary PLA/PA11 blend, followed by EMA while PBS and PBAT result in the least changes in morphology and properties. Self-assembled droplets of EMA at the PLA/PA11 interface result in a major increase in the ductility of the blend with an elongation at break of 260% as compared to 4% for the binary blend. A substantial increase in the notched Izod impact strength is also achieved with partially wet droplets of EMA with a value of 73 J/m, a four-fold increase as compared to the impact strength of the pure PLA and the PLA/PA11 binary blend. The blends with partially wet EMA demonstrate significant interfacial cavitation after the impact fracture test. This work shows that self-assembled rubbery EMA droplets at a co-continuous PLA/PA11 interface combine to compatibilize the system, improve interfacial adhesion and, after fracture, to interfacially cavitate through the continuous system. This interfacial percolation results in the shear yielding of the matrix and a

---

[3] Submitted to *Polymer.*

significant toughening effect ensues. These results indicate the potential of partially wet droplets to compatibilize and toughen co-continuous structures.

6.2 INTRODUCTION

Generally binary polymer blends display two types of morphologies: matrix/dispersed phase and co-continuous structures. The formation of these morphologies depend on the blend composition, the rheological and interfacial properties of the components, and processing conditions [1]. Over the last 15 years, co-continuous morphologies, have received significant attention since they have the potential to significantly broaden the application range of polymer blends [2,3]. The interfacial stabilization of the co-continuous morphology in an immiscible polymer blend is crucial since its highly interconnected nature renders it inherently unstable and it can coarsen rapidly during annealing or reprocessing [4,5]. Common approaches to modify the interface are the addition of copolymers as compatibilizers [4,6] or reactive blending [7,8] based on the in situ formation of block/graft copolymer at the interface. More recently, nonofillers [9–11] and Janus polymeric nanoparticles [8,12] have also been used to compatibilize/stabilize the co-continuous morphology of polymer blends. These partially wet particles have shown a potential to stabilize the interface.

Multicomponent blends, such as ternary and quaternary polymer blends, have also attracted increasing attention in recent years as they allow for the generation of diverse morphologies. Generally two types of wetting regimes are identified in three phase systems: complete wetting and partial wetting [13]. These wetting behaviors can result in a variety of complex phase structures such as core-shell and tri-continuous structures in the case of complete wetting [14,15] and multiple stacked morphologies in the case of partial wetting [16].

The equilibrium morphology in ternary blends can be predicted by spreading coefficients as proposed in Harkins spreading theory [17–20]. Three spreading coefficients (λ) are defined based on the interfacial tensions (γ) between components where three negative spreading coefficients predict partial wetting and one positive and two negative spreading coefficients predict complete wetting. Figure 6.1 schematically demonstrates these two cases in a ternary blend with the corresponding coefficients. The theory has been examined and proven to be quite reliable in the analysis of the morphology of a variety of ternary blends [21–23]. Although a number of studies

have examined the formation of complete wetting in ternary polymer blends [24–27], very few have reported on the partial wetting case [28–30]. In one of the first detailed studies on the partial wetting of polymers, Virgilio et al. [29] reported the self-assembly of polystyrene (PS) as segregated droplets at the interface of high density polyethylene (HDPE) and polypropylene (PP) through a partial wetting mechanism.

$$\lambda_{BAC} = \gamma_{BC} - (\gamma_{AB} + \gamma_{AC}) > 0 \qquad \lambda_{BAC} = \gamma_{BC} - (\gamma_{AB} + \gamma_{AC}) < 0$$
$$\lambda_{ABC} = \gamma_{AC} - (\gamma_{AB} + \gamma_{BC}) < 0 \qquad \lambda_{ABC} = \gamma_{AC} - (\gamma_{AB} + \gamma_{BC}) < 0$$
$$\lambda_{ACB} = \gamma_{AB} - (\gamma_{AC} + \gamma_{BC}) < 0 \qquad \lambda_{ACB} = \gamma_{AB} - (\gamma_{AC} + \gamma_{BC}) < 0$$
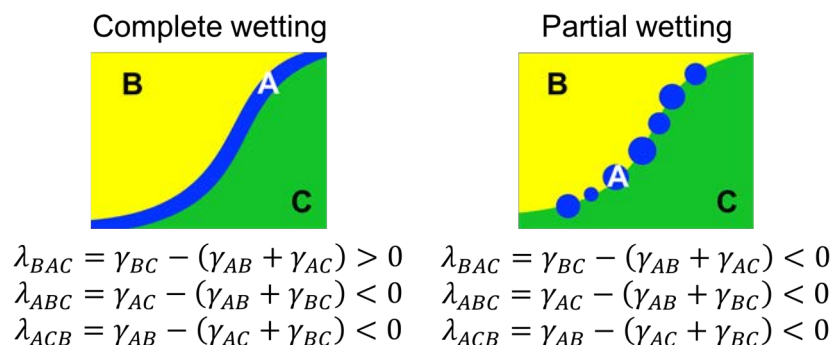
Figure 6.1. Schematics demonstrating complete and partial wetting morphologies in ternary polymer blends of minor component of A and two major components of B and C with the corresponding spreading coefficients.

The correlation between the morphology and mechanical properties of multiphase polymer blends has been well established and the control of morphology can be used to access a wide range of mechanical property sets [31–37]. It has been shown that changing from a matrix/dispersed structure to a co-continuous morphology can significantly improves the impact and tensile properties in different binary blends [3,31]. Co-continuous polylactide (PLA)/acrylonitrile-butadiene-styrene (ABS) compatibilized by styrene-acrylonitrile-glycidyl methacrylate copolymer (SAN-GMA) can improve impact strength and elongation at break [32]. Significant improvements in the impact strength and tensile properties have been obtained through the formation of core-shell structures in ternary blends [24,33–35]. Luzinov et al. [24] observed improvements in the tensile properties of core-shell polymers (PE/styrene-butadiene rubber) dispersed in a matrix of PS and correlated it to stress transfer through the rubbery shell to the core. In another work, the toughening mechanism in ternary PP/PA6/polyethylene-octene elastomer (POE) blends was analyzed through dilatometry experiments [36]. The results showed that that the volume strain decreases with increasing (PA6+POE) content up to 60 wt% which implies a significant increase in shear yielding

in the PP matrix. The observed enhanced toughness was attributed to the development of the intermediate completely wet phase of POE at the interface of the PP/PA6 system. High impact strength, with significantly enhanced heat resistance, was reported in quaternary blends of PLA, polycarbonate (PC), styrene-ethylene/butylene-styrene (SEBS), and ethylene methyl acrylate–glycidyl methacrylate (EMA-GMA). In that case, dispersed SEBS droplets effectively dilated the highly continuous PLA and PC matrices due to an effective compatibilization effect of EMA-GMA at the interface [37].

PLA and polyamide 11 (PA11) are both renewable materials which are promising alternatives to petroleum-based polymers [38–40]. PLA possesses high strength and stiffness, and excellent processability, but its broader application is limited due to the brittleness and low heat deflection temperature (HDT) [38,39]. On the other hand, PA11 is an engineering plastic with high thermal stability, high impact and chemical resistance, and excellent dimensional stability [40]. Biobased PA11 has been melt blended with PLA to improve its properties [41–44]. Despite the strong interfacial interactions between PLA and PA11 [45,46], very limited enhancements in the impact strength and elongation at break have been reported [41,42]. However, the formation of the co-continuous morphology for that system has been shown to significantly increase the HDT [43,44].

To date, it is still not clear how the incorporation of partially wet droplets at the interface of a co-continuous system can influence the mechanical properties in a ternary system. In this work, four different components, poly(butylene succinate) (PBS), poly(butylene adipate-co-terephthalate) (PBAT), ethylene methyl acrylate (EMA), and EMA-GMA will be examined to assess their potential to assemble as partially wet droplets at the interface of co-continuous PLA/PA11. The morphology of the blends and the effectiveness of the third component in the compatibilization of the co-continuous PLA/PA11 morphology will also be examined. The notched Izod impact strength and tensile properties of the blends will be evaluated and will be related to the morphology and thermal properties of the materials.

6.3 EXPERIMENTAL

6.3.1 Materials and Sample Preparation

Commercial homopolymers of polylactide (PLA) and polyamide-11 (PA11) were used as the main components. Poly(butylene succinate) (PBS), poly(butylene adipate-co-terephthalate) (PBAT), ethylene methyl acrylate (EMA) copolymer with 24 wt% of methyl acrylate content, and a terpolymer of ethylene methyl acrylate–glycidyl methacrylate (EMA-GMA) with 24 and 8 wt% of methyl acrylate and glycidyl methacrylate content, respectively, were employed as the third component to modify the morphology and mechanical properties. Table 6.1 summarizes the suppliers and grades for all materials used in this study. All the materials were dried at 70 °C under vacuum over night before being used in the experiments except EMA and EMA-GMA.

Table 6.1. Materials used in this work.

Material	Supplier	Grade	Density at 25 °C (g/cm^3)	η^* (Pa.s) at 200°C & 25 rad/s*	η_0 (Pa.s) at 200°C*
PLA	NatureWorks	3001D	1.24	405	420
PA11	Arkema	Rilsan BMNO	1.03	390	640
PBS	Showa Denko	Bionelle 1001MD	1.26	220	250
PBAT	BASF	Ecoflex	1.26	170	195
EMA	DuPont	Elvaloy AC 12024s	0.94	310	950
EMA-GMA	Arkema	Lotader AX8900	0.94	420	2400

η^*: complex viscosity.

η_0: zero shear viscosity calculated by fitting Carreau-Yassuda model.

* See Supporting Information in ANNEX B.

Ternary blends of PLA/x/PA, where x represents either PBS, PBAT, EMA, or EMA-GMA, were prepared through a melt blending process based on volume composition. This strategy of formulation resulted in a co-continuous structure for the supporting PLA/PA11 phases in the systems which was confirmed by solvent extraction experiments. All sample preparations were carried out on a co-rotating twin screw extruder (TSE), Leistritz ZSE 18HP with an L/D ratio of 40, at a screw speed of 100 rpm with a temperature profile of 170/180/190/200/200/200/200 °C from hopper to die. The extrudates were quenched in a cold-water bath and pelletized and dried

prior to the injection molding. A Sumimoto SE50S injection molding machine was used to mold dog-bone specimens of Type I (ASTM D638) and impact test bars (dimensions 12.7×63.5×3.2 mm). The temperature profile and screw speed were set to 190/200/210 °C from hopper to nozzle and 100 rpm, respectively.

Binary blends of PLA/EMA, PLA/EMA-GMA, PA11/EMA, and PA11/EMA-GMA, all at an 80/20 composition, were also melt blended in order to evaluate the miscibility between components through thermal analysis.

6.3.2 Scanning Electron Microscopy

SEM observations were performed on a Field Emission SEM machine (JSM 7600TFE, JEOL) operated at a voltage of 2 keV. The specimens were either microtomed using a microtome (Leica RM 2065) equipped with a glass knife and a cryo-chamber (LN21) or cryo-fractured in liquid nitrogen. PLA and PBAT were extracted from the microtomed samples using tetrahydrofuran (THF), 1,2,3-trichloropropane (TCP) in order to create a contrast between phases. Chloroform was also used to extract both PLA and PBS. EMA and EMA-GMA were both etched using cyclohexane in the same way. The Izod impact fractured samples were examined directly. The specimens were then coated with gold/palladium by plasma deposition and the surfaces were then observed using SEM unit.

6.3.3 Atomic Force Microscopy

Samples for AFM analysis were cut using a Leica EM UC7 ultra-microtome equipped with Leica EM FC7 cryo-chamber and a cryo 45° DiAtome diamond knife. The specimens were then placed under an AFM in PeakForce tapping mode with quantitative nanomechanical analysis (QNM) to map the surface morphology. ScanAsyst-Air probes (Bruker AFM Probes Camarillo, CA) consisting of a SiN cantilever with Si probe, 5 nm nominal tip radius, and 0.4 N/m nominal spring constant were used for all experiments. Nanoscope (v8) and Nanoscope Analysis (v1.40) software were used for AFM operation and image analysis.

6.3.4 Morphology Characterization, Solvent Extraction and Gravimetry

SEM and AFM micrographs were analyzed to measure both the number average, d_n, and volume average, d_v, of partially wet droplets at interface. A digitizing table from Wacom and SigmaScan V.5 software were employed to calculate the values of d_n and d_v, which were then modified applying the Saltikov correction procedure to consider the fact that droplets are not cut exactly at their equator [47]. An average of 300 to 400 droplets was measured for each diameter calculation.

The continuous galleries in the PLA/PA co-continuous network were assumed to be successions of cylinders of a diameter D. The specific interfacial area S between the PLA and PA phases were determined through the image analysis which corresponds to the porous PA specific surface area and the average pore size diameter D after the extraction of the PLA phase. The specific interfacial area S was calculated using equation 6.1 [48]:

$$S = \frac{P}{A} \tag{6.1}$$

where P is the measured interfacial perimeter of the PLA/PA interface and A is the area of the analyzed micrograph. The average pore size was then determined with equation 6.2 [49]:

$$D = \frac{4\phi_p}{S} \tag{6.2}$$

where D represents the average pore diameter, ϕ_p is the volume fraction of the extracted phase.

The continuity of the PLA phase was determined through the solvent extraction technique. The following equation was used to calculate the continuity of the PLA phase:

$$\% \; continuity \; of \; PLA = \left(\frac{m_i - m_f}{m_{PLA,i}}\right) \times 100 \tag{6.3}$$

in which m_i and m_f are the mass of the sample before and after extraction, respectively, and $m_{PLA,i}$ is the mass of PLA based on the blending formulation before extraction. The weight of samples was measured before and after extraction. A soxhlet extractor setup filled by chloroform as the solvent was utilized to perform the extraction measurements for a week. At least five measurements were performed for each reported value.

6.3.5 Interfacial Tension Measurement

The interfacial tension between components was measured using the breaking thread method which is based on the break-up of a cylindrical liquid in a liquid matrix due to the growth of sinusoidal distortions [50]. In this method, the component with the higher melting temperature is spun out of the melt to form a cylindrical thread with a diameter ranging from 40-70 μm, which is then placed between two thin films (thickness ranging from 200-500 μm) of the other polymer. All the threads were annealed at 60 °C overnight in order to remove the residual stresses frozen in during spinning. A hot-stage (Mettler FP-82HT) equipped with an optical microscope from Nikon (Optiphot-2) was used to measure the distortions of the thread at 190 °C. The digital images captured during the experiments using Streampix v.III software were then analyzed using SigmaScan v.5 software. The reported interfacial tension values are an average of at least ten measurements.

6.3.6 Differential Scanning Calorimetry

A DSC Q2000 (TA Instruments) machine was used to carry out the thermal analysis. The machine was calibrated with an indium standard under a dry nitrogen atmosphere flow of 50 mL/min. Samples of about 5-10 mg were weighed in aluminum pans. A modulated DSC (MDSC) mode was utilized to measure the glass transition temperature (T_g) of the components. The heating rate was set at 2 °C/min with an oscillation amplitude of ±1.27 °C and an oscillation period of 60 s over the temperature range of -80 °C to 100 °C. Conventional DSC heating and cooling runs were performed from 25 °C to 210 °C at a heating rate of 10 °C/min to evaluate other thermal transitions.

6.3.7 Mechanical tests

A universal testing machine (Instron 4400R) equipped with an extensometer was used at a crosshead speed of 5 mm/min to perform tensile experiments according to ASTM D638. Notched Izod impact measurements were carried out using a CS-137C-176 CSI Custom Scientific Instrument impact testing machine according to the ASTM D256 standard. The reported values are the average value of at least five replicated specimens for each sample.

6.4 RESULTS AND DISCUSSION

In this study a co-continuous PLA/PA11 is prepared and four components, PBS, PBAT, EMA and EMA-GMA are examined in order to assess their potential for partial wetting, compatibilization of the interface and influence on mechanical properties.
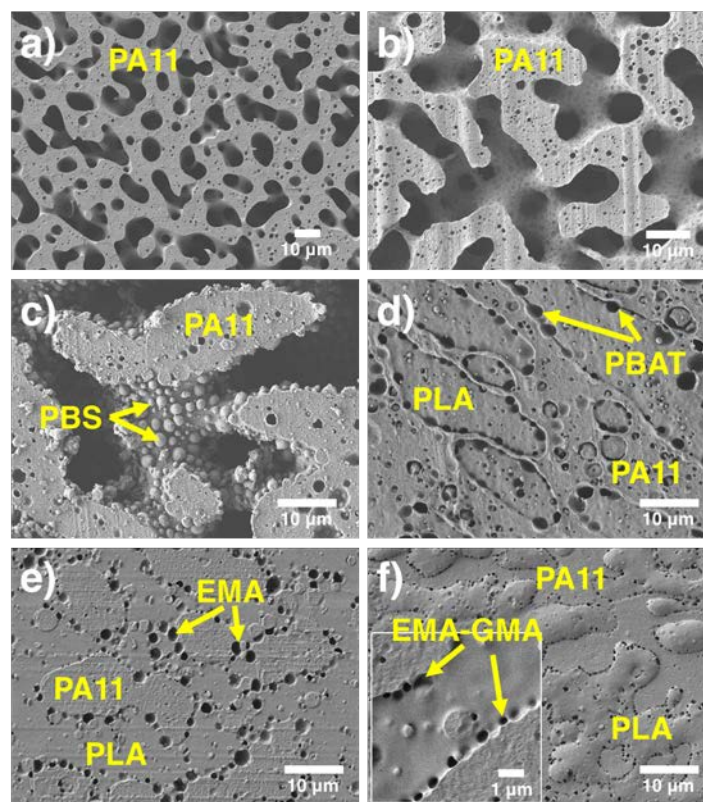
Figure 6.2. SEM micrographs of a) PLA/PA11 50/50, the PLA phase is extracted by chloroform; PLA45%/PBS10%/PA45%: b) after extraction of both PLA and PBS by chloroform, c) after extraction of PLA by THF; d) PLA45%/PBAT10%/PA45%, the PBAT phase is extracted by TCP; e) PLA45%/EMA10%/PA45%, the EMA phase is extracted by cyclohexane; f) PLA45%/EMA-GMA10%/PA45%, the EMA-GMA phase is extracted by cyclohexane.

6.4.1 Morphology

Both SEM and AFM were employed to identify the phase structure of the prepared ternary blends. Figure 6.2 shows the SEM micrographs of the PLA/PA11 (50/50) blends with and without 10% of

a third component. The binary PLA/PA11 50/50 clearly possesses a co-continuous morphology (see Figure 6.2a). By selectively extracting a specific phase it is possible to distinguish different phases. It is observed that the PLA/PA11 matrix retains the co-continuous structure and all of the third component polymers were found to localize at the interface of the PLA/PA11 phases. Figure 6.2b shows the co-continuous structure of the PLA/PBS/PA11 ternary blend after extraction of both PLA and PBS where the traces of PBS droplets are clearly detectable at the interface. PBS droplets can be clearly seen at the interface after extraction of PLA in the PLA/PBS/PA11 ternary blend demonstrating partial wetting behavior (Figure 6.2c). The voids in Figure 6.2d correspond to extracted PBAT droplets in the ternary PLA/PBAT/PA11 blend which, for the most part, partially wet the PLA/PA11 interface and which show a finer dispersed PBAT droplet size (1.6 microns) than that for the PBS droplets (2.1 microns) in the PLA/PBS/PA11 blend. Both EMA and EMA-GMA also form partially wet droplets at the interface of the PLA/PA11 system and the EMA-GMA droplets are much finer at 0.45 microns than EMA at 1.1 microns (Figure 6.2e,f).
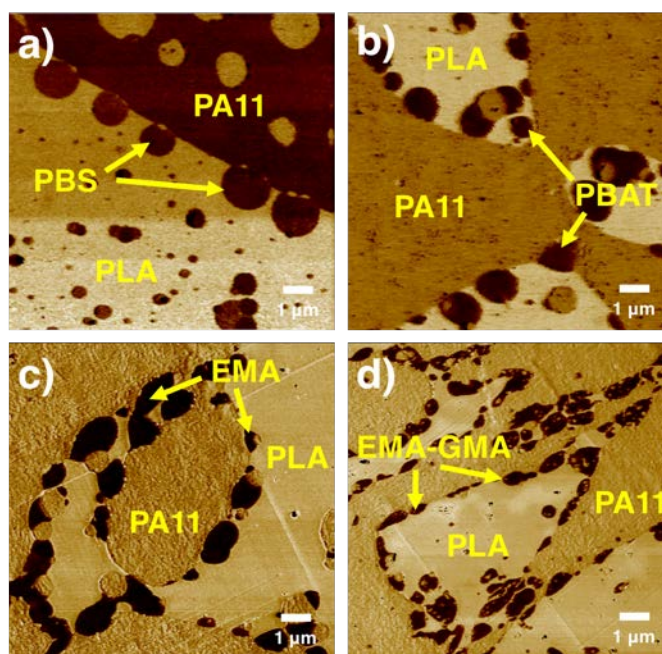
Figure 6.3. AFM micrographs of a) PLA45%/PBS10%/PA45%; b) PLA45%/PBAT10%/PA45%; c) PLA45%/EMA10%/PA45%; d) PLA45%/EMA-GMA10%/PA45%.

AFM micrographs in Figure 6.3 further illustrate the phase morphology of the ternary blends with even more detail related to the geometry of the droplets. PBS and PBAT were situated at the interface with a preference for the PLA side (see Figure 6.3a,b) which is attributed to the very low interfacial tensions between PLA/PBS and PLA/PBAT as reported in the literature [51,52]. However, EMA and EMA-GMA form more symmetrical droplets at the interface due to their similar affinity towards both PLA or PA11 as presented in Figure 6.3c,d.

Table 6.2. Effect of the third phase at the interface on the morphology characteristics of blends. dn, dv and L are the characteristics of droplets and their surface to surface distance at the interface.

Sample	d_n (μm)	d_v (μm)	L (μm)	D_{PLA} (μm)	D_{PA11} (μm)	PLA phase continuity %	% of droplets at the interface
PLA50/PA50	-	-	-	10±3	9.5±4	90±10	-
PLA45/PBS10/PA45	2.1	2.7	1.2±0.4	12±6	11±5	92±8	57±8
PLA45/PBAT10/PA45	1.6	2	1.0±0.8	11±5	8.5±5	96±5	78±5
PLA45/EMA10/PA45	1.1	1.6	0.6±0.5	8±4	8±3	98±6	91±3
PLA45/EMA-GMA10/PA45	0.45	0.65	0.35±0.2	6±2	5±3	98±5	94±2

The results of the image analysis and continuity measurements for the ternary blends are presented in Table 6.2. The PLA phase shows full continuity at 92-98%, which along with the remaining self-supporting porous PA11 implies a co-continuous morphology for the all blends. The PLA (D_{PLA}) and PA11 (D_{PA11}) phase sizes increased by the addition of PBS and PBAT from about 10 microns to about 12 microns. However, the partially wet droplets of EMA and especially EMA-GMA were markedly effective in reducing D_{PLA} and D_{PA11} of the ternary blends to 6-8 microns and 5-8 microns which is about half that of the binary PLA/PA11 system. This is significantly important since it shows that soft polymeric particles can act as a compatibilizer at the interface of two other polymeric phases similar to the effects of solid particles in Pickering emulsions. In order to get a better understanding of the compatibilization mechanism, the phase characteristics of the droplets

were analyzed and the results are presented in Table 6.2. The size of the PBS and PBAT droplets were 2.1 and 1.5 μm in which 67% and 78% of those phases were located at the interface, respectively. In contrast, more than 90% of the EMA and EMA-GMA droplets are situated at the PLA/PA11 interface with a droplet size of 1.2 and 0.45 μm, respectively. The inter particle distance (*L*) at the interface was also significantly decreased by replacing PBS or PBAT with EMA or EMA-GMA.

Based on the morphology studies above, the ternary PLA/EMA/PA11 and PLA/EMA-GMA/PA11 systems were selected based on their apparent enhanced interactions with both PLA and PA11 for further examinations.

6.4.2 Interfacial Interactions

The interfacial tension results obtained for the ternary PLA/EMA/PA11 system shows that EMA has similar interfacial tensions of 2.1 and 2.4 mN/m with PLA and PA11 respectively (Table 6.3), which confirms its almost equal tendency for PLA and PA11. The three negative spreading coefficients shown in Table 6.3 were determined based on the measured interfacial tensions and predict a partial wetting morphology for PLA/EMA/PA11. The interfacial tension results obtained for the ternary PLA/EMA-GMA/PA11 system shows that EMA-GMA also has similar interfacial tensions of 1.5 and 1.8 mN/m with PLA and PA11 respectively (Table 6.3), which also confirms its almost equal tendency for PLA and PA11. The three negative spreading coefficients for the PLA/EMA-GMA/PA11 system predicts partial wetting for this system, although the driving force for partial wetting is somewhat weaker than for PLA/EMA/PA11. The chemical reactions between the epoxy groups of EMA-GMA with either PLA or PA11 can further enhance the assembly of EMA-GMA droplets at the interface. These results underline the thermodynamic basis of the stable morphology development in these systems.

Table 6.3. Interfacial tension values and Spreading coefficients at 200 °C.

Ternary system	Interfacial tension (mN/m) @ 200°C	Spreading coefficient (mN/m)	Predicted morphology
PLA/EMA/PA11	$\gamma_{PLA/PA11} = 3.2 \pm 0.6$ $\gamma_{PLA/EMA} = 2.1 \pm 1.2$ $\gamma_{PA11/EMA} = 2.4 \pm 1.0$	$\lambda_{PLA/EMA/PA11} = -1.3 < 0$ $\lambda_{EMA/PLA/PA11} = -3.5 < 0$ $\lambda_{EMA/PA11/PLA} = -2.9 < 0$	Partial wetting: EMA minor phase partially wets the interface of PLA and PA11
PLA/EMA-GMA/PA11	$\gamma_{PLA/PA11} = 3.2 \pm 0.6$ $\gamma_{PLA/EGMA} = 1.5 \pm 0.9$ $\gamma_{PA11/EGMA} = 1.8 \pm 1.1$	$\lambda_{PLA/EGMA/PA11} = -0.1 < 0$ $\lambda_{EGMA/PLA/PA11} = -2.9 < 0$ $\lambda_{EGMA/PA11/PLA} = -3.5 < 0$	Partial wetting: EMA-GMA minor phase partially wets the interface of PLA and PA11

These observations can be explained by the high thermodynamic driving force of the EMA or EMA-GMA droplets for partial wetting at the interface of PLA/PA11 compared to the PBS or PBAT droplets. For example, the interfacial tension between PLA and PBAT is about 0.4 mN/m as reported in the literature [51]. The thermodynamic tendency to form a partially wet droplet of PBAT at the interface of PLA/PA11 can be determined by the absolute value of $\lambda_{PLA/PBAT/PA11}$. The absolute value for $\lambda_{PLA/PBAT/PA11}$ is low, due to the very low interfacial tension of 0.5 mN/m for PLA/PBAT [51,52] and assuming that the interfacial tension of PA11/PBAT is similar to that of PLA/PA11. PLA and PBAT are partial miscible polymers with a very low interfacial tension [52], thus, they could have similar interfacial tensions with a third polymer. In contrast, the spreading coefficient in the PLA/EMA/PA11 system ($\lambda_{PLA/EMA/PA11}$), shows an absolute value of 1.3 mN/m, which suggests a higher driving force for partial wetting for the EMA droplets. The high percentage at the interface and the low droplet sizes of the EMA and EMA-GMA droplets at the interface also support this this thermodynamic tendency.

The interfacial analysis above also confirms the selection of the PLA/EMA/PA11 and PLA/EMA-GMA/PA11 systems based on their apparent enhanced interactions with both PLA and PA11.

6.4.3 Thermal Analysis

The possible interfacial interactions of the third component at the PLA/PA11 interface were evaluated through the thermal analysis with an emphasis on EMA and EMA-GMA (Table 6.4). The analysis of the glass transition temperature showed that both EMA and EMA-GMA highly interact with PLA and PA11 as the glass transition temperatures of EMA and EMA-GMA both significantly increase and shift towards that of PLA and PA11.

Table 6.4. Thermal properties of the pure polymers and binary blends.

Samples	T_g (°C)*	T_{cc} (°C)	T_m (°C)	X_c (%)
PLA[a]	61	113	170	2
PA11[b]	43	–	189	57
EMA[c]	-48, -10	-	61	-
EMA-GMA[d]	-34	-	50	-
PLA/EMA 80/20	59[a]/-30[c]	122[a]	166[a]	4[a]
PA11/EMA 80/20	41[b]/-34[c]	-	189[b]	23[b]
PLA/EMA-GMA 80/20	59[a]/-34[d], -8[d]	128[a]	167[a]	7[a]
PA11/EMA-GMA 80/20	41[b]/-35[d], -6[d]	-	189[b]	22[b]

*See Supporting Information.

The glass transition temperature of EMA (-48 °C) increases to -30 °C and -34 °C in the blends of PLA/EMA 80/20 and PA11/EMA 80/20 and thus demonstrates a shift towards the glass transition temperature of PLA (61 °C) and PA11 (43 °C), respectively. These results indicate partial miscibility between EMA and the PLA, PA11 matrices. It has been reported that PLA is miscible with poly(methyl methacrylate) (PMMA) [53,54]. Thus, the methyl acrylate segments of EMA can promote miscibility between the PLA and EMA chains while the ethylene segments impose immiscibility.

For the PLA/EMA-GMA and PA11/EMA-GMA systems, the glass transition temperature change of EMA-GMA shows a 5 °C increase (from -35 to -30 °C) for both PLA/EMA-GMA and PA11/EMA-GMA blends. In addition to the interactions of the EMA segments with PLA and PA11, epoxide groups of the GMA segments can readily react with the terminal groups of PLA (hydroxyl and carboxyl groups) and PA11 (amine and carboxyl groups) and form graft copolymers at the interface [37,55,56]. This markedly influences the interfacial interactions between

PLA/EMA-GMA and PA11/EMA-GMA and is responsible for the glass transition temperature increase of EMA-GMA in the respective binary blends. The glass transition temperature of PLA was undetectable due to the overlap of the melting temperature of EMA and EMA-GMA with the glass transition temperature of PLA. In addition, the glass transition temperature of PA11 was almost unchanged in all the blends as it possesses very strong intra-molecular hydrogen bonding. The reduced melting temperature of PLA in the systems also supports a conclusion of partial miscibility between PLA with EMA and EMA-GMA.

Based on all of the morphology, interfacial and thermal analysis, the interfacial affinity and interactions of the four components studied with a PLA/PA11 blend are expected to increase in the order of PBS<PBAT<EMA<EMA-GMA. The strong interfacial affinity enhances the adsorption of the partially wet droplets to the blend interface. Thus, the reduced droplet size and a low interparticle distance of the thermodynamically stable droplets of EMA (or EMA-GMA) at the interface favor the compatibilization of the PLA/PA11 system. Similar results using polymeric Janus nanoparticles have been reported in the compatibilization of polymer blends [8,12]. Bahrami et al. [12] reported that poly(2,6-dimethyl-1,4-phenylene ether) (PPE) blended with poly(styrene-co-acrylonitrile) (SAN) is compatibilized using polymeric Janus nanoparticles. They attributed the compatibilization effect to the adsorption of the Janus particles to the interface. The facile and effective compatibilization approach demonstrated in this study uses readily available commodity polymers as opposed to specialized copolymers.

6.4.4 Tensile and Impact Properties

Tensile stress-strain curves of the neat PLA, binary PLA/PA11 50/50, and ternary blends containing 10% of either PBS, PBAT, EMA, or EMA-GMA are presented in Figure 6.4. The neat PLA shows a tensile strength of about 70 MPa and an elongation at break of only 4% indicating its poor ductility and high stiffness. A brittle behavior with lower tensile strength and modulus is obtained by the addition of 50% PA11 to PLA, which does not generate a ductile blend despite the high ductility of the neat PA11. In contrast, the incorporation of the third components to the binary PLA/PA11 50/50 changes the brittle fracture to a ductile fracture. All the ternary blends demonstrated ductile behavior with distinct tensile yielding followed by considerable cold drawing.
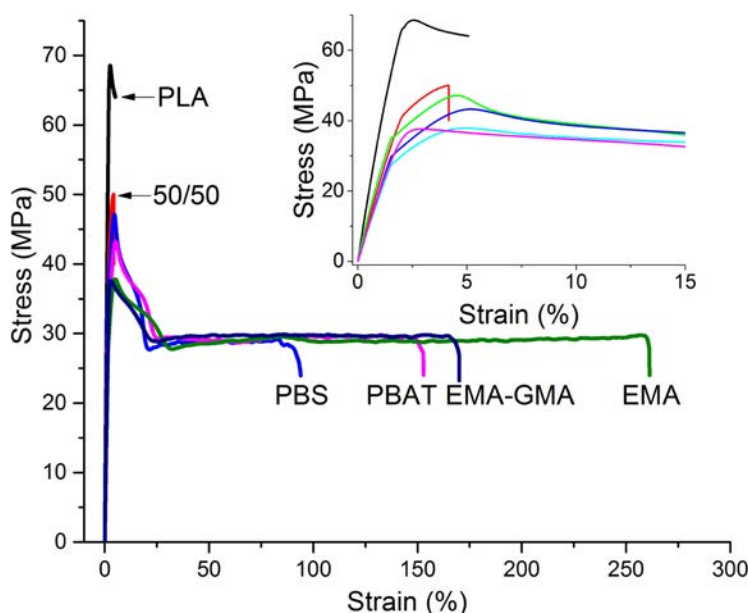
Figure 6.4. Tensile stress-strain plots of PLA, the binary PLA/PA 50/50 blend, and ternary blends containing 10% of different third components.

Figure 6.5 summarizes some tensile properties and notched Izod impact strength of the neat PLA and blends. Excellent tensile toughness was obtained for the ternary blends. The ternary blends demonstrate a significantly improved elongation at break with moduli in the same range as the binary PLA/PA11 50/50 blend. The decrease of the tensile strength for the ternary blends can be seen in Figure 6.5 which is attributed to the presence of the third component with lower strength as is typically reported for rubber toughened plastics. Among the ternary blends, the PLA/EMA/PA11 blend shows the highest elongation at about 260%, which is a dramatic improvement over the pure PLA and the binary PLA/PA11 50/50 blend. The ternary blends containing PBAT and EMA-GMA yield virtually the same elongation at break (150%) while the lowest improvement was obtained from the blend containing PBS (77%). As expected, the notched Izod impact strength follows the same trend as the elongation at break (Figure 6.5a). The impact strength of the ternary PLA/EMA/PA11 blend reaches 73 J/m, which is an important increase of more than 400% with respect to that of the neat PLA and 50/50 binary blend.
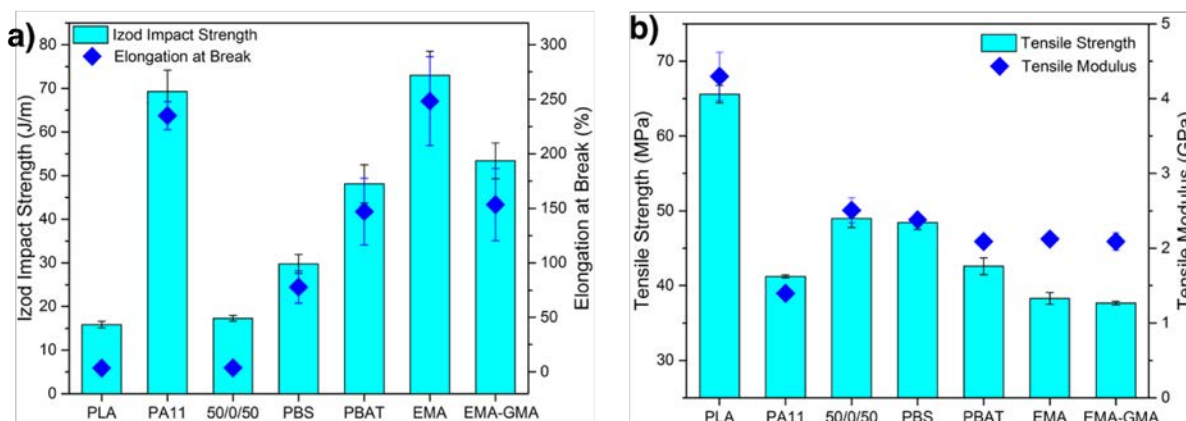
Figure 6.5. Mechanical properties of pure components and blends containing 10% of different types of third components.

The difference between PBS, PBAT, EMA, and EMA-GMA in the toughening of the binary co-continuous PLA/PA11 50/50 blend are, for the most part, in line with the results of the morphology and interfacial analysis carried out earlier in the paper. EMA and EMA-GMA both are much more effective in the compatibilization of the co-continuous PLA/PA11 matrices and form finer self-assembled partially wet droplets at the interface when compared with PBS and PBAT. EMA and EMA-GMA also have lower inherent modulus (E_{EMA} and $E_{EMA-GMA}$ < 30 MPa vs. E_{PBS}=620 MPa and E_{PBAT}=105 MPa). It will be shown in the next section that the rubbery nature of EMA and EMA-GMA facilitates the rubber cavitation process [57].

The ternary PLA/EMA/PA11 system with different EMA contents was also examined to define the optimum EMA content. The best impact strength and elongation at break results are obtained from the blend containing 10% EMA (See Supporting Information in ANNEX B). The increase in the EMA content increases the impact strength, but no considerable difference between 10% and 20% is found. In addition to the elongation at break, the tensile modulus drops in the blend containing 20% EMA suggesting the optimum EMA content in PLA/EMA/PA11 to be about 10%.

Figure 6.6 shows SEM micrographs of the impact fracture surface of the PLA/PA11 50/50 blend in the vicinity of the notch. A featureless fracture surface with no matrix plastic deformation and a large number of cavities are observed which imply a typical brittle fracture characterized by rapid crack propagation due to a weak interfacial adhesion (Figure 6.6a). It is known that the crazing is the main fracture mechanism in rigid-rigid polymer blends and that it can toughen polymer blends

in the presence of effective termination mechanisms [58]. However, the propagation of crazes can lead to the crack formation and consequently failure of blends. Close examination of the cryo-fractured cross-section underneath the impact fracture surface in Figure 6.6b clearly indicates multiple imprints where dispersed phase was pulled from the binary PLA/PA11 50/50 blend sample. This is a clear indication of interfacial debonding and the poor impact data for this blend presented in Figure 6.5 is not surprising in light of these fracture surfaces.
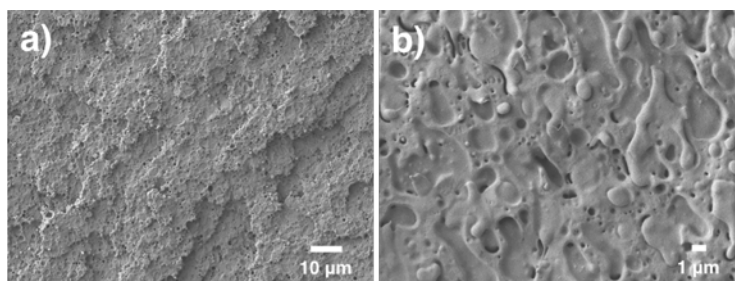
Figure 6.6. SEM micrographs of the fracture surface of the binary PLA/PA11 50/50 blend at a) the vicinity of the notch of impact fractured specimen; b) a cryo-fractured cross-section underneath the impact fracture surface.

The SEM micrographs of the impact fracture surface of the ternary blends are presented in Figure 6.7. The addition of 10% PBS results in no appreciable plastic deformation in the matrices (Figure 6.7a) as manifested in the impact strength results. Although improvements were obtained in the tensile and impact properties, the evident interfacial debonding of PBS with PLA and PA11 combined with no adequate termination mechanism results in only a very modest improvement in impact. This observation is also in line with the lower level of interfacial interactions for PBS with PLA and PA11 observed earlier in this paper. A rough fracture surface with obvious shear zones is observed in the ternary blend containing 10% PBAT along with local fibrillation of some PBAT particles (Figure 6.7b). This suggests that the partially wet PBAT droplets have been effective in triggering the plastic deformation of the PLA and PA11 matrices. A much rougher fracture surface with intense shear zones and fibrillated structures is observed in the ternary blends with EMA and EMA-GMA as presented in Figure 6.7c,d. These localized plastic deformations of the matrices can be associated with the finer co-continuous structure of PLA/PA11 and the strong interfacial adhesion of the dispersed particles at the interface of PLA/PA11. These results correlate well with

the high impact strength properties obtained for the PLA/EMA/PA11 and PLA/EMA-GMA/PA11 blends.
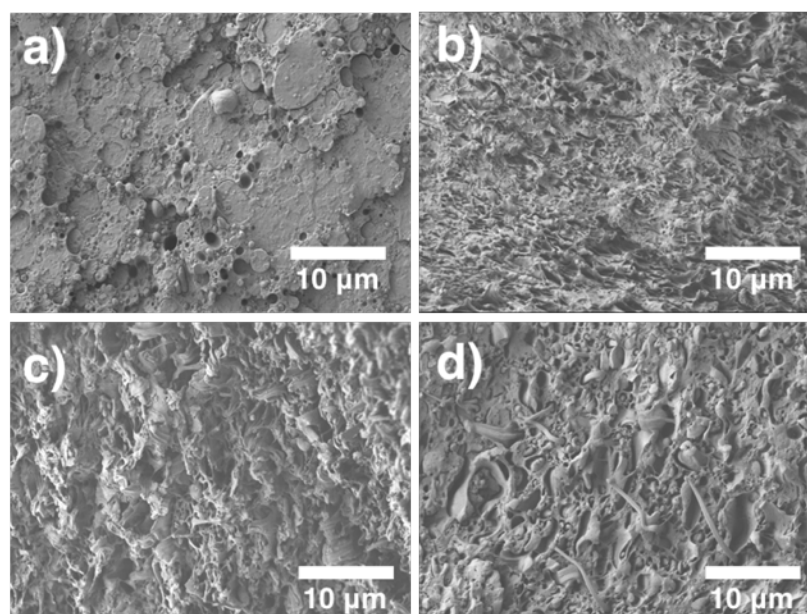
Figure 6.7. SEM micrographs of the Izod fracture surface at the notch root of the PLA/PA 50/50 blends containing 10% of a) PBS; b) PBAT; c) EMA; and d) EMA-GMA.

The cryo-fractured cross section underneath the impact fracture surface of the ternary samples were examined under SEM to gain a better understanding of the underlying mechanisms behind the obtained toughening. Figure 6.8a shows the debonding of the dispersed PBS particles from the matrix as the result of the stress concentration around relatively large PBS particles. It should be noted that the ternary blend with the PBS particles had the largest size and the lowest percentage of the partially wet droplets at the interface. The better impact strength of the ternary PLA/PBAT/PA11 blend can be related to the higher presence of PBAT particles at the interface of PLA and PA11 as indicated by arrows in Figure 6.8b. The soft PBAT particles act as stress concentrators and alter the stress state at the interface of the PLA and PA11 phases which can locally release the triaxial stress and lead to plastic deformation.
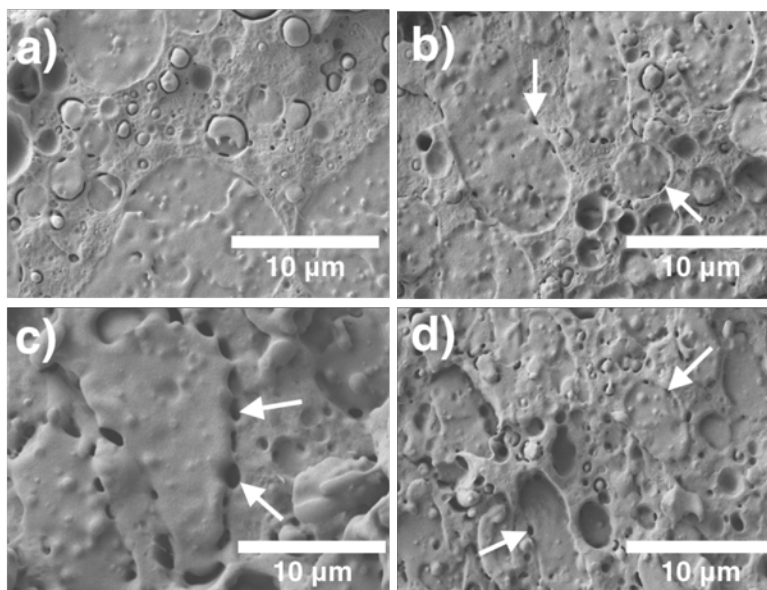
Figure 6.8. SEM micrographs of the fracture surface of a cross-section underneath the impact fracture surface of the PLA/PA 50/50 blends containing 10% of a) PBS; b) PBAT; c) EMA; and d) EMA-GMA.

Internal rubber cavitation is regarded as one of the most effective mechanisms to delocalize the triaxial stress in rubber toughened plastics [59,60]. Cavitation is an important process that enables a blend to yield at moderate stresses under a plane strain condition as in notched impact specimens. Two conditions to achieving a high toughness in a rubber modified system are to create extensive cavitation ahead of the crack tip and to considerably involve the matrix in the plastic deformation [59,61]. A much more marked internal rubber cavitation is observed in Figure 6.8c when EMA was localized at the interface of the co-continuous PLA/PA11. Indeed, due to the balanced interfacial adhesion between the PLA and PA11 phases and also the low modulus of EMA, internal cavitation of EMA develops (see white arrows) rather than interfacial debonding. The array of cavitated EMA particles at the PLA/PA11 interface effectively reduce the detrimental dilational stress throughout the blend. In contrast, no appreciable internal cavitation is observed in the blend containing EMA-GMA (Figure 6.8d). Based on an energy balance model, Bucknall and coworkers [59,61–63] have shown that cavitation in rubber particles cannot occur below a critical rubber particle size. The energy required to drive cavitation increases as the rubber particle size becomes smaller and thus, a limited number of cavitation events occur. This explains the lower impact

strength and elongation at break in the ternary PLA/EMA-GMA/PA11 blend as compared to the PLA/EMA/PA11 system. Despite the very strong interfacial adhesion between EMA-GMA and the matrices, the very fine EMA-GMA particles (ca. 450 nm) are unable to develop the large numbers of internal cavitation required to saturate the PLA/PA11 interface.

On the basis of the above results, Figure 6.9 illustrates the toughening process in ternary blends of co-continuous PLA and PA11 with partially wet EMA droplets at the interface. The rubbery EMA particles of 1.1 microns in size partially wet the PLA/PA11 interface with an interparticle distance of about 600 nm. It is reasonable to assume that the PLA matrix, due to its inherent brittleness, is the component that most likely limits the impact properties of the binary PLA/PA11 blend. Considering that the EMA interparticle distance (600 nm) is well below the critical ligament thickness reported for the PLA matrix in the literature [64], it is reasonable to consider that the stress field around the partially wet droplets at the interface (red dash lines) results in EMA cavitation which interfacially percolates and spreads through the sample. This leads to significant shear yielding in PLA and PA11 and a better than 400% increase in impact strength as compared to the co-continuous binary PLA/PA11.
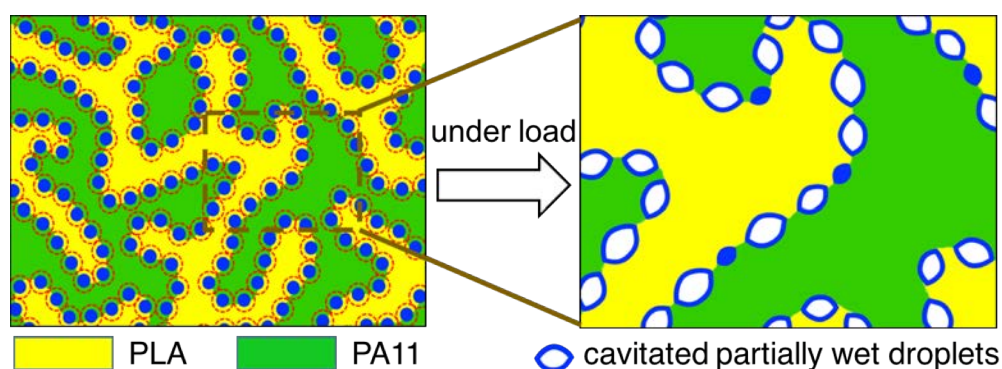
Figure 6.9. Schematic of the toughening process in PLA/EMA/PA11 with cavitated partially wet droplets percolating the PLA/PA11 interface throughout the sample.

6.5 CONCLUSION

This paper reports on significant improvements in the compatibilization and toughening of a co-continuous PLA/PA11 blend through a new approach based on the assembly of partially wet droplets at the PLA/PA11 interface. Four different polymers, EMA, EMA-GMA, PBS and PBAT

were shown to partially wet the PLA/PA11 interface. The partially wet EMA-GMA droplets demonstrate the most significant compatibilization effect by reducing the co-continuous phase thickness from 10 μm to about 5 μm. The interfacial assembly of very fine 450 nm EMA-GMA droplets, with a 350 nm interparticle distance, appears to enhance the compatibilization effect. The combined effect of the interfacial affinity and tendency towards partial wetting plays an important role in the compatibilization of the PLA/PA11 system by the fine EMA-GMA particles.

A brittle-to-ductile transition is achieved for PLA/PA11 when a partially wet droplet phase assembles at the interface. The addition of 10% of PBS, PBAT, and EMA-GMA components improve the tensile properties and the notched Izod impact strength, however, the best results are obtained for the ternary PLA/EMA/PA11 blend. PLA/EMA/PA11 45/10/45 shows a 4-fold increase in the notched Izod impact strength (73 J/m) and a high elongation at break of about 250%. The results of the fracture surface analysis reveal significant cavitation for the partially wet EMA droplets whereas very limited cavitation is observed for EMA-GMA, PBS, and PBAT. EMA provides suitable interfacial adhesion, an inherent capability for cavitation, and particularly an appropriate interfacial morphology (d_n=1.1 μm and L=600 nm) to form micro-cavitation. Thus, the stress-field overlap through an interconnected network path created by the partially wet droplets at the interface enhances the shear yielding and consequently the toughening of the ternary systems.

This work opens new opportunities to improve both toughening and interfacial compatibilization in co-continuous systems through the use of partially wet droplets.

6.6 ACKNOWLEDGMENT

6.7 REFERENCES

[1] B.D. Favis, Factors influencing the morphology of immiscible polymer blends in melt processing, in: D.R. Paul, C.B. Bucknall (Eds.), Polym. Blends Vol. 1 Formul., John Wiley & Sons, New York, 2000: pp. 501–538.

[2] H. Pernot, M. Baumert, F. Court, L. Leibler, Design and properties of co-continuous

nanostructured polymers by reactive blending, Nat. Mater. 1 (2002) 54–58.

[3]   J.P.. Inberg, R.. Gaymans, Co-continuous polycarbonate/ABS blends, Polymer. 43 (2002) 2425–2434.

[4]   C.L. Zhang, L.F. Feng, J. Zhao, H. Huang, S. Hoppe, G.H. Hu, Efficiency of graft copolymers at stabilizing co-continuous polymer blends during quiescent annealing, Polymer. 49 (2008) 3462–3469.

[5]   J.A. Galloway, H.K. Jeon, J.R. Bell, C.W. Macosko, Block copolymer compatibilization of cocontinuous polymer blends, Polymer. 46 (2005) 183–191.

[6]   U. Sundararaj, C.W. Macosko, Drop Breakup and Coalescence in Polymer Blends: The Effects of Concentration and Compatibilization, Macromolecules. 28 (1995) 2647–2657.

[7]   T.S. Omonov, C. Harrats, G. Groeninckx, Co-continuous and encapsulated three phase morphologies in uncompatibilized and reactively compatibilized polyamide 6/polypropylene/polystyrene ternary blends using two reactive precursors, Polymer. 46 (2005) 12322–12336.

[8]   H. Wang, W. Dong, Y. Li, Compatibilization of Immiscible Polymer Blends Using in Situ Formed Janus Nanomicelles by Reactive Blending, ACS Macro Lett. 4 (2015) 1398–1403.

[9]   Y. Cao, J. Zhang, J. Feng, P. Wu, Compatibilization of Immiscible Polymer Blends Using Graphene Oxide Sheets, ACS Nano. 5 (2011) 5920–5927.

[10]   S. Huang, L. Bai, M. Trifkovic, X. Cheng, C.W. Macosko, Controlling the Morphology of Immiscible Cocontinuous Polymer Blends via Silica Nanoparticles Jammed at the Interface, Macromolecules. 49 (2016) 3911–3918.

[11]   H.J. Chung, K. Ohno, T. Fukuda, R.J. Composto, Self-regulated structures in nanocomposites by directed nanoparticle assembly, Nano Lett. 5 (2005) 1878–1882.

[12]   R. Bahrami, T.I. Löbling, A.H. Gröschel, H. Schmalz, A.H.E. Müller, V. Altstädt, The Impact of Janus Nanoparticles on the Compatibilization of Immiscible Polymer Blends under Technologically Relevant Conditions, ACS Nano. 8 (2014) 10048–56.

[13]   P.-G. de Gennes, F. Brochard-Wyard, D. Quere, Capillarity and Wetting Phenomena: Drops,

Bubbles, Pearls, Waves, Springer, New York, 2004.

[14] I. Luzinov, C. Pagnoulle, R. Jerome, Ternary polymer blend with core-shell dispersed phases: effect of the core-forming polymer on phase morphology and mechanical properties, Polymer. 41 (2000) 7099–7109.

[15] J.H. Zhang, S. Ravati, N. Virgilio, B.D. Favis, Ultralow percolation thresholds in ternary cocontinuous polymer blends, Macromolecules. 40 (2007) 8817–8820.

[16] K. Zhang, V. Nagarajan, M. Misra, A.K. Mohanty, Supertoughened Renewable PLA Reactive Multiphase Blends System: Phase Morphology and Performance., ACS Appl. Mater. Interfaces. 6 (2014) 12436–48.

[17] W.D. Harkins, A General Thermodynamic Theory of the Spreading of Liquids to Form Duplex Films and of Liquids or Solids to Form Monolayers, J. Chem. Phys. 9 (1941) 552.

[18] W.D. Harkins, A. Feldman, Films. The spreading of liquids and the spreading coefficient, J. Am. Chem. Soc. 44 (1922) 2665–2685.

[19] S. Torza, S.. G. Mason, Three-phase interactions in shear and electrical fields, J. Colloid Interface Sci. 33 (1970) 67–83.

[20] S.Y. Hobbs, M.E.J. Dekkers, V.H. Watkins, Effect of interfacial forces on polymer blend morphologies, Polymer. 29 (1988) 1598–1602.

[21] S. Shokoohi, A. Arefazar, A review on ternary immiscible polymer blends: morphology and effective parameters, Polym. Adv. Technol. 20 (2009) 433–447.

[22] A.R. Kolahchi, Surface Morphology and Properties of Ternary Polymer Blends : Effect of the Migration of Minor Components, J. Phys. Chem. B. 118 (2014) 6316–6323.

[23] H. Rastin, S.H. Jafari, M.R. Saeb, H.A. Khonakdar, U. Wagenknecht, G. Heinrich, On the reliability of existing theoretical models in anticipating type of morphology and domain size in HDPE/PA-6/EVOH ternary blends, Eur. Polym. J. 53 (2014) 1–12.

[24] I. Luzinov, K. Xi, C. Pagnoulle, G. Huynh-Ba, R. Jerome, Composition effect on the core-shell morphology and mechanical properties of ternary polystyrene/styrene butadiene rubber polyethylene blends, Polymer. 40 (1999) 2511–2520.

[25]   T.S. Valera, A.T. Morita, N.R. Demarquette, Study of morphologies of PMMA/PP/PS ternary blends, Macromolecules. 39 (2006) 2663–2675.

[26]   L. Li, B. Yin, Y. Zhou, L. Gong, M. Yang, B. Xie, C. Chen, Characterization of PA6/EPDM-g-MA/HDPE ternary blends: The role of core-shell structure, Polymer. 53 (2012) 3043–3051.

[27]   C. Shen, Y. Zhou, R. Dou, W. Wang, B. Yin, M. Yang, Effect of the core-forming polymer on phase morphology and mechanical properties of PA6/EPDM-g-MA/HDPE ternary blends, Polymer. 56 (2015) 395–405.

[28]   S. Horiuchi, N. Matchariyakul, K. Yase, T. Kitano, Morphology development through an interfacial reaction in ternary immiscible polymer blends, Macromolecules. 30 (1997) 3664–3670.

[29]   N. Virgilio, C. Marc-Aurele, B.D. Favis, Novel Self-Assembling Close-Packed Droplet Array at the Interface in Ternary Polymer Blends, Macromolecules. 42 (2009) 3405–3416.

[30]   S. Ravati, B.D. Favis, Interfacial coarsening of ternary polymer blends with partial and complete wetting structures, Polymer. 54 (2013) 6739–6751.

[31]   R.C. Willemse, A. Speijer, A.E. Langeraar, A.P. de Boer, Tensile moduli of co-continuous polymer blends, Polymer. 40 (1999) 6645–6650.

[32]   Y. Li, H. Shimizu, Improvement in toughness of poly(l-lactide) (PLLA) through reactive blending with acrylonitrile-butadiene-styrene copolymer (ABS): Morphology and properties, Eur. Polym. J. 45 (2009) 738–746.

[33]   Z.-Z. Yu, Y.-C. Ou, Z.-N. Qi, G.-H. Hu, Toughening of nylon 6 with a maleated core-shell impact modifier, J. Polym. Sci. Part B Polym. Phys. 36 (1998) 1987–1994.

[34]   Z. Yu, M. Lei, Y. Ou, G. Hu, The Role of Interfacial Modifier in Toughening of Nylon-6 with a Core-Shell Toughener, J. Polym. Sci. Part B Polym. Phys. 37 (1999) 2664–2672.

[35]   Z. Ke, D. Shi, J. Yin, R.K.Y. Li, Y.W. Mai, Facile method of preparing supertough polyamide 6 with low rubber content, Macromolecules. 41 (2008) 7264–7267.

[36]   C. G'Sell, S.-L. Bai, J.-M. Hiver, Polypropylene/polyamide 6/polyethylene–octene

elastomer blends. Part 2: volume dilatation during plastic deformation under uniaxial tension, Polymer. 45 (2004) 5785–5792.

[37]   K. Hashima, S. Nishitsuji, T. Inoue, Structure-properties of super-tough PLA alloy with excellent heat resistance, Polymer. 51 (2010) 3934–3939.

[38]   M. Vert, G. Schwarch, J. Coudane, Present and Future of PLA Polymers, J. Macromol. Sci. Part A. 32 (1995) 787–796.

[39]   D. Garlotta, A literature review of poly (lactic acid), J. Polym. Environ. 9 (2001) 63–84.

[40]   R. Rulkens, C. Koning, Chemistry and Technology of Polyamides, in: Polym. Sci. A Compr. Ref. 10 Vol. Set, 2012: pp. 431–467.

[41]   G. Stoclet, R. Seguela, J.-M. Lefebvre, Morphology, thermal behavior and mechanical properties of binary blends of compatible biosourced polymers: Polylactide/polyamide11, Polymer. 52 (2011) 1417–1425.

[42]   R. Patel, D.A. Ruehle, J.R. Dorgan, P. Halley, D. Martin, Biorenewable blends of polyamide-11 and polylactide, Polym. Eng. Sci. 54 (2014) 1523–1532.

[43]   A. Nuzzo, S. Coiai, S.C. Carroccio, N.T. Dintcheva, C. Gambarotti, G. Filippone, Heat-Resistant Fully Bio-Based Nanocomposite Blends Based on Poly(lactic acid), Macromol. Mater. Eng. 299 (2014) 31–40.

[44]   a. Nuzzo, E. Bilotti, T. Peijs, D. Acierno, G. Filippone, Nanoparticle-induced co-continuity in immiscible polymer blends – A comparative study on bio-based PLA-PA11 blends filled with organoclay, sepiolite, and carbon nanotubes, Polymer. 55 (2014) 4908–4919.

[45]   Y. Lin, K.Y. Zhang, Z.M. Dong, L.S. Dong, Y.S. Li, Study of hydrogen-bonded blend of polylactide with biodegradable hyperbranched poly(ester amide), Macromolecules. 40 (2007) 6257–6267.

[46]   F. Feng, L. Ye, Structure and Property of Polylactide/Polyamide Blends, J. Macromol. Sci. Part B. 49 (2010) 1117–1127.

[47]   S.A. Saltikov, Proceedings of the Second International Congress for Stereology, in: H. Elias (Ed.), Proc. Second Int. Congr. Stereol., Springer-Verlag, Berlin, 1967: pp. 163–173.

[48]   J. a. Galloway, M.D. Montminy, C.W. Macosko, Image analysis for interfacial area and cocontinuity detection in polymer blends, Polymer. 43 (2002) 4715–4722.

[49]   J. Li, B.D. Favis, Characterizing co-continuous high density polyethylene/polystyrene blends, Polymer. 42 (2001) 5047–5053.

[50]   P.H.M. Elemans, J.M.H. Janssen, H.E.H. Meijer, The measurement of interfacial tension in polymer/polymer systems: The breaking thread method, J. Rheol. 34 (1990) 1311–1325.

[51]   A.M. Zolali, B.D. Favis, Partial and Complete Wetting in Ultra-low Interfacial Tension Multiphase Blends with Polylactide, J. Phys. Chem. B. (2016) Submitted.

[52]   E.J. Dil, P.J. Carreau, B.D. Favis, Morphology, Miscibility and Continuity Development in Poly(lactic acid)/Poly(butylene adipate-co-terephthalate) Blends, Polymer. 68 (2015) 202–212.

[53]   J.L. Eguiburu, J.J. Iruin, M.J. Fernandez-Berridi, J. San Román, Blends of amorphous and crystalline polylactides with poly(methyl methacrylate) and poly(methyl acrylate): a miscibility study, Polymer. 39 (1998) 6891–6897.

[54]   C. Samuel, S. Barrau, J.-M. Lefebvre, J.-M. Raquez, P. Dubois, Designing Multiple-Shape Memory Polymers with Miscible Polymer Blends: Evidence and Origins of a Triple-Shape Memory Effect for Miscible PLLA/PMMA Blends, Macromolecules. 47 (2014) 6791–6803.

[55]   H.T. Oyama, Super-tough poly(lactic acid) materials: Reactive blending with ethylene copolymer, Polymer. 50 (2009) 747–751.

[56]   H. Liu, W. Song, F. Chen, L. Guo, J. Zhang, Interaction of Microstructure and Interfacial Adhesion on Impact Performance of Polylactide (PLA) Ternary Blends, Macromolecules. 44 (2011) 1513–1522.

[57]   D. Dompas, G. Groeninckx, M. Isogawa, T. Hasegawa, M. Kadokura, Toughening behaviour of rubber-modified thermoplastic polymers involving very small rubber particles: 3. Impact mechanical behaviour of poly(rmvinyl chloride)/methyl methacrylate-butadiene-styrene graft copolymer blends, Polymer. 35 (1994) 4760–4765.

[58]   G.X. Wei, H.J. Sue, J. Chu, C. Huang, K. Gong, Toughening and strengthening of

polypropylene using the rigid-rigid polymer toughening concept. Part I. Morphology and mechanical property investigations, Polymer. 41 (2000) 2947–2960.

[59]   C.B. Bucknall, D.R. Paul, Notched impact behavior of polymer blends: Part 1: New model for particle size dependence, Polymer. 50 (2009) 5539–5548.

[60]   F. Ramsteiner, G.E. McKee, M. Breulmann, Influence of void formation on impact toughness in rubber modified styrenic-polymers, Polymer. 43 (2002) 5995–6003.

[61]   C.B. Bucknall, D.R. Paul, Notched impact behaviour of polymer blends: Part 2: Dependence of critical particle size on rubber particle volume fraction, Polymer. 54 (2013) 320–329.

[62]   A. Lazzeri, C.B. Bucknall, Dilatational bands in rubber-toughened polymers, J. Mater. Sci. 28 (1993) 6799–6808.

[63]   A. Lazzeri, C.B. Bucknall, Applications of dilatational yielding model to rubber-toughened polymers, Polymer. 36 (1995) 2895–2902.

[64]   K.S. Anderson, S.H. Lim, M.A. Hillmyer, Toughening of polylactide by melt blending with linear low-density polyethylene, J. Appl. Polym. Sci. 89 (2003) 3757–3768.

CHAPTER 7   ARTICLE 4: ULTRATOUGH CO-CONTINUOUS PLA/PA11 BY INTERFACIALLY PERCOLATED POLY(ETHER-B-AMIDE)[4]

Ali M. Zolali, Vahid Heshmati and Basil D. Favis

CREPEC, Department of Chemical Engineering, École Polytechnique de Montréal, Montréal, QC, Canada H3C3A7

7.1 Abstract

In this work it will be shown that when polyether-*b*-amide (PEBA) is added to a PLA/PA11 blend it tends towards the interface and results in a significant increase in the impact strength when all three phases are fully percolated. The addition of the elastomeric PEBA phase to the binary PLA/PA11 blend replaces a rigid PLA/PA11 interface with a much more deformable one. The further addition of PEO to PLA results in an ultratough material with an impact strength of ~ 750 J/m which is approximately forty times greater than the original co-continuous PLA/PA11 blend. The tensile toughness and notched Izod impact strength are significantly influenced by the critical co-continuous composition region of the PLA/PA11 binary system and a minimum concentration to form a fully percolated PEBA layer at the co-continuous PLA/PA11 interface. The added PEO is also found to enhance the interfacial interactions and the chain mobility of PLA. The combined effects of co-continuity, strong interfacial interactions, a deformable interface and sufficient PLA chain mobility are all essential to achieving ultratough behavior in PLA/PA11. Examination of the fracture surface of the ultratough material after impact indicates significant voiding. It is suggested that the stress-field overlap within the deformable PEBA phase in conjunction with suitable interfacial adhesion changes the failure mode from crazing to shear yielding. These results establish

---

a strategy for the toughening of multiphase polymer blends, especially in the vicinity of the co-continuous region.

7.2 INTRODUCTION

Polylactide (PLA), which is derived from renewable resources, has attracted much attention as a promising alternative to some petroleum-based polymers because of its high strength and stiffness, biocompatibility, compostability and excellent processability [1,2]. However, PLA suffers from inherent drawbacks, notably brittleness and a low heat deflection temperature (HDT), which limit its large-scale commercial application [2]. Improving the toughness of PLA has been the subject of several studies in the literature [3], and the melt blending of PLA with other polymers has been considered as one of the best ways to compensate for these disadvantages.[4] Binary blends of PLA with various flexible polymers like linear low density polyethylene (LLDPE),[5] acrylonitrile-butadiene-styrene (ABS) [6], polyurethane [7,8] and poly(ethylene-glycidyl methacrylate) (EGMA) [9,10], have been employed to toughen PLA. A number of such studies include the addition of poly(ε-caprolactone) (PCL) [11,12], poly(butylene succinate) (PBS) [13,14], and plant oil derivatives [15,16].

Polyamide (PA) polymers, which can be derived from biobased resources such as castor oil [17], are engineering plastics with high thermal stability impact and chemical resistance as well as excellent dimensional stability. The melt blending of biobased polyamide-11 (PA11) with PLA has been reported to augment PLA's properties [18,19]. However, very limited improvements in impact and tensile toughness has been obtained [18,19] while a considerable enhancement in heat deflection temperature can be achieved through the addition of nanoparticles to induce a stable co-continuous structure [20–22].

Multicomponent blends have attracted much interest and many researchers have reported obtaining high performance materials through the generation of complex morphologies in multiphase polymer blends. In a pioneering work, Cheng et al. [23] showed that the toughness of ternary blends of polycarbonate (PC) strongly depends on the morphology, interfacial adhesion and inherent properties of components. Core-shell morphologies have been shown to be effective in modifying the mechanical properties, i.e. impact and tensile properties, of three-phase systems and has been

the subject of several studies [24–27]. Luzinov et al.[24] studied the relationship between the morphology and mechanical properties of ternary blends with polystyrene (PS) as the matrix and a dispersed core-shell phase of polyethylene (PE)/styrene-butadiene rubber. They observed some synergism in tensile properties through the control of the phase morphology and correlated it to the excellent stress transfer from the matrix through the shell to the core. Following this concept, the ultra high impact of polyamide (PA) have been achieved through the incorporation of well-controlled in-situ formed core-shell droplets in a matrix of PA [25–27].

Willemse et al. [28] showed that changing a matrix/dispersed phase morphology to a co-continuous morphology in binary PE/PS and PE/polypropylene (PP) systems results in a significant enhancement in modulus. Two separate studies have supported that generating co-continuous morphologies leads to the important improvement of impact and tensile properties of binary blends with acrylonitrile butadiene styrene (ABS) [29,30], in which the intrinsic properties of ABS, i.e. the polybutadiene content, appeared to effectively influence the impact resistance [30]. Modification of the interface of a co-continuous PLA/ABS system by styrene-acrylonitrile-glycidyl methacrylate copolymer (SAN-GMA) compatibilizes the morphology and improves the impact strength and elongation at break [31].

In a series of papers, the morphology, mechanical properties and toughening mechanism have been investigated in ternary PP/PA6/polyethylene-octene elastomer (POE) blends [32–34]. The POE phase separates PA6 dispersed droplets from PP by forming a middle layer between them which represents a complete wetting behavior from the thermodynamic point of view. The highest toughness values were obtained at a 40/40/20 composition of the PP/PA6/POE blend where the two phases have a high level of continuity. The dilatometry results reveal that the volume strain decreases with increasing (PA6+POE) content from 0 to 60 wt% where the PA6/POE weight ratio was maintained at 2. In other words, the amount of POE interphase cavitation at the interface of PP and PA6 was reduced, implying the profuse expansion of plastic shear yielding in the PP matrix through the development of the completely wet layer of POE phase at the interface of the PP/PA6 system. In another work, a high impact strength PLA blend with significantly enhanced heat resistance was reported for quaternary blends of PLA, PC, styrene-ethylene/butylene-styrene copolymer (SEBS), and EGMA [35]. The dilational stress evolved in the PLA phase from the negative pressure effect of SEBS effectively transfers to the PC phase as the result of the

compatibilization effect of EGMA at the interface of PLA and PC. This results in a high performance PLA blend. Sarazin et al. [36] reported a brittle-ductile transition in ternary blends of PLA/PCL/thermoplastic starch (TPS). Significant improvements in elongation at break and impact strength are achieved through the addition of PCL and TPS to PLA giving promise to the ternary blend approach as a useful technique to expand the property range of PLA materials.

However, it is still unknown how co-continuity and interfacial interactions between the phases of ternary blends contribute to the toughness of multicomponent blends. The morphology development of PLA, PA11, and thermoplastic elastomer poly(ether-b-amide) (PEBA) ternary blends, including their interfacial modification and plasticization, will be investigated and their effect on the impact strength of the blends will be examined.

7.3 EXPERIMENTAL

7.3.1 Materials

Commercial polymers of polylactide (PLA), polyamide-11 (PA11), poly(ether-b-amide) (PEBA), and poly(ethylene oxide) (PEO) were used as main components. Table 7.1 summarizes the grades of all materials used in this study. All the materials were dried at 70 °C (except PEO which was dried at 40 °C) under vacuum overnight before being used in the experiments.

Table 7.1. Main characteristics of materials

Material	Supplier	Grade	M_w (kg/mol)	Density at 25 °C (g/cm^3)
PLA	NatureWorks	2003D	199.6[a]	1.24
PA11	Arkema	Rilsan BMNO	50[b]	1.03
PEBA	Arkema	Pebax MV1074	134[c]	0.94
PEO	Dow Chemicals	Polyox WSR-N10	100[c]	1.13

a Obtained from Ref.[53]
b Obtained from Ref.[54]
c Provided by the corresponding manufacturers.

7.3.2 Sample Preparation

The PLA, PEBA and PA11 were prepared on a component weight fraction with the total of those three components equal to 100% in all blends. Since PEO is miscible with PLA, the quantity of PEO in the quaternary blend is presented as a wt% based on the PLA weight fraction. All samples were first dry-mixed and were then melt blended using a co-rotating twin screw extruder (TSE), Leistritz ZSE 18HP with an L/D ratio of 40, at a screw speed of 100 rpm and a temperature profile of 170/180/190/200/200/200/200 °C from hopper to die. The extrudates were quenched in a cold water bath and then pelletized and dried prior to injection molding. For blends containing PEO, a master-batch of PLA/PEO was first melt blended and was then melt-mixed with PA11 and PEBA. A Sumimoto SE50S injection molding machine was used to mold dog-bone specimens of type I (ASTM D638) and impact test bars (dimensions 12.7×63.5×3.2 mm). The temperature profile and screw speed were set to 190/200/210 °C from hopper to nozzle and 100 rpm, respectively.

7.3.3 Scanning Electron Microscopy

SEM observations were performed on a Field Emission SEM machine (JSM 7600TFE, JEOL) operated at a voltage of 2 keV. The specimens were either microtomed using a microtome (Leica RM 2065) equipped with a glass knife and a cryo-chamber (LN21) or cryo-fractured in liquid nitrogen. The Izod impact fractured samples were used as is after testing. PLA was extracted from the microtomed samples using tetrahydrofuran in order to create a contrast between phases. The specimens were then coated with gold/palladium by plasma deposition and the surfaces were observed using the SEM unit.

7.3.4 Atomic Force Microscopy

Samples for AFM analysis were cut using a Leica EM UC7 ultra-microtome equipped with a Leica EM FC7 cryo-chamber and a cryo 45° DiAtome diamond knife. The specimens were then placed under an AFM in PeakForce tapping mode with quantitative nanomechanical analysis (QNM) to map the surface morphology. ScanAsyst-Air probe (Bruker AFM Probes Camarillo, CA) consisting of a SiN cantilever with Si probe, 5 nm nominal tip radius, and 0.4 N/m nominal spring

constant were used for all experiments. Nanoscope (v8) and Nanoscope Analysis (v1.40) software were used for the AFM operation and image analysis.

7.3.5 Image Analysis, Solvent Extraction and Gravimetry

SEM and AFM micrographs were analyzed using a digitizing table from Wacom and SigmaScan V.5 software to characterize the morphology. The thickness and interfacial coverage of the PEBA layer at the interface of PLA and PA11 were estimated from the average length of the cross-sectional measurements perpendicular to the tangent line of the interface and the percentage of the covered to total interfacial perimeter of PLA/PA11, respectively [37,38]. An average value of 5 different measurements using different specimens was obtained and an average error value of less than 10% was reported for each sample.

A solvent extraction technique was used to extract and measure the continuity of the PLA phase. The continuity of the PLA phase was determined using equation 7.1:

$$\% \; continuity \; of \; PLA = \left(\frac{m_{initial} - m_{final}}{m_{PLA,initial}} \right) \times 100 \tag{7.1}$$

where $m_{initial}$ and m_{final} are the mass of sample before and after extraction, respectively, and $m_{PLA,initial}$ is the mass of PLA before extraction. The extraction measurements were carried out using chloroform in a soxhlet extractor setup for a week. At least four measurements were performed for each reported value.

7.3.6 Interfacial Tension Measurement

The interfacial tensions between components were measured using the breaking thread technique. In this method a cylindrical thread of the pair with higher melting temperature was placed between two films of the other pair and the growth of distortions over time was recorded. For each pair, threads with diameters ranging from 40-70 μm were spun out of the melt and then annealed at 60 °C for 24 h under vacuum to remove the residual stress. Measurements were then performed at 200 °C using a Mettler FP-82HT hot-stage. The thread distortions and breakup were filmed using an optical microscope from Nikon (Optiphot-2). Results were then analyzed using SigmaScan v.5. Details of the technique can be found elsewhere [39].

7.3.7 Differential Scanning Calorimetry

Thermal analysis was carried out on a DSC Q2000 (TA Instruments) under a dry nitrogen atmosphere flow of 50 mL/min. The machine was calibrated with an indium standard in a nitrogen atmosphere. Samples of about 5-10 mg were placed in aluminum cells, and conventional DSC heating and cooling runs were performed from 25 °C to 210 °C at a heating rate of 10 °C/min. The specific enthalpy of fusion of the perfect crystal, ΔH_f=93.7 (J/g) for PLA [2] and ΔH_f=189 (J/g) for PA11 [40] were used to calculate the crystalline weight fractions. The glass transition temperature (T_g) of the polymeric phases were evaluated through modulated DSC (MDSC) experiments. The heating rate was operated at 2 °C/min with an oscillation amplitude of ±1.27 °C and an oscillation period of 60 s over the temperature range of -80 °C to 100 °C.

7.3.8 Mechanical tests

Tensile tests were performed according to ASTM D638 using a universal testing machine (Instron 4400R) at a crosshead speed of 5 mm/min while the initial strain was recorded using an extensometer. Notched Izod impact strength was measured using a CS-137C-176 CSI Custom Scientific Instrument impact machine according to the ASTM D256 standard. Five specimens were analyzed for each sample.

7.4 RESULTS AND DISCUSSION

7.4.1 Interfacial Tensions and Spreading Behavior

Among several theoretical models, the spreading coefficient model has been widely used to predict the morphology of immiscible ternary blends [41–43]. This method requires the interfacial tensions γ_{ij} between components which were measured through the breading thread method and are listed in Table 7.2. The spreading coefficient describes the tendency of a component to segregate the two other components from each other. It is defined using equation 7.2 [41]:

$$\lambda_{ijk} = \gamma_{ik} - \gamma_{ij} - \gamma_{jk} \qquad (7.3)$$

where λ_{ijk} are the spreading coefficients. The calculated spreading coefficients associated with the PLA/PEBA/PA11 system are presented in Table 7.2. The positive value of $\lambda_{PLA/PEBA/PA}$ indicates

the existence of a wetting behavior known as complete wetting. In other words, it predicts the tendency of the minor PEBA phase to completely spread at the interface of PLA and PA11.

It is well known that PEO promotes the mobility of PLA chains and in order to examine this effect on mechanical properties, it was also decided to add PEO to the PLA/PEBA/PA11 mixture. It has been reported that melt blended PEO with PLA shows a limited miscibility up to 50 wt% [44]. Thus, a masterbatch of PLA+PEO blended with PA11 and PEBA can be considered as one phase which constitutes a three-phase system with PA11 and PEBA. The interfacial tensions between PLA modified with 20% PEO, PLA(PEO), and PA11 and PEBA were measured and are listed in Table 7.2. This reduces the interfacial tension between PLA and PA11 from 3.2±0.6 mN/m to 2.8±0.8 mN/m. A reduced interfacial tension from 1.9±0.5 mN/m to 1.4±1.0 mN/m is also observed between PLA and PEBA due to the interactions between PLA and the polyether blocks of PEBA and also due to the possible interactions between PLA and the PA12 blocks of PEBA. These interfacial interactions will be discussed in the following sections. Based on the obtained interfacial tensions, a complete wetting behavior is predicted for the quaternary PLA(PEO)/PEBA/PA11 system in which PEBA forms a completely wet layer between the PLA(PEO) and PA11 phases.

Table 7.2. Interfacial tension values and spreading coefficients at 200 °C.

	Interfacial tension (mN/m) @ 200°C	Spreading coefficient (mN/m)	Predicted morphology
No PEO	$\gamma_{PLA/PA} = 3.2 \pm 0.6$ $\gamma_{PA/PEBA} = 1.0 \pm 0.2$ $\gamma_{PLA/PEBA} = 1.9 \pm 0.5$	$\lambda_{PLA/PEBA/PA} = +0.3 > 0$ $\lambda_{PEBA/PLA/PA} = -4.1 < 0$ $\lambda_{PEBAA/PA/PLA} = -2.3 < 0$	Complete wetting: PEBA completely spreads at the interface of PLA and PA11
With PEO	$\gamma_{PLA(PEO)/PA} = 2.8 \pm 0.8$ $\gamma_{PA/PEBA} = 1.0 \pm 0.2$ $\gamma_{PLA(PEO)/PEBA} = 1.4 \pm 1.0$	$\lambda_{PLA(PEO)/PEBA/PA} = +0.4 > 0$ $\lambda_{PEBA/PLA(PEO)/PA} = -3.2 < 0$ $\lambda_{PEBA/PA/PLA(PEO)} = -2.4 < 0$	Complete wetting: PEBA completely spreads at the interface of PLA(PEO) and PA11

7.4.2 Morphology

Figure 7.1 shows the microstructure of the PLA/PEBA/PA11 45/10/45 system. A co-continuous structure of PLA and PA11 forms with the PEBA phase forming a layer at the interface of PLA and PA11. This suggests a tri-continuous structure where all phases are interconnected throughout the sample. Although the continuity of PEBA was not determined due to the lack of a selective

solvent, the image analysis results clearly support the existence of an interfacially percolated PEBA phase. The results confirm the thermodynamic prediction from above and also suggest the formation of a thermodynamically driven double percolated structure.
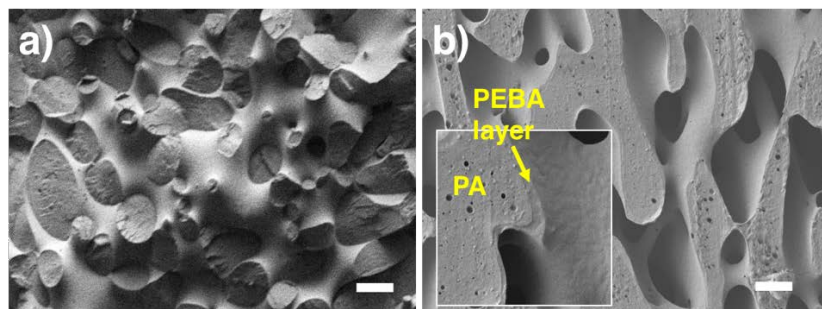
Figure 7.1. SEM micrographs of PLA/PEBA/PA11 45/10/45 a) cryo-fractured surface, b) PLA solvent extracted surface. The white bars denote 10 μm.
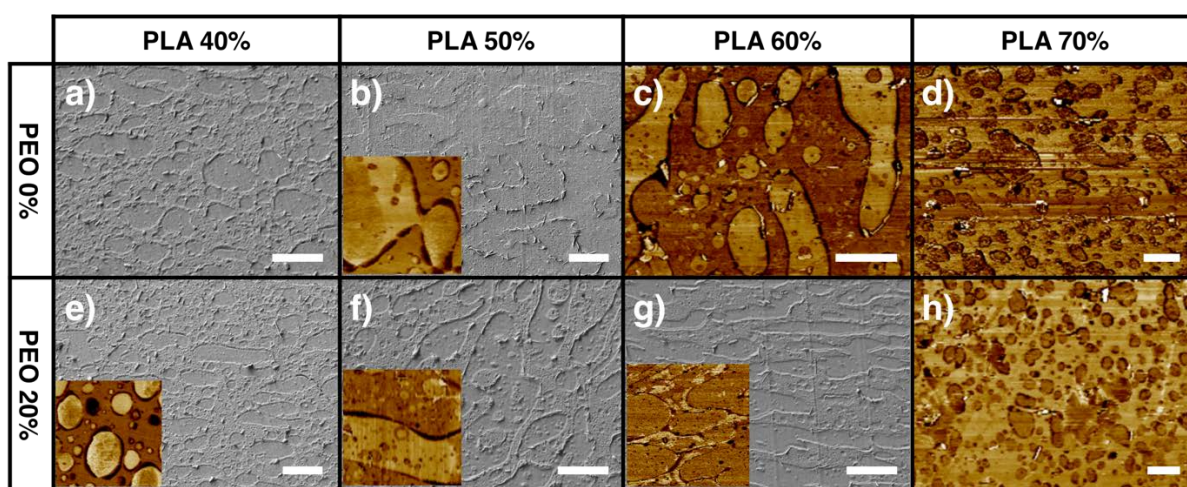
Figure 7.2. SEM and AFM micrographs of a) PLA/PEBA/PA11 x/10/y and b) PLA(PEO)/PEBA/PA11 x(20)/10/y. The white bars denote 10 μm.

Figure 7.2a-d displays the AFM and SEM micrographs of various PLA/PEBA/PA11 blends with a constant PEBA content of 10%. In all of these samples PEBA forms a distinct layer between the PLA and PA11 phases which is clearly shown as the dark phase in AFM micrographs. Upon increasing the concentration of PLA from 40% to 70%, phase transitions from dispersed phase/matrix (Figure 7.2a) to co-continuous (Figure 7.2b) and then to matrix/dispersed phase (Figure 7.2c,d) PLA/PA11 are observed. The addition of 20% PEO based on the PLA content to

the ternary PLA/PEBA/PA11 appears to shift the PLA/PA11 dual continuity region from about 50% to 60% (Figure 7.2f,g), while dispersed phase/matrix morphologies are observed at lower (40%) and higher (70%) concentrations of PLA (Figure 7.2e,h). These results are also in agreement with the thermodynamic predictions as the complete wetting behavior of PEBA in the PLA/PA11 system is preserved even after addition of PEO.

7.4.3 Mechanical Properties

The mechanical properties of the pure components, as well as their binary, ternary, and quaternary blends are listed in Table 7.3. PLA demonstrates a brittle behavior as expected while PA11 possesses a balanced impact and tensile properties. The binary blend of PLA/PA11 50/50 shows very poor impact and tensile properties. However, the addition of PEBA to the binary 50/50 PLA/PA11 blend results in a significant improvement in the impact and tensile properties. The notched Izod impact strength increases more than eight times to 142.4 J/m compared to 17.3 J/m for the binary PLA/PA11 system and the elongation at break is more than 200%. The mechanical properties of the binary blends of PLA and PA11 containing 20% PEBA are also shown in Table 7.3. Although the tensile properties of these blends are considerably enhanced, the impact strength at 31.6 and 35.2 J/m only show limited improvements.

The mechanical properties of the ternary PLA/PEBA/PA11 45/10/45 system in Table 7.3 indicates a clear role between the phase structure and mechanical properties. The impact and elongation at break of the ternary PLA/PEBA/PA11 45/10/45 system significantly increase to 142.4 J/m for the impact strength and 250% for the elongation at break.

When PEO is also added to the PLA/PEBA/PA11 ternary blend, this quaternary system exhibits a remarkable ultra-tough behavior with an impact strength of 728.6 J/m and an elongation at break of 465% (Table 7.3). This synergy does not occur when either PEBA or PEO is absent from the quaternary blend. As shown in Table 7.3 the impact strength of the ternary PLA(PEO)/PA11 50(20)/50 blend is significantly lower than that the quaternary system. This results underline the importance of the mutual presence of PEBA and PEO in the ultra-toughening of the PLA/PA11 system. In the following sections an emphasis will be placed on understanding this dramatic increase in impact strength for the quaternary PLA(PEO)/PEBA/PA11 system.

Table 7.3. Mechanical properties of the pure components as well as binary, ternary and quaternary systems.

Sample	Izod Impact Strength (J/m)	Young's Modulus (GPa)	Tensile Strength (MPa)	Elongation at Break (%)
PLA	15.9±0.7	4.3±0.3	65.6±1.2	3.6
PA11	69.4±4.6	1.4±0.04	41.2±0.2	235
PLA/PEBA 80/20	31.6±3.6	2.7±0.1	44.0±0.1	145
PA11/PEBA 80/20	35.2±1.1	1.1±0.1	33.4±0.1	450
PLA/PEO 80/20	16.8±1.0	1.8±0.2	28.3±1.0	>500
PLA/PA11 50/50	17.3±0.6	2.5±0.16	49.0±1.2	3.7
PLA(PEO)/PA11 50(20)/50	58.2±3.0	1.6±0.1	30.0±1.3	250
PLA/PEBA/PA11 45/10/45	142.4±15.9	2.1±0.04	43.2±3.4	230
PLA(PEO)/PEBA/PA11 45(20)/10/45	728.6±53.0	1.2±0.05	28.2±0.7	465

7.4.4 Relationship between Impact Strength and PEBA, PEO Contents

The concentration of PEBA was varied from 0 to 20 wt% in the ternary PLA/PEBA/PA11 and quaternary PLA(PEO)/PEBA/PA11 systems in order to examine its effect on the impact strength (see Figure 7.3). The impact strength of both the ternary and quaternary systems increase with PEBA content and level off at 10% PEBA at values of 140 J/m and 730 J/m, respectively. As discussed earlier, PEBA spreads at the interface of the PLA and PA11 phases and forms a layer in both systems with and without PEO. The interfacial coverage of the PEBA phase has been estimated through image analysis and is presented in Figure 7.3. Full interfacial coverage of PEBA at the PLA(PEO)/PA11 interface is obtained at and above 10% PEBA. Full interfacial coverage correlates very well with the dramatic improvement in impact strength. The layer thickness at 10% PEBA is approximately 350 nm.
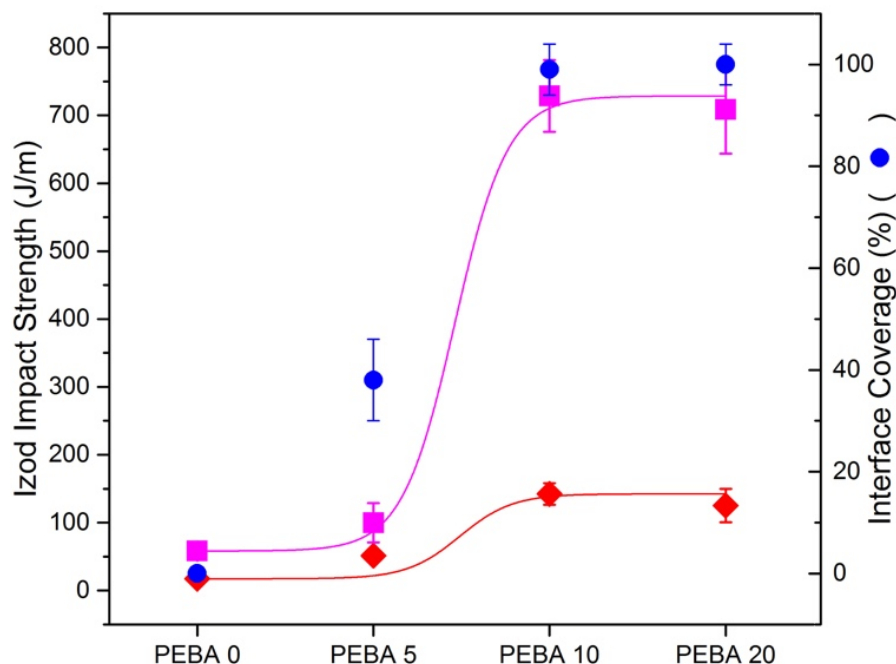
Figure 7.3. Impact strength as a function of PEBA content in PLA/PEBA/PA11 where the PLA:PA11 ratio is maintained at 1:1 (◆) and PLA(PEO)/PEBA/PA11 with 20% PEO (based on the PLA content) and a PLA:PA11 ratio of 1:1. (■). Also shown is the PEBA interfacial coverage (●) in both the ternary and quaternary systems as a function of PEBA content.

PEO appears to be a crucial component in toughening the PLA/PEBA/PA11 system. The Izod impact strength of the quaternary PLA(PEO)/PEBA/PA11 45(x)/10/45 blends containing 0 to 25% of PEO is presented in Figure 7.4. The optimum amount of PEO in the system to achieve the highest impact strength is approximately 20% (based on the PLA content). This concentration is well within the miscibility range reported in the literature [44]. Figure 7.4 shows that a broad range of impact strengths from about 100 to 800 J/m can be obtained by adjusting the PEO concentration. It should be noted that the impact strength drops upon increasing the PEO concentration above the optimum concentration. It is likely that this effect at the higher PEO content is due to an onset of phase separation of PEO in PLA. Phase separated PEO would be expected to accumulate at the PLA/PEBA interface and significantly weaken the interfacial adhesion. It is worth noting that the high molecular weight of PEO used in this study almost completely eliminates possible aging effects as observed in plasticized systems with low molecular weight plasticizers such as PEG.
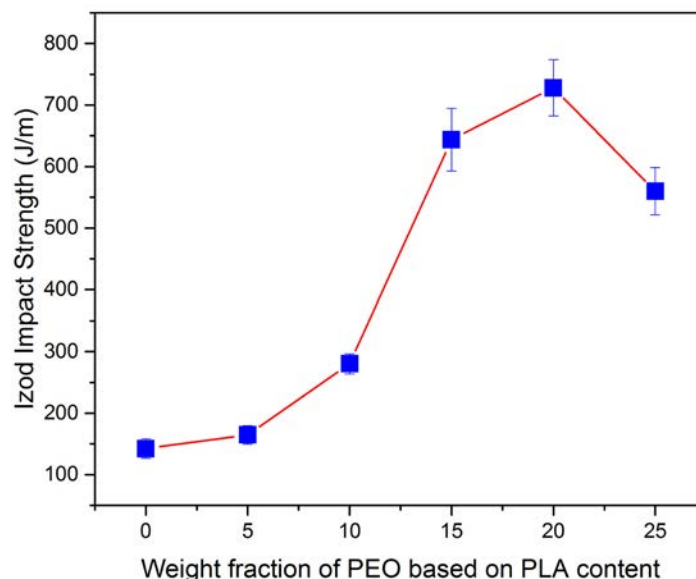
Figure 7.4. Impact strength as a function of PEO content in PLA(PEO)PEBA/PA11 with 45PLA(xPEO)/10PEBA/45PA11.

7.4.5 Relationship between Impact Toughness and Continuity

The effect of the composition ratio of PLA to PA11 on the impact strength was also examined in the systems containing a fixed concentration of PEBA (10%). Figure 7.5 demonstrates the notched Izod impact strength of the ternary PLA/PEBA/PA11 systems as a function of PLA content. It should be noted that the continuity of the PLA phase is examined as a function of the % concentration of PLA in (PLA plus PA11) where PLA plus PA11 always equals 90% in the ternary and quaternary blends with PEBA as mentioned earlier. Thus 100% PLA refers to the 90%PLA/10%PEBA/0%PA11 blend while 50% PLA in Figure 7.5 refers to the 45%PLA/10%PEBA/45%PA11 blend. Although, limited improvements in impact strength are observed under 40% and above 60% PLA, an important increase is obtained at 50% PLA with an impact strength of 142.4 J/m achieved. The continuity levels of PLA and PA11 are also presented in Figure 7.5 along with the impact strength results. The high toughness achieved at 50% PLA in the ternary blend corresponds to the region of co-continuity PLA/PA11 where both PLA and PA11 possess very high levels of phase continuity. The phase morphologies presented in Figure 7.2 are in accordance with the continuity results obtained for the ternary PLA/PEBA/PA11 blends. Since

the PEBA phase completely spreads at the interface of the PLA and PA11 phases, a tri-continuous morphology is generated in the PLA/PEBA/PA11 45/10/45 blend.
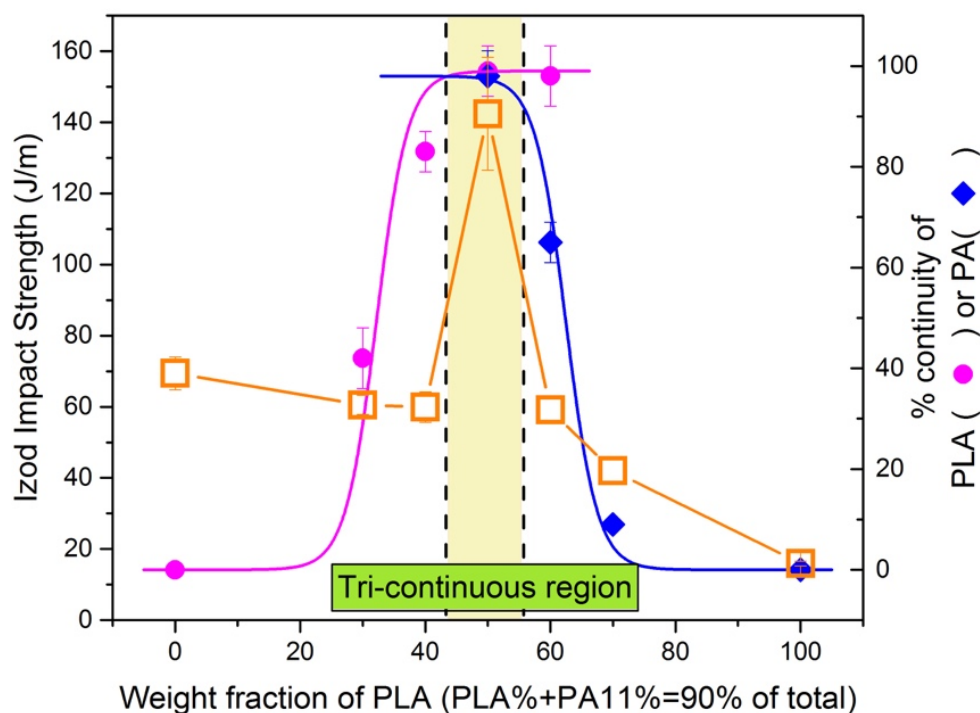
Figure 7.5. Impact strength (□) as a function of the weight content of PLA in PLA/PEBA/PA11 with 10% PEBA. Phase continuity of PLA (●) or PA11 (◆) in the same blends.

Figure 7.6 demonstrates the effect of PLA composition on the Izod impact strength of the quaternary PLA(PEO)/PEBA/PA11 systems with constant 10% PEBA and 20% PEO contents. Ultra-toughening was achieved at a PLA concentration of about 50 to 60 % while below and beyond this range very limited improvements were observed. The phase morphology results presented in Figure 7.2 imply a tri-continuous structure in the range of 50 to 60% of PLA where PEBA forms a continuous layer between the continuous PEO modified PLA phase and the continuous PA11 phase. The % continuity results from the solvent extraction/gravimetry procedure are shown in Figure 7.6 and confirm the formation of a co-continuous structure of PLA and PA11 in which the PEBA phase is localized at the interface of PLA/PA11. Note that the continuity reported as PLA in Figure 6 is actually for both PLA and PEO and is represented as PLA(PEO).
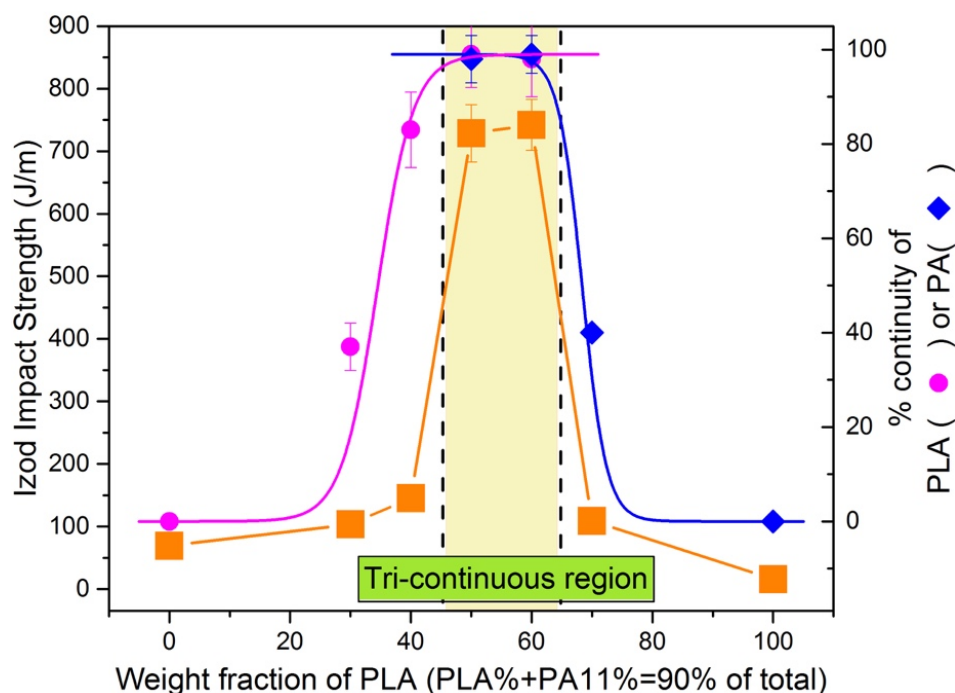
Figure 7.6. Impact strength (■) as a function of the weight content of PLA in PLA(PEO)/PEBA/PA11 with 10% PEBA and 20% PEO based on the PLA content. Phase continuity of PLA(PEO) (●) or PA11 (◆) in the same blends.

7.4.6 Interfacial Interactions

There are a range of interfacial interactions possible between the various components in the ternary (PLA/PEBA/PA11) and quaternary (PLA(PEO)/PEBA/PA11) systems studied here. In this study the addition of PEBA, in the case of the ternary blend, and of a further addition of PEO, in the quaternary system, are essential components in the dramatic improvements in impact strength observed in this work. Some studies have reported that PLA can be partially miscible with polyamides due to hydrogen bonding between the ester groups of PLA and amine groups of polyamide [45,46]. Nevertheless, the impact strength of the PLA/PA11 blend, as reported in Table 7.3, is very low at 17.3 J/m. Hence these interactions, though possible, are clearly insufficient to improve a high deformation property such as impact strength.

PLA and PA11 are both stiff polymers that form a rigid interface which fails to effectively transfer stress at the interface and becomes the weakest point during fracture. In this work, the rigid interface of PLA/PA11 is converted into a much more deformable one by the self-assembling of

thermoplastic elastomer PEBA at the interface as discussed earlier. Furthermore, PEBA at the interface of PLA/PA11 can provide good compatibility with PLA and PA11. The PEBA used in this study consists of hard segments of polyamide 12 and soft segments of polyethylene oxide [47]. The PEO segments are compatible with PLA while the polyamide segments in PEBA possess a natural affinity for PA11. The binary blend of PLA/PEO 80/20 shows a single glass transition temperature emphasizing the high compatibility between PLA and PEO chains as presented in Table 7.4. The binary blend of PLA/PEBA 80/20 was also prepared to analyze the interactions between PLA and PEBA. The glass transition temperature of the PEO segments in the PEBA rich phase increases significantly (about 10 °C) and the glass transition temperature of the PLA rich phase decreases (about 2 °C) which indicate partial miscibility between PLA and PEBA. The melting temperature of both phases was also changed confirming the interfacial interactions between PLA and PEBA phases. Further evidence of interfacial interactions between PLA and PEBA is also observed in ternary PLA/PEBA/PA11 45/10/45 blends where the glass transition temperatures of PLA and PEBA components move towards each other and the melting temperature of the PLA phase is reduced (Table 7.4).

Table 7.4. Thermal properties of the pure polymers and binary, ternary, and quaternary blends. In the table a, b, and c denotes PLA, PA11 and PEBA respectively.

Samples	T_g (°C)	T_{cc} (°C)	T_m (°C)	X_c (%)
PLA[a]	59	108	154	1
PA11[b]	43	–	189	57
PEBA[c]	-59, 42	–	8, 158	–
PLA/PEBA 80/20	58[a], -49[c]	112[a]	148[a], -7[c], 159[c]	5[a]
PA11/PEBA 80/20	43[b,c], -56[c]	–	148[b], 154[b], 157[c]	57
PLA/PEO 80/20	40[a]	–	154[a]	22[a]
PLA/PA11 50/50	–	121[a]	150[a], 189[b]	20[a], 40[b]
PLA/PEBA/PA11 45/10/45	57[a], -50[c]	128[a]	151[a], 189[b]	2[a], 42[b]
PLA(PEO)/PEBA/PA11 45(20)/10/45	32[a], -50[c]	82[a]	154[a], 189[b]	9[a], 68[b]

The further addition of PEO to the PLA(PEO)/PEBA/PA11 in the quaternary blend allows for even significantly further enhanced interactions between PLA(PEO) and PEBA. The PEO chains within

the PLA phase have a natural compatibility with the PEO segments of PEBA. Furthermore, the addition of PEO to PLA renders the PLA much less rigid and thus also contributes to the creation of a more elastic interface with PEBA and PA11. It was shown earlier that the interfacial tensions between components decreases with the addition of PEO to PLA (see Table 7.2). Furthermore, the lowered glass transition temperature of PLA in the miscible blend of PLA/PEO 80/20 conveys the plasticization effect of PEO molecules on PLA.
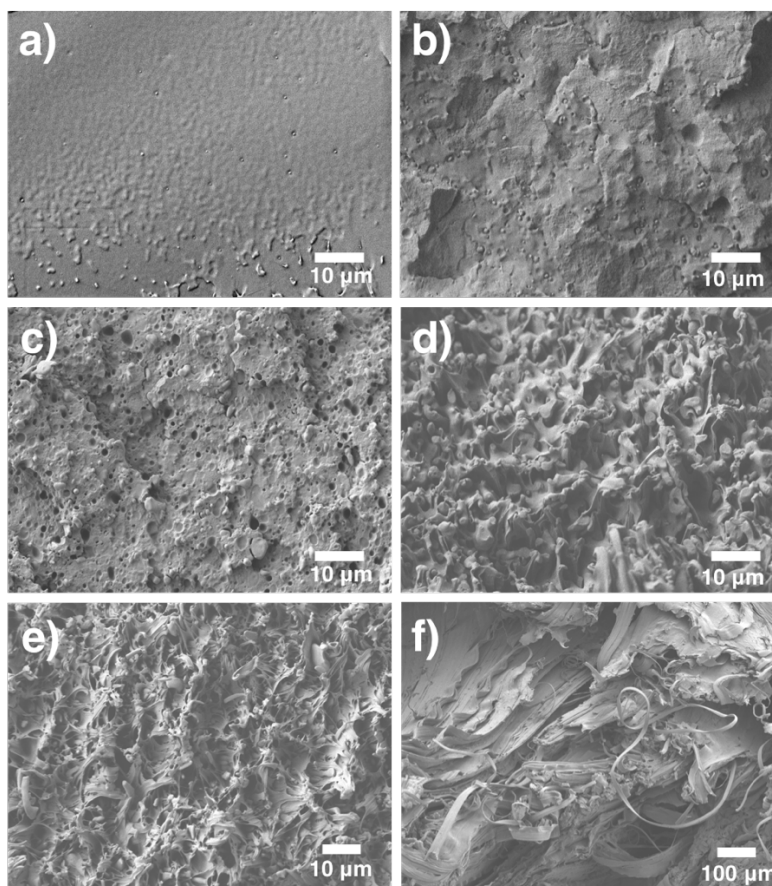
Figure 7.7. SEM micrographs of the impact fracture surface adjacent to the notch of a) neat PLA, b) PLA/PA11 50/50, c) PLA/PEBA/PA11 27/10/67, d) PLA/PEBA/PA11 45/10/45, e) PLA(PEO)/PEBA/PA11 27(20)/10/67 and f) PLA(PEO)/PEBA/PA11 45(20)/10/45.

7.4.7 Toughening Mechanism

Figure 7.7 shows the micrographs of the impact fracture surfaces of the pure PLA, PLA/PA11, PLA/PEBA/PA11 and PLA(PEO)/PEBA/PA11 systems. PLA displays a smooth and featureless

fracture surface indicating a typical brittle fracture behavior as reported in the literature (Figure 7.7a) [45]. Similarly, the fracture surface of the binary PLA/PA11 50/50 is a smooth surface demonstrating a brittle fracture behavior with no perceptible deformation of PLA or PA11 phases (Figure 7.7b). To explain the observed results, generally crazing and shear yielding are two main mechanisms that are discussed in the toughening of polymeric systems [48]. In rigid-rigid polymer blends, crazing is the dominant fracture mechanism which easily develops into a catastrophic crack in the absence of an effective termination mechanism [49]. The results suggest that the PLA and PA11 matrices experience brittle failure mode through unstable crazing. The modulus mismatch between PLA and PA11 results in stress-concentration at the interface and consequently interfacial failure and crack propagation.

When the fracture surfaces of the PLA/PEBA/PA11 blend is examined a number of interesting features are observed. Firstly, the PLA/PEBA/PA11 27/10/67 fracture surface shown in Figure 7.7c does not appear to indicate any matrix shear yielding. Only a moderate toughening effect is observed in this case (see Figure 7.7c) and the fracture surface shows a rougher surface with some voids and debonding at the dispersed phase interface.

In comparison to the PLA/PEBA/PA11 27/10/67 blend, the impact fracture surface of the PLA/PEBA/PA11 45/10/45 system shows a much rougher surface with more shear zones and fibrillation in the PLA and PA11 (Figure 7.7d). These results suggest that localized plastic deformation of the co-continuous PLA and PA11 matrices occurred near the PEBA continuous phase indicating that percolated PEBA at the interface of PLA and PA11 is effective in triggering pervasive plastic deformation of the PLA and PA11. These results show a clear distinction in fracture mechanisms when PLA and PA11 are in a matrix/dispersed phase morphology as compared to a co-continuous one.

The addition of PEO in the quaternary PLA(PEO)/PEBA/PA11 system completely changes the fracture behavior. Extensive plastic deformation is observed for the 45(20)/10/45 blend as presented in Figure 7.7f. The results indicate that shear yielding occurs and runs through the entire sample. These results clearly support the ultra-high impact results observed in Figure 7.6. In contrast, the fracture surface of samples beyond the tri-continuous region (<50% and >60% of PLA based on PLA plus PA11 equal to 90% of total) show considerably less plastic deformation as

presented in Figure 7.7e. These observations also emphasize the importance of the tri-continuous morphology in the quaternary blend of PLA(PEO)/PEBA/PA11 in achieving ultra-tough systems.

In order to get a more in-depth understanding of the toughening mechanism, the cryo-fractured cross section underneath the impact fracture surface of the samples was analyzed by SEM and is shown in Figure 7.8. The quaternary PLA(PEO)/PEBA/PA11 45(20)/10/45 system shows the formation of submicron-size cavitation within the PEBA layer (indicated by the arrow). PEBA is a copolymer of blocks of PEO and PA12 which can form a co-continuous nanostructure through the PEBA phase. The hard PA12 blocks can act as physical crosslink sites for the PEO segments, which are considerably above their glass transition temperature at room temperature (about 80 °C). Therefore, owing to the excellent interfacial adhesion between PEBA and plasticized PLA and PA11, the rubbery PEO domains in PEBA cavitate within the interconnected network of PEBA throughout the sample. It is well known that rubber particle cavitation is an important part of the toughening mechanism in rubber-modified polymers [50] and that cavitation is the main dilatational deformation process in rubber toughened systems [51,52]. The high level of percolated cavitation within the PEBA phase can achieve this similar effect and thus provide a critical stress-relief mechanism.
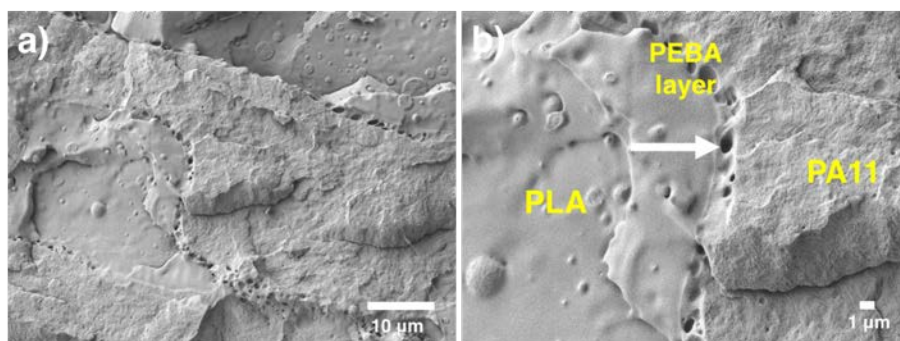
Figure 7.8. SEM micrographs of the cryo-fractured surface of a cross-section underneath the impact fracture surface of the PLA(PEO)/PEBA/PA11 45(20)/10/45 blend showing cavitation.

Figure 7.9 displays a schematic qualitatively describing the toughening mechanism in these systems. The PEBA phase forms an interconnected structure throughout the blend in the tri-continuous systems (Figure 7.9b). The good interfacial adhesion of the PEBA layer with PA11 and the plasticized PLA effectively promotes stress transfer during the fracture process, which

facilitates cavitation of the soft segments of PEBA. A percolated stress field forms around the PEBA layer upon cavitation which initiates plastic deformation of the surrounding matrices (Figure 7.9b'). Consequently, the yielding process propagates over the entire deformation zone and results in a toughened blend through a shear yielding mechanism. Since the PEBA is fully continuous within the quaternary blend, this cavitation propagates as a network over the entire sample in a stable fashion. The presence of PEO also lowers the yield strength of the PLA matrix which would be expected to facilitate the dilatational deformation of the PLA matrix. This mechanism is absent in the matrix/dispersed morphologies shown in Figure 7.9a and c. Clearly more detailed fracture analysis will be necessary in order to fully understand this complex system. Nevertheless, this work shows the excellent potential of ternary and quaternary polymer blends with co-continuous structures, a rubbery intermediate phase and good interfacial interactions to generate ultratough polymeric materials. In summary, the synergetic effect of PEBA and PEO along with the unique tri-continuous structure were believed to promote the toughness of the blends.

PLA   PA   PEBA
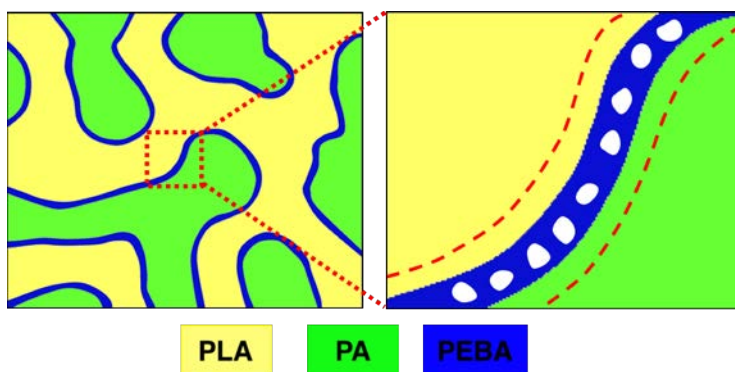
Figure 7.9. Schematic of toughening in the PLA(PEO)/PEBA/PA11system comprised of a 3D interconnected network of a cavitated middle rubbery PEBA layer. The dashed lines along the rubbery layer demonstrate an effective stress-field surrounding the layer.

7.5 CONCLUSION

It is shown that a PEBA thermoplastic elastomer completely wets the interface of PLA and PA11 and assembles into a fully percolated rubbery network at the interface of PLA/PA11 constituting a tri-continuous phase morphology. The polyether component of PEBA is capable of strong

interfacial interactions with PLA and the amide component in the copolymer has a natural affinity for the PA11. The addition of the elastomeric PEBA phase to the binary PLA/PA11 blend also replaces a rigid PLA/PA11 interface with a much more deformable one. An optimum concentration of PEBA (10%) was required to completely cover the interfacial area of the co-continuous PLA/PA11 system where a 350 nm thick PEBA layer effectively increases the toughness from 17.3 to 142.4 J/m in the ternary and to 728.6 J/m in the quaternary systems. The addition of PEO (up to 20%) to the ternary PLA/PEBA/PA11 blend with tri-continuous morphology generates ultratough blends with an impact strength reaching 800 J/m. The added PEO maintains the potential for strong interfacial interactions with PEBA, but also results in a significant increase in the chain mobility of PLA which further enhances the capability for interfacial interactions. The surface analysis of the fractured samples shows a brittle-ductile transformation for the ultratough tri-continuous quaternary blends and the presence of significant interfacial cavitation within the PEBA layer.

7.6 ACKNOWLEDGMENT

7.7 REFERENCES

[1]   M. Vert, G. Schwarch, J. Coudane, Present and Future of PLA Polymers, J. Macromol. Sci. Part A. 32 (1995) 787–796.

[2]   D. Garlotta, A literature review of poly (lactic acid), J. Polym. Environ. 9 (2001) 63–84.

[3]   K.S. Anderson, K.M. Schreck, M.A. Hillmyer, Toughening polylactide, Polym. Rev. 48 (2008) 85–108.

[4]   H. Liu, J. Zhang, Research progress in toughening modification of poly(lactic acid), J. Polym. Sci. Part B Polym. Phys. 49 (2011) 1051–1083.

[5]   K.S. Anderson, S.H. Lim, M.A. Hillmyer, Toughening of polylactide by melt blending with linear low-density polyethylene, J. Appl. Polym. Sci. 89 (2003) 3757–3768.

[6]   W. Dong, M. He, H. Wang, F. Ren, J. Zhang, X. Zhao, Y. Li, PLLA/ABS Blends Compatibilized by Reactive Comb Polymers: Double T_g Depression and Significantly

Improved Toughness, ACS Sustain. Chem. Eng. 3 (2015) 2542–2550.

[7] Y. Li, H. Shimizu, Toughening of polylactide by melt blending with a biodegradable poly(ether)urethane elastomer., Macromol. Biosci. 7 (2007) 921–8.

[8] Z. Liu, Y. Luo, H. Bai, Q. Zhang, Q. Fu, Remarkably Enhanced Impact Toughness and Heat Resistance of poly(L-Lactide)/Thermoplastic Polyurethane Blends by Constructing Stereocomplex Crystallites in the Matrix, ACS Sustain. Chem. Eng. 4 (2016) 111–120.

[9] H.T. Oyama, Super-tough poly(lactic acid) materials: Reactive blending with ethylene copolymer, Polymer. 50 (2009) 747–751.

[10] K. Zhang, V. Nagarajan, M. Misra, A.K. Mohanty, Supertoughened Renewable PLA Reactive Multiphase Blends System: Phase Morphology and Performance., ACS Appl. Mater. Interfaces. 6 (2014) 12436–48.

[11] M. Todo, S.-D. Park, T. Takayama, K. Arakawa, Fracture micromechanisms of bioabsorbable PLLA/PCL polymer blends, Eng. Fract. Mech. 74 (2007) 1872–1883.

[12] H. Bai, H. Xiu, J. Gao, H. Deng, Q. Zhang, M. Yang, Q. Fu, Tailoring impact toughness of poly(L-lactide)/poly(ε-caprolactone) (PLLA/PCL) blends by controlling crystallization of PLLA matrix., ACS Appl. Mater. Interfaces. 4 (2012) 897–905.

[13] T. Yokohara, M. Yamaguchi, Structure and properties for biomass-based polyester blends of PLA and PBS, Eur. Polym. J. 44 (2008) 677–685.

[14] V. Ojijo, S.S. Ray, R. Sadiku, Toughening of biodegradable polylactide/poly(butylene succinate-co-adipate) blends via in situ reactive compatibilization., ACS Appl. Mater. Interfaces. 5 (2013) 4266–76.

[15] M.L. Robertson, J.M. Paxton, M. a. Hillmyer, Tough blends of polylactide and castor oil, ACS Appl. Mater. Interfaces. 3 (2011) 3402–3410.

[16] W.M. Gramlich, M.L. Robertson, M. a. Hillmyer, Reactive compatibilization of poly(L-lactide) and conjugated soybean oil, Macromolecules. 43 (2010) 2313–2321.

[17] R. Rulkens, C. Koning, Chemistry and Technology of Polyamides, in: Polym. Sci. A Compr. Ref. 10 Vol. Set, 2012: pp. 431–467.

[18] G. Stoclet, R. Seguela, J.-M. Lefebvre, Morphology, thermal behavior and mechanical properties of binary blends of compatible biosourced polymers: Polylactide/polyamide11, Polymer. 52 (2011) 1417–1425.

[19] R. Patel, D.A. Ruehle, J.R. Dorgan, P. Halley, D. Martin, Biorenewable blends of polyamide-11 and polylactide, Polym. Eng. Sci. 54 (2014) 1523–1532.

[20] A. Nuzzo, S. Coiai, S.C. Carroccio, N.T. Dintcheva, C. Gambarotti, G. Filippone, Heat-Resistant Fully Bio-Based Nanocomposite Blends Based on Poly(lactic acid), Macromol. Mater. Eng. 299 (2014) 31–40.

[21] a. Nuzzo, E. Bilotti, T. Peijs, D. Acierno, G. Filippone, Nanoparticle-induced co-continuity in immiscible polymer blends – A comparative study on bio-based PLA-PA11 blends filled with organoclay, sepiolite, and carbon nanotubes, Polymer. 55 (2014) 4908–4919.

[22] Y. Shi, W. Zhang, J. Yang, T. Huang, N. Zhang, Y. Wang, G. Yuan, C. Zhang, Super toughening of the poly(l-lactide)/thermoplastic polyurethane blends by carbon nanotubes, RSC Adv. 3 (2013) 26271.

[23] T.W. Cheng, H. Keskkula, D.R. Paul, Property and morphology relationships for ternary blends of polycarbonate, brittle polymers and an impact modifier, Polymer. 33 (1992) 1606–1619.

[24] I. Luzinov, K. Xi, C. Pagnoulle, G. Huynh-Ba, R. Jerome, Composition effect on the core-shell morphology and mechanical properties of ternary polystyrene/styrene butadiene rubber polyethylene blends, Polymer. 40 (1999) 2511–2520.

[25] Z.-Z. Yu, Y.-C. Ou, Z.-N. Qi, G.-H. Hu, Toughening of nylon 6 with a maleated core-shell impact modifier, J. Polym. Sci. Part B Polym. Phys. 36 (1998) 1987–1994.

[26] Z. Yu, M. Lei, Y. Ou, G. Hu, The Role of Interfacial Modifier in Toughening of Nylon-6 with a Core-Shell Toughener, J. Polym. Sci. Part B Polym. Phys. 37 (1999) 2664–2672.

[27] Z. Ke, D. Shi, J. Yin, R.K.Y. Li, Y.W. Mai, Facile method of preparing supertough polyamide 6 with low rubber content, Macromolecules. 41 (2008) 7264–7267.

[28] R.C. Willemse, A. Speijer, A.E. Langeraar, A.P. de Boer, Tensile moduli of co-continuous

polymer blends, Polymer. 40 (1999) 6645–6650.

[29] A. Mamat, T. VuKhanh, P. Cigana, B.D. Favis, Impact fracture behavior of nylon-6/ABS blends, J. Polym. Sci. Part B-Polymer Phys. 35 (1997) 2583–2592.

[30] J.P.. Inberg, R.. Gaymans, Co-continuous polycarbonate/ABS blends, Polymer. 43 (2002) 2425–2434.

[31] Y. Li, H. Shimizu, Improvement in toughness of poly(l-lactide) (PLLA) through reactive blending with acrylonitrile-butadiene-styrene copolymer (ABS): Morphology and properties, Eur. Polym. J. 45 (2009) 738–746.

[32] S.L. Bai, G.T. Wang, J.M. Hiver, C. G'Sell, Microstructures and mechanical properties of polypropylene/polyamide 6/polyethelene-octene elastomer blends, Polymer. 45 (2004) 3063–3071.

[33] C. G'Sell, S.-L. Bai, J.-M. Hiver, Polypropylene/polyamide 6/polyethylene–octene elastomer blends. Part 2: volume dilatation during plastic deformation under uniaxial tension, Polymer. 45 (2004) 5785–5792.

[34] S.L. Bai, C. G'Sell, J.M. Hiver, C. Mathieu, Polypropylene/polyamide 6/polyethylene-octene elastomer blends. Part 3. Mechanisms of volume dilatation during plastic deformation under uniaxial tension, Polymer. 46 (2005) 6437–6446.

[35] K. Hashima, S. Nishitsuji, T. Inoue, Structure-properties of super-tough PLA alloy with excellent heat resistance, Polymer. 51 (2010) 3934–3939.

[36] P. Sarazin, G. Li, W.J. Orts, B.D. Favis, Binary and ternary blends of polylactide, polycaprolactone and thermoplastic starch, Polymer. 49 (2008) 599–609.

[37] S. Ravati, B.D. Favis, Interfacial coarsening of ternary polymer blends with partial and complete wetting structures, Polymer. 54 (2013) 6739–6751.

[38] J. Wang, A. Reyna-Valencia, B.D. Favis, Assembling Conductive PEBA Copolymer at the Continuous Interface in Ternary Polymer Systems: Morphology and Resistivity, Macromolecules. 49 (2016) 5115–5125.

[39] P.H.M. Elemans, J.M.H. Janssen, H.E.H. Meijer, The measurement of interfacial tension in

polymer/polymer systems: The breaking thread method, J. Rheol. 34 (1990) 1311–1325.

[40] Q. Zhang, Z. Mo, S. Liu, H. Zhang, Influence of annealing on structure of Nylon 11, Macromolecules. 33 (2000) 5999–6005.

[41] S.Y. Hobbs, M.E.J. Dekkers, V.H. Watkins, Effect of interfacial forces on polymer blend morphologies, Polymer. 29 (1988) 1598–1602.

[42] T.S. Valera, A.T. Morita, N.R. Demarquette, Study of morphologies of PMMA/PP/PS ternary blends, Macromolecules. 39 (2006) 2663–2675.

[43] A.M. Zolali, B.D. Favis, Partial and Complete Wetting in Ultra-low Interfacial Tension Multiphase Blends with Polylactide, J. Phys. Chem. B. (2016) Submitted.

[44] A.J. Nijenhuis, E. Colstee, D.W. Grijpma, A.J. Pennings, High molecular weight poly(L-lactide) and poly(ethylene oxide) blends: Thermal characterization and physical properties, Polymer. 37 (1996) 5849–5857.

[45] F. Feng, L. Ye, Structure and Property of Polylactide/Polyamide Blends, J. Macromol. Sci. Part B. 49 (2010) 1117–1127.

[46] Y. Lin, K.Y. Zhang, Z.M. Dong, L.S. Dong, Y.S. Li, Study of hydrogen-bonded blend of polylactide with biodegradable hyperbranched poly(ester amide), Macromolecules. 40 (2007) 6257–6267.

[47] V.I. Bondar, B.D. Freeman, I. Pinnau, Gas sorption and characterization of poly(ether-b-amide) segmented block copolymers, J. Polym. Sci. Part B Polym. Phys. 37 (1999) 2463–2475.

[48] D.R. Paul, C.B. Bucknall, Polymer Blends, John Wiley & Sons, Inc., New York, 2000.

[49] G.X. Wei, H.J. Sue, J. Chu, C. Huang, K. Gong, Toughening and strengthening of polypropylene using the rigid-rigid polymer toughening concept. Part I. Morphology and mechanical property investigations, Polymer. 41 (2000) 2947–2960.

[50] C.B. Bucknall, a. Karpodinis, X.C. Zhang, A model for particle cavitation in rubber-toughened plastics, J. Mater. Sci. 29 (1994) 3377–3383.

[51] D. Dompas, G. Groeninckx, M. Isogawa, T. Hasegawa, M. Kadokura, Toughening

behaviour of rubber-modified thermoplastic polymers involving very small rubber particles: 3. Impact mechanical behaviour of poly(rmvinyl chloride)/methyl methacrylate-butadiene-styrene graft copolymer blends, Polymer. 35 (1994) 4760–4765.

[52] C.B. Bucknall, D.R. Paul, Notched impact behavior of polymer blends: Part 1: New model for particle size dependence, Polymer. 50 (2009) 5539–5548.

[53] V.T. Phuong, M.B. Coltelli, P. Cinelli, M. Cifelli, S. Verstichel, A. Lazzeri, Compatibilization and property enhancement of poly(lactic acid)/polycarbonate blends through triacetin-mediated interchange reactions in the melt, Polymer. 55 (2014) 4498–4513.

[54] E. Landreau, L. Tighzert, C. Bliard, F. Berzin, C. Lacoste, Morphologies and properties of plasticized starch/polyamide compatibilized blends, Eur. Polym. J. 45 (2009) 2609–2618.

CHAPTER 8   GENERAL DISCUSSION

The work presented in this dissertation has provided valuable insights for the understanding of partial and completely wet phase structuring and associated toughness enhancement in multicomponent blends with PLA. We investigated the structuring of some complex morphologies in multiphase biobased blends. Since almost all the biodegradable polymers are biopolyesters, the ternary and quaternary biodegradable system studied in the first part of this study, i.e. PLA/PBS/PBAT and PLA/PBS/PBAT/PHBV, are the most relevant multicomponent blends and represent a good model system to evaluate and understand morphology development in biodegradable systems. Duo to the similar molecular structure of these polymers, they possess very low interfacial tension which limits the credibility of the thermodynamic analysis. Thus, a rigorous examination of the interfacial tensions using multiple methods was performed to obtain the most accurate results. It was found that the final structures of the systems are in accordance with the thermodynamic predictions after quiescent annealing process. However, composition dependent morphologies were observed for the quaternary system which is not occurred in the ternary PLA/PBS/PBAT system. These results indicate that composition control during the mixing of multiphase systems with low interfacial tensions can result in a complete change of spreading behavior. In terms of mechanical properties, the best results have been obtained for the ternary PLA/PBS/PBAT system which demonstrates a significant improvement in toughness; however, no considerable enhancement was observed for the quaternary systems. Thus, further attempts were made to understand the morphology development in biobased systems based on PLA and to examine their potential in toughening of PLA.

Partial wetting was involved in all of these morphology transitions which is less understood as compared to complete wetting behavior. Thus, in the second part of this research work, an attempt has been made to understand some aspects of morphology development in systems with partial wetting behavior. Three different systems PLA/PHBV/PBS, PLA/PBAT/PE and PLA/PE/PBAT which demonstrate a range of partial wetting tendencies were prepared to study the evolution of the morphology of an intermediate phase demonstrating partial wetting morphology. Two distinct wetting behaviors were observed: a) stable partially wet droplets despite high composition of the intermediate phase and even after long annealing process for the PLA/PE/PBAT system, b) a

composition dependent wetting transition from partially wet droplets to a complete wet layer for the PLA/PHBV/PBS and PLA/PBAT/PE systems. Through an examination of interfacial tensions and thermodynamic analysis, two classes of partial wetting were defined: strong and weak partial wettings. The system with strong partial wetting is found to retain its morphology whereas the wetting transition only occurs in the systems with weak partial wetting. The systems were examined through a dewetting/coalescence model and it was found that the wetting behavior is dominated by the dewetting speed. The confinement of the partially wet droplets at the interface significantly influences the wetting behavior. These results show the excellent potential for controlled wetting and structuring in ternary polymer systems and presents a route towards the preparation of a range of new morphological structures.

In the two last parts of this research work, the two wetting behaviors, namely partial and complete wettings, were examined for their potential in enhancing the mechanical performance of PLA/PA11 biobased system. It was found that through control of the morphology, significantly improved properties are achieved with both wetting structures. The interfacial assembly of four different partially wet polymeric droplets, i.e. PBS, PBAT, EMA, and EMA-GMA, at the co-continuous PLA/PA11 interface was examined. The partially wet droplets at the interface result in a concurrent compatibilization and brittle to ductile transition effects for the various blends. The fractured surface analysis revealed that the percolation of the stress field around the cavitated partially wet droplets at the interface effectively changes failure mode from crazing to shear yielding. On the other hand, suitable interfacial interactions and inherent rubbery properties for cavitation are essential in partially wet droplets for achieving a significant compatibilization effect and enhanced tensile toughness and notched Izod impact strength in PLA/PA11. These results indicate the significant potential of the partially wet morphology as a promising strategy to compatibilize and toughen materials.

A completely different strategy consisting of morphology control along with the plasticization of the PLA phase was employed for the ultra-toughening of the PLA/PA11 system. The toughening strategy presented in the PLA/PEBA/PA11 system, which demonstrates complete wetting behavior, clearly accentuates the prominent role of morphology in achieving high performance materials. The enhanced toughening was only observed when all the phases form fully percolated structure, in which beyond this critical tri-continuous composition region poor toughness is

obtained. In addition, it was shown that interfacial interactions play an important role in enhancing the mechanical properties. The further incorporation of PEO due to its plasticization effect increases the mobility of the PLA chains and consequently enhances the interfacial interactions between the PLA and PEBA phases. These results clearly indicate that both morphology and interfacial adhesion must be controlled to achieve high toughening effect in multiphase systems. A significantly enhanced notched Izod impact strength of over 730 J/m is achieved for the quaternary PLA(PEO)/PEBA/PA11 45(20)/10/45 blend in this study which is considerably higher than typical values reported for common engineering compounds in the market such as HIPS with notched impact strength below 200 J/m and in the range of values obtained for super tough nylon at about 900 J/m. However, as is often observed with rubber toughening(Bartczak & Galeski 2014) and plasticization(Immergut & Mark 1965) of glassy polymers, the modulus and yield strength relative to the binary PLA/PA11 50/50 decreases by 40-45%. Several approaches can be taken to compensate for the reduced modulus and strength in these systems. First, the type and amount of plasticizer, in particular the molecular weight of PEO, can be optimized to lower the loss associated with the use of the plasticizer. Second, the crystallinity of the PLA phase can play an important role in setting the mechanical properties of these systems. Increasing the crystallinity of PLA can significantly improve the modulus and tensile strength of the blends, although a reduction in the toughness is also expected.

The results obtained from this dissertation are promising for the future of bioplastics as alternative materials to petroleum based plastics. The approaches developed in this study can be used to generate high performance biobased materials for value added application, which currently are reserved for a limited number of engineering plastics. Most importantly, these structures, as opposed to the typical high performance blend materials available in the market which possess a matrix/dispersed morphology, have a co-continuous structure. They can be designed to meet specific requirements through tailored structures for multi-functional applications such as high impact electro-conductive materials.

CHAPTER 9   CONCLUSION AND RECOMMENDATIONS

In this dissertation, we studied the structuring of the phase morphology in ternary and quaternary bioplastic blends in order to generate novel high performance PLA-based material with significantly enhanced impact strength. This dissertation examines and evaluates the potential of two different categories of wetting behaviors i.e. complete wetting and partial wetting in toughening of PLA blends.

In order to achieve the aforementioned objectives, a comprehensive study was performed on the phase structuring of the ternary and quaternary PLA based systems. First, the morphology development and its stability before and after quiescent annealing in PLA/PBS/PBAT and PLA/PBS/PBAT/PHBV were investigated. It was found that a variety of precise interfacial tension methods as well as multiple phase identification techniques in order to characterize the phase structuring of immiscible ternary and quaternary polymer systems. Thus, FTIR-imaging as a novel phase identification and morphology analysis method was proposed for characterizing multiphase systems of similar chemical structures such as the biopolyesters used in this work. The results revealed that both systems demonstrate multiple percolated structures right after melt mixing process. A tri-continuous morphology was observed for the ternary the 33PLA/33PBS/33PBAT blend and a fully quadruple continuous completely wet morphology was obtained for the 25PLA/25PBS/25PBAT/25PHBV system. However, these systems demonstrated different behaviors upon quiescent annealing. The ternary system showed coarsening with no change in the order of the phases. The morphology of the quaternary system, however, coarsened with a change in the wetting behavior of the PBAT phase. It was found that this change in the wetting behavior is concentration dependent where at low concentration of PBAT (10 vol%), PBAT forms partially wet droplets at the interface of PBS/PHBV both after mixing and after annealing. It was found that the morphological results after annealing strongly correlate with the thermodynamic predictions. These results indicate that composition control during the mixing of multiphase systems with ultra-low interfacial tensions can result in complete change of wetting behavior.

The morphology development in systems with partial wetting behavior was examined for the first time. It was found that systems with weak and strong thermodynamic tendencies towards partial wetting demonstrate different morphology development with composition. The three different melt

blended ternary systems, PLA/PHBV/PBS, PLA/PBAT/PE and PLA/PE/PBAT were prepared which demonstrate diverse partial wetting behaviors. It was observed that the PE intermediate phase in the PLA/PE/PBAT system with strong partial wetting tendency remained stable even at high PE content of 20% and after 30 min of quiescent annealing. However, the partially wet PHBV and PBAT intermediate phases with weak partial wetting tendencies in the PLA/PHBV/PBS and PLA/PBAT/PE systems, respectively, form a completely wet layer at the interface by increasing their concentration above 10 vol% demonstrating a composition dependent wetting behavior. This behavior is attributed to the low dewetting speed and the interfacial confinement where the dewetting/coalescence equilibrium favors coalescence. It is shown that dewetting speed, concentration of the intermediate phase, annealing time and interfacial confinement significantly influence the morphology development in both partial and complete wetting morphologies and can be controlled to generate a wide range of new morphological structures.

With the knowledge acquired from the previous section, we tried to enhance the toughness of the PLA/PA11 blend by assembling partially wet droplets of various polymers at the interface of co-continuous PLA/PA11. It was shown that a brittle-to-ductile transition is achieved for PLA/PA11 when a partially wet droplet phase assembles at the interface. The tensile properties and the notched Izod impact strength were significantly improved by the addition of 10% of either PBS, PBAT, EMA, or EMA-GMA. However, the best results were obtained for the PLA/EMA/PA11 blend which shows about a 4-fold increase in the notched Izod impact strength (73 J/m) and a high elongation at break at about 250% which is almost 80 times the binary PLA/PA11 50/50 blend. In addition, a novel compatibilization effect is achieved upon assembly of partially wet droplets with strong interfacial affinity to the interface. Among the four partially wet droplets used here, the partially wet EMA-GMA droplets demonstrate a marked compatibilization effect by reducing the co-continuous phase size from 10 μm to about 5 μm. The interfacial adsorption of the very fine 450 nm EMA-GMA droplets with a 350 nm interparticle distance enhances the compatibilization effect due to the combination of strong interfacial affinity and Pickering emulsion effect. The PW droplets used in this study are commercial homopolymers which in spite of copolymers or other compatibilizers are rather cheap and promise a very viable way for polymer blend compatibilization. In addition, they act as an impact modifier and significantly improve the

mechanical properties. This opens new opportunities to exploit interfacial compatibilization and toughening using PW droplets and should be of great significance in multiphase polymer blends.

The assembly of a completely wet PEBA thermoplastic elastomer at the interface of PLA and PA11 was found to be even more effective in the toughening of the PLA/PA11 blend. When PEBA assembles at the interface of the co-continuous PLA/PA11, a fully percolated rubbery network forms which constructs a tri-continuous phase morphology. The correlation between the impact toughness and the results reveals that the strong interfacial interactions of PEBA with both PLA and PA11 along with the unique double percolated structure significantly enhances the impact properties. PEBA plays a critical role in the toughening of the PLA/PA11 based ternary blends. The polyether component of PEBA is capable of strong interfacial interactions with PLA and the amide component in the copolymer has a natural affinity for the PA11. The addition of the elastomeric PEBA phase to the binary PLA/PA11 blend also replaces a rigid PLA/PA11 interface with a much more deformable one. The further addition of PEO to PLA results in an ultratough material with an impact strength of ~ 750 J/m which is approximately forty times greater than the original co-continuous PLA/PA11 blend. The added PEO maintains the potential for strong interfacial interactions with PEBA, but also results in a significant increase in the chain mobility of PLA which further enhances the capability for interfacial interactions. The tensile toughness and notched Izod impact strength are significantly influenced by the critical co-continuous composition region of the PLA/PA11 binary system. The surface analysis of the fractured samples suggests that the high impact toughness observed for the quaternary blends is attributed to the tri-continuous morphology and the interfacially cavitated PEBA layer coupled with suitable interfacial adhesion. Therefore, shear yielding begins to take place due to the relief of triaxial tension by extensive percolated cavitation within the PEBA phase.

Based on the results obtained in this study, it was shown that through control of the phase structuring in multiphase PLA based blends, a significant improvement in the mechanical properties can be achieved. Both partially wet droplets and interfacially percolated complete wet layer were utilized to enhance the mechanical properties of co-continuous PLA/PA11 systems. The partially wet system has the potential to compatibilize co-continuous structures while demonstrates a moderate toughening effect. It is found that when all phases are fully percolated where a thin interfacially percolated thermoplastic elastomer is assembled at the interface of a co-continuous

structure, a significant increase in the tensile toughness and notched Izod impact strength is obtained over the original binary blend. Ultra-toughening is achieved through the combined effects of a double percolated structure and an enhanced interfacial adhesion. However, the blends beyond the critical tri-continuous composition region demonstrate a poor toughness.

PLA has shown much promise in the development of a bioplastic paradigm. It can play a critical role in the implementation of bioplastics due to its affordable cost and useful property attributes. Novel research approaches must be encouraged to broaden the properties of PLA. The present study reveals that the multicomponent blending of PLA can provide such a research gateway in the field of biobased materials. There is still enormous opportunity available for researchers in understanding the phase structuring in multiphase bioplastics in order to generate high performance novel structures with value added multi-functional applications.

In the present work, the morphology and mechanical properties of systems with partial wetting morphology are examined. However, a more comprehensive study is needed to understand the morphology development in systems demonstrating partial wetting behavior. It is also shown that interfacial confinement plays an important role on the morphology transition from partial wetting to complete wetting at the interface in systems with partial wetting morphology. It is still unknown how this confinement influence the morphology development in systems with complete wetting behavior.

Systems with partial and complete wetting morphologies are examined for their potential for toughening of PLA based multiphase systems. Despite our attempt to understand the toughening mechanisms behind the enhanced toughness achieved for these system, it will be necessary to further examine the fracture mechanisms in these novel structures. This will help in designing materials with optimized structures and properties. The low temperature performance of these materials is another important aspect which can be studied in future attempts. It was also shown that the plasticization of PLA in multicomponent blends effectively improves the impact toughness of the blends. This can be further explored to find the most effective strategy for the plasticization and toughening of PLA based systems with less/no negative influence on the modulus and strength of those systems.

BIBLIOGRAPHY

Ajioka, M., Enomoto, K., Suzuki, K., & Yamaguchi, A. (1995). Basic properties of polylactic acid produced by the direct condensation polymerization of lactic-acid. *Bulletin of the Chemical Society of Japan*, *68*(8), 2125–2131.

Al-Mulla, A., & Gupta, R. K. (2000). Droplet coalescence in the shear flow of model emulsions. *Rheologica Acta*, *39*(1), 20–25.

Anderson, K. S., Schreck, K. M., & Hillmyer, M. A. (2008). Toughening polylactide. *Polymer Reviews*, *48*(1), 85–108.

Argon, a. S., & Cohen, R. E. (2003). Toughenability of polymers. *Polymer*, *44*(19), 6013–6032.

Auras, R., Lim, L. T., Selke, S. E. M., & Tsuji, H. (2010). *Poly(lactic acid) : synthesis, structures, properties, processing, and applications*. (R. F. Grossman & D. Nwabunma, Eds.), *Wiley Series on Polymer Engineering and Technology*. Hoboken, New Jersey: John Wiley & Sons, Inc.

Avérous, L., & Pollet, E. (2012). Biodegradable Polymers. In L. Avérous & E. Pollet (Eds.), *Environmental Silicate Nano-Biocomposites* (pp. 13–39). London: Springer London.

Babu, R. P., O'Connor, K., & Seeram, R. (2013). Current progress on bio-based polymers and their future trends. *Progress in Biomaterials*, *2*(1), 8.

Bai, H., Xiu, H., Gao, J., Deng, H., Zhang, Q., Yang, M., & Fu, Q. (2012). Tailoring impact toughness of poly(L-lactide)/poly(ε-caprolactone) (PLLA/PCL) blends by controlling crystallization of PLLA matrix. *ACS Applied Materials & Interfaces*, *4*(2), 897–905.

Bai, S. L., G'Sell, C., Hiver, J. M., & Mathieu, C. (2005). Polypropylene/polyamide 6/polyethylene-octene elastomer blends. Part 3. Mechanisms of volume dilatation during plastic deformation under uniaxial tension. *Polymer*, *46*(17), 6437–6446.

Bai, S. L., Wang, G. T., Hiver, J. M., & G'Sell, C. (2004). Microstructures and mechanical properties of polypropylene/polyamide 6/polyethelene-octene elastomer blends. *Polymer*, *45*(9), 3063–3071.

Bai Chin, H., & Han, C. D. (1979). Studies on Droplet Deformation and Breakup. I. Droplet Deformation in Extensional Flow. *Journal of Rheology*, *23*(5), 557.

Baiardo, M., Frisoni, G., Scandola, M., Rimelen, M., Lips, D., Ruffieux, K., & Wintermantel, E. (2003). Thermal and mechanical properties of plasticized poly(L-lactic acid). *Journal of Applied Polymer Science*, *90*(7), 1731–1738.

Bentley, B. J., & Leal, L. G. (1986). Computer-controlled four-roll mill for investigations of particle and drop dynamics in two-dimensional linear shear flows. *Journal of Fluid Mechanics*, *167*, 219–240.

Biodegradable Plastics Market by Type (PLA, PHA, PBS, Starch-Based Plastics, Regenerated Cellulose, PCL), by Application (Packaging, Fibers, Agriculture, Injection Molding, and Others) - Global Trends & Forecasts to 2020. (2015).

Bourry, D., & Favis, B. D. (1998). Cocontinuity and phase inversion in HDPE/PS blends: Influence of interfacial modification and elasticity. *Journal of Polymer Science Part B-Polymer Physics*, *36*(11), 1889–1899.

Bousmina, M. (1999). Rheology of polymer blends: linear model for viscoelastic emulsions. *Rheologica Acta*, *38*(1), 73–83.

Braunegg, G., Lefebvre, G., & Genser, K. F. (1998). Polyhydroxyalkanoates, biopolyesters from renewable resources: Physiological and engineering aspects. *Journal of Biotechnology*, *65*(2–3), 127–161.

Bucknall, C. B., & Paul, D. R. (2009). Notched impact behavior of polymer blends: Part 1: New model for particle size dependence. *Polymer*, *50*(23), 5539–5548.

Carriere, C. J., Cohen, A., & Arends, C. B. (1989). Estimation of Interfacial Tension Using Shape Evolution of Short Fibers. *Journal of Rheology*, *33*(5), 681–689.

Cheng, T. W., Keskkula, H., & Paul, D. R. (1992). Property and morphology relationships for ternary blends of polycarbonate, brittle polymers and an impact modifier. *Polymer*, *33*(8), 1606–1619.

Chesters, A. K. (1991). The modelling of coalescence processes in fluid-liquid dispersions : a review of current understanding. *Chemical Engineering Research & Design*, *69*, 259–270.

Cohen, A., & Carriere, C. J. (1989). Analysis of a retraction mechanism for imbedded polymeric

fibers. *Rheologica Acta*, *28*(3), 223–232.

Corre, Y.-M., Bruzaud, S., Audic, J.-L., & Grohens, Y. (2012). Morphology and functional properties of commercial polyhydroxyalkanoates: A comprehensive and comparative study. *Polymer Testing*, *31*(2), 226–235.

Coulaloglou, C. A., & Tavlarides, L. L. (1977). Description of interaction processes in agitated liquid-liquid dispersions. *Chemical Engineering Science*, *32*(11), 1289–1297.

Dae Han, C., & Funatsu, K. (1978). An Experimental Study of Droplet Deformation and Breakup in Pressure-Driven Flows through Converging and Uniform Channels. *Journal of Rheology*, *22*(2), 113.

de Freitas, C. A., Valera, T. S., Catelli de Souza, A. M., & Demarquette, N. R. (2007). Morphology of Compatibilized Ternary Blends. *Macromolecular Symposia*, *247*(1), 260–270.

de Gennes, P.-G., Brochard-Wyard, F., & Quere, D. (2004). *Capillarity and Wetting Phenomena: Drops, Bubbles, Pearls, Waves*. New York: Springer.

Demarquette, N. R. (2003). Evaluation of experimental techniques for determining interfacial tension between molten polymers. *International Materials Reviews*, *48*(4), 247–269.

Dou, R., Li, S., Shao, Y., Yin, B., & Yang, M. (2016). Insight into the formation of a continuous sheath structure for the PS phase in tri-continuous PVDF/PS/HDPE blends. *RSC Adv.*, *6*(1), 439–447.

Dou, R., Shao, Y., Li, S., Yin, B., & Yang, M. (2016). Structuring tri-continuous structure multiphase composites with ultralow conductive percolation threshold and excellent electromagnetic shielding effectiveness using simple melt mixing. *Polymer*, *83*, 34–39.

Dou, R., Zhou, Y., Shen, C., Li, L., Yin, B., & Yang, M. (2015). Toughening of PA6/EPDM-g-MAH/HDPE ternary blends via controlling EPDM-g-MAH grafting degree: the role of core–shell particle size and shell thickness. *Polymer Bulletin*, *72*(2), 177–193.

Elemans, P. H. M., Janssen, J. M. H., & Meijer, H. E. H. (1990). The measurement of interfacial tension in polymer/polymer systems: The breaking thread method. *Journal of Rheology*, *34*(8), 1311–1325.

Elmendorp, J. J., & Van Der Vegt, A. K. (1986). A study on polymer blending microrheology: Part IV. The influence of coalescence on blend morphology origination. *Polymer Engineering and Science*, *26*(19), 1332–1338.

Engelberg, I., & Kohn, J. (1991). Physicomechanical properties of degradable polymers used in medical applications - A comparative-study. *Biomaterials*, *12*(3), 292–304.

Erickson, B., & Winters, P. (2012). Perspective on opportunities in industrial biotechnology in renewable chemicals. *Biotechnology Journal*, *7*(2), 176–185.

Favis, B. D. (1990). The effect of processing parameters on the morphology of an immiscible binary blend. *Journal of Applied Polymer Science*, *39*(2), 285–300.

Favis, B. D. (1991). Polymer alloys and blends - Recent advances. *Canadian Journal of Chemical Engineering*, *69*(3), 619–625.

Favis, B. D. (2000). Factors influencing the morphology of immiscible polymer blends in melt processing. In D. R. Paul & C. B. Bucknall (Eds.), *Polymer Blends Volume 1: Formulation* (pp. 501–538). New York: John Wiley & Sons.

Favis, B. D., & Chalifoux, J. P. (1988). Influence of composition on the morphology of polypropylene/polycarbonate blends. *Polymer*, *29*(10), 1761–1767.

Favis, B. D., & Willis, J. M. (1990). Phase size composition dependence in immiscible blends - experimental and theoretical considerations. *Journal of Polymer Science Part B-Polymer Physics*, *28*(12), 2259–2269.

Filippone, G., Netti, P. A., & Acierno, D. (2007). Microstructural evolutions of LDPE/PA6 blends by rheological and rheo-optical analyses: Influence of flow and compatibilizer on break-up and coalescence processes. *Polymer*, *48*(2), 564–573.

Florence, A., & Mechael, C. (2015). *Bio-based Building Blocks and Polymers in the World Capacities, Production and Applications: Status Quo and Trends towards 2020*. nova-Institute.

Fortelný, I. (2001). Analysis of the effect of breakup frequency on the steady droplet size in flowing polymer blends. *Rheologica Acta*, *40*(5), 485–489.

Fortelný, I. (2006). Theoretical aspects of phase morphology development. *Micro-and Nanostructured Multiphase Polymer Blend Systems: Phase Morphology and Interfaces, C. Harrats, S. Thomas, and G. Groeninckx, Eds., Taylor and Francis, Boca Raton, 43*.

Fortelný, I., & Jůza, J. (2012). Modeling of the influence of matrix elasticity on coalescence probability of colliding droplets in shear flow. *Journal of Rheology*, *56*(6), 1393.

Fortelný, I., & Jůza, J. (2013). Modeling of interface mobility in the description of flow-induced coalescence in immiscible polymer blends. *Colloid and Polymer Science*, *291*(8), 1863–1870.

G'Sell, C., Bai, S.-L., & Hiver, J.-M. (2004). Polypropylene/polyamide 6/polyethylene–octene elastomer blends. Part 2: volume dilatation during plastic deformation under uniaxial tension. *Polymer*, *45*(17), 5785–5792.

Gabriele, M., Pasquino, R., & Grizzuti, N. (2011). Effects of Viscosity-Controlled Interfacial Mobility on the Coalescence of Immiscible Polymer Blends. *Macromolecular Materials and Engineering*, *296*(3–4), 263–269.

Grace, H. P. (1982). Dispersion Phenomena in High Viscosity Immiscible Fluid Systems and Application of Static Mixers As Dispersion Devices in Such Systems. *Chemical Engineering Communications*, *14*(3–6), 225–277.

Graebling, D., Muller, R., & Palierne, J. F. (1993). Linear viscoelastic behavior of some incompatible polymer blends in the melt. Interpretation of data with a model of emulsion of viscoelastic liquids. *Macromolecules*, *26*(2), 320–329.

Gu, S.-Y., Zhang, K., Ren, J., & Zhan, H. (2008). Melt rheology of polylactide/poly(butylene adipate-co-terephthalate) blends. *Carbohydrate Polymers*, *74*(1), 79–85.

Guild, F. J., & Young, R. J. (1989). A predictive model for particulate-filled composite materials. *Journal of Materials Science*, *24*(1), 298–306.

Guo, H. F., Gvozdic, N. V, & Meier, D. J. (1997). Prediction and manipulation of the phase morphologies of multiphase polymer blends: II. Quaternary systems. *Polymer*, *38*(19), 4915–4923.

Guo, H. F., Packirisamy, S., Gvozdic, N. V, & Meier, D. J. (1997). Prediction and manipulation of

the phase morphologies of multiphase polymer blends: 1. Ternary systems. *Polymer*, *38*(4), 785–794.

Ha, M. H., Kim, B. K., & Kim, E. Y. (2004). Effects of dispersed phase composition on thermoplastic polyolefins. *Journal of Applied Polymer Science*, *93*(1), 179–188.

Harkins, W. D. (1941). A General Thermodynamic Theory of the Spreading of Liquids to Form Duplex Films and of Liquids or Solids to Form Monolayers. *The Journal of Chemical Physics*, *9*(7), 552.

Harkins, W. D., & Feldman, A. (1922). Films. The spreading of liquids and the spreading coefficient. *Journal of the American Chemical Society*, *44*(12), 2665–2685.

Hashima, K., Nishitsuji, S., & Inoue, T. (2010). Structure-properties of super-tough PLA alloy with excellent heat resistance. *Polymer*, *51*(17), 3934–3939.

Hedegaard, A. T., Gu, L., & Macosko, C. W. (2015). Effect of extensional viscosity on cocontinuity of immiscible polymer blends. *Journal of Rheology*, *59*(6), 1397–1417.

Hemmati, M., Nazokdast, H., & Panahi, H. S. (2001a). Study on morphology of ternary polymer blends. I. Effects of melt viscosity and interfacial interaction. *Journal of Applied Polymer Science*, *82*(5), 1129–1137.

Hemmati, M., Nazokdast, H., & Panahi, H. S. (2001b). Study on morphology of ternary polymer blends. II. Effect of composition. *Journal of Applied Polymer Science*, *82*(5), 1138–1146.

Hobbs, S. Y., Dekkers, M. E. J., & Watkins, V. H. (1988). Effect of interfacial forces on polymer blend morphologies. *Polymer*, *29*(9), 1598–1602.

Horiuchi, S., Matchariyakul, N., Yase, K., & Kitano, T. (1997). Morphology development through an interfacial reaction in ternary immiscible polymer blends. *Macromolecules*, *30*(12), 3664–3670.

Hsu, A. S., Roy, A., & Leal, L. G. (2008). Drop-size effects on coalescence of two equal-sized drops in a head-on collision. *Journal of Rheology*, *52*(6), 1291.

Huang, S., Bai, L., Trifkovic, M., Cheng, X., & Macosko, C. W. (2016). Controlling the Morphology of Immiscible Cocontinuous Polymer Blends via Silica Nanoparticles Jammed

at the Interface. *Macromolecules*, *49*(10), 3911–3918.

Ichikawa, Y., & Mizukoshi, T. (2012). Bionolle (Polybutylenesuccinate). In B. Rieger, A. Künkel, G. W. Coates, R. Reichardt, E. Dinjus, & T. A. Zevaco (Eds.), *Synthetic Biodegradable Polymers* (Vol. 245, pp. 285–313). Springer Berlin Heidelberg.

Imre, B., Bedo, D., Domján, A., Schön, P., Vancso, G. J., & Pukánszky, B. (2013). Structure, properties and interfacial interactions in poly(lactic acid)/polyurethane blends prepared by reactive processing. *European Polymer Journal*, *49*(10), 3104–3113.

Inberg, J. P. ., & Gaymans, R. . (2002). Co-continuous polycarbonate/ABS blends. *Polymer*, *43*(8), 2425–2434.

Jacobsen, S., & Fritz, H. G. (1999). Plasticizing polylactide - The effect of different plasticizers on the mechanical properties. *Polymer Engineering and Science*, *39*(7), 1303–1310.

Jamshidian, M., Tehrany, E. A., Imran, M., Jacquot, M., & Desobry, S. (2010). Poly-Lactic Acid: Production, Applications, Nanocomposites, and Release Studies. *Comprehensive Reviews in Food Science and Food Safety*, *9*(5), 552–571.

Jeelani, S. A. K., & Hartland, S. (1991). Collision of oscillating liquid drops. *Chemical Engineering Science*, *46*(7), 1807–1814.

Karam, H. J., & Bellinger, J. C. (1968). Deformation and Breakup of Liquid Droplets in a Simple Shear Field. *Industrial & Engineering Chemistry Fundamentals*, *7*(4), 576–581.

Ke, Z., Shi, D., Yin, J., Li, R. K. Y., & Mai, Y. W. (2008). Facile method of preparing supertough polyamide 6 with low rubber content. *Macromolecules*, *41*(20), 7264–7267.

Kim, B. K., Kim, M. S., & Kim, K. J. (1993). Viscosity effect in polyolefin ternary blends and composites. *Journal of Applied Polymer Science*, *48*(7), 1271–1278.

Kinloch, A. J., & Young, R. J. (1995). *Fracture Behaviour of Polymers*. Dordrecht: Springer Netherlands.

Kulinski, Z., & Piorkowska, E. (2005). Crystallization, structure and properties of plasticized poly(L-lactide). *Polymer*, *46*(23), 10290–10300.

Kulinski, Z., Piorkowska, E., Gadzinowska, K., & Stasiak, M. (2006). Plasticization of poly(L-

lactide) with poly(propylene glycol). *Biomacromolecules*, *7*(7), 2128–35.

Labrecque, L. V, Kumar, R. A., Dave, V., Gross, R. A., & McCarthy, S. P. (1997). Citrate esters as plasticizers for poly(lactic acid). *Journal of Applied Polymer Science*, *66*(8), 1507–1513.

Lacroix, C., Bousmina, M., Carreau, P. J., Favis, B. D., & Michel, A. (1996). Properties of PETG/EVA blends .1. Viscoelastic, morphological and interfacial properties. *Polymer*, *37*(14), 2939–2947.

Lai, W. C., Liau, W. B., & Lin, T. T. (2004). The effect of end groups of PEG on the crystallization behaviors of binary crystalline polymer blends PEG/PLLA. *Polymer*, *45*(9), 3073–3080.

Le Corroller, P., & Favis, B. D. (2011). Effect of viscosity in ternary polymer blends displaying partial wetting phenomena. *Polymer*, *52*(17), 3827–3834.

Lee, J. K., & Han, C. D. (1999). Evolution of polymer blend morphology during compounding in an internal mixer. *Polymer*, *40*(23), 6277–6296.

Li, J., & Favis, B. D. (2001). Characterizing co-continuous high density polyethylene/polystyrene blends. *Polymer*, *42*(11), 5047–5053.

Li, J. M., Ma, P. L., & Favis, B. D. (2002). The role of the blend interface type on morphology in cocontinuous polymer blends. *Macromolecules*, *35*(6), 2005–2016.

Li, Y., & Shimizu, H. (2009). Improvement in toughness of poly(l-lactide) (PLLA) through reactive blending with acrylonitrile-butadiene-styrene copolymer (ABS): Morphology and properties. *European Polymer Journal*, *45*(3), 738–746.

Li, Y., Wang, D., Zhang, J.-M., & Xie, X.-M. (2010). Influences of component ratio of minor phases and charge sequence on the morphology and mechanical properties of PP/PS/PA6 ternary blends. *Polymer Bulletin*, *66*(6), 841–852.

Lim, L. T., Auras, R., & Rubino, M. (2008). Processing technologies for poly(lactic acid). *Progress in Polymer Science*, *33*(8), 820–852.

Liu, H., Chen, F., Liu, B., Estep, G., & Zhang, J. (2010). Super toughened poly(lactic acid) ternary blends by simultaneous dynamic vulcanization and interfacial compatibilization. *Macromolecules*, *43*(14), 6058–6066.

Liu, H., Guo, L., Guo, X., & Zhang, J. (2012). Effects of reactive blending temperature on impact toughness of poly(lactic acid) ternary blends. *Polymer*, *53*(2), 272–276.

Liu, H., Song, W., Chen, F., Guo, L., & Zhang, J. (2011). Interaction of Microstructure and Interfacial Adhesion on Impact Performance of Polylactide (PLA) Ternary Blends. *Macromolecules*, *44*(6), 1513–1522.

Liu, H., & Zhang, J. (2011). Research progress in toughening modification of poly(lactic acid). *Journal of Polymer Science Part B: Polymer Physics*, *49*(15), 1051–1083.

Liu, Z., Luo, Y., Bai, H., Zhang, Q., & Fu, Q. (2016a). Remarkably Enhanced Impact Toughness and Heat Resistance of poly(L-Lactide)/Thermoplastic Polyurethane Blends by Constructing Stereocomplex Crystallites in the Matrix. *ACS Sustainable Chemistry & Engineering*, *4*(1), 111–120.

Liu, Z., Luo, Y., Bai, H., Zhang, Q., & Fu, Q. (2016b). Remarkably Enhanced Impact Toughness and Heat Resistance of poly(l -Lactide)/Thermoplastic Polyurethane Blends by Constructing Stereocomplex Crystallites in the Matrix. *ACS Sustainable Chemistry and Engineering*, *4*(1), 111–120.

Ljungberg, N., Colombini, D., & Wesslen, B. (2005). Plasticization of poly(lactic acid) with oligomeric malonate esteramides: Dynamic mechanical and thermal film properties. *Journal of Applied Polymer Science*, *96*(4), 992–1002.

Ljungberg, N., & Wesslen, B. (2002). The effects of plasticizers on the dynamic mechanical and thermal properties of poly(lactic acid). *Journal of Applied Polymer Science*, *86*(5), 1227–1234.

Ljungberg, N., & Wesslen, B. (2003). Tributyl citrate oligomers as plasticizers for poly (lactic acid): thermo-mechanical film properties and aging. *Polymer*, *44*(25), 7679–7688.

López-Barrón, C. R., & Macosko, C. W. (2010). A new model for the coarsening of cocontinuous morphologies. *Soft Matter*, *6*(12), 2637.

Luciani, A., & Jarrin, J. (1996). Morphology development in immiscible polymer blends. *Polymer Engineering and Science*, *36*(12), 1619–1626.

Luzinov, I., Pagnoulle, C., & Jerome, R. (2000a). Dependence of phase morphology and mechanical properties of PS/SBR/PE ternary blends on composition: transition from core-shell to triple-phase continuity structures. *Polymer*, *41*(9), 3381–3389.

Luzinov, I., Pagnoulle, C., & Jerome, R. (2000b). Ternary polymer blend with core-shell dispersed phases: effect of the core-forming polymer on phase morphology and mechanical properties. *Polymer*, *41*(19), 7099–7109.

Luzinov, I., Xi, K., Pagnoulle, C., Huynh-Ba, G., & Jerome, R. (1999). Composition effect on the core-shell morphology and mechanical properties of ternary polystyrene/styrene butadiene rubber polyethylene blends. *Polymer*, *40*(10), 2511–2520.

Lyngaae-Jørgensen, J., & Utracki, L. A. (1991). Dual phase continuity in polymer blends. *Makromolekulare Chemie. Macromolecular Symposia*, *48–49*(1), 189–209.

Macosko, C. W. (2000). Morphology development and control in immiscible polymer blends. *Macromolecular Symposia*, *149*(1), 171–184.

Mamat, A., VuKhanh, T., Cigana, P., & Favis, B. D. (1997). Impact fracture behavior of nylon-6/ABS blends. *Journal of Polymer Science Part B-Polymer Physics*, *35*(16), 2583–2592.

MarketsandMarkets. (2016). *Bioplastics & Biopolymers Market by Type, Application, and by Region - Trends & Forecast to 2021*.

Martin, O., & Avérous, L. (2001). Poly(lactic acid): plasticization and properties of biodegradable multiphase systems. *Polymer*, *42*(14), 6209–6219.

Mascia, L., & Xanthos, M. (1992). An overview of additives and modifiers for polymer blends: Facts, deductions, and uncertainties. *Advances in Polymer Technology*, *11*(4), 237–248.

McMASTER LEE P. (1975). Aspects of Liquid-Liquid Phase Transition Phenomena in Multicomponent Polymeric Systems. In *Copolymers, Polyblends, and Composites* (Vol. 142, pp. 43–65).

Meijer, H. E. H., Janssen, J. M. H., & Anderson, P. D. (2009). Mixing of Immiscible Liquids. In I. Manas-Zloczower (Ed.), *Mixing and compounding of polymers: theory and practice* (2nd Editio, pp. 41–182). Munich, Cincinnati: Hanser.

Mekhilef, N., Favis, B. D., & Carreau, P. J. (1997). Morphological stability, interfacial tension, and dual-phase continuity in polystyrene-polyethylene blends. *Journal of Polymer Science Part B-Polymer Physics*, *35*(2), 293–308.

Merz, E. H., Claver, G. C., & Baer, M. (1956). Studies on heterogeneous polymeric systems. *Journal of Polymer Science*, *22*(101), 325–341.

Michler, G. H., & Bucknall, C. B. (2001). New toughening mechanisms in rubber modified polymers. *Plastics, Rubber and Composites*, *30*(3), 110–115.

Mighri, F., Carreau, P. J., & Ajji, A. (1998). Influence of elastic properties on drop deformation and breakup in shear flow. *Journal of Rheology*, *42*(6), 1477.

Miles, I. S., & Zurek, A. (1988). Preparation, structure, and properties of two-phase co-continuous polymer blends. *Polymer Engineering & Science*, *28*(12), 796–805.

Momoko Ishii, Masaki Okazaki, Yuji Shibasaki, and, Ueda*, M., & Teranishi, T. (2001). Convenient Synthesis of Aliphatic Polyesters by Distannoxane-Catalyzed Polycondensation.

Nagarajan, V., Zhang, K., Misra, M., & Mohanty, A. K. (2015). Overcoming the Fundamental Challenges in Improving the Impact Strength and Crystallinity of PLA Biocomposites: Influence of Nucleating Agent and Mold Temperature. *ACS Applied Materials & Interfaces*, *7*(21), 11203–11214.

Nemirovski, N., Siegmann, A., & Narkis, M. (1995). Morphology of ternary immiscible polymer blends. *Journal of Macromolecular Science, Part B*, *34*(4), 459–475.

Nijenhuis, A. J., Colstee, E., Grijpma, D. W., & Pennings, A. J. (1996). High molecular weight poly(L-lactide) and poly(ethylene oxide) blends: Thermal characterization and physical properties. *Polymer*, *37*(26), 5849–5857.

Ojijo, V., Ray, S. S., & Sadiku, R. (2013). Toughening of biodegradable polylactide/poly(butylene succinate-co-adipate) blends via in situ reactive compatibilization. *ACS Applied Materials & Interfaces*, *5*(10), 4266–76.

Omonov, T. S., Harrats, C., & Groeninckx, G. (2005). Co-continuous and encapsulated three phase morphologies in uncompatibilized and reactively compatibilized polyamide

6/polypropylene/polystyrene ternary blends using two reactive precursors. *Polymer*, *46*(26), 12322–12336.

Omonov, T. S., Harrats, C., Groeninckx, G., & Moldenaers, P. (2007). Anisotropy and instability of the co-continuous phase morphology in uncompatibilized and reactively compatibilized polypropylene/polystyrene blends. *Polymer*, *48*(18), 5289–5302.

Paul, D. R., & Barlow, J. W. (1980). Polymer Blends. *Journal of Macromolecular Science, Part C: Polymer Reviews*, *18*(1), 109–168.

Paul, D. R., & Bucknall, C. B. (2000). *Polymer Blends*. New York: John Wiley & Sons, Inc.

Perego, G., & Cella, G. D. (2010). Mechanical Properties. In R. Auras, L. T. Lim, S. E. M. Selke, & H. Tsuji (Eds.), *Poly(lactic acid) : synthesis, structures, properties, processing, and applications*. Hoboken, New Jersey: John Wiley & Sons, Inc.

Piorkowska, E., Kulinski, Z., Galeski, a., & Masirek, R. (2006). Plasticization of semicrystalline poly(l-lactide) with poly(propylene glycol). *Polymer*, *47*(20), 7178–7188.

Pötschke, P., & Paul, D. R. (2003). Formation of Co-continuous Structures in Melt-Mixed Immiscible Polymer Blends. *Journal of Macromolecular Science, Part C: Polymer Reviews*, *43*(1), 87–141.

Rasal, R. M., Janorkar, A. V, & Hirt, D. E. (2010). Poly(lactic acid) modifications. *Progress in Polymer Science*, *35*(3), 338–356.

Ravati, S., Beaulieu, C., Zolali, A. M., & Favis, B. D. (2014). High performance materials based on a self-assembled multiple-percolated ternary blend. *AIChE Journal*, *60*(8), 3005–3012.

Ravati, S., & Favis, B. D. (2010a). Low percolation threshold conductive device derived from a five-component polymer blend. *Polymer*, *51*(16), 3669–3684.

Ravati, S., & Favis, B. D. (2010b). Morphological states for a ternary polymer blend demonstrating complete wetting. *Polymer*, *51*(20), 4547–4561.

Ravati, S., & Favis, B. D. (2011). 3D porous polymeric conductive material prepared using LbL deposition. *Polymer*, *52*(3), 718–731.

Ravati, S., & Favis, B. D. (2013a). Interfacial coarsening of ternary polymer blends with partial

and complete wetting structures. *Polymer*, *54*(25), 6739–6751.

Ravati, S., & Favis, B. D. (2013b). Tunable morphologies for ternary blends with poly(butylene succinate): Partial and complete wetting phenomena. *Polymer*, *54*(13), 3271–3281.

Rayleigh, L. (1878). On The Instability Of Jets. *Proceedings of the London Mathematical Society*, *s1-10*(1), 4–13.

Reignier, J., & Favis, B. D. (2000a). Control of the subinclusion microstructure in HDPE/PS/PMMA ternary blends. *Macromolecules*, *33*(19), 6998–7008.

Reignier, J., & Favis, B. D. (2000b). Control of the subinclusion microstructure in HDPE/PS/PMMA ternary blends. *Macromolecules*, *33*(19), 6998–7008.

Reignier, J., & Favis, B. D. (2003a). Core-shell structure and segregation effects in composite droplet polymer blends. *AIChE Journal*, *49*(4), 1014–1023.

Reignier, J., & Favis, B. D. (2003b). On the presence of a critical shell volume fraction leading to pseudo-pure droplet behavior in composite droplet polymer blends. *Polymer*, *44*(18), 5061–5066.

Reignier, J., Favis, B. D., & Heuzey, M. C. (2003). Factors influencing encapsulation behavior in composite droplet-type polymer blends. *Polymer*, *44*(1), 49–59.

Roland, C. M., & Böuhm, G. G. A. (1984). Shear-induced coalescence in two-phase polymeric systems. I. Determination from small-angle neutron scattering measurements. *Journal of Polymer Science: Polymer Physics Edition*, *22*(1), 79–93.

Rother, M. A., & Davis, R. H. (2001). The effect of slight deformation on droplet coalescence in linear flows. *Physics of Fluids*, *13*(5), 1178.

Rulkens, R., & Koning, C. (2012). Chemistry and Technology of Polyamides. In *Polymer Science: A Comprehensive Reference, 10 Volume Set* (Vol. 5, pp. 431–467).

Rumscheidt, F. ., & Mason, S. . (1961). Particle motions in sheared suspensions XII. Deformation and burst of fluid drops in shear and hyperbolic flow. *Journal of Colloid Science*, *16*(3), 238–261.

Saito, H., Yoshinaga, M., Mihara, T., Nishi, T., & Jinnai, H. (2009). The interface dynamics of

bicontinuous phase separating structure in a polymer blend. *Journal of Physics: Conference Series*, *184*(1), 12029.

Sarazin, P., Li, G., Orts, W. J., & Favis, B. D. (2008). Binary and ternary blends of polylactide, polycaprolactone and thermoplastic starch. *Polymer*, *49*(2), 599–609.

Scher, H., & Zallen, R. (1970). Critical Density in Percolation Processes. *Journal of Chemical Physics*, *53*, 3759–3761.

Serpe, G., Jarrin, J., & Dawans, F. (1990). Morphology-processing relationships in polyethylene-polyamide blends. *Polymer Engineering and Science*, *30*(9), 553–565.

Shao, Y., Dou, R., Li, S., Yin, B., & Yang, M. (2016). Morphology evolution and the tri-continuous morphology formation of a PVDF/PS/HDPE ternary blend in melt mixing. *RSC Adv.*, *6*(45), 38803–38810.

Shen, C., Zhou, Y., Dou, R., Wang, W., Yin, B., & Yang, M. (2015). Effect of the core-forming polymer on phase morphology and mechanical properties of PA6/EPDM-g-MA/HDPE ternary blends. *Polymer*, *56*, 395–405.

Shen, L., Haufe, J., & Patel, M. K. (2009). *Product overview and market projection of emerging bio-based plastics PRO-BIT 2009*. Utrecht, Netherlands: Utrecht University.

Shen, L., Worrell, E., & Patel, M. (2010). Present and future development in plastics from biomass. *Biofuels, Bioproducts and Biorefining*, *4*(1), 25–40.

Shi, D., Hu, G.-H., Ke, Z., Li, R. K. Y., & Yin, J. (2006). Relaxation behavior of polymer blends with complex morphologies: Palierne emulsion model for uncompatibilized and compatibilized PP/PA6 blends. *Polymer*, *47*(13), 4659–4666.

Shirahama, H., Kawaguchi, Y., Aludin, M. S., & Yasuda, H. (2001). Synthesis and enzymatic degradation of high molecular weight aliphatic polyesters. *Journal of Applied Polymer Science*, *80*(3), 340–347.

Siggia, E. D. (1979). Late stages of spinodal decomposition in binary mixtures. *Physical Review A*, *20*(2), 595–605.

Sinclair, R. G. (1996). The case for polylactic acid as a commodity packaging plastic. *Journal of

Macromolecular Science Pure and Applied Chemistry, *A33*(5), 585–597.

SJOERDSMA, S. D. (n.d.). The tough-brittle transition in rubber-modified polymers. *Polymer Communications*, *30*(4), 106–108.

Sodergard, A., & Stolt, M. (2002). Properties of lactic acid based polymers and their correlation with composition. *Progress in Polymer Science*, *27*(6), 1123–1163.

Song, W., Liu, H., Chen, F., & Zhang, J. (2012). Effects of ionomer characteristics on reactions and properties of poly(lactic acid) ternary blends prepared by reactive blending. *Polymer*, *53*(12), 2476–2484.

Stauffer, D., & Amnon, A. (1994). *Introduction to percolation theory*. London: Taylor and Francis.

Steinmann, S., Gronski, W., & Friedrich, C. (2002). Quantitative rheological evaluation of phase inversion in two-phase polymer blends with cocontinuous morphology. *Rheologica Acta*, *41*(1–2), 77–86.

Stoclet, G., Seguela, R., & Lefebvre, J.-M. (2011). Morphology, thermal behavior and mechanical properties of binary blends of compatible biosourced polymers: Polylactide/polyamide11. *Polymer*, *52*(6), 1417–1425.

Sue, H.-J., Huang, J., & Yee, A. . (1992). *Interfacial adhesion and toughening mechanisms in an alloy of polycarbonate/polyethylene*. *Polymer* (Vol. 33). Elsevier.

Sundararaj, U., & Macosko, C. W. (1995). Drop Breakup and Coalescence in Polymer Blends: The Effects of Concentration and Compatibilization. *Macromolecules*, *28*(8), 2647–2657.

Taylor, G. I. (1932). The Viscosity of a Fluid Containing Small Drops of Another Fluid. *Proceedings of the Royal Society of London. Series A, Containing Papers of a Mathematical and Physical Character*, *138*(834), 41–48.

Taylor, G. I. (1934). The Formation of Emulsions in Definable Fields of Flow. *Proceedings of the Royal Society of London. Series A, Containing Papers of a Mathematical and Physical Character*, *146*(858), 501–523.

Tchomakov, K. P., Favis, B. D., Huneault, M. A., Champagne, M. F., & Tofan, F. (2004). Composite droplets with core/shell morphologies prepared from HDPE/PS/PMMA ternary

blends by twin-screw extrusion. *Polymer Engineering and Science*, *44*(4), 749–759.

Thurber, C. M., Xu, Y., Myers, J. C., Lodge, T. P., & Macosko, C. W. (2015). Accelerating Reactive Compatibilization of PE/PLA Blends by an Interfacially Localized Catalyst. *ACS Macro Letters*, *4*(1), 30–33.

Tomotika, S. (1935). On the Instability of a Cylindrical Thread of a Viscous Liquid Surrounded by Another Viscous Fluid. *Proceedings of the Royal Society of London Series A*, *150*(870), 322–337.

Torza, S., & Mason, S. . G. (1970). Three-phase interactions in shear and electrical fields. *Journal of Colloid and Interface Science*, *33*(1), 67–83.

Valera, T. S., Morita, A. T., & Demarquette, N. R. (2006). Study of morphologies of PMMA/PP/PS ternary blends. *Macromolecules*, *39*(7), 2663–2675.

Van Oene, H. (1972). Modes of dispersion of viscoelastic fluids in flow. *Journal of Colloid and Interface Science*, *40*(3), 448–467.

Veenstra, H., Van Dam, J., & de Boer, A. P. (2000). On the coarsening of co-continuous morphologies in polymer blends: effect of interfacial tension, viscosity and physical cross-links. *Polymer*, *41*(8), 3037–3045.

Veenstra, H., van Lent, B. J. J., van Dam, J., & de Boer, A. P. (1999). Co-continuous morphologies in polymer blends with SEBS block copolymers. *Polymer*, *40*(24), 6661–6672.

Veenstra, H., Verkooijen, P. C. J., van Lent, B. J. J., van Dam, J., de Boer, A. P., & Nijhof, A. (2000). On the mechanical properties of co-continuous polymer blends: experimental and modelling. *Polymer*, *41*(5), 1817–1826.

Virgilio, N., Desjardins, P., L'Esperance, G., & Favis, B. D. (2009). In Situ Measure of Interfacial Tensions in Ternary and Quaternary Immiscible Polymer Blends Demonstrating Partial Wetting. *Macromolecules*, *42*(19), 7518–7529.

Virgilio, N., Desjardins, P., L'Esperance, G., & Favis, B. D. (2010). Modified interfacial tensions measured in situ in ternary polymer blends demonstrating partial wetting. *Polymer*, *51*(6), 1472–1484.

Virgilio, N., & Favis, B. D. (2011a). Self-Assembly of Janus Composite Droplets at the Interface in Quaternary Immiscible Polymer Blends. *Macromolecules*, *44*(15), 5850–5856.

Virgilio, N., & Favis, B. D. (2011b). Self-Assembly of Janus Composite Droplets at the Interface in Quaternary Immiscible Polymer Blends. *Macromolecules*, *44*(15), 5850–5856.

Virgilio, N., Marc-Aurele, C., & Favis, B. D. (2009). Novel Self-Assembling Close-Packed Droplet Array at the Interface in Ternary Polymer Blends. *Macromolecules*, *42*(9), 3405–3416.

Virgilio, N., Sarazin, P., & Favis, B. D. (2010). Towards ultraporous poly(L-lactide) scaffolds from quaternary immiscible polymer blends. *Biomaterials*, *31*(22), 5719–5728.

Virgilio, N., Sarazin, P., & Favis, B. D. (2011). Ultraporous poly(l-lactide) scaffolds prepared with quaternary immiscible polymer blends modified by copolymer brushes at the interface. *Polymer*, *52*(7), 1483–1489.

Wang, J., Reyna-Valencia, A., & Favis, B. D. (2016). Assembling Conductive PEBA Copolymer at the Continuous Interface in Ternary Polymer Systems: Morphology and Resistivity. *Macromolecules*, *49*(14), 5115–5125.

Willemse, R. C., de Boer, A. P., van Dam, J., & Gotsis, A. D. (1998). Co-continuous morphologies in polymer blends: a new model. *Polymer*, *39*(24), 5879–5887.

Willemse, R. C., de Boer, A. P., van Dam, J., & Gotsis, A. D. (1999). Co-continuous morphologies in polymer blends: the influence of the interfacial tension. *Polymer*, *40*(4), 827–834.

Willemse, R. C., Ramaker, E. J. J., Van Dam, J., & De Boer, A. P. (1999). Coarsening in molten quiescent polymer blends: The role of the initial morphology. *Polymer Engineering and Science*, *39*(9), 1717–1725.

Willemse, R. C., Speijer, A., Langeraar, A. E., & de Boer, A. P. (1999). Tensile moduli of co-continuous polymer blends. *Polymer*, *40*(24), 6645–6650.

Williams, C., & Hillmyer, M. (2008). Polymers from Renewable Resources: A Perspective for a Special Issue of Polymer Reviews. *Polymer Reviews*, *48*(1), 1–10.

Willis, J. M., Favis, B. D., & Lunt, J. (1990). Reactive Processing of Polystyrene-co-maleic

Anhydride Elastomer Blends - Processing-Morphology-Property Relationships. *Polymer Engineering and Science*, *30*(17), 1073–1084.

Witt, U., Einig, T., Yamamoto, M., Kleeberg, I., Deckwer, W. D., & Müller, R. J. (2001). Biodegradation of aliphatic–aromatic copolyesters: evaluation of the final biodegradability and ecotoxicological impact of degradation intermediates. *Chemosphere*, *44*(2), 289–299.

Wu, M., Wu, Z., Wang, K., Zhang, Q., & Fu, Q. (2014). Simultaneous the thermodynamics favorable compatibility and morphology to achieve excellent comprehensive mechanics in PLA/OBC blend. *Polymer*, *55*(24), 6409–6417.

Wu, S. (1971). Calculation of interfacial tension in polymer systems. *Journal of Polymer Science Part C: Polymer Symposia*, *34*(1), 19–30.

Wu, S. (1974). Interfacial and Surface Tensions of Polymers. *Journal of Macromolecular Science, Part C: Polymer Reviews*, *10*(1), 1–73.

Wu, S. (1982). *Polymer interface and adhesion*. New York: M. Dekker.

Wu, S. (1987). Formation of dispersed phase in incompatible polymer blends: Interfacial and rheological effects. *Polymer Engineering & Science*, *27*(5), 335–343.

Wu, S. (1992). Control of intrinsic brittleness and toughness of polymers and blends by chemical structure: A review. *Polymer International*, *29*(3), 229–247.

Xing, P. X., Bousmina, M., Rodrigue, D., & Kamal, M. R. (2000). Critical experimental comparison between five techniques for the determination of interfacial tension in polymer blends: Model system of polystyrene/polyamide-6. *Macromolecules*, *33*(21), 8020–8034.

Young, R. J. (1991). Introduction to Polymers. Chapman and Hall, London.

Yu, Z.-Z., Ou, Y.-C., Qi, Z.-N., & Hu, G.-H. (1998). Toughening of nylon 6 with a maleated core-shell impact modifier. *Journal of Polymer Science Part B: Polymer Physics*, *36*(11), 1987–1994.

Yu, Z., Lei, M., Ou, Y., & Hu, G. (1999). The Role of Interfacial Modifier in Toughening of Nylon-6 with a Core-Shell Toughener. *Journal of Polymer Science Part B: Polymer Physics*, *37*, 2664–2672.

Yuan, Z., & Favis, B. D. (2005). Coarsening of immiscible co-continuous blends during quiescent annealing. *AIChE Journal*, *51*(1), 271–280.

Zhang, J. H., Ravati, S., Virgilio, N., & Favis, B. D. (2007). Ultralow percolation thresholds in ternary cocontinuous polymer blends. *Macromolecules*, *40*(25), 8817–8820.

Zhang, K., Mohanty, A. K., & Misra, M. (2012). Fully Biodegradable and Biorenewable Ternary Blends from Polylactide, Poly(3-hydroxybutyrate-co-hydroxyvalerate) and Poly(butylene succinate) with Balanced Properties. *ACS Applied Materials & Interfaces*, *4*(6), 3091–3101.

Zhang, K., Nagarajan, V., Misra, M., & Mohanty, A. K. (2014). Supertoughened Renewable PLA Reactive Multiphase Blends System: Phase Morphology and Performance. *ACS Applied Materials & Interfaces*, *6*(15), 12436–12448.

Zhou, L., Zhao, G., Feng, Y., Yin, J., & Jiang, W. (2015). Toughening polylactide with polyether-block-amide and thermoplastic starch acetate: Influence of starch esterification degree. *Carbohydrate Polymers*, *127*, 79–85.

APPENDIX A – SUPPOTING INFORMATION FOR ARTICLE 2

A.1. In-situ measurement of interfacial tensions and contact angles

A method based on the Neumann triangle method combined with a microscopy technique is used to measure the interfacial tensions of PLA/PBS, PBS/PHBV, PLA/PHBV, and PLA/PBAT and contact angles between phases at the line of 3-phase contact. This technique is based on the geometrical analysis of contact angles between three immiscible phases in a ternary polymer blend. The balance between three interfacial tensions at the line of 3-phase contact is described by a Neumann triangle. This method gives relative values of the interfacial tensions between components, therefore, one can calculate the interfacial tensions when one of the interfacial tensions is known. Three melt blended ternary PLA/PHBV/PBS, PLA/PBAT/PE, and PLA/PE/PBAT systems with partial wetting morphology were prepared. AFM and SEM micrographs of the blends were used to fit geometrical constructions for a minimum 20 partially wet droplets at the interface. Further details of the technique can be found elsewhere [1,2].
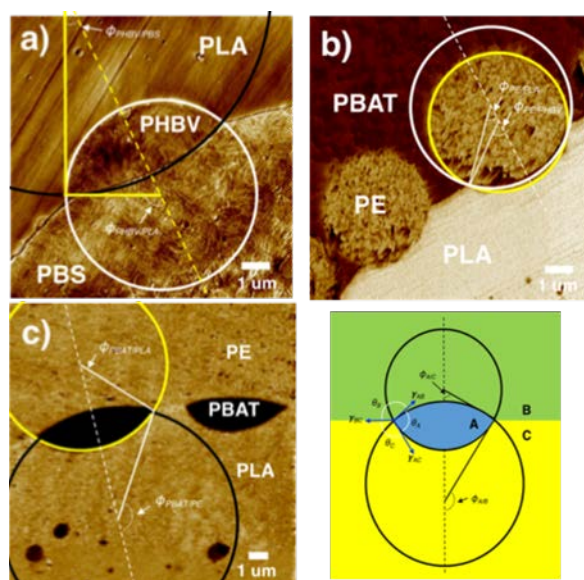

Figure A1. Geometrical constructions fitted to AFM micrographs of partially wet droplets at interface to calculate the θ contact angles in a) PLA/PHBV/PBS 50/5/50, b) PLA/PE/PBAT 50/5/50, and c) PLA/PBAT/PE 50/5/50.

A.2. AFM micrographs of the ternary PLA/PBS/PBAT system

The ternary PLA 47.5%/PBS 5%/PBAT 47.5% blend were prepared to show formation of a completely wet layer of PBS at the interface of the PLA/PBAT. This system consists of components with very low interfacial tensions.
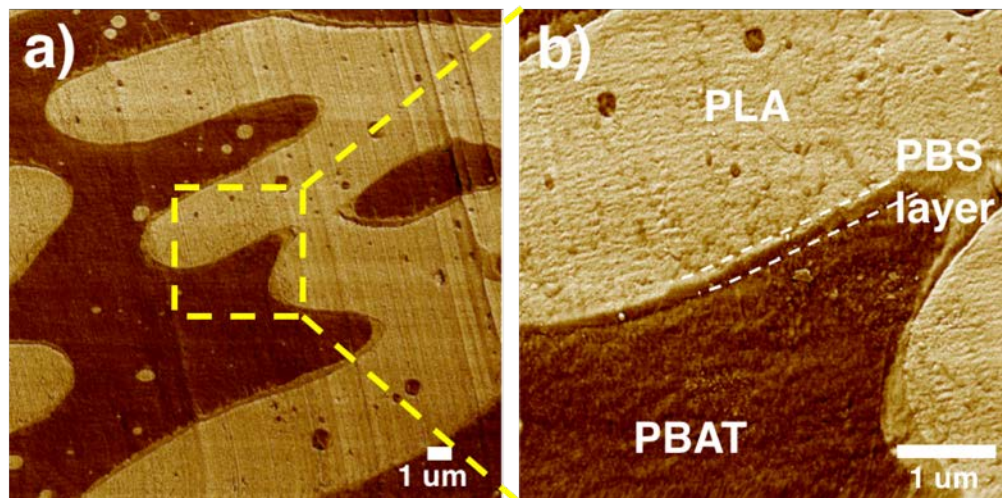

Figure A2. a, b) AFM micrographs of the PLA/PBS/PBAT 50/5/50 system with complete wetting morphology.

A.3. Rheological properties of pure components

The results of the complex viscosities of the neat polymers examined at 190°C are presented in Figure S3.
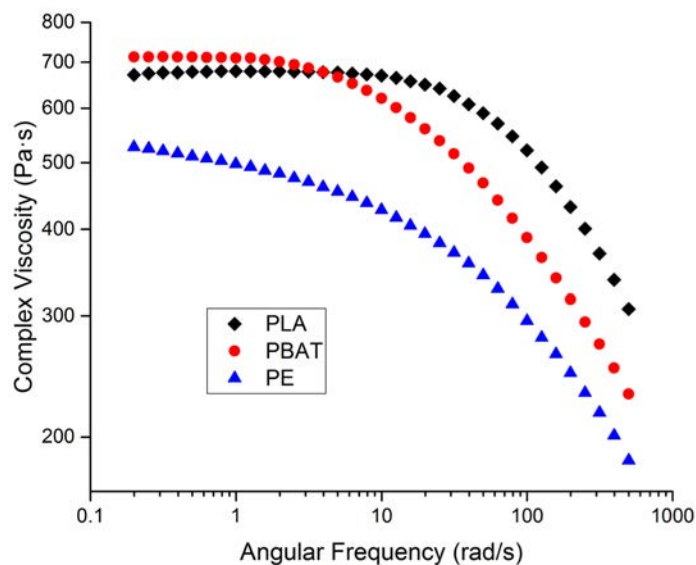

Figure A3. Complex viscosity vs. frequency of pure homopolymers used in this study at 190°C.

A.4. References

[1]   S. Horiuchi, N. Matchariyakul, K. Yase, T. Kitano, Morphology development through an interfacial reaction in ternary immiscible polymer blends, Macromolecules. 30 (1997) 3664–3670.

[2]   N. Virgilio, P. Desjardins, G. L'Esperance, B.D. Favis, In Situ Measure of Interfacial Tensions in Ternary and Quaternary Immiscible Polymer Blends Demonstrating Partial Wetting, Macromolecules. 42 (2009) 7518–7529.

APPENDIX B – SUPPOTING INFORMATION FOR ARTICLE 3

B.1. Rheological analysis

A controlled-stress rheometer (Physica MCR 301, Anton Paar) equipped with a 25 mm parallel plate disk geometry with a gap of 1 mm was used to perform rheological measurements. All rheological measurements were performed on compression molded disks of 25mm diameter and 1.2mm thickness at 200 °C under nitrogen atmosphere. Strain and time sweep tests were performed to determine the linear viscoelastic region and thermal stability of samples. All polymers showed acceptable thermal stability (less than 10% viscosity reduction) at the set temperature in the time sweep experiment at 10% strain and 1 rad/s after 40 min. The results are presented in Figure S1.
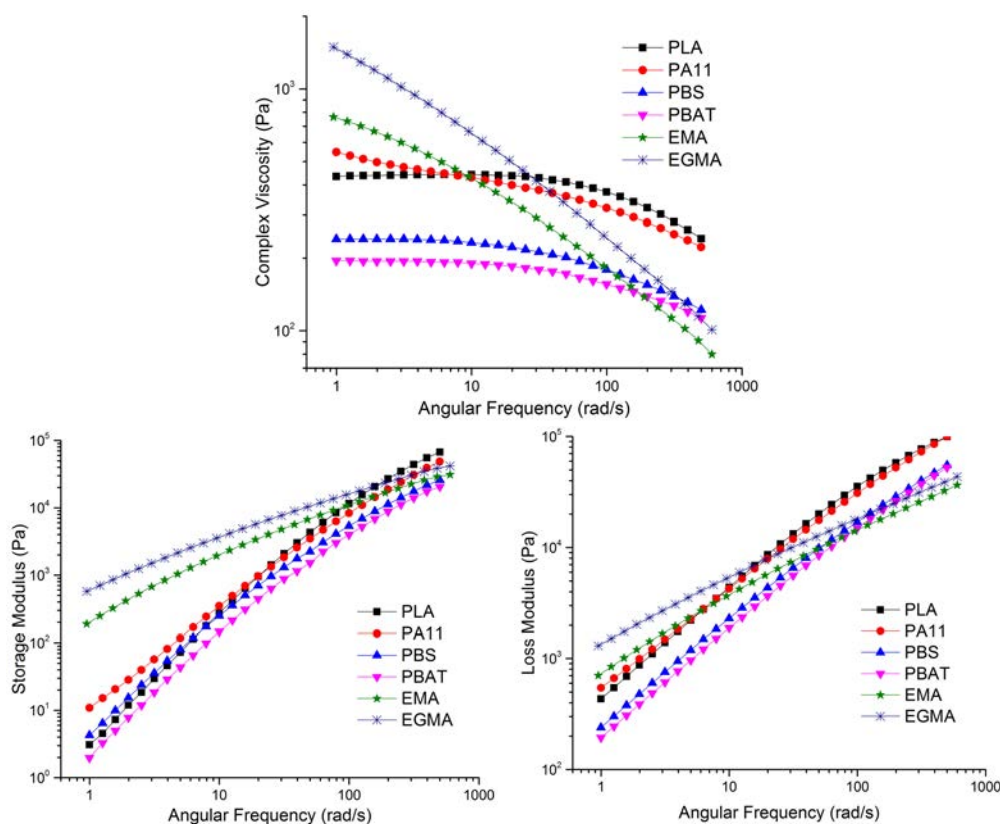

Figure B1. Complex viscosity, storage and loss moduli of the neat polymers at 200 °C.
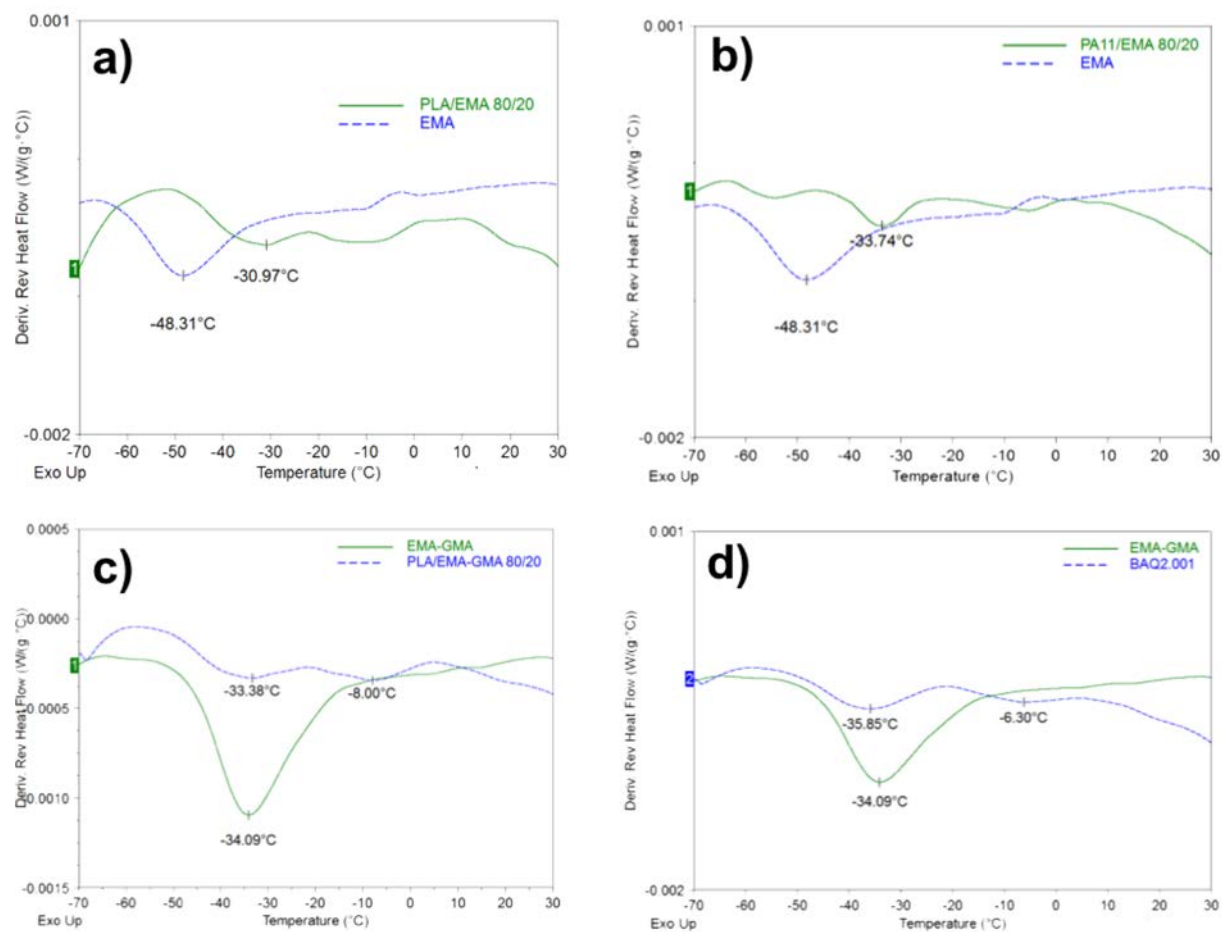
B.2. Thermal analysis

Figure B2. MDSC data for the pure polymers and the 80/20 w/w blends heated at 2°C/min.

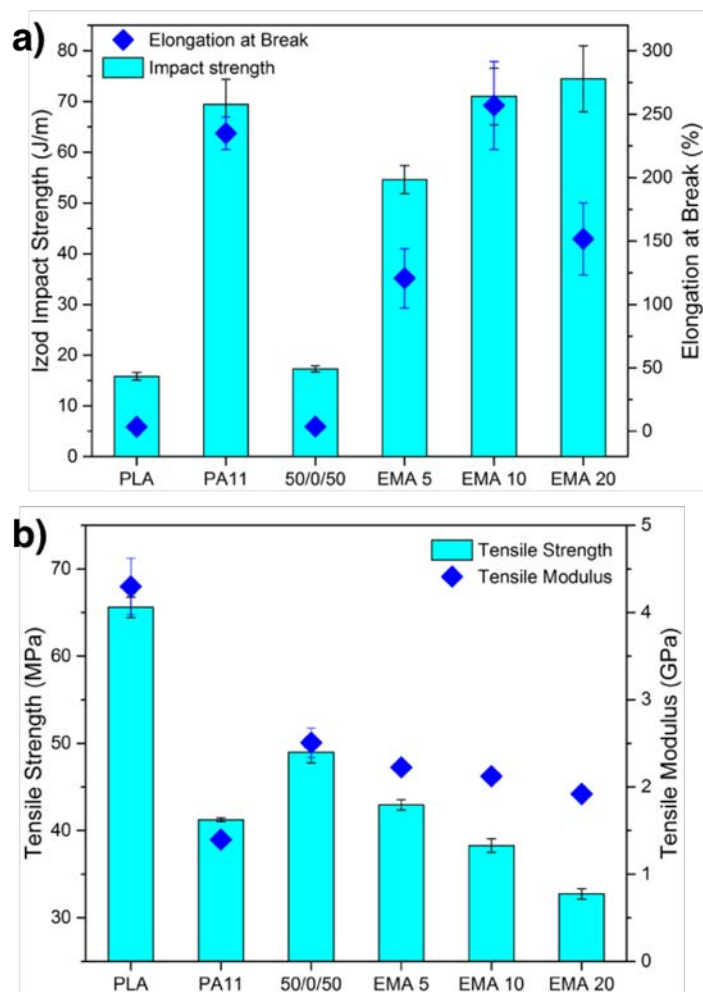## B.3. Tensile properties and notched Izod impact strength

Figure B3. Mechanical properties of pure components and blends containing EMA.